ISSN 0915-6348

NATIONAL INSTITUTE FOR FUSION SCIENCE

U.S.-Japan Workshop on "RF Heating and Current Drive in Confinement Systems Tokamaks"

Nov. 18-21, 1991

(Received – Dec. 26, 1991)

NIFS-PROC-10 Jan. 1992

RESEARCH REPORT
NIFS-PROC Series

NAGOYA, JAPAN

U.S.-Japan Workshop on

"RF Heating and Current Drive in Confinement Systems Tokamaks"

Nov. 18-21, 1991

National Institute for Fusion Science

Nagoya, Japan

Keywords: RF Heating, Current Drive, Helicity Injection, Current Profile Control, Diverter Condition, Biasing, Consistency Analysis

Contents

Opening Address Iiyoshi, A. 1

Workshop Program 2

Abstracts of Presentations 7

Summary Reports

Group A 46

Group B 48

Group C 54

Grand Summary 57

Highlights of Workshop (in Japanese) 60

Appendix (Viewgraphs) 61

Welcome address for the US-Japan workshop

A. Iiyoshi

National Institute for Fusion Science (NIFS)

It is my great pleasure to welcome you to NIFS on occasion of this Japan-US workshop.

One of the purposes of this institute is to study the physics of plasmas so as to establish the basic and general understanding of toroidal plasma properties. The research on the heating, current-drive and the divertor has long history since the C-Stellarator, on which I had a chance to work in the very beginning of my academic life. Now the JET has achieved D-T plasma experiment and the fusion research is coming into a new era. The problem still remains the largest obstacle for us to realize the stationary burning. These problems, I understatnd, require multiple approaches in both experimental and theoretical aspects.

The topic of this workshop is very important and is an urgent issue. We know that US research is more dedicated to ITER, however, we also have to consider the physics and technology beyond ITER. Japanese fusion society is paying efforts for the progress in this area. I believe that the workshop will surely be successful and creative for the new research in this field. I look forward to seeing the outcome of the workshop.

Program for US-Japan workshop (p181) on

" RF heating and current drive in confinement systems tokamaks "

Nov. 18 1991

9.30 Registration

:Opening session:

9.55 Opening Announcement — S.-I. Itoh (NIFS)

10.10 Opening Address — A. Iiyoshi (NIFS)

10.20 Self-introduction — all participants

:Overview session:

Chair S. Tanaka (Kyoto U)

10.35 Recent Fast Wave Results on DIII-D Experiments
V. S. Chan (GA)

11.15 Combined Current Drive of EC and LH waves in WT-3
T. Maekawa (Kyoto U)

11.40 Plan of RF Heating and Related R&D for Large Helical Device(LHD)
K. Ohkubo (NIFS)

12.00 - 13.30 lunch

Chair V.S.Chan (GA)

13.30 Fast Wave Heating and Current Drive in JT-60/60U
H. Kimura (JAERI)

14.15 Wave Particle Interactions of Fast and Slow Waves in JIPP-T-II-U
T. Seki (NIFS)

14.40 Wave Heating and Current Drive Experiments in JFT-2M
Y. Uesugi (Nagoya U)

15.05 - 15.40 break

Chair T. Imai (JAERI)

15.40 High-Density and Long-Pulse Operation by LHCD in TRIAM-1M
Y. Nakamura (Kyushu U)

16.30 Experiments on Current Profile Control with LH waves in View of the PBX-M Experiment
S. Bernabei (PPPL)

17.10 Ice breaking shots + Video
(4210 sec discharge in TRIAM-1M)

Adjourn

Nov.19 1991

:RF Technology and Applications:

Chair M. Taguchi(Nihon U)

9.15 Modelling DIII-D/ITER FWCD Experiments with a Full Wave Code P. Bonoli (MIT)

9.55 Helicity Injection and Current Drive by RF Waves A. Fukuyama (Okayama U)

10.35 - 10.50 break

Chair T. Watari (NIFS)

10.50 Improved Confinement and Stability Through Current Profile Modification T. Taylor (GA)

11.30 Profile control by LH Wave Application K. Ushigusa (JAERI)

11.55 Sawtooth Stabilization by ECH near q=1 Surface in WT-3 K. Hanada (Kyoto U)

12.20 - 13.45 lunch

Chair M. Shimada (JAERI)

14.00 ITER Current Drive Requirements H. Kimura (JAERI)

:Helicity, Transport, Current/Rotation Drive:

14.25 Current Drive Experiment on CDX-U : Helicity Injection and Pressure Driven Currents C. Forest (PPPL)

15.05 Model of Divertor Biasing and SOL Plasma Response K. Nagasaki (Kyoto Heliotron)

15.30 - 16.00 break

Chair T. Taylor (GA)

16.00 Divertor Biasing Experiments in DIII-D R. Stambaugh (GA)

16.40 Divertor biasing and Helicity Injection K. Itoh (NIFS)

17.20 Adjourn

18.00 Group Dinner (Faculty Club, Nagoya Univ.)

Nov.20 1991

:Heating/Current-Drive and SOL/Divertor Conditions:

Chair M. Fujiwara (NIFS)

9.30 Initial Results of LHCD in JT-60U and Limitation of the LHCD Application T. Imai (JAERI)

10.10 SOL/Divertor Plasma Performance during Auxiliary Heating/ Current-Drive on JT-60 M. Shimada (JAERI)

10.45 - 11.10 break

Chair P. Bonoli (MIT)

11.10 Simulation Study of SOL Plasma Transport and the Scaling Laws S.-I. Itoh (NIFS)

11.45 Anomalous Transports Associated with the Helicity Transport Z. Yoshida (Tokyo U)

12.10- 13.30 lunch

13.30 Consistency of Current-Drive and the Divertor Conditions (ITER & beyond ITER needs) M. Sugihara (JAERI)

14.15 Working session grand leader K. Itoh (NIFS)
group discussions on

1) Perspectives on RF technology and the applications
leaders: *S. Bernabei & S. Tanaka & H. Kimura

2) Helicity, Transport, New Concept on Current/Rotation Drives leaders: *K. Itoh & V.S.Chan

3) Heating/Current-Drive and SOL/Divertor Conditions
-ITER and beyond ITER Phys. R & D for Long Pulse Operation-
leaders: S.-I.Itoh & *M. Sugihara

Three topic leaders(indicated by *) will report the discussion record in the summary session for further discussion.

Adjourn

Nov.21 1991

:Summary session:

Chair A. Fukuyama

9.30 summary and discussions of group 1) S. Bernabei

9.55 summary and discussions of group 2) K. Itoh

10.20 summary and discussions of group 3) M. Sugihara

10.45-11.00 break

Chair S. Bernabei

11.00 grand summary and outcome of the workshop V.S. Chan

11.40 a comment to the workshop M. Yoshikawa

11.50 a comment & memo learned from the workshop R. Freeman

12.05 Closing S.-I. Itoh

List of participants Nov. 18-21 1991 NIFS

US

S. Bernabei (PPPL)

P. Bonoli (MIT)

V.S. Chan (GA)

C. Forest (PPPL)

R. Freeman (GA)

R. Stambaugh (GA)

T. Taylor (GA)

S. Yoshikawa (PPPL & Tokyo Univ.)

Japan

H. Abe (Ryukoku Univ.)

M. Fujiwara (NIFS)

A. Fukuyama (Okayama Univ.)

Y. Hamada (NIFS)

K. Hanada (Kyoto Univ.)

A. Iiyoshi (NIFS, Director general)

T. Imai (JAERI)

K. Itoh (NIFS)
S.-I. Itoh (NIFS)
H. Kimura (JAERI)
S. Kubo (NIFS)
R. Kumazawa (NIFS)
K. Kusano (Hiroshima Univ.)
T. Maekawa (Kyoto Univ.)
K. Miyamoto (Tokyo Univ.)
T. Mutoh (NIFS)
K. Nagasaki (Kyoto Heliotron)
Y. Nakamura (Kyushu Univ.)
K. Ohkubo (NIFS)
H. Sanuki (NIFS)
T. Seki (NIFS)
M. Shimada (JAERI)
M. Sugihara (JAERI)
H. Takase (Toshiba, R & D Center)
M. Taguchi (Nihon Univ.)
S. Tanaka (Kyoto Univ., WT-3 leader)
Y. Uesugi (Nagoya Univ.)
K. Ushigusa (JAERI)
T. Watari (NIFS)
Z. Yoshida (Tokyo Univ.)
M. Yoshikawa (JAERI, Executive Director)

Recent Fast Wave Results on DIII–D

Reported by
V.S. Chan for the DIII–D RF Group

General Atomics
San Diego, California 92186-9784, U.S.A.

The DIII–D program has, as its long term goal, the integrated demonstration of fully noninductive current drive with good confinement in a high beta plasma. This goal will be achieved with a combination of FWCD/ECH, ECCD, and bootstrap current. Present DIII–D program systematically studies each of these current drive elements to achieve detailed understanding of the physics which is crucial for attaining the long term goal.

Recently, efficient direct electron heating by fast waves has been observed on DIII–D. A four-strap antenna with $(0, \pi, 0, \pi)$ phasing launched up to 1.7 MW of fast wave power with $|n_{\parallel}| \simeq 11$. The fast wave electron heating was weak for central electron temperature below 1 keV, but improved substantially with increasing T_e. For $P_{rf} \simeq 0.8$ MW and $B_T = 2$ T, the central T_e increased from 1.1 to 2.5 keV. The plasma stored energy during rf increased with toroidal field at variance with single pass absorption theory. Multiple pass absorption of the fast waves appears to be occurring since at 2 T nearly 100% efficient plasma heating is observed even though the calculated single pass absorption is only 8%. This is consistent with full wave calculation.

Electron heating with fast waves has also been observed with $\pi/2$ (current drive) phasing. When combined with ECH, significant central electron heating was achieved indicating that wave-particle interaction was enhanced at higher target temperature as expected from theory and in a direction favorable for current drive. Analysis of changes in loop voltage to ascertain possible current drive effect is in progress.

This is a report of work sponsored by the U.S. Department of Energy under Contract No. DE-AC03-89ER51114.

Combined Current Drive of EC and LH Waves in WT-3

T. Maekawa, T. Maehara, T. Kishino, Y. Kishigami, K. Makino
T. Minami, K. Hanada, M. Nakamura,*) Y. Terumichi, S. Tanaka

Department of Physics, Kyoto University
*) Osaka Institute of Technology

The efficiency of electron cyclotron (EC) current drive is strongly dependent on the drift velocity of EC resonant electrons along the toroidal field. If one generates a fast electron tail in addition to the bulk electron by lower hybrid (LH) current drive and injects EC wave in such a manner that the EC wave couples to the fast electron tail, one can expect an efficient ECCD comparable to LHCD. Another aspect of interest is the combined effect on the resonant interaction of the both waves with the fast electron tail. To explore these points we have carried out experiments of combined current drive by use of EC and LH waves on the WT-3 tokamak (R_0=65cm, a=20cm, $B_t \leq 1.75$T).

Figure 1 shows a typical shot of the experiments. First, the plasma current is initiated and increased to $I_p \simeq 40$ kA by the Ohmic heating (OH) power. Second, LH power from a klystron (f=2 GHz) is injected and at the same time the primary winding of the OH transformer is short-circuited. After a while the current settles to a constant value of $I_p \simeq 35$ kA and the loop voltage at the vacuum vessel cut settles to slightly negative value of $V_L \simeq -0.1$ V. Its negative value is ascribed to a small resistance of the OH coil. Third, EC power from a gyrotron (f=56 GHz) is injected from the low field side as the X-mode via a Vlasov antenna. Then, the current starts to ramp up with a rate of $dI_p/dt \simeq 100$ kA/sec and the loop voltage becomes to a further negative value of $V_L \simeq -0.25$ V. At the same time electron cyclotropn emission (ECE), which is radiated mainly from the tail electrons, and the Shafranov lamda $\Lambda = \beta_p + \ell_i/2$ increase.

The negative loop voltage and the current increase manifest increase of poloidal magnetic field energy. The rate of increment may be evaluated by a formula $P_M = -V_L I_p + (d/dt)\{\int B_\theta^2/2\mu_0 \, dV\}$, where the first term is the Poynting out flux at the vessel cut and the second term is the time derivative of the magnetic energy inside the vessel. The result is $P_M \simeq 3.5$ kW before EC injection and $P_M \simeq 12$ kW during EC injection for the additional injection power of $P_{EC} \simeq 150$ kW.

Such a ramp-up discharge as Fig.1 is obtained in rather narrow parameter range of the density $\bar{n}_e \leq 2\times10^{12}$ cm^{-3} and the toroidal field $\Omega_e(0)/\omega \simeq 0.75 \sim 0.83$, where $\Omega_e(0)$ is the EC frequency at $R=R_0$. An examination of the EC resonance condition of the fast electrons, $\gamma[1-N_{//}(v_{//}/c)] = \ell\Omega_e/\omega$, and the propagation

characteristics of EC waves suggests that absorption of EC waves via fundamental resonance (ℓ=1) of oblique X-mode ($N_{//}$ ~0.7) is the dominant process of the interaction.

Current ramp-up is also obtained by stepping up the LH power at t=80 msec instead of EC power in Fig.1. In this case current ramp-up rate is nearly equal or slightly larger compared with the EC case for the same additional power in the range of 0 ~ 200 kW, while increments of the ECE signal and Λ is much larger in the EC case. This result suggests that the current is carried away by more energitic electrons in the EC case compared with the LH case. Figure 2 shows energy spectra of hard X-ray emitted forward and perpendicularly to the fast electron drift direction along the toroidal field in the three cases of LHCD flat top discharge, and ramp-up discharges with nearly the same additional EC or LH power of ≃120 kW. In the EC case enhancement of photon counts in high energy range for the forward direction is remarkable, suggesting that the fast electrons are being further accelerated against the opposite loop voltage of $V_L \simeq -0.25$ V.

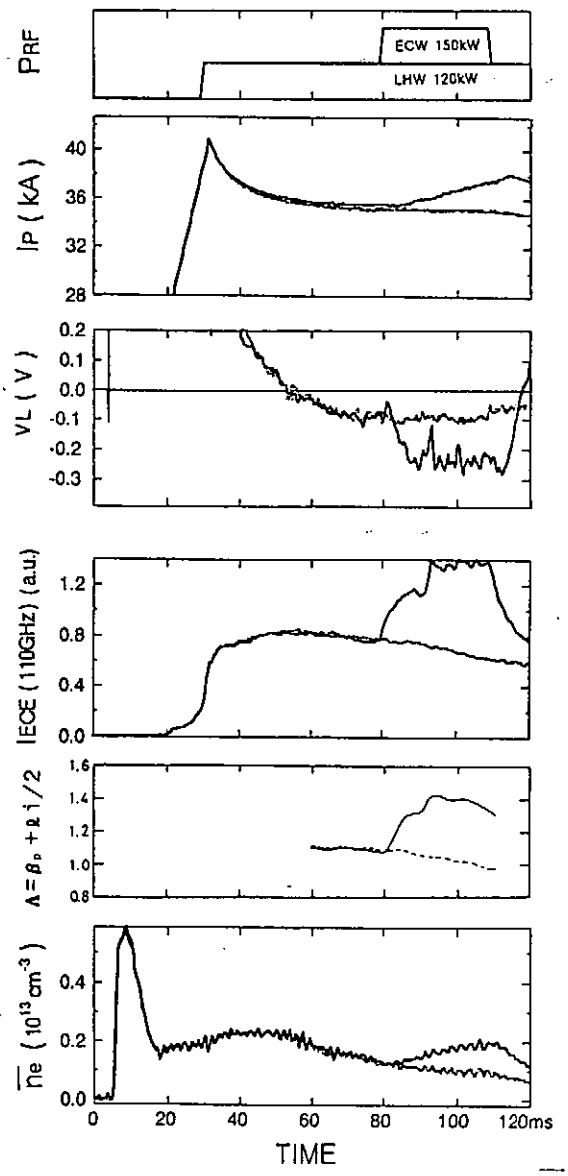

Fig. 1

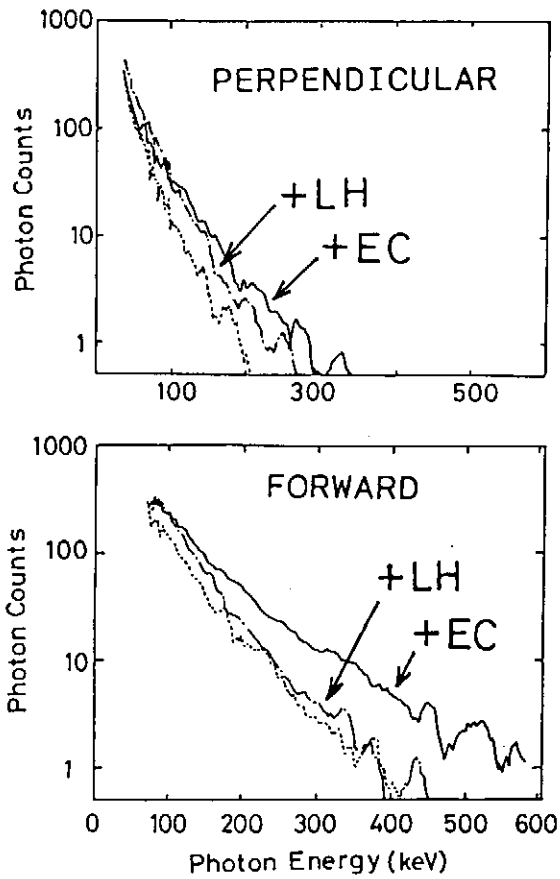

Fig. 2

Japan-US Workshop at NIFS,
Nagoya Oct.18-21 1991

Plans of RF Heating and Related R&D for LHD

K. Ohkubo, M. Hosokawa, S. Kubo, R. Kumazawa,
T. Motoh, M. Sato, T. Watari and T. Kuroda

National Institute for Fusion Science, Nagoya, 464-01

Large Helical Device (LHD) is a superconducting heliotron/torsatron type device (l=2, m=10) with R=3.9m, ap=0.55-0.6m, B=3-4T and with the helical divertor fully around the torus. Its physical objectives are to produce currentless high temperature plasma in a steady state and to conduct various experimental programs for development of helical fusion system as an alternative approach of tokamak. In the LHD, heating power of 20 MW for a 10 sec pulse and about 3 MW for CW is planned. To satisfy the requirements, ECH, ICRF and NBI methods are adopted.

The goal of this investigation is to define both ECH and ICRF systems for LHD on the grounds of the art from the experimental and theoretical points of views.

The main objectives and specification of ECH and ICRF system are as follows: for ECH, plasma production, transport analysis, electron root confinement study, potential control and steady state heating are main objectives. For ICRF, heating and profile control, high Ti mode operation and simulation of alpha particle behavior are main subjects. Each heating method can supply the rf power of 3MW for the long pulse steady state operation of around 30 minutes at the first stage. In the first stage the frequencies of ECH and ICRF are 84 GHz and 30-90 MHz, respectively.

The schedule of R&D for rf heating system and LHD machine is shown in Table 1. Until 1994, R&D and design of rf heating system will be contiunued.

The R&D program for ECH is composed of fabrication of MW-class gyrotron and transmission line with good performance from the viewpoint of mode purity and withstanding voltage. With fabricating the MW-class gyrotron, the development of high dc voltge (-80kV) power supply connected to both the commercial power line and flywheel generator is being progressed. The design of control system by the LHD central control computer and the ECH subcomputer is also being advanced.

Engineering issue for ICRF system is of an antenna development including the waveguide lauching, its related design with plasma-antenna interaction, and establishment of matching procedure. During an R&D period, the ICRF heating experiment on the JIPP T-IIU tokamak and the CHS helical device is continued to get the know-how from the physical and engineering viewpoints of ICRF.

The R&D started when the NIFS was established in 1989. As for the gyrotron fabication for testing, two types of whispering gallery mode and quasi-optical gyrotron are considered as the candidate. Quasi-optical

gyrotron is attractive for frequency tunability and the capability of second harmonic oscillation. The experiments of quasi-optical gyrotron with standard resonator of curved mirrors is being carried out. The whispering gallery mode gyrotron which will install in spring of 1992 is being fabricated.

By using the test stands for quasi-optical and corrugated waveguide transmission which were installed in 1990 and 1991, respectively, the experiment on microwave transmission with cylindrical elipsoid mirrors is carried out. The design method of the mirror taken into account of phase front of gaussian beam is developed. The new evaluation method of the corrugated waveguide components based on the fast Fourier trasnsform is developed. The calculation code for radiation pattern launched from the opening of the component is also completed and is now served to evaluate the perfomance of the component.

In FY 1990, an ICRF oscillator of which power is 3 MW/30 mimutes (4 MW/ 2 sec.) for 25-60 MHz and 2 MW/30 minutes (3 MW/10 sec.) for 60-100 MHz was fablicated. The oscillator is consist of the two amplifiers and the outputs are added by the 3 db power combiner. The investigation of matching methods with plasma admittance is being carried out from the viewpoint of frequency feedback and stub tuner controls. The calculation shows that the frequency control method is well applicable for the change in the plasma surface admittance, As if megawatts power had been introduced continuously, the temperature increase in the coaxial line was simulated experimentally by inserting the electric heater inside the coaxial line. From experimental results, it is being discussed how to cool the transmission line.

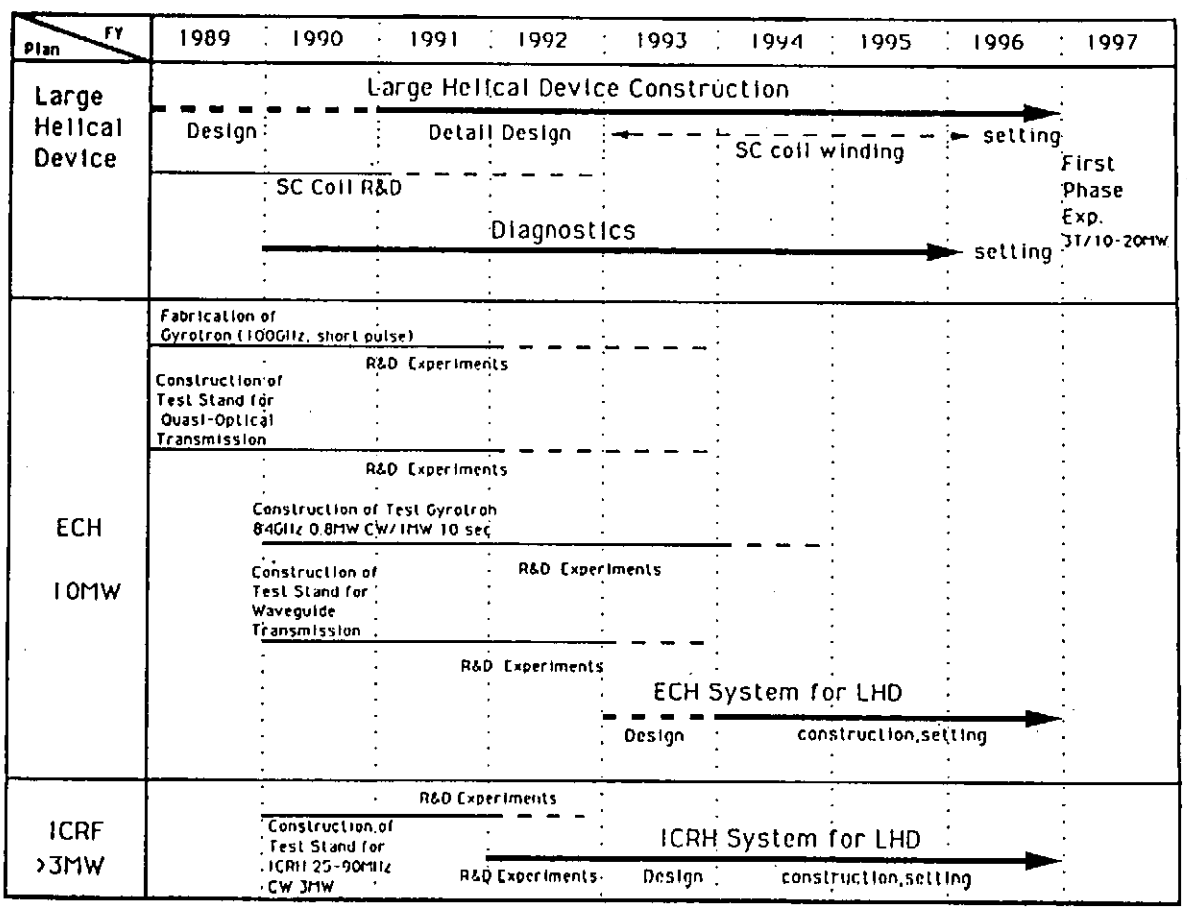

Abstract for US-Japan Workshop on RF Heating and Current Drive in Confinement System Tokamaks, Nagoya, Nov. 18-21, 1991

FAST WAVE HEATING AND CURRENT DRIVE IN JT-60/60U

H. Kimura and T. Fujii

Naka Fusion Research Establishment
Japan Atomic Energy Research Institute

With acknowledgements to
M. Saigusa, S. Moriyama, M. Yamagiwa, K. Hamamatsu, Y. Kusama, K. Tobita, M. Nemoto, K. Nagashima, H. Takeuchi, M. Kuriyama, T. Imai, T. Yamamoto and A. Fukuyama*

Summary of the ICRF heating experiments on JT-60 and ICRF experimental plan and analyses for JT-60U are presented. The JT-60 ICRF experiments (120MHz and 131MHz) are characterized by higher harmonic heating with phase control of the compact 2×2 loop antenna array. The antenna power density at the Faraday shield reached 16MW/m^2, which is the highest value among the ICRF systems in the world. It is found that power injection capability is inversely dependent on the antenna-plasma distance between in-phase (low-$k_{||}$) mode and out-of-phase (high-$k_{||}$) mode. Interactions between edge plasma and the antenna are enhanced significantly only with low-$k_{||}$ mode when the plasma comes close to the antenna. The result may be explained by the RF sheath model. The frequency feedback control is quite useful for automatic antenna impedance matching. Second harmonic heating is optimized by the antenna phase control. The incremental energy confinement time (τ_E^{inc}) of the high-$k_{||}$ mode is about 50% better than that of the low-$k_{||}$ mode. Minority hydrogen second harmonic heating in helium discharges is found to be more effective in the wide electron density range than majority hydrogen second harmonic heating. τ_E^{inc} of the minority heating is ~110ms, which is twice as high as that of NBI heating of hydrogen discharges. Efficient beam ion acceleration is observed in combined second harmonic ICRF and NBI heating. Enhancement of the plasma stored energy is explained quantitatively by the Fokker-Planck analysis. Strong central electron heating associated with beam ion acceleration is also observed in combined third harmonic ICRF and NBI heating. Sawtooth stabilization is observed both in second and third harmonic heating. A parameter space for the sawtooth stabilization with the second harmonic minority heating is characterized by relatively high density and low q ($\bar{n}_e \leq 6.5\times10^{19}$m^{-3}, $q_{eff} \geq 2.6$) and low threshold power (~ 2MW). Fast ions can be produced efficiently by the second harmonic minority heating even in high density discharges and play an important role in sawtooth stabilization. FWEH experiment ($f/f_{cH} \sim 2.5$) in combination with LHCD of relatively low

* Faculty of Engineering, Okayama University

power (f = 2GHz, P_{LH}/P_{IC} = 0.3~0.6) is performed. Power absorption efficiency of fast wave is improved due to presence of fast electrons produced by LHCD. Bulk electron heating is observed with high-$k_{\parallel}$ mode and coupling with fast electrons is confirmed in hard X-ray emission with low-$k_{\parallel}$ mode. The results are consistent with theoretical prediction based on 1-D full wave code.

The JT-60 ICRF heating system has been upgraded for JT-60U. Two new antennas have been constructed. They are also 2×2 loop antenna arrays, essentially similar to the old one, but have three times larger size to improve power injection capability, especially for H-mode plasmas. Objectives of ICRF heating in JT-60U will be also focused on the investigation of the higher harmonic heating with emphasis on the sawtooth stabilization in high density plasma with larger power (~4.5MW). High D-^{3}He fusion yield can be expected with fourth harmonic ICRF heating of ^{3}He in combination with ^{3}He beam injection into deuterium plasma, especially in high density regime [1]. Local current profile control by uni-directional minority ion heating or beam ion acceleration in combination with tangential NBI will be tested. Synergetic effects between FWEH and LHCD will be also investigated more systematically than before.

Fast wave current drive (FWCD) ability on JT-60U is analyzed for future programme. $N_{\parallel}$-range required for FWCD on JT-60U is found to be 3~6, in analyzing single-pass absorption rate (η_s) of two operation regimes (low field regime and high field regime). Coupling calculation indicates that eight-loop antenna is favourable for keeping high directivity in the required $N_{\parallel}$-range. Current drive efficiency is calculated with 1-D full wave code including trapped particle effects and higher harmonic ion cyclotron damping. We can expect driven current of ~1MA with 4MW ICRF power at $N_{\parallel}(p)$=4.5, T_{e0}=10keV and $n_{e0}=2\times10^{19}m^{-3}$ (corresponding current drive figure of merit of $\sim0.11\times10^{20}AW^{-1}m^{-2}$) with reasonable assumptions of wall resistivity = $10^{-3}\Omega m$, n_H/n_e=2% and Z_{eff}=2. It is found that very low $N_{\parallel}$ modes appear due to an eigen mode effect and still affect the current drive efficiency even in large single-pass absorption regime ($\eta_s \leq 0.6$).

REFERENCE

[1] YAMAGIWA, M. and KIMURA, H., Nucl. Fusion, **31** (1991) 1519.

WAVE PARTICLE INTERACTIONS OF FAST AND SLOW WAVES IN JIPP T-IIU

T. Seki, JIPP T-IIU group

National Institute for Fusion Science, Nagoya 464-01, Japan

INTRODUCTION

In JIPP T-IIU tokamak, a series of experiments using the 130 MHz radio frequency (RF) system has been conducted in the last two years. The objective of the experiments is in the investigation of the wave particle interactions in the intermediate frequency range, which extends from the 3rd harmonic ion cyclotron frequency to the lower hybrid frequency and is important in the thermonuclear fusion studies.

Fast wave experiments was conducted in the deuterium plasma mixed with 10 % hydrogen. There were two competitive heating regimes, that is, electron and ion heating regimes. The electron heating regime is associated with the fast wave current drive. On the other hand, the ion heating is caused by the higher (3rd) harmonic ion cyclotron damping mechanism, which is related to the finite Larmor radius effects and is thought to be enhanced as the plasma parameters are improved.

The heating experiments using the slow wave (Ion Bernstein Wave) have been also carried out. The frequency used is the highest frequency in the Ion Bernstein Wave heating experiments thus far performed and are also interesting as the references of the fast wave experiments.

ELECTRON HEATING REGIME IN FAST WAVE EXPERIMENT

This regime exists in the density region smaller than 2×10^{19} m^{-3}. In this regime, the central electron temperature increases (see Fig.1) and the drop of loop voltage is observed. From the pulse height analysis of soft X-rays, it is found that the wave interacts with the electrons whose energy range is from 10 to 25 keV. We investigated the four antenna phasings, $(0,0,0,0)$, $(0,\pi/2,\pi,3\pi/2)$, $(0,-\pi/2,-\pi,-3\pi/2)$, and $(0,\pi,0,\pi)$. As a result, the increase of the electron temperature and the drop of the loop voltage are most clearly observed in $(0,\pi,0,\pi)$ phasing. In this phasing, parallel refractive index of wave, $n_{//}$, is about 4.5 and this corresponds to 20 keV of electron energy. Other phasing corresponds to much higher electron energy range, in which there are few electrons. It is thought that the degradation of heating efficiency in the high density is due to the absence of slide-away electrons, which can interact with wave. This density range of the experiment is two orders of magnitude higher than the lower hybrid current drive density limit.

ION HEATING REGIME IN FAST WAVE EXPERIMENT

In the density above 2×10^{19} m^{-3}, the heating efficiency decreases. However, the ion heating is observed when the RF power is applied to the auxiliary heated plasma. On the

injection of 130 MHz RF power, the growth of the hydrogen tail is observed in the energy spectrum obtained from the charge-exchange fast neutral analysis (see Fig.2). Stored energy and neutron yield increase with the input of 130 MHz RF power. This ion heating is attributed to the 3rd harmonic cyclotron damping. The antenna phasing effect on the stored energy and radiation loss does not exist. The heating efficiency of this heating regime is comparable to those of the established heating methods such as neutral beam injection (NBI) and 40 MHz fast wave heating.

SLOW WAVE (ION BERNSTEIN WAVE) EXPERIMENT

Ion Bernstein Wave heating (IBWH) experiments have been performed in the hydrogen plasma and the 3rd harmonic cyclotron resonance layer was situated at the central chord. The ion and electron temperatures increase both in the case of the IBWH only and in the case of the NBI + IBWH. The profiles of ion and electron temperature peak at the plasma center on the injection of IBW (see Fig.3 for ion). The density profile also peaks at the center of plasma by the IBWH and the intensity of H_α signal near the antennas decreases or is constant in spite of the density increment induced by the IBWH. Different from the fast wave heating, the high energy ion tail produced by IBWH shows non-runaway feature (see Fig.4).

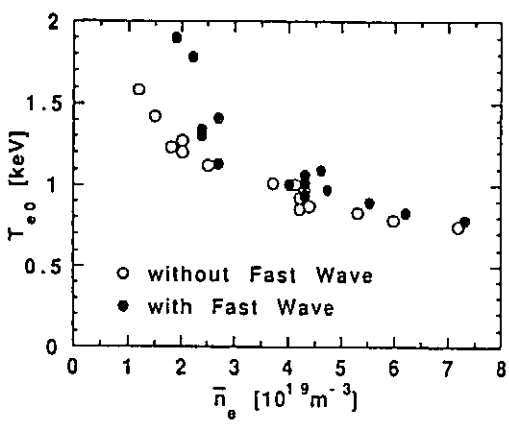

Fig.1 The dependence of the electron temperature on the density in the electron heating regime of fast wave.

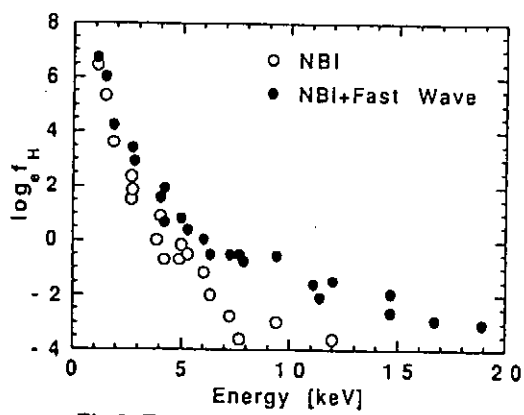

Fig.2 Energy spectrum of hydrogen in the ion heating regime of fast wave.

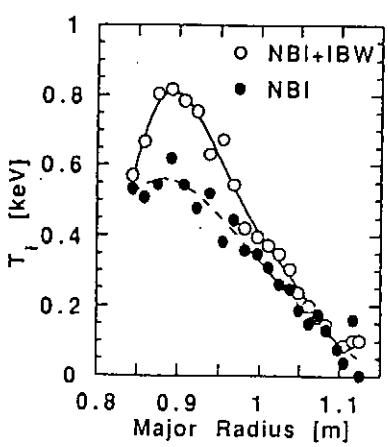

Fig.3 Ion temperature profile obtained by the IBW heating.

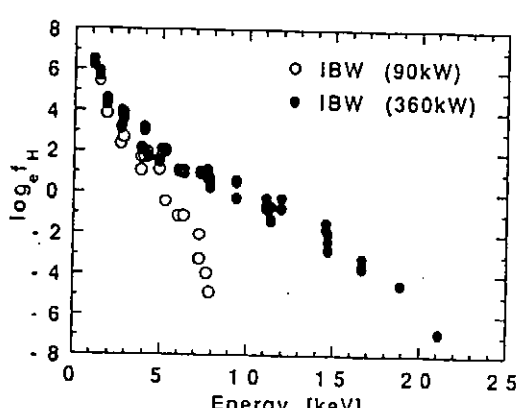

Fig.4 Energy spectrum of hydrogen in the two cases of the IBW power.

US-Japan Workshop on RF Heating and Current Drive in
Confinement Systems Tokamaks, Nov. 18-21, '91 NIFS

Wave Heating and Current Drive Experiments in JFT-2M

Y. Uesugi*, T. Yamamoto, H. Kawashima and JFT-2M Group
*Dept. of Electrical Engineering and Electronics
Nagoya University, Nagoya, Japan

JAERI, Naka, Ibaraki, Japan

ABSTRACT

The coupling and absorption characteristics of the fast waves launched from a phased four loop antenna array have been investigated in JFT-2M. The parallel wavenumber of the excited fast waves is determined by the relative phase of the rf current on each antenna strap. The coupling characteristics are similar to those observed in ICRF experiments. The loading resistance increases with density and strongly depends on the antenna phasing. The maximum loading due to surface wave excitation is obtained at $\Delta\phi=\pi$ and minimum at $\Delta\phi=\pi/2$. These observation shows that the present four loop antenna array excites the fast magnetosonic waves dominantly.

The previous low power FWCD experiment up to 50 kW at 200 MHz shows that the plasma current is driven in the low density region below $\bar{n}_e=2\times10^{18}$ m^{-3} and the current drive efficiency is $\eta_{CD}\sim0.4\times10^{19}$ $m^{-2}A/W$ as high as that of LHCD in JFT-2M. Although the density dependence of FWCD is similar to that of LHCD, the density limit for 200 MHz FWCD is twice higher than that expected

from the LHCD empirical scaling law. Recent high power experiment up to 650 kW, however, indicates that the interaction of excited fast waves with electrons at $v_{ph}/v_{te} \leq 3$ brings us the high efficiency electron heating at high density region above $\bar{n}_e = 1 \times 10^{19}$ m^{-3}. Clear FWCD at $\Delta\phi = \pi/2$ has not been observed yet in JFT-2M. The absorption efficiency deduced from an increase of the electron temperature increases with electron density and temperature, and with increasing the parallel refractive index. These experimental results are consistent qualitatively with the theoretical damping rate based on the electron Landau damping. The central electron heating efficiency is $\eta_e \sim 4 \times 10^{19}$ eVm^{-3}/kW as high as that of 2nd harmonic ECH in JFT-2M. The power deposition profile obtained from synchronous detection of the electron cyclotron emission modulated by the periodic fast wave power shows a peaked profile at the plasma center. The net electron absorption efficiency calculated from the power deposition profile is $\eta_{abs} \sim 0.4$ at $\bar{n}_e = 2 \times 10^{19}$ m^{-3} and Teo=0.7 keV, which agrees roughly with that deduced from the change of the plasma stored energy. In order to demonstrate the high density FWCD at $\pi/2$ phasing the loop antenna array was modified to excite the slower fast waves with Nz~6 at $\pi/2$ phasing. So far we have observed an enhancement of the energetic electrons with the energy of several tens keV at $\pi/2$ phasing but not observed clear FWCD yet since the antenna loading is not high enough to demonstrate it.

US-Japan Workshop on
RF Heating and Current Drive in Confinement Systems Tokamaks
National Institute for Fusion Science
November 18-21, 1991

High-Density and Long-Pulse Operation by LHCD in TRIAM-1M

Y. Nakamura, S. Kawasaki, E. Jotaki,
T. Fujita, A. Nagao, K. Nakamura, S. Itoh

Advanced Fusion Research Center
Research Institute for Applied Mechanics
Kyusyu University, Kasuga 816, Japan

The TRIAM-1M research program has the demonstration of high density and long pulse operation with non-inducting current drive to provide a basis for tokamak progress toward steady-state reactors. Recent experiments on the superconducting tokamak TRIAM-1M have focused on the extension of operational regime of long pulse tokamak discharges and high density current drive with LH waves (2.45 GHz, 50 kW). The plasma discharge duration was extended up to 4210 sec (more than one hour) and a high density discharge with $\bar{n}_e = 1.0 \times 10^{13}$ cm^{-3} was maintained for 14 sec. We report here the recent progress on long-pulse and high-density tokamak operation by LHCD in TRIAM-1M.

Long-pulse operation has been realized by two important plasma parameter control (plasma position and density control). It was impossible to detect the plasma current and position with accuracy over a long time by using a conventional method with magnetic coils and analog integrators because the offset voltage in the integrator output signal increased with time (1,2). A new plasma position control system based on Hall-effect sensors, which can measure a magnetic field directly, was developed (3) and it allowed us to keep the plasma position within the displacement of 5 mm during 1-hour discharge. Plasma density control was required for keeping the peaked profile of high energy electrons unchanged and preventing them from interacting with the limiters (4). In order to keep the plasma density constant, the neutral pressure in the plasma chamber was controlled with the feedback loop including the ionization gauge, the gas feed controller and the piezovalve.

Impurity behaviour in the long duration discharges was investigated by VUV spectroscopic measurements. The main impurities in the plasma were molybdenum (0.2 %) from the limiters and oxygen (2 %) resulting from recycling and desorption. The accumulation of these impurities was not observed during the long duration discharge. It seems that the content of the impurities in the plasma remains at a quasi-stationary level without an adverse effect on the discharges.

The ring limiters of TRIAM-1M suffered a variety of modifications such as melting, cracking, deformation and segregation of surface composition (5). In long duration discharges, the limiter was gradually heated up and became white-hot locally. Ejection of molten droplets was occasionally observed through TV monitor. The impurity influx into the plasma seems to be due to the evaporation from the molten surface of the limiters.

The long pulse operation has been performed within the upper limit of the temperature at the ceramic break, which is a component of the plasma chamber. There is no essential problem in long pulse operation under our experimental conditions. However, the improvement in heat removal from plasma facing components and impurity control will be required to operate at high RF power and higher density.

High density operation was limited by plasma current disruption or abrupt drop of plasma current in the early experimental stage. This density limit is caused by the strong interaction of high energy electrons with the limiters due to the deterioration of the accessibility of the plasma to LH waves (4). In order to improve the accessibility of the high density plasma, the current drive discharge was carried out at higher toroidal magnetic field and consequently a high density current drive discharge with $\bar{n}_e = 1.0 \times 10^{13}$ cm^{-3} was obtained. Therefore, a sharp RF power spectrum accessible to the central plasma will be required for higher density discharge.

In high density discharges, it was found that the current drive efficiency increased with the plasma density in spite of the deterioration of wave accessibility. The efficiency reached up to 0.9 (10^{19}m^{-2}kA/kW) at $\bar{n}_e = 1.0 \times 10^{13}$cm^{-3}. This density dependence seems to be due to the improvement of the confinement of high energy electrons. The direct loss of high energy electrons decreases with increasing the plasma density because of the reduction of the collisional slowing-down time. Therefore, the current drive efficiency is improved by increasing the plasma density.

Next operation program in TRIAM-1M is aimed to achieving long pulse operation at higher plasma density of the order of 10^{13} cm^{-3}. A new high frequency (8.2 GHz) LHCD system, which has an output power of 200 kW and a launcher with sharp power spectra, has been installed to the machine for that purpose. The properties of steady-state tokamak discharge with high plasma density will be also investigated.

(1) S. Itoh, N. Hiraki, Y. Nakamura, et al., in Plasma Physics and Controlled Nuclear Fusion Research 1988 (Proc. 12th Int. Conf. Nice, 1988), Vol.1, IAEA, Vienna (1989) 629.

(2) S. Moriyama, Y. Nakamura, A. Nagao, et al., Nucl. Fusion, 30 (1990) 47.

(3) S. Itoh, N. Hiraki, Y. Nakamura, et al., in Plasma Physics and Controlled Nuclear Fusion Research 1990 (Proc. 13th Int. Conf. Washington, D.C., 1990), Vol.1, IAEA, Vienna (1991) 733.

(4) Y. Nakamura, Y. Takabatake, E. Jotaki, et al., Nucl. Fusion, 30 (1990) 689.

(5) K. Tokunaga, T. Fujiwara, N. Yoshida, et al., J.Nucl. Mater., 179-181 (1991) 353.

Experiments on current profile control with LH waves in view of the PBX-M experiment.

Stefano Bernabei
Princeton University
Plasma Physics Laboratory
P.O. Box 451, Princeton, NJ 08543

ABSTRACT

Several current drive experiments have shown that Lower Hybrid waves modify the current density profile: in order to achieve a good degree of control of the profile it is necessary to predict precisely the damping location of the waves and to estimate the radial diffusion of the current carrying electrons. There are two damping conditions: one for high values of $n_{||}$ (typically $n_{||}>2.5$) which characterizes waves with low phase velocity, in which most of the damping occurs during the first pass of the waves through the plasma. This means that for a given electron temperature the condition of wave-electrons resonance is satisfied. The other case is for low values of $n_{||}$, corresponding to high phase velocity of the waves, in which there are no resonant electrons. In this case, several passes of the waves through the plasma with subsequent $n_{||}$-upshift are needed to obtain damping. This second condition is often referred to as the energy gap. The first-pass damping case has the advantage that the power deposition can be readily calculated, from which the current profile modification can be inferred . The disadvantage comes from the fact that low phase velocity waves have low current drive efficiency: furthermore for a given coupler, high $n_{||}$ are usually obtained by imposing a large phase difference between adjacent waveguides which produces weaker directivity in the launched waves. The opposite situation happens for low $n_{||}$, or low phase difference: the advantage of high current drive efficiency is offset by the disadvantage of the difficulty of predicting the damping location. Therefore the ability of controlling the current density profile maybe greatly reduced. On the ASDEX experiment we made combined use of high $n_{||}$ and low $n_{||}$ launching in order to achieve a remarkable degree of current density profile control. Results from the modelling with the CQL3D/LH code (developed by Harvey and McCoy) have been compared to the experimental results with very good success. The experience gained will be applied to the upcoming LH experiment on PBX-M, which is intended to facilitate the achievement of second stability by properly modifying the current density profile.

Abstract for US Japan Workshop on RF Heating and Current Drive in Confinement Systems Tokamaks

Nagoya, Japan; November 18–21, 1991

Modelling DIII-D/ITER Fast Wave Current Drive Experiments with a Full Wave Code*

P.T. Bonoli and M. Porkolab
MIT Plasma Fusion Center
Cambridge, MA 02139, USA

Current drive in the ion cyclotron range of frequencies is of great interest in the present generation of toroidal confinement devices and is expected to play an important role in the steady state operation of future thermonuclear reactors, such as the proposed ITER device[1]. In order to better understand recent results for electron heating and current drive by ICRF fast waves,[2,3] a toroidal full-wave code[4] has been modified to evaluate direct electron heating in the ICRF regime by the combined effects of transit time magnetic pumping (TTMP) and electron Landau damping (ELD). Numerical results, confirming an earlier analysis,[5] indicate that for arbitrary phase speeds ($\omega/k_{\|}v_e \lesssim 1$) the contribution to the electron absorption via TTMP is cancelled by the cross-term between TTMP and ELD. Extensive full-wave results will be presented for wave propagation and absorption in the DIII-D electron heating and current drive experiments. Issues will be addressed related to the coupling of fast wave power at high negative parallel wavenumber ($k_{\|}$) in the launched wave spectrum, the possibility of large decreases in $k_{\|}$, and the possibility of a sign reversal in $k_{\|}$.

An accurate evaluation of the fast wave current drive efficiency in these experiments is obtained by combining the full-wave results for wave propagation and absorption with an adjoint solution of the Fokker Planck equation[6]. Finally, model results relevant to the proposed ITER fast wave current drive scenario will be presented.

* Work supported by the U.S. Department of Energy Contract No. DE-AC02-78ET51013

REFERENCES

[1]K. Tomabechi, J.R. Gilleland, Yu.A. Sokolov, R. Tosci et al., Nucl. Fusion **31**, 1135 (1991).

[2]C.C. Petty et al., Bull. Am. Phys. Soc. **36**, 2470 (1991).

[3]R.I. Pinsker, et al., Bull. Am. Phys. Soc. **36**, 2470 (1991).

[4]M. Brambilla and T. Krücken, Nucl. Fusion **28**, 1813 (1988).

[5]M. Porkolab, General Atomics Memos D3DPM-8813 and D3DPM-8817 (1988).

[6]D.A. Ehst and C.F.F. Karney, Argonne National Laboratory Report ANL/FPP/TM-247 (1990).

US-Japan Workshop
RF Heating and Current Drive
NIFS, 1991/11/18-21

Helicity Injection and Current Drive by RF Waves

A. Fukuyama, K. Hamamatsu†, K. Itoh‡ and S.-I. Itoh‡

Faculty of Engineering, Okayama University, Okayama 700
†Japan Atomic Energy Research Institute, Naka, Ibaraki 311-01
‡National Institute for Fusion Science, Nagoya 464-01

Current drive via non-resonant wave-particle interaction is studied both analytically and numerically and is compared with conventional resonant current drive.

In the presence of inhomogeneity of the wave amplitude or the equilibrium plasma parameters, the non-resonant interaction generates a force, which mainly acts as an internal force among plasma species. The net momentum input from the wave to the plasma is small in this process. The current driven by this force is associated with the change of the wave helicity. Since non-resonant particles carry the current, the reduction of the current drive efficiency due to the toroidally trapped particle is not severe as the case of resonant current drive.

Quantitative analysis is carried out for ICRF and Alfvén waves in a large tokamak. The one dimensional full wave code (TASK/W1) is emplyed to calculate the profile of the non-resonant force and the driven current as well as the helicity flux carried by the wave. The current drive efficiency η increases with the increase of the wave number until the kinetic Alfvén wave is strongly excited. In the low phase velocity region, η of the non-resonant current drive exceeds that of the conventional resonant current drve. It is also confirmed that η scales strongly with electron temperature and toroidal magnetic field but only weakly with plasma density. In the case of low-frequency compressional Alfvén wave, the efficiency can be comparable with the case of minority-ion cyclotron resonance.

Improved Confinement and Stability Through Current Profile Modification

T.S. Taylor

General Atomics
San Diego, California 92186-9784, U.S.A.

Detailed control of the current density can lead to increased beta limits and improved confinement in tokamaks. Improved stability to ideal pressure-driven modes, local high n ballooning and global low n kink, is attained with peaked current density profiles and high magnetic shear (high internal inductance, ℓ_i) where the entire discharge is in the first regime of stability. The increase of the maximum achievable beta with increasing internal inductance has been shown in DIII–D where dynamic current ramps have been used to alter the current profile. In similarly controlled discharges on DIII–D, TFTR, and JET, and in dynamically-shaped DIII–D discharges, the thermal energy confinement also increases with increasing ℓ_i. Stability to high n ballooning modes can also be improved with reduced magnetic shear, by accessing the second regime of stability to ballooning modes. In DIII–D strongly shaped discharges with negative central shear, the central region is in the second stable regime and very peaked pressure profiles ($p_0/\langle p\rangle \sim 4$) and high central beta [$\beta(0) \gtrsim 40\%$] are obtained.. Very high confinement, VH–mode, discharges are observed in DIII–D with large bootstrap current and an extended high pressure gradient region near the plasma boundary. This improvement in confinement might be a result of second regime access of an increasing volume of the edge plasma. The use of rf current drive, ECCD, FWCD, LHCD, and neutral beam current drive for detailed current profile control has the potential of greatly improving the performance of the tokamak.

This is a report of work sponsored by the U.S. Department of Energy under Contract No. DE-AC03-89ER51114.

US-Japan Workshop on "RF heating and Current Drive in Confinement System Tokamak", Nagoya, 18-21, Nov. 1991

Profile Control by Lower Hybrid Wave Application

K. Ushigusa and the JT-60 Team

Japan Atomic Energy Research Institute
Naka Fusion Establishment
Naka-machi, Naka-gun, Ibaraki-ken,
Japan

Abstract

Control of the current profile and MHD activities in JT-60/60U by the lower hybrid current drive(LHCD) are discussed. The multi-junction launcher, which was installed in 1989, can excite wave with narrow wave spectrum for wide $N_{||}$ regime ($N_{||}^{peak}$ = 1 - 2.9) without causing degradation of the directivity. This permits us to study MHD behaviors in non-inductive plasmas with various current profile.

The plasma internal inductance does not change so much in the injection of low $N_{||}$ wave, while high $N_{||}$ wave decreases the internal inductance with a long time constant. Hard X-ray measurement indicates that broad (peaked) RF current profile is formed in high (low) $N_{||}$ injection. The change in MHD activities are also observed according to the change in the internal inductance. Edge MHD modes (m = 2 or 3 mode) are sometimes destabilized when very broad current profile was formed by high $N_{||}$ wave injection. Sawteeth are suppressed with high $N_{||}$ ($N_{||}^{peak}$ > 2.5) injection, however, about 2 sec from the onset of LH pulse is required for the sawtooth suppression and sawteeth reappear at 0.5-1 sec after LH pulse. These behaviors indicate that sawteeth are suppressed by the change in current profile. Low $N_{||}$ wave can also suppress the sawteeth. In low $N_{||}$ ($N_{||}^{peak}$ < 1.6) case, sawteeth disappears at several hundred msec after the LH onset and appears quickly (within ~ 100msec) after the LH pulse. This time

delay is shorter than that of the case of high $N_{||}$ injection. There is no sawtooth suppression for the injection of medium $N_{||}$ wave ($N_{||}^{peak}$ = 1.9 - 2.3) with the same LH power and the density as previous two cases. These results suggest that the mechanism of sawtooth suppression for low $N_{||}$ case is different from that of high $N_{||}$ injection. We also observed the correlation of the sawtooth free period and the central hard X-ray emission for low $N_{||}$ wave injection. Some kinetic effect of energetic electron may play some role to the sawtooth suppression by low $N_{||}$ wave injection.

Preliminary experiments on current profile control by LHCD were performed in JT-60U at low density regime (n_e ~ $0.5 \times 10^{19} m^{-3}$, hydrogen plasma). Sawteeth were suppressed by low $N_{||}$ wave injection just after the onset of LH pulse. We observed similar $N_{||}$ dependence of the change in the internal inductance during LHCD as in the JT-60 experiments. Sawtooth does not appear in an additional ~10MW of neutral beam injection during low $N_{||}$ LH pulse and reappears at ~0.3s after the LH pulse. In the LHCD plasma with high $N_{||}$ wave in JT-60U, we observed an instability which is accompanied by the loss of high energy electrons at relatively low density and high power injection. Large drop in the diamagnetic poloidal beta was observed during such instability. Energetic electron pulse within ~a/2 propagates to the plasma edge and reaches in the divertor plates with the time delay of ~ 30msec. This instability occurs repeatedly with the period of ~200ms. The internal inductance is still decreasing during such instabilities. Small m=3 mode appears after the disappearance of this instability. Additional ~10MW of NB injection enhances this m=3 mode, however, sawtooth are still not observed during NB pulse. Further study of profile control on NB heated D^+- plasmas by LHCD in JT-60U is planned in next year to achieve stable high temperature plasma.

Sawtooth Stabilization by ECH near q=1 surface in WT-3

K. HANADA, T. MAEKAWA, M. IIDA, Y. KISHIGAMI, T. KISHINO,
T.MAEHARA, K. MAKINO, T. MINAMI, M. NAKAMURA,
Y. TERUMICHI and S.TANAKA

Department of Physics, Kyoto University, Kyoto 606, Japan

ABSTRACT

A study of the effect on Sawtooth Oscillations (STO) by localized electron-cyclotron-resonance heating (ECH) on the WT-3 tokamak is reported. The effect of ECH on STO is very sensitive to the toroidal field B_T which determines the location where the ECH is localized. STO in the Ohmically heated WT-3 tokamak are strongly modified or suppressed by ECH near the q=1 surface, where q refers to the safety factor. In addition to the influence of B_T, the normalized power P_{EC}/P_{OH} play an important role for the stabilization of STO as well. When ECH is applied on the HFS of q=1 surface there is an initial linear phase where the period of STO τ_S increases linearly with P_{EC}/P_{OH}, and at larger value of P_{EC}/P_{OH} τ_S increases rapidly and complete stabilization is achieved. The effect of ECH is much stronger when it is applied on the high field side (HFS) as compared to the low field side (LFS). The threshold power for complete stabilization of STO decreases with the increasing safety factor at the limiter, q_L and in the range of $q_L \geq 4.8$ the complete suppression can be obtained even when ECH is applied on the LFS. In the case of $q_L \geq 5.0$, the threshold power is almost the same regardless of the heating on HFS or LFS.

In q_L = 6 - 7, where there is no STO in the OH plasma, STO can be excited by ECH. This excitation is also sensitive to the location of resonance layer of ECH and the injected power, P_{EC}. In order to excite STO the ECH is applied inside the certain boundary which is smoothly connected with a boundary for suppression of STO at q_L=6.0. However, one must take a care that if the strong ECH is applied into plasma, STO cannot be excited by the ECH

applied near the magnetic axis, while the ECH applied slightly inside the boundary can excite STO. This result suggests that STO are not controlled by the change of q(0) as expected by Kadomtsev's model.

The mechanism of the stabilizing and exciting of STO is discussed. The theoretical model that the stabilization is due to a modification of the current profile in such a manner as to lower the shear at the q=1 surface, thus stabilizing the resistive m/n=1/1 mode is proposed. Specifically, when the ECH is applied, Te increases locally and the electron collisionality and hence the plasma resistivity is reduced, driving more current in this region. This increment of the current density may result in a local reduction of the shear. If this reduction in shear occurs at the q=1 surface, it will have a stabilizing effect on the m/n=1/1 resistive mode which plays an important role in STO. In fact, The growth rate of precursor oscillations of STO consisting of m/n=1/1 structure decrease with increasing of P_{EC} and finally it becomes zero when the complete suppression of STO takes place. Moreover, our theoretical model can explain the difference when the ECH is applied on HFS and LFS. When ECH is applied on the HFS, the high-energy electrons accelerated by ECH can traverse most of the surface enhancing a locally peaked current profile on the entire surface. In contrast, when the ECH is applied on the LFS, many of the high-energy electrons are easily trapped in the banana region and do not contribute to an enhancement of the current density. As a result there is smaller influence on the shear and hence the stability. However, in high qL region, the mirror ratio on the q=1 magnetic surface decreases because of the reduction of the q=1 surface and it must be hard to trap the high energy electrons produced by the ECH. This can also explain the reduction of the difference on the threshold power for the suppression of STO when ECH is applied on the HFS and LFS in the experiment.

Abstract for US-Japan Workshop on RF Heating and Current Drive in Confinement System Tokamaks, Nagoya, Nov. 18-21, 1991

ITER CURRENT DRIVE REQUIREMENTS

H. Kimura

Naka Fusion Research Establishment
Japan Atomic Energy Research Institute

ITER current drive and heating (CD&H) systems, defined during Conceptual Design Activities (CDA), are briefly reviewed. Two scenarios (reference and alternative) were identified according to experimental data base and modelling calculations during CDA. Both are indicated in Table 1. A difference between them is only in the choice of the main current drive and heating system. NB was selected as a reference system, since some data base exists for the current drive and a theoretical current drive efficiency shows the best value among all schemes. On the other hand, IC was regarded as an alternative, because the system has merits of low cost and small R&D need but its data base of current drive was sparse. Main critical issues on physics for each system, listed in Table 1, are discussed.

Table 1 ITER CURRENT DRIVE AND HEATING SYSTEMS

REFERENCE:

SYSTEM	POWER	ROLE	REMARKS
NB	75MW	Current Drive (central region)	Alfven instability
(1.3MeV)		Heating to Ignition	
		Burn Control	beam penetration ?
LH	50MW	Current Drive (outer region)	
(5GHz)		Current Ramp-up Assist	divertor heat load ?
EC	20MW	Plasma Start-up Assist	
(120GHz)		Current Drive (q=2 surface)	trapped electron ?

ALTERNATE:

SYSTEM	POWER	ROLE	REMARKS
IC	130MW	Current Drive (central region)	data base ?
(15-			$k_{\parallel}$-upshift, eigenmode
80MHz)		Heating to Ignition	
		Burn Control	
LH	50MW	Current Drive (outer region)	
(5GHz)		Current Ramp-up Assist	divertor heat load ?
EC	20MW	Plasma Start-up Assist	
(120GHz)		Current Drive (q=2 surface)	trapped electron ?

CURRENT DRIVE EXPERIMENTS ON CDX-U: HELICITY INJECTION AND PRESSURE DRIVEN CURRENTS

C. B. Forest and the CDX-U Team
Princeton University, P. O. Box 451, Princeton, NJ 08543

ABSTRACT

A general overview of the CDX-U physics program will be presented with an emphasis on current drive experiments. The primary focus of the the project has been DC helicity injection current drive and current transport studies in a low-aspect-ratio torus, and evidence supporting tokamak formation will be shown. The CDX-U helicity injection scenario consists of a high current (<400 Amps,) low energy ($< 500 Volts$) electron beam injected from a heated, LaB_6 cathode. Up to 6000 Amps have been driven in this method, the primary requirement being a careful programing of the externally imposed poloidal field. Another set of experiments has observed pressure driven currents in an ECH heated plasma. A novel poloidal field configuration is able to provide confinement in the absence of toroidal plasma current. In the initial stages of the discharge, however, field-aligned currents flow along open field lines to eliminate the charge separation due to ∇B and curvature drifts and trapped electrons precess toroidally to produce a net toroidal current. The toroidal current of as large as 850 amps was generated with $\sim$ 8 kWatts of ECH power. At this current level, the poloidal field created by these currents is significantly larger than the vacuum field and may produce closed flux surfaces. This internally driven current may offer an attractive method to start up and maintain a low-aspect-ratio tokamak by generating the seed current required for a bootstrap current driven equilibrium.

Model of Divertor Biasing and SOL Plasma Response

K. Nagasaki, K. Itoh†, S.-I. Itoh†
Plasma Physics Laboratory, Kyoto University
† National Institute for Fusion Science

Recently the importance of the scrape-off layer (SOL) and divertor plasmas has been widely recognized. The boundary plasma, which surrounds the main plasma, has a critical role in determining the global confinement, particularly for the appearance of improved confinement modes. The long and stable discharge in the high power heating regime is possible only if the SOL and divertor plasmas are controlled so that the rapid impurity generation is suppressed. It has been also noticed that the condition which is imposed on the divertor plasma often limits the parameter regime of the consistent fulfillment of various physics and technological constraints. Motivated by these results, the divertor biasing have been done in search of the control of the SOL/divertor plasmas. It has been found that there is a spontaneous force free current driven by the thermoelectric field in the SOL/divertor region. Applying a DC voltage between two divertor plates may control the SOL/divertor plasmas.

In this workshop, we will show the theoretical analysis of the divertor biasing. A simple slab model is used to describe the classical parallel transport. Assuming the particle flux enhancement factor in the divertor region, we evaluate the SOL/divertor plasma parameters as a function of the externally applied DC electric field, for the given fluxes from the core plasma. The necessary voltage to equalize the plasma temperature or sheath potential at the divertor regions is calculated. These parameters are key factors of estimating the erosion rate and the impurity source.

The plasma region of our interest is illustrated schematically in Fig.1. We take a simple slab plasma model by choosing the SOL width to be constant. Figure 2 shows a simplified geometry of our analysis. The heat and particle fluxes are supplied from the main plasma at the distance $L1$ from the divertor plate 1. The source asymmetry appears in the experience. It is usually considered that the supplies are made in the vicinity of the outer mid-plane. In our model, this asymmetry is made by the difference of the distance between two plates, $L1 \neq L2$. The distances $L1$ and $L2$ are chosen as given parameters. We discuss the effect of the divertor biasing on plasma parameters such as temperature, density, sheath potential and heat flux in the SOL/divertor plasma.

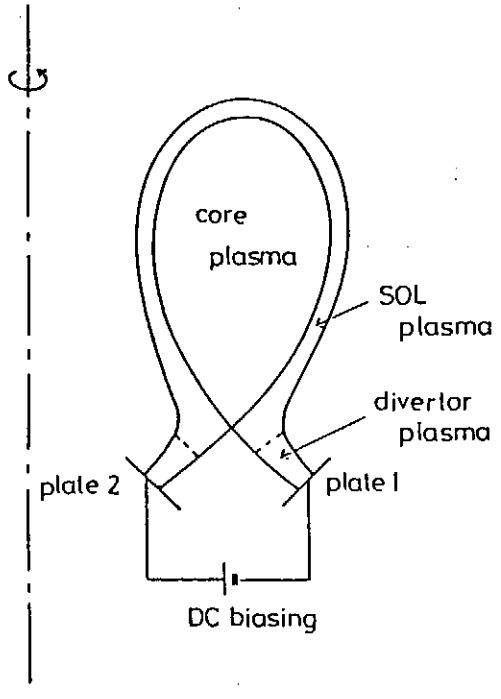

Fig.1

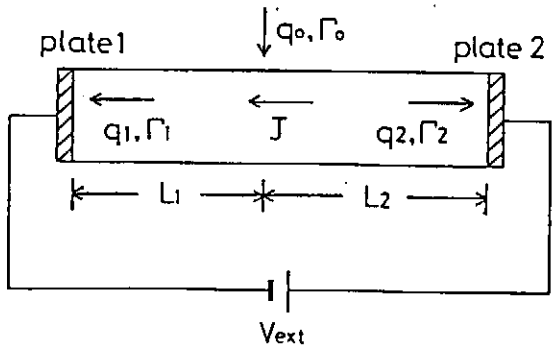

Fig. 2

Abstract for US-Japan Workshop on RF Heating and Current Drive in Confinement System Tokamaks, Nagoya, November 18–21, 1991.

BIASED DIVERTOR EXPERIMENTS ON DIII-D

Reported by
R.D. Stambaugh for the DIII–D Group
General Atomics
San Diego, California 92186-9784 USA

A summary of divertor biasing experiments in the DIII–D tokamak was presented. The talk focussed on the two areas in which substantial results have been obtained: the use of biasing to increase neutral pressures in the pumping plenum and the use of bias to alter the H–mode power threshold. In addition, because of the subject of the workshop, some remarks on helicity injection current drive were made. Other effects of bias, e.g. on confinement and ELMs, have been small and inconclusive.

The biasing hardware consists of a toriodally continuous electrode in the lower outer corner of the DIII–D vacuum vessel. This bias ring has graphite tiles as plasma facing components. Boron-nitride tiles insulate the ring from other structures. It is water cooled. There is a 3 cm gap under the ring leading into a pumping plenum. Later, a cryopump will be installed in the pumping plenum.

Initial studies have foccused on maximizing the neutral pressure in the pumping plenum. Without bias, a maximum pressure of 10 mTorr is produced when the outer divertor strike point is 3 cm from the edge of the divertor bias ring. The neutral pressure increases in proportion to neutral beam power. With bias, the electric field points either toward or away from the ring. Hence $E_b \times B_T$ is parallel to the ring surface and either into (negative bias) or out of (positive bias) the pumping plenum region. The resulting $E \times B$ drift constitutes a powerful plasma pump. In DIII–D geometry this pumping speed can be 10^6 liters/sec! Positive bias is found to decrease the neutral pressure in the plenum. Negative bias increases it. The difference is an

order of magnitude; pressures up to 16 mTorr have been produced. The pressure varies linearly with bias voltage. Even with the outer strike point located far up on the ring, far from the optimum location without bias, the $E \times B$ drift around the ring keeps the pressure in the plenum high. This effect may be very useful in future applications to guide plasma down ducts. Even without pumping, negative bias has been able to store particles in the pumping plenum, lowering the plasma density and increasing the plasma temperature. With the future cryopump installation, this lower density operating path may lead to enhanced confinement.

DC helicity injection current drive results so far are encouraging but inconclusive. The reconnection of the OH coil in the middle of the observational period produced complicating loop voltage transients. A comparison of the two best shots with and without bias shows some reduction in loop voltage and ℓ_i with bias.

Divertor bias alters the H–mode power threshold. With the grad-B drift either toward or away from the X–point, a bias voltage of +75 volts reduces the power threshold by about 30%. Large voltages either negative or positive can increase the power threshold up to a factor of 4. $E_p \times B_T$ drift effects probably are not involved in this result, since the sign of the optimum voltage does not depend on the sign of B_T and since for positive bias, the $E_p \times B_T$ drift is radially outward, which should raise the threshold power. Bias produced changes in the radial E field shear might be involved, since the radial E field profiles are different with negative and positive bias. Current driven instabilities in the SOL, produced by the bias current, could explain a minimum in the power threshold at non-zero bias current if +75 volts is required to cancel normal thermo-electrically driven SOL current. This effect of bias on the H–mode power threshold needs theoretical attention.

US-Japan Workshop on
RF Heating and Current Drive in Confinement Systems
(1991, November, NIFS)

Divertor Biasing and Helicity Injection

Kimitaka Itoh

National Institute for Fusion Science, Nagoya 464-01, Japan

The DC helicity injection has been studied as the innovative method for current drive. In this scheme, the current is driven (by helicity injection) near edge and transported to the core plasma. One of the candidate is to drive the parallel current in the scrape-off layer. The existence of the toroidal current in the scrape-off layer has been known experimentally. The question is the process in the core to transport the current. In order to study the validity of this scheme, we investigate the steady state of the core plasma in which the resistive dissipation is sustained by the cross field transport of the current.

We take a cylindrical tokamak model for the simplicity. The cylindrical coordinates (r, θ, z) are used. The Ohm's law is written as, in the stationary state without equilibrium flow,

$$\eta J - \lambda \Delta J = 0, \tag{1}$$

where J is the current, η is the resistivity, and λ is the current diffusivity. λ is the coefficient for the current diffusion. For the simplicity, we look for the solution with the cylindrical symmetry, and assume that the coefficient λ/η is constant in space. The solution is given as

$$J(r) = J(0) I_0(\sqrt{\eta/\lambda}\, r), \tag{2}$$

where J(0) is the current density at the axis, and I_0 is the zero-th order modified Bessel function of the first kind. The shape of the current is dictated by the parameter $\Lambda = a\sqrt{\eta/\lambda}$, where a is the minor radius of the plasma. For the actual application, the current density cannot be too high at the edge to avoid the violent MHD activity. The internal inductance must be of the order of 1/2 or higher. This condition requires that Λ has to be of the order of unity.

The requirement of the low value of Λ set a lower boundary for the current diffusivity. The current diffusivity cannot be enhanced alone. The enhancement of the current diffusivity is associated by the increment of the other transport coefficient, such as the thermal diffusivity χ. For instance, when the cross field transport is driven by the magnetic braiding, λ and χ are estimated as $\lambda = [\sqrt{\pi}c^2/2\omega_p^2]\mu_0 v_{te} D_M$ and $\lambda/\chi = \pi\mu_0 c^2/6\omega_p^2$, where c is the speed of light, ω_p is the plasma oscillation frequency, v_{te} is the electron thermal velocity and D_M is the diffusion coefficient of the magnetic field line. Noting these relations, we have the relation

$$\chi \simeq 2\Lambda^{-2} a_m^2 n_{20} T_{keV}^{-3/2} \times 10^5 \quad [m^2/s] \qquad (3)$$

where a_m T_{kev} and n_{20} are the minor radius [in m], temperature in [keV] and the density [in $10^{20} m^{-3}$]. From this relation we see that the condition on Λ, i.e., $\Lambda \sim O(1)$, requires very large transport coefficient, which is too large for the real experiments. This indicates the importance of the current transport, for which the rf helicity current drive was shown to work.

* This work is performed in collaboration with S.-I. Itoh and A. Fukuyama.

US-Japan Workshop on "RF heating and Current Drive in Confinement System Tokamak" , Nagoya, 18-21, Nov. 1991

Initial Results of LHCD in JT-60U and Limitation of the LHCD Application

T. Imai and JT-60 Team
Japan Atomic Energy Research Institute
Naka Fusion Research Establishment
Naka, Ibaraki, Japan

LHCD in JT-60 had finished successfully in 1989. Non-inductive current drive of 2 MA, efficient current drive performance with efficiency $0.34 \times 10^{20} m^{-2} A/W$ and high power LHCD up to ~5 MW were demonstrated. In JT-60U, plasma current is increased up to 6 MA in divertor discharge and deuterium plasma operation is possible. LHCD program in JT-60U aims further progress of LHCD to explore steady state tokamak reactor and study the profile control. The LHCD power of 2-3 MW from 24x4 multi-junction (MJ) launcher is prepared from 1991 and will be about 10 MW in 1993 by adding new 48x4 MJ launcher. Multi-channel hard X-ray detectors are equipped to investigate the power deposition profile. Plan to increase the HX measurement and current profile measurement is progressing.

Initial results of JT-60U LHCD

Maximum LHCD power of ~1.5 MW has been injected into JT-60U plasma with Bt=4T, Ip=1-2 MA and hydrogen gas in divertor discharge, and ~2MA current has been driven. In spite of the carbon first wall, density control was easy and very low density plasma far less than $1 \times 10^{19} m^{-3}$ was routinely possible in this series of experiment by keeping the wall temperature 150°C and overnight GDC. $N_{||}$ dependence of current drive efficiency ($\eta_{CD} \equiv n_e R_p I_{RF} / P_{LH}$) roughly agrees with theory. The η_{CD} at present is $\sim 0.2 \times 10^{20} m^{-2} A/W$ and is still low, since the present density region is less than $0.7 \times 10^{19} m^{-3}$. Both consistent with the previous results on JT-60. We still need further conditioning of the launcher to get higher performance in the higher density and current region.

Some HX profile data were obtained which indicate the change of the power deposition profile with change of the phasing of the launcher. Identification of the dispersion relation of the lower hybrid wave in tokamak was studied using the NBI as a probe. Both NBI and LH power were simultaneously injected and density was linearly ramped up from 0.4 to $3.0 \times 10^{19} m^{-3}$ in time. The dependence of the critical density, where

the coupling of the LHW changes from electrons to ions, by changing the beam energy was examined. The results are interpreted to dispersion relation and agrees well with theoretical one.

Power balance and limitation of the LHCD

Localized heat load to the first wall due to the fast electrons accelerated by the LHW is sometimes emphasized in the LHCD experiments. This kind of problem, so called, "hot spot" was especially remarkable in the early experiment of the LHCD since the experiments were done in the limiter configuration and in the very low density region usually less than $1x10^{19}m^{-3}$. It has been anticipated to damage the first wall and divertor plates due to the intense fast electron beam produced by the 50-100 MW LH power required in an application of the LHCD to the reactor.

In JT-60, however, there were no serious problem of the hot spot or localized heat load except some special conditions. High power of 4.5 MW was injected without any problem of the divertor plate, if the operational density is higher than $1x10^{19}m^{-3}$. The FWHM (full width of half maximum) of the heat flux profile to the divertor plate is almost similar to the OH and NBI plasma. Ratios of the radiation loss and divertor heat loss to the total absorbed power in the normal LHCD discharge are almost same as the OH and NBI heated ones. In normal case of δ_{30} (distance between launcher and outer most surface of the plasma) > 1.5 cm, heat load to the divertor and radiation loss are ~40% and ~50%, respectively. Confinement time of the LHCD plasma was similar or better than that of the NBI heated plasma, which indicates power absorbed by the fast electrons transferred to the bulk plasma through slowing down process and there were no direct loss of the fast electrons.

In some cases, the hot spot phenomena and data which indicate the localized heat load and/or the direct loss of the fast electrons were observed even in the JT-60 and in 60U, too. Example of these will be discussed in the meeting. These phenomena were observed in the case of quite low density with relatively high power LHCD or some disalignment of the first wall or error field. In conclusion, the hot spot and/or localized heat load in LHCD are unlikely to occur in normal divertor operation and the LHCD seems to be applicable to the ITER class tokamak, though we need further quantitative studies of these phenomena.

US-Japan Workshop on "RF Heating and Current Drive in Confinement Systems Tokamaks", Nov. 18-21 1991, NIFS, Nagoya, Japan

SOL/Divertor Plasma Performance during the Auxiliary Heating/Current Drive in JT-60U

M. Shimada, K. Itami, N. Asakura, H. Kubo, K. Shimizu, and JT-60 team

Profiles of electron temperature and density on the divertor plates were measured with an array of 15 Langmuir probes installed on the divertor plate. In hydrogen ohmically-heated discharges with I_p=2 MA and B_T=3.7-3.8 T, an increase of the main plasma density from 0.6×10^{19} m^{-3} to 2.8×10^{19} m^{-3} results in reduction of the peak electron temperature from 80 eV to ~10 eV and increase of the peak electron density from 0.2×10^{19} m^{-3} to 2.8×10^{19} m^{-3}. Both particle and heat fluxes as well as electron pressure of the electron side are large compared to those of the ion side when the direction of the gradient B_T drift is toward the divertor plates. Parallel current in the scrape-off layer from the electron side to the ion side. The magnitude of the scrape-off layer current is close to the ion saturation current. When the toroidal field is reversed, the asymmetry in electron pressure, and scrape-off layer current reverse direction as well. The sum of heat flux and the total radiation loss roughly equals to the joule input power of 1.3-1.5 MW. Neither temperature nor density of divertor plasmas are affected by the change of B_T. The total ionized neutrals S_{total} supplied to the whole plasma including the scrape-off-layer obtained from the H_α emission signals is consistent with the particle flux to the divertor plate Γ_{div}. The particle confinement times of global τ_p($\tau_p^{global}=\bar{n}_e V_p/\Gamma_{div}$) are derived. In the density region of $\bar{n}_e>1.3\times10^{19}$ m^{-3}, τ_p^{global} decreases proportionally to $\bar{n}_e^{-1}$.

During neutral beam heating, an increase in the main plasma density results in increase of radiation loss in the divertor(remote radiative cooling) up to 50-60 % of the total input power. The radiation power in the main plasma is ~20 %. Analysis of divertor heat load and divertor characteristics during neutral beam heating and LH current drive experiments is in progress and will be presented at the meeting.

US-Japan Workshop
NIFS,1991/11 18-21

Simulation Study of SOL Plasma Transport and the Scaling Laws

Sanae-I. Itoh, Noriaki Ueda* and Kimitaka Itoh
National Institute for Fusion Science, Chikusaku, Nagoya 464-01
*Mitsubishi Atomic Power Industries, Inc., Minatoku, Tokyo 105

Numerical analysis on Scrape-Off Layer (SOL) plasma and divertor plasma in tokamaks is made by using two-dimensional time-dependent transport code (UEDA code). Plasma transport in SOL and the divertor region is calculated for given particle and heat sources from the main plasma. Scaling study of the density, the temperature and their fall-off lengths is done for JFT-2M tokamak. The results show us inter-relations between the divertor plasma parameters and the core plasma confinement. The operational conditions of the core to guarantee the divertor performance are discussed.

We consider the single-null divertor plasma in JFT-2M tokamak. Using the model transport coefficients of SOL plasma, we solve the 2-D structure, where the width of heat flux channel, motions of neutral particles in a realistic geometory of the chamber and changes of plasma parameters in SOL are calculated in a consistent manner. Using the total particle flux, Γ_{out}, and the heat flux, P_{out}, from the core as parameters, we study the dependences of the edge density (n_b), the density fall-off length (λ_n), the electron temperature ($T_{b,e}$) and its fall-off length (λ_T) (measured at the mid-plane), as wel as the density and the electron temperature at the divertor plate, n_d and $T_{d,e}$. T_d represents the peak value on the plate. Independent of $T_{d,e}$, the dense divertor plasma can be established when the high recycling condition, i.e., the multiplication of the neutrals is sufficient. We do the simulation in parameter ranges where the dense divertor plasma condition holds.

The results on n_b, $T_{b,e}$, n_d and $T_{d,e}$ are as follows,

$$n_b \propto \Gamma_{out}{}^{1} P_{out}{}^{-0.3}, \quad (1) \qquad T_{b,e} \propto \Gamma_{out}{}^{-0.25} P_{out}{}^{0.5}. \quad (2)$$

We see that the reduction of particle flux yields the decrease of the edge density and the moderate increase of the temperature for the fixed output power. We also obtain the dependences of λ_n and λ_T as

$$\lambda_n = d\Gamma_{out}^{-0.24} P_{out}^{0.15}, \quad (3) \qquad \lambda_T = d\Gamma_{out}^{0.4} P_{out}^{-0.23} \quad (4)$$

where the value of d is 1.8 cm in JFT-2M for $\Gamma_{out} = 10^{21}$/sec and P_{out} = 100kW. The λ_n expands while λ_T contracts with the higher P_{out} for given Γ_{out}. On the divertor plate we find

$$n_d \propto \Gamma_{out}^{1.1} P_{out}^{-0.35}, \quad (5) \qquad T_{d,e} \propto \Gamma_{out}^{-1} P_{out}^{1} \quad (6)$$

The divertor density is roughly proportional to the edge density, i.e.,

$$n_d \propto \Gamma_{out}^{1.1} / P_{out}^{0.35} \simeq (\Gamma_{out} / P_{out}^{0.3})^{1.1} \propto (n_b)^{1.1} \quad (7)$$

The dense plasma condition in the divertor region is correlated to the edge density, i.e., the particle confinement. The cold divertor condition is also strong-ly affected by the outflux from the core plasma. The absolute value of the $T_{d,e}$ is $30 P_{out}(MW)/\Gamma_{out}(10^{22}/sec)$ eV.

Using the obtained scaling relations, Eqs.(1)-(6), we consider the divertor performance and the core confinement. Neglecting a radiative cooling term, the cold divertor condition in a stationary phase is derived from the relation as $T_d = P_{out}/\gamma G \Gamma_{out}$. The value of Γ_{out} from the plasma is simply evaluated by τ_p of the core, as $\Gamma_{out} \equiv \langle n \rangle V_p/\tau_p$, where V_p is the plasma volume and $\langle n \rangle$ is the averaged density. This leads to $T_d = P_{out}\tau_p/\gamma G n V_p$. If we use an empirical law, $\tau_p \simeq 0.05 P_{MW}^{-1/2} n_{e20}^{-1} I_p^0$ (P in MW, $\langle n \rangle$ in $10^{20} m^{-3}$), which is obtained in particle control experiment in JT-60 of diverted configuration, we obtain $T_d \propto P^{1/2}/\langle n \rangle^2$. This naturally leads to the fact that the high density opeartion is essential in high power regime in order to guarantee the divertor performance.

References

N. Ueda, K. Itoh and S.-I. Itoh, Nucl. Fusion 29 (1989) 173.

S-I. Itoh, N. Ueda and K. Itoh, Plas. Phys. Cont. Fus. 32(1990) 415.

Anomalous transports associated with the helicity transport in a plasma

Z. Yoshida

Department of Nuclear Engineering, University of Tokyo

Hongo, Tokyo 113, Japan

Heat and particle transports which are associated with the helicity transport are obtained in a current-carrying plasma. The helicity flux represents the transport of parallel current density and is produced by an electric field with a circularly polarized component. Fluctuations with circularly polarized components induce finite average in cross-field nonlinear parallel current, which leads to generation of frictional electron heat flux as well as ion nonlinear polarization current which produces particle flux. The circular polarization of the perturbed electric field thus relates the helicity flux, electron heat flux and the particle flux in such a manner that the heat and the particle transport in the direction opposite to the helicity flux. This result applies whether the helicity is injected externally by oscillating fields or it is generated internally in the plasma.

We take the coordinate system such that x is normal to the flux surface and y in the direction of the wave vector. The ambient magnetic field exists in the y-z plane. When we choose a specific gauge such that $\varphi = 0$ at $x = 0$, the helicity flux F_h across the surface $x = 0$ is given by

$$\langle F_h \rangle_x \equiv \left\langle -(\partial_t A_1) \times A_1 \cdot \nabla x \right\rangle,$$

or expressing in Fourier amplitudes,

$$\langle F_{h,k} \rangle_x = \frac{i\omega}{2} \left\langle A_k \times A_k^* \cdot \nabla x \right\rangle + \text{c.c.}$$

These relations show that, for the helicity flux to be finite, the perturbation should have a circularly polarized component.

For the tearing-mode turbulence we observe that $\nabla \cdot (\langle F_h \rangle)$ corresponds to the hyper-resistivity term;

$$\langle F_h \rangle = -B_{z,0}^2 D_0 \nabla j_{//,0},$$

where D_0 is the hyper-resistivity.

The nonlinear parallel current, as well as the the nonlinear polarization current, become finite in the tearing-mode turbulence, and both are related to the helicity flux. We obtain

$$\langle j_{//k} \rangle_x = \frac{-x_k (\partial_x v_{z,0}) \lambda^2}{\mu_0 B_0^2} \left(\frac{k_\perp}{\gamma}\right)^2 \langle F_{h,k} \rangle_x,$$

and accordingly the frictional heat flux

$$\langle q_{u,k}^e \rangle_x = \frac{C_z T_e}{e} \frac{x_k (\partial_x v_{z,0}) \lambda^2}{\mu_0 B_0^2} \left(\frac{k_\perp}{\gamma}\right)^2 \langle F_{h,k} \rangle_x,$$

where $\nabla \times \boldsymbol{B}_0 \approx \lambda \boldsymbol{B}_0$, $v_{z,0} = -j_{//,0} / e n_e$, $k_{//}(x_k) = 0$, and C_z is a positive number of the order of 1. We require a balances finite average in the perturbed perpendicular current, which is primarily an ion current, to retain the charge neutrality. A particle flux results; using the helicity flux, we may write

$$\langle \Gamma_k \rangle_x = \frac{1}{e} \frac{x_k (\partial_x v_{z,0}) \lambda^2}{\mu_0 B_0^2} \left(\frac{k_\perp}{\gamma}\right)^2 \langle F_{h,k} \rangle_x.$$

The perpendicular ion current is primarily produced by the nonlinear polarization drift. The polarization current is dependent upon the perturbed radial electrostatic potential. The average charge neutrality condition $\langle j_{//} \rangle_x + \langle j_p \rangle_x = 0$ yields an ambipolar relation for the perturbed electric field.

Consistency of Current Drive and Divertor Conditions

M. Sugihara, Y. Murakami, H. Kimura, T. Nakazato,
T. Tsunemastu, Y. Shimomura

Japan Atomic Energy Research Institute
Naka-machi, Naka-gun, Ibaraki-ken, Japan

Systems analysis on the operational capability of steady state and long pulse operation in ITER (International Thermonuclear Experimental Reactor) are studied with particular emphasis on the consistency of current drive and divertor conditions. In ITER, the steady state or long pulse operation with reasonably high fusion power or neutron wall loading ($\approx$ 1 MW/m^2 at test region) must be achieved for the nuclear testing of blanket. Most critical issue for this operation is the consistency of current drive and divertor conditions, since the additional power input is necessary for current drive and the efficient current drive requires relatively low plasma density. In fact, the steady state operation with the neutron wall loading higher than 0.4 MW/m^2 is considered difficult to be achieved due to severe divertor heat load. Divertor peak heat load is expected in the range of 5 MW/m^2 for the ignition operation with relatively high density, while it becomes more than 20 MW/m^2 for the steady state operation with the neutron wall loading of 0.7 MW/m^2.

In this paper, we will perform the wide range of systems analysis to identify the operational capability for steady state and long pulse operation in ITER based on the simple scaling laws for divertor peak heat load. It should be noted, however, that the estimation of the divertor conditions contain substantial uncertainty due to the incomplete database and modeling for SOL and divertor plasmas. Operational capability will be altered to substantial extent by this uncertainty. Thus, we will employ two representative scaling laws; Harrison-Kukushkin's (HK) scaling [1] and Itoh's scaling [2] in the analysis. Importance to establish reliable scaling law is also pointed out by the comparisons of resultant operational capability obtained by these scaling laws.

In the analysis of steady state operation, operation space on the plasma current and temperature plane (Ip-T) and various restricting conditions for the operation space are identified. On this operation space, the divertor peak heat load is examined by the above scaling laws.

In the analysis of long pulse operation, hybrid operation (plasma current is partially driven by non-inductive means with the supplement of inductive drive) space is first identified to achieve the required neutron wall loading and burn time for the nuclear testing (here we assume 1 MW/m^2 and 2000 seconds). Possible improvement on the

divertor peak heat load with the extension of various restricting conditions, such as current drive efficiency, confinement enhancement factor, beta, available inductive flux, are quantitatively evaluated. An example of hybrid operation space is shown in Fig. 1, where operation point A provides the longest burn time within all of the restricting conditions (in this case confinement of power law is most restricting), and operation point B provides the best divertor condition with the burn time of 2000 seconds. Peak divertor heat load of this point is 7 MW/m^2 as shown by the left hand side of open circle in Fig. 2. With increasing the inductive flux (equivalently increasing the radius of OH coil, R_{OH}), the divertor peak heat load is improved as shown in Fig. 2.

Lastly, we will examine the experimental capability to explore the high heat load condition on divertor in DT steady state and hybrid operation with use of the H and H/D operation in Physics Phase.

References

[1] M.F.A. Harrison, A. Kukushkin, ITER-IL-PH-13-9-E12 (1989).

[2] S-I. Itoh, N. Ueda, K. Itoh, Plasma Physics and Controlled Fusion, 32 (1990) 415.

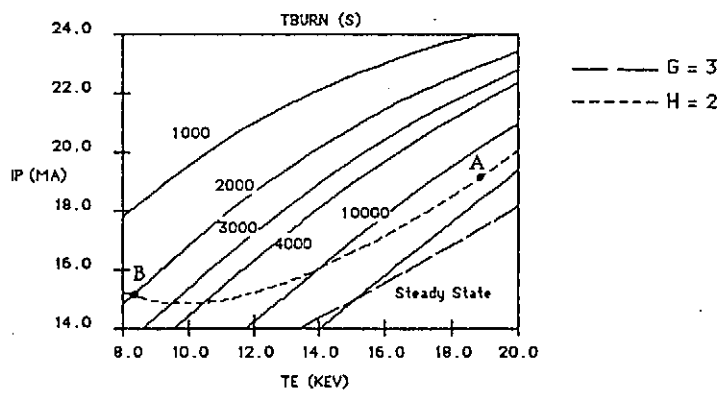

Fig. 1 An example of operation space for hybrid long pulse operation.

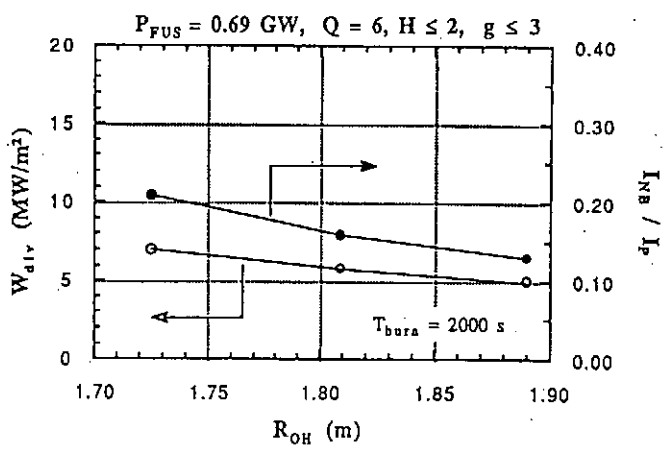

Fig. 2 Divertor peak heat load and fraction of non-inductive driven current as a function of inductive flux for 2000 seconds of burn.

Summary Report **Group A** **S. Bernabei**

Perspectives on RF Technology and Applications

The discussion on RF current drive focussed on the comparison of the three leading methods, Fast Wave, Lower Hybrid and Electron Cyclotron Current Drive, and on their main characteristics and problems.

In summary there was almost unanimous agreement that FWCD is the most promising method from the physics and technology points of view, followed by ECCD and then by LHCD, but there was also agreement that the inverse order applies for what concerns present experimental demonstration of steady state current drive.

Infact in theory FWCD presents many advantages over the other methods: it has no density limit and because of the low frequency does not suffer the same limitation in penetration as for the LHCD (this indeed is the most serious limitation for an otherwise very succesful current drive method: the accessibility condition in a reactor plasma imposes a phase velocity for the launched wave which resonates with electrons at temperature around Ú 15 keV. Beacause of the strong damping, regions at higher temperatures are inaccessible). Efficiency can be as high as for the LHCD, and the technology seems well at hand. During the discussion there was not total agreement that coupling by means of loops is the most desirable, even without the Faraday shield, but it was noted that even the LH waveguide array may not be the easiest owing to the difficulty of cooling the thin septa between adjacent waveguides.

ECCD seems equally good from the physics point of view but the RF sources are a continuous problem, even if often overstated.

The whole situation reverses when experimental results are considered. Infact LHCD has sustained currents up to 2 MA (JT60), and currents in excess of one hour (4210 seconds in TRIAM-1M) with a maximum figure of merit of 0.4 (10E20 A m^{-2}/W). This figure of merit approaches the theoretical value and should reach 0.5- 0.6 (the ITER realistic value is 0.35).

By comparison ECCD has driven 100kA (DIIID) but without reaching the condition of steady state characterized by V_L=0 and even if the predicted figure of merit for ITER is 0.25, the best value so far obtained is 0.01. It was noted that trapping effects may enhance bootstrap current, but the value is still Ú40 times less than LHCD.

Finally FWCD has not yet shown unequivocal sign of current drive. It has shown ability of heating electrons in good agreement with theory;

unidirectional effects are observed but the current is independent of the phasing (DIIID): this was one of the most tantalizing results presented at the workshop.

As for the current profile control again the only clear results are provided by LHCD (JT60 and ASDEX results were presented), but the best theoretical localization of the driven current is with ECCD.

The group briefly discussed the major oustanding misteries and problems and the suggested priorities for the experiments: the above mentioned FWCD phase independence, the need for more data on sawteeth and m=2 stabilization with ECCD and the study of the importance of the fast electron diffusion in LH current profile control. In the case of LHCD the mechanism for the bridging of the spectral gap is still not completely understood, however it appears that computer modelling follows closely the experimental results.

It was noted that JT-60U and JET are in the position of demonstrating the inaccessibility of the LH waves into the hot core of the Tokamak.

Attendant: S. Bernabei, P. Bonoli, R. Freeman, K. Hanada, T. Imai, H. Kimura, T. Maekawa, K. Nagasaki, K. Ohkubo, T. Seki, S. Tanaka, K. Ushigusa, T. Watari

Summary Report for the Discussion Group B

K. Itoh (NIFS)

Attendant: V. S. Chan, C. Forest, A. Fukuyama, K. Itoh, Y. Taguchi, Z. Yoshida

This group discusses topics (1)Motivation of the research in this direction, (2) Physics of Helicity Injection/Transport, (3)Synergies in the Innovative Current Drive.

1. Motivation of the Research

We firstly reviewed why and in what direction the research on innovative current drive must be performed and strengthened.

It is widely recognized that the present method of the current drive is not yet efficient enough. This is particularly true for the high density plasma, which is necessary from the view point of the divertor control. It is also known that although the profile of the current can be externally controlled, the applicability is limited to some parameter range. In short, to open up the parameter for flexibility is still an urgent task of the research.

The necessary direction would be as follows: Key concept for the steady state plasma would be the circulating power, which we must minimize. As the plasma beta or temperature increases,

the required circulating power for sustenance/control is reduced owing to the improved current drive efficiency and spontaneous current such as Bootstrap current. On the other hand, if the high beta value is required, the current profile cannot be freely chosen. [Clear example was shown by T. Taylor. The Bootstrap current profile will give lower beta limit for MHD stability. Additional current profile control is requested to achieve high beta value.] The necessary power would behave as a U-curve as is shown in Fig.1. The reduction of the minimum circulating power is clearly the direction of the future research.

Another way to reduce the necessary current is to improve the plasma confinement. If the quality of plasma confinement, such as τ_E/I_p is enhanced [as is the case of H-mode or VH-mode and so on], then the necessary current is reduced. This allows a straightforward reduction of the circulating power.

In addition to these research to look for the break through, the impact on the physics understanding must not be bypassed.

The innovative experiment, which is different from conventional experiments in dimensionless parameter or boundary condition, may yield an unique touch stone for the plasma modelling. For instance, the transport of the current, which is a key physics in studying the DC helicity current drive, on the other hand casts a new aspects of the understanding of the anomalous transport of the core plasma. Other example can be seen from the study on the rf helicity current drive. This scheme is theoretically formulated in terms of the nonresonant force of the wave on the plasma. This force can also be a candidate to drive the

plasma rotation, thus giving a chance for the improved confinement experiments.

We conclude that this workshop has contributed quite a lot in these two aspects. Examples are seen in the following.

2. Helicity Current Drive

RF Helicity Current Drive

Through this series of workshops (this time and the last San Diego WS) the physics picture of the rf helicity current drive is firmly formulated.

The particle picture was developed by Chan and GA group with the local drive efficiency. The current is reformulated in terms of the nonresonant force from the RF wave to the plasma by Fukuyama et al. The latter formalism allows to combine the global wave analysis with rf helicity current drive. The over all efficiency was calculated. The weak density dependence was confirmed. The experimental evidence, however, will be obtained only the plasma temperature is high. Only small and finite wave momentum (vacuum part) is necessary to cause net electro-motive force in plasma.

DC Helicity Current Drive

CDX-U experiment has demonstrated that the DC helicity injection into open field line can, in the end, form the closed magnetic surface. Toroidal current is found to flow mainly in the closed magnetic surface. The shape of the current profile in the closed surfaces are of large interest. [Can the plasma have

peaked current density? If so, then what mechanism carries the current into the axis?] The presentation leave us with this desire for the further knowledge, which will be given in a year or two.

One interesting point is remarked that the e-beam experiment may be able to check whether or not the generalized term $\int(e\vec{A}/m+\vec{v})\cdot(e\vec{B}/m+\nabla\times\vec{v})$ rather than $\int\vec{A}\cdot\vec{B}$ is conserved. It is also noted that the SPAC experiment (by A. Mohri) should be revisited.

Helicity and Current Transport

The transport of the current is of vital importance for the sustenance by means of the DC helicity injection. During the workshop, it is argued that the current diffusion across the magnetic surface must be associated with thermal transport, and this value is too large for the application to large devices. Other calculation has also shown that the heat flux is in the opposite direction of the helicity flux, and obtained the heat flux driven by current density gradient through tearing mode.

This kind of calculations is deeply connected with the anomalous transport of the core plasma. The hypothesis of the so called "heat pinch" has been discussed (i.e., the heat flux q is driven by some gradient, in addition to ∇T, so that q has and offset $q = -\chi\nabla T - q_{in}$), and the heat flux driven by ∇J is one candidate. This term was considered to be small for the drift wave frequency, but future research is necessary. The current diffusivity was predicted to play an important role in the collapse of sawtooth.

Rotation drive

Chan and GA group reported their calculation on the rotation drive by the nonresonant force of rf waves. The nonresonant force on ions are calculated for the low frequency waves. It was found that the force is given by the formula F^{NR}[Newton] = $0.4n_{20}P_{kW}/B_T^2N_z$. This force can be compared to the force driven by NBI for which $F_{NBI}=7.5\times10^{-4}P_{kW}$ for the deuterium beam at 80 keV. This estimation shows that the rotation drive by the rf nonresonant force can be more efficient than NBI, and propose a new experimental method to improve the plasma confinement.

3. Synergies

The synergetic effect between two different mechanism of current drive may enhance the overall efficiency. Although the Bootstrap current has been studied, not all of the plasma free energy was investigated as a possible source of the plasma current.

The Bootstrap current has been shown by large devices that it can sustain considerable part of the total plasma current. For it there has been a long argument of the seed current, which cannot be eliminated for the conventional BS current drive scheme.

ECH experiment on CDX-U has shown that the perpendicular heating of the plasma can sustain almost all of the toroidal plasma current. The dependence of direction of the toroidal current on B_t and B_v suggests that the seed current is generated by the toroidal precession of trapped particles, thus realizing the tokamak equilibrium without any external current drive. (The directional preference in the ECH absorption cannot be completely denied, but the state is close to the stationary state.)

A theory was presented that the current diffusion can supply the seed current near the core. Example of the solution that the Bootstrap current equilibrium with no external drive is shown. This provides a possibility to realize steady state ignition in tokamaks.

Associated with this, Taguchi reported the calculation of the Bootstrap current carried by α-particles. This component was found small (about 10% compared to the conventional one). However, the other driving mechanisms of the seed current must be pursued in future, to reduce the circulating power, and the stability of these states must be more carefully studied.

4. Final Note

In short, many new ideas were presented during this workshop. We would like to emphasize, many of them are opening the new tool to control plasmas, and at the same time, cast new insight of the fundamental problems in plasma confinement. The future research will surely provide further steps into the break through of the current drive/control and the improvement of the physics understanding.

Fig. 1.

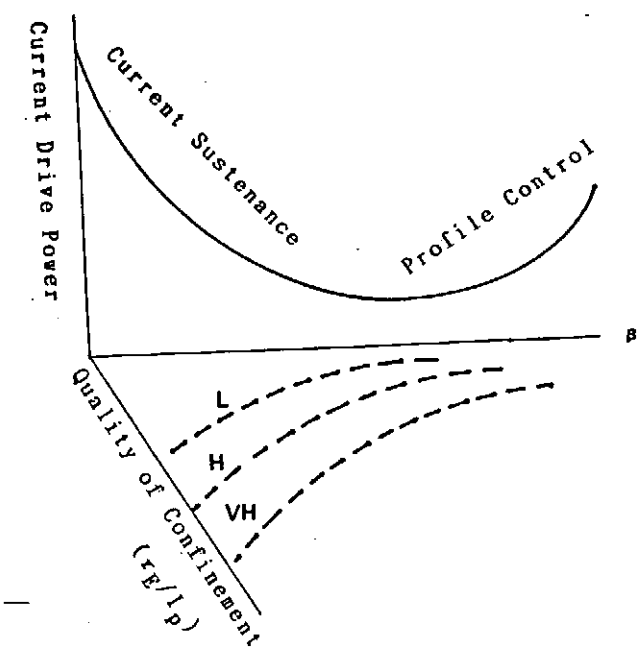

Group C - Summary

S-I. Itoh, M. Shimada, M. Sugihara, T. Taylor

In this group, following four major topics with respect to SOL/divertor conditions under heating/current drive are discussed :
1) View on steady state operation, 2) Compatibility, 3) Understanding,
4) New future progress.

1) View on steady state operation

First of all, the typical requests in achieving the steady state operation in fusion experimental device such as ITER are summarized as follows;

- Plasma current	$\geq$ 15 MA	(restrictions by confinement and beta)
- Wall loading	$\geq$ 1 MW/m^2	(request for nuclear testing)
- Operation density	$\approx 5\times10^{19}$ m^{-3}	(request from low current drive efficiency)
- Z_{eff}	$\leq$ 2	
- Total power (α + CD)	$\geq$ 250 MW	
- Divertor heat load	$\leq$ 15 MW/m^2	(for reliable heat removal)
- Divertor temperature	$\leq$ 30 eV	(for substantial erosion life)

Requirements for the divertor conditions to meet these requests can simply be expressed as achieving high density and low temperature divertor. Details of these conditions and its feasibility, possible improvements are discussed in the following.

2) Compatibility of steady state operation and divertor

Group conclude that the steady state operation is difficult to achieve from divertor view point based on the assessment by using the present simple models, since low density and high power operation demands large peak heat load, which is higher by a factor of 2-3 than in the high density and high Q (low external power) operation mode, and also fairly high divertor temperature, e.g., higher than 100 eV. However, the group also recognize that the present divertor models need substantial improvement to draw definite conclusions on the feasibility of steady state operation.

Several possibilities to improve divertor conditions in steady state operation, and their remarks are listed as follows:

-Radiative divertor ; Concern exists in the compatibility with good confinement and maintenance of low impurity level in the main plasma, especially in low density operation required for steady state operation.

-Higher q_Ψ operation ; High bootstrap fraction, long connection length, radiative divertor, favorable MHD stability, grassy ELMs will be obtained by higher q_Ψ operation.

However, confinement capability and available absolute beta are degraded in this scheme. Although both deficiencies can be improved by increasing toroidal field, concerns are raised on the increase of synchrotron radiation loss and technical difficulty for high field coils.

-Edge density control
-Divertor biasing
-Sweeping (either magnetic and electro-static by using biasing)
-Pumped divertor
-Ergodization

In addition, group recognize the importance of the effort to reduce the plasma current. Two possibilities are discussed based on the present knowledge, i.e., VH mode with 2nd stability both observed in DIII-D, and high aspect ratio. It is expected that VH mode and 2nd stability will not be realized simultaneously, since the required edge current in VH mode will not be compatible with 2nd stability in the former possibility. As for the latter possibility, though the high performance database is still needed, the necessary plasma current can definitely be reduced by increasing aspect ratio when based on power law confinement scaling, while the essential point should be increasing q_ψ to increase the bootstrap fraction. Some concern on the error field as decreasing the aspect ratio is raised with respect to the production of hot spot by fast electrons, while, in CDX-U, the error field is not necessarily large.

3) Understanding

Group concluded that the present status of understanding on the divertor/SOL plasma is poor, and that the approach of core plasma confinement, where the development of empirical scalings and the study on the basic transport process are progressed in parallel, is valuable in order to improve the situation. For the derivation of empirical scalings on peak heat load, temperature, global particle confinement time, dependences of these quantities on power, density, plasma current, field, divertor configuration (SN/DN) and so on should be systematically studied under ITER-relevant current driven conditions. For the study on the basic transport process, divertor/SOL profile data of density, temperature, current, radiation power must be examined systematically. Main target for this study is to derive $\chi_\perp$, $D_\perp$. Other important transport processes are power fraction carried by ion and electron across the separatrix, fast ion trajectories in SOL, impurity-related physics such as generation, shielding, transport effects on τ_p and τ_E. Improvement of the modelling must also be promoted in parallel. For this purpose, systematic check against experimental data, modeling of non-stationary state such as ELM, impurity modeling are important.

Group also recognize the importance of the identification of the operation regime and operation parameters, which are relevant to the steady state operation with respect to the divertor/SOL conditions. Typical examples are listed below.

- Grassy ELMs discharge (It may not be achieved in low q_ψ discharge as observed in DIII-D so far?)
- High bootstrap fraction discharge with high density
- Effect of fast electrons (In JT-60, the effect can be diminished substantially when density exceeds 1×10^{19} m^{-3}, and further broad information should be important)
- Operation regime to maintain SOL plasma in Maxwellian

Remaining mysteries in the understanding of the divertor/SOL plasmas are discussed, and some of them are listed below, though they are far from complete.

- High energy ions in SOL
- Non-divergence free SOL current
- Factor of two discrepancy in total and hydrogen particle flux to divertor plate
- Isotope effect on confinement, recycling and so on
- Material effect on confinement, recycling and so on

4) New future progress

New future progress, which can be expected in DIII-D and JT-60U, are discussed and the major areas are listed below.

<u>DIII-D</u>

-Systematic database are being developed
-Biasing effect
-Pumping effect
-Bootstrap current (with 2nd stability)

<u>JT-60U</u>

-Database on density, temperature, current in OH discharge
-τ_p, heat flux data for high power (up to 40 MW) discharge
-Impurity data;
  generation
  shielding
  transport (parallel, perpendicular)
-Boronization effect
-Bootstrap current

General Summary of US-Japan Workshop on RF Heating and Current Drive

November 18-21, 1991

Nagoya, Japan

Vincent Chan, General Atomics Workshop Co-Organizer

The workshop was attended by 8 US scientists (5 official and 3 observers) and 30 Japanese scientists (5 from JAERI). The agenda was divided into 2 1/2 days of presentations, 1/2 day group discussions and 1/2 day summary session. There were 10 papers on rf physics, technologies and applications; 6 papers on new concepts, helicity injection and transport; and 6 papers on heating/current drive and scrape-off-layer/divertor conditions. They can be broken down in specifics as follows:

FWH/CD 5
ICRF/IBW 3
ECCD/ECH 2
LHCD 4
Helicity Injection 5
Profile Control/Sawtooth Stabilization 4
ITER/Reactor Requirements 2
Bootstrap Currents 2
Divertor/SOL Models 4

The wide range of topics discussed is an indication of the impressive growth, both in depth and breadth, of the US-Japan workshop in RF Heating and Current Drive. It also benefitted by being combined with the new current drive concepts workshop and the active participation of JAERI scientists.

The technical content of the workshop is best summarized according to the respective topical discussion groups.

1. RF Physics, Technologies and Applications

In the area of FWCD, direct electron heating is established. Multiple pass absorption is in evidence and consistent with full wave theory. Launching of FW with phased spectrum and efficient coupling are demonstrated. However, a question concerning the compatibility of loop antennae with ITER/reactor is raised. CD is observed but current is independent of phasing and steady-state CD has not been achieved. Theoretically, FWCD holds great promise. Alpha particle damping can be avoided, there is no density limit for penetration, the efficiency can be comparable to LHCD and the technology is available.

In LHCD, a large data base has been established for steady-state CD and a maximum duration of over 1 hour has been demonstrated. Experimental efficiency of 0.4 has been achieved compared with ITER requirement of 0.35. Profile control capability is established but penetration may be limited by high temperature. Anomalous diffusion of fast electrons is still a question.

In ECCD, CD is demonstrated and in agreement with Fokker-Planck theory. Sawtooth suppression is proven but $m = 2$ stabilization and disruption control remain as challenges. Also reliable theoretical models do not exist. Theory predicts CD efficiency of 0.25 for ITER. Recovering trapped particle reduction through bootstrap current enhancement may improve efficiency and more theory and experiments are encouraged. EC launchers are highly efficient but sources are a serious problem. RF generators are not yet available.

2. New Concepts

Presently available methods to sustain steady-state noninductive current by rf is marginal at best for reactors, hence it is important to develop high efficiency CD at high densities. While largely bootstrap driven tokamak looks attractive, one has to seriously consider compatibility with MHD stability. Improved confinement may relax CD requirements and need to be explored. Further research on the simultaneous control of both pressure and current profile will be necessary for the achievement of higher β plasmas. Since the bootstrap current profile is determined by both the pressure and current profile in rf sustained plasmas and it is known that edge bootstrap current lowers the critical β, tailoring of the wave phase spectrum may be required to enhance the beta value. Fundamental understanding of new concepts may provide further insights.

Theoretical understanding of rf helicity injection is much improved over the last 2 years. Experimental confirmation is still lacking and predicted efficiency is low so far. The formation of closed flux surfaces is established by dc helicity injection. Current diffusion and transport are still not well understood. Theoretical models of helicity diffusion are proposed but experimental verification is not available. It is pointed out that if this can be validated, full bootstrap current drive tokamak may be feasible.

Significant bootstrap current has been observed in many machines. In CDX-U, close to 100% of the current is internally generated. Study to ascertain whether externally supplied seed current is necessary will be crucial.

Other new concepts include synergetic effects and plasma rotation. Some preliminary observations of synergetic effects by combining two CD/heating schemes can be found but were not convincingly demonstrated. Non-resonant rf force can drive plasma rotation (e.g. for confinement improvement) which can be comparable to NBI. Experimental verification is needed.

3. Divertor/SOL Issues

Study of compatibility with divertor and wall loading provides visualization of the power flow in a tokamak from cradle to grave, i.e. the input from the antenna to the flux onto the divertor. The divertor condition favors high q, high density and low temperature operation. Simple SOL model with specific confinement scaling and available CD efficiency shows steady-state difficult to achieve. Constraints may be relaxed by improved energy confinement, judicious utilization of ELMs, or innovative divertor concepts e.g., radiative divertor, sweeping x-point. Significant trade-offs are still required. Reliability of divertor models needs to be improved and experimental verification of models is lacking.

Experiments observed runaways at low densities which often led to hot spots and impurity enhancement. The increase in runaways may be due to error fields, which led to the question of error fields tolerance in order to minimize runaways. ICRH generates energetic ions which can result in impurity generation also. High q_{edge} operation is compatible with ELMy discharges for impurity control. New ideas to utilize this feature will be beneficial.

Assumptions used in many 1-D models may not be realistic, although some interesting predictions have come forth, yet 2-D models are difficult and time consuming to develop. We need some middle ground approach which combines measured boundary conditions with 1-D models for useful near term applications.

In conclusion, it is particularly significant that Dr. M. Yoshikawa, the executive director of JAERI, made a special trip to Nagoya to address this workshop. He stressed the significance of the occasion, not only because of the importance of the topic at hand, but the fact that it marked the first Ministry of Education/JAERI joint workshop which opens up an arena for all-Japan collaboration. He is looking forward to more extensive collaborations in the future, particularly in some aspects of fusion engineering, as Japan readies itself to participate in the next large fusion project.

Finally, special thanks go to Professor A. Iiyoshi, Professor S. Tanaka and our host Dr. S.-I. Itoh for their hospitality and an extremely well organized meeting.

RF Heating and Current Drive in Confinement System Tokamaks ハイライト

達成データの進展:

*電流駆動は、4210秒(TRIAM-1M),2MA(JT-60)のプラズマ電流を維持した(LH).

*内部インダクタンスℓ_iを0.2程度上下させ(ASDEX,JT-60)、プロファイル・コントロールの実績も示した(LH).

*Fast Waveによる,高密度電流駆動可能性を示す予備的データ(DIII-D).

*ベータ値は44%(中心)に達し、中心部でも第二安定化状態になった可能性大(DIII-D).

*不純物発生率のin situの観測が初めて報告された(JT-60U).

新たな発見と見通し

*エネルギー閉じ込め時間やベータ限界値がℓ_iに比例するとの実験則が提案され(DIII-D)、圧力と電流分布制御の重要性と研究意義を刺激.

*CDX-Uがほぼ100%自発電流で維持されるプラズマを示した(ECH).

*トカマクの外部駆動ゼロでの定常解が理論的に示された.

*ダイバータ・バイアスでH-modeの閾値を上下した(DIII-D)他、SoL/ダイバータ・プラズマを制御する検討が進んだ.

理論モデルの進展:

*電流駆動について定量的に満足ゆくものが(高温になると)出来つつある.

*アンテナ・フェイジングにより、分布制御し(ℓ_iと$p(r)$)、ベータ限界を高く維持すると言った予言も近々可能.

*定常維持のために必要なパワーの「揺り籠から墓場まで」一貫した流れを把握出来る様になった.

*RFヘリシティ駆動については、このWSを契機として、ほぼ、理論的な構成が出来た.

残されたミステリー:

*RF制御により、鋸歯状波抑制が実証された(WT-3他)が、理論モデルが無い.

*Fast Wave電流駆動は、自発電流も含めると、相当部分の電流を維持したが、入射スペクトルを反対符号にしても余り変わらない(DIII-D).

*DCヘリシティ駆動法では、閉じた磁気面を作ることは出来たが電流がピーク分布になったか分かっていない.

*スクレイプ・オフ層では、磁力線を横切るかなりの電流がある(JT-60U).等.

今後の動向と課題

*高密度領域での駆動電流の分布制御性の確立と,限界ベータ値上昇の実証.

*高ベータプラズマの加熱による自発電流(ブート・ストラップ電流を含む)の評価.

*プラズマの内部エネルギーの活用には,今後の研究の必要大.

*電流の輸送は、今後の大切な研究課題である.

*長時間維持のためのクリティカル・パスを見つけ、整合性有る解決を目指す研究.

運営:

*出席者数、JAERI6人を含め日本側30人以上と言う、この課題にたいする日本の総力(All Japan)を示しうる研究会.

*定常化研究が、個々の成果ではなく、整合性あるプラズマ状態の制御であるとの認識が進み、その新しい考え方を纏める会合になった.

*核融合実験炉段階に進む上で、考え・決心せねばならぬ多く事(吉川)のなかにあって、本ワークショップは,整合性,両立性を考えながらプラズマ開発を進める方法論の一例となったのではなかろうか.

Appendix

Recent Fast Wave Results on DIII-D

Reported by

V.S. Chan for the DIII-D RF Group

General Atomics

at
the U.S.-Japan Workshop
on RF Heating and Current Drive
in Confinement System Tokamaks

Nov. 18-21, 1991
Nagoya, Japan

Current Drive Program for DIII-D

- The long range goal is to demonstrate full noninductive current drive with good confinement in a high beta plasma.
- A second objective is to fully explore the potential of rf current drive for profile control and plasma performance enhancement.
- To achieve these objectives requires the combined use of FWCD/ECH, ECCD, and bootstrap current.

Key Steps Toward Long Term Goals

- Demonstrate effective ECCD, and compare with FP theory
- Demonstrate efficient launching of FW
- Demonstrate interaction of FW with electrons
- Demonstrate ability to phase the antenna
- o Demonstrate FWCD at <2 MW
- o Raise FW and ECH power; new FW antenna
- o Demonstrate 1 MA noninductive CD
- o Raise FW power to 8 MW and ECH power to 10 MW
- o Demonstrate 2 MW noninductive CD

FAST WAVE CURRENT DRIVE

FWCD refers to the application of fast waves in the ICRF with an asymmetric spectrum in the toroidal direction.

Fast waves may be absorbed directly by electrons (unlike FW minority heating) through the processes of Landau damping and transit-time magnetic pumping, when the resonance condition $\omega - k_{\|} v_{\|} = 0$ is satisfied.

The resulting current drive is expected to be comparable to that of neutral beam current drive under ITER-like conditions, but experimental verification is required.

GENERAL ATOMICS

DIII-D fast wave current drive antenna

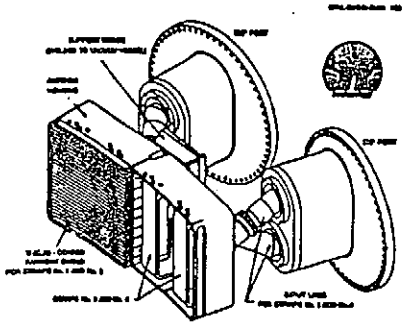

Spectrum of $(0,\pi,0,\pi)$ phasing has peak $n_\parallel$ of 11, damps optimally on 2 keV electrons; $(0,\pi/2,\pi,3\pi/2)$ phasing has $n_\parallel$ of 5.5.

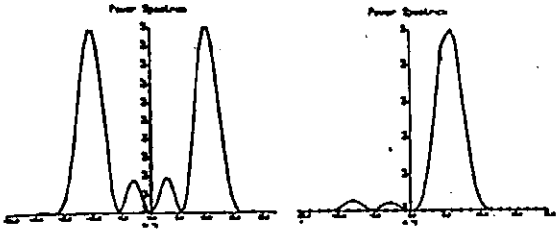

GENERAL ATOMICS

FUNDAMENTAL H MINORITY HEATING

- Efficient heating is found
  - — compares well with NBI at same power level in same discharge in DIII–D
  - — heating results agree with ITER-89P scaling
- Produces centrally peaked electron heating when resonance is at plasma center

Conclusion: The FW antenna is highly effective at launching the fast wave.

GENERAL ATOMICS

FW ICH produces centrally-peaked electron heating

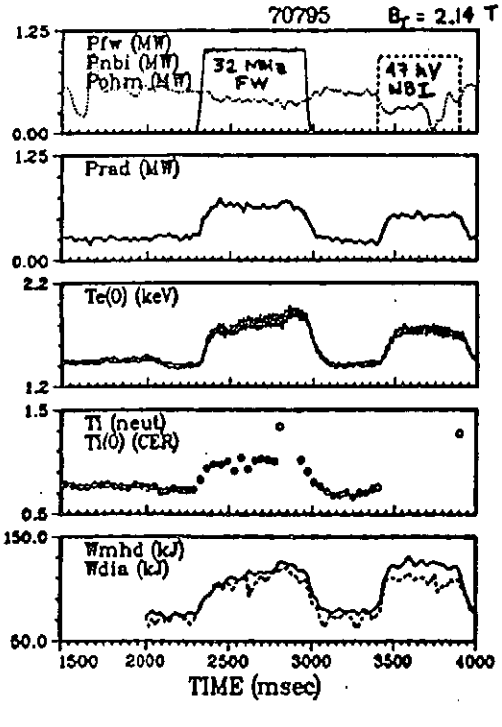

GENERAL ATOMICS

FW heating efficiency at 32 MHz agrees with ITER-89 offset linear scaling

This permits measurement of heating efficiency η for other scenarios (IBW, FW at $2\Omega_H$, FW direct electron heating)

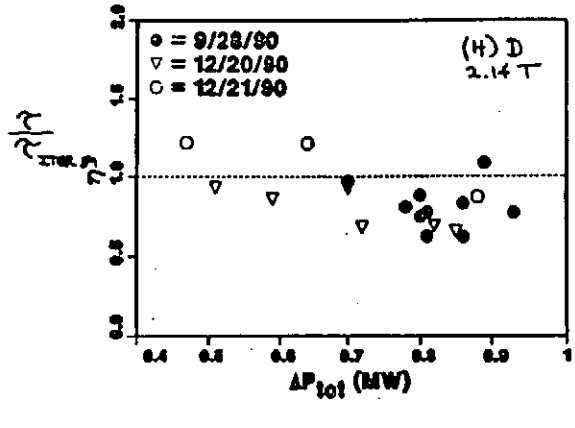

DIRECT INTERACTION OF FAST WAVES WITH ELECTRONS

- Experiments performed with symmetric phasing of antenna straps
- Single pass damping of rays is small theoretically: ≈ 30% at 1 T and ≈ 5% at 2 T
- However, FW heating with high efficiency was found for all B_T, suggesting effective multiple pass damping
- There appears to be a threshold in target temperature below which the heating is weak; this is in agreement with theory of single pass damping
- Electron heating is centrally peaked, in agreement with full wave code results

Strong plasma heating by fast waves is observed

$B_T = 2.1$ T

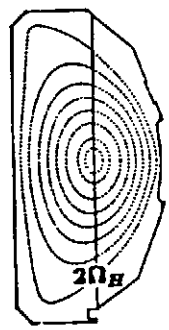

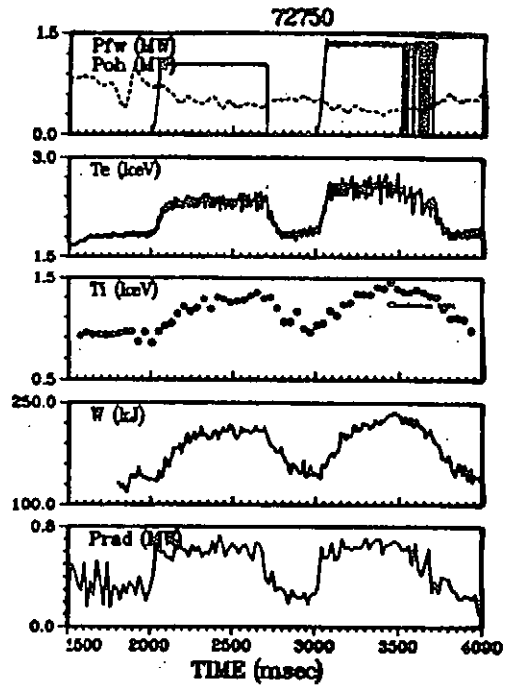

Centrally peaked electron heating is observed

$B_T = 2.1$ T

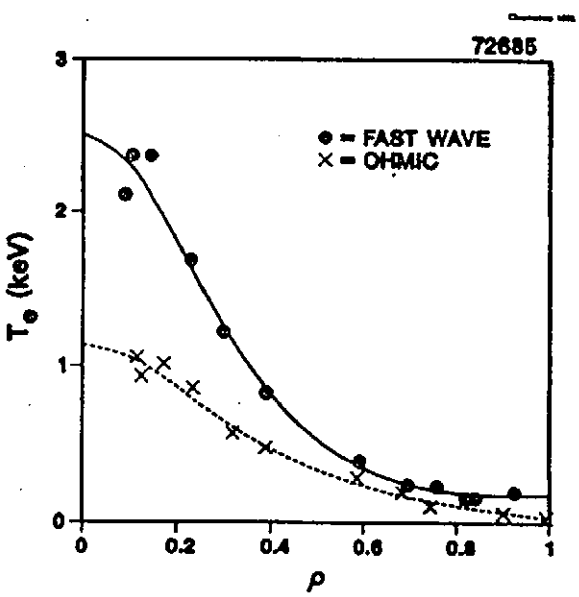

Strong central electron heating is observed even with no central ion cyclotron resonance

$B_T = 1.71$ T

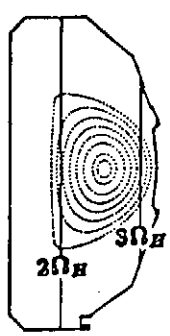

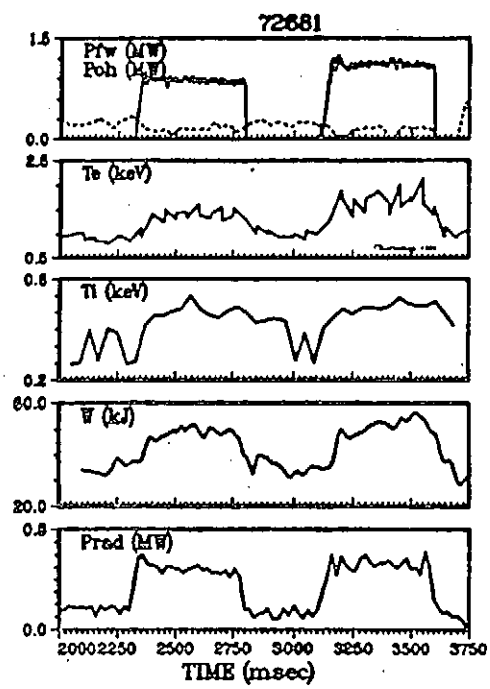

Fast wave heats efficiently for all B_T

$$\tau_{ITER} = 0.048 I^{.85} R^{1.2} a^{.3} n^{.1} B^{.2} (A\kappa/P)^{.5}$$

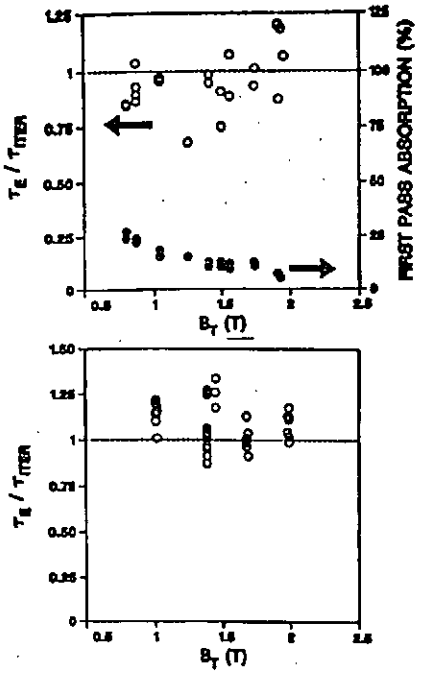

High aspect ratio

Low aspect ratio

Multiple pass absorption appears to be occurring.

GENERAL ATOMICS

Full wave code predicts that direct electron absorption is ≈ 5 times stronger than second harmonic hydrogen absorption

$B_T = 2$ T

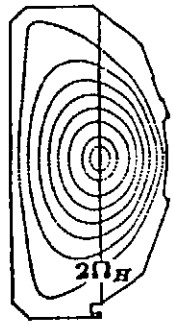

Courtesy of P. Bonoli, M.I.T.

Poster 3S16

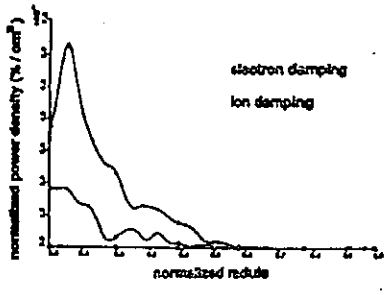

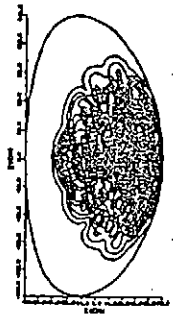

mod (E)

GENERAL ATOMICS

Power modulation experiments were performed to measure the fast wave deposition profile

$B_T = 2$ T

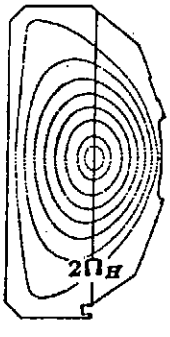

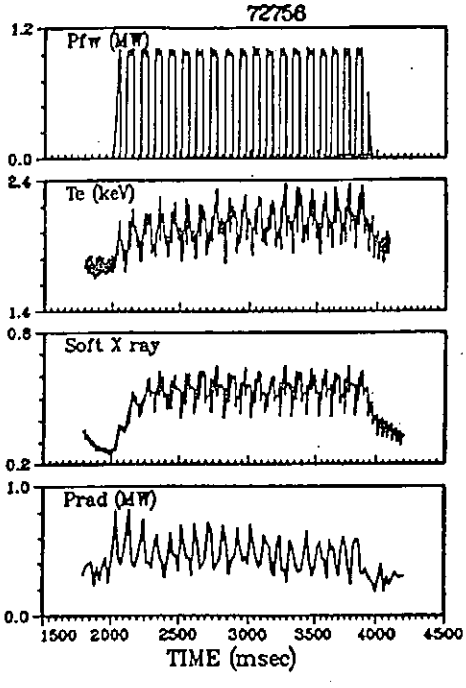

GENERAL ATOMICS

The experimental deposition profile is consistent with the full wave code calculation

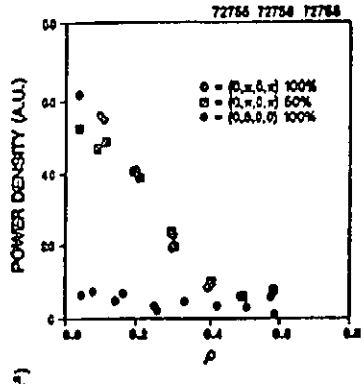

From modulated FW experiments

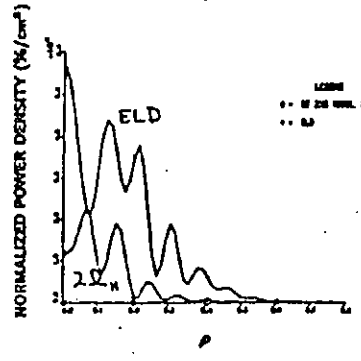

Full wave calculation

GENERAL ATOMICS

A target temperature threshold of $T_e \approx 1$ keV is observed for efficient fast wave heating

$B_T = 1.39$ T

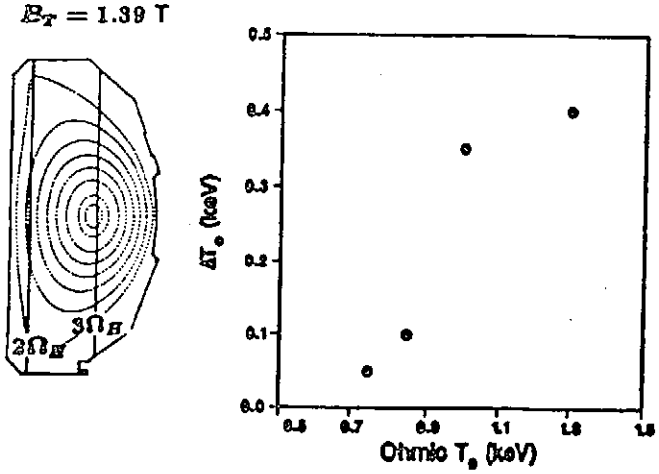

The ohmic electron temperature was scanned by varying the plasma density.

GENERAL ATOMICS

H-mode was obtained with fast wave heating alone for $\omega = 4\Omega_H = 8\Omega_D$

$B_T = 1$ T

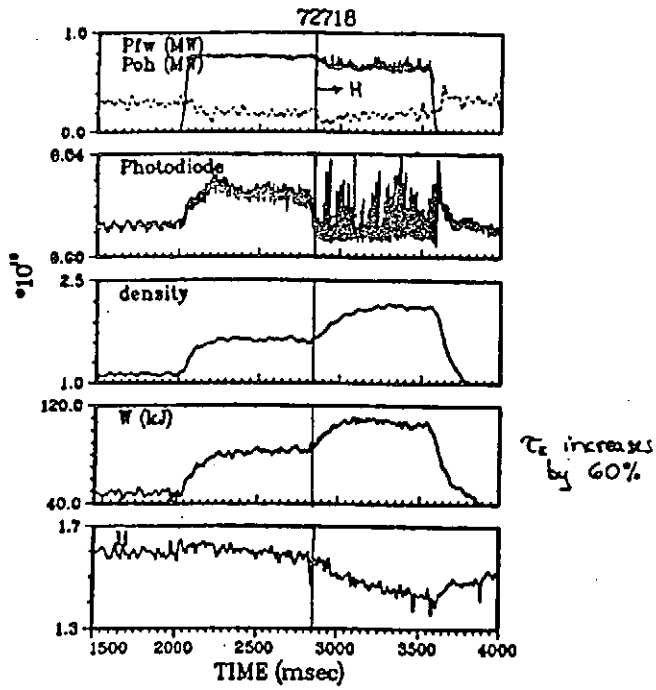

GENERAL ATOMICS

FAST WAVE CURRENT DRIVE

- $\pi/2$ phasing maintained for $P_{FW} \leq 1.2$ MW
- Boronization is highly effective at suppressing impurity generation and radiated power, and it reduces the density increase when the fast waves are applied.
- Electron heating and loop voltage drop are observed.
- Current drive is inferred from comparison of plasma resistance determined from loop voltage with that calculated from neoclassical resistivity.
- Detailed kinetic analysis of best current drive shots indicates a non-inductive current of about 100 kA was driven by 1 MW of fast waves.
- However, the current drive effect is nearly independent of phasing of the antenna ($\pi/2$, $-\pi/2$, 0 π π 0)

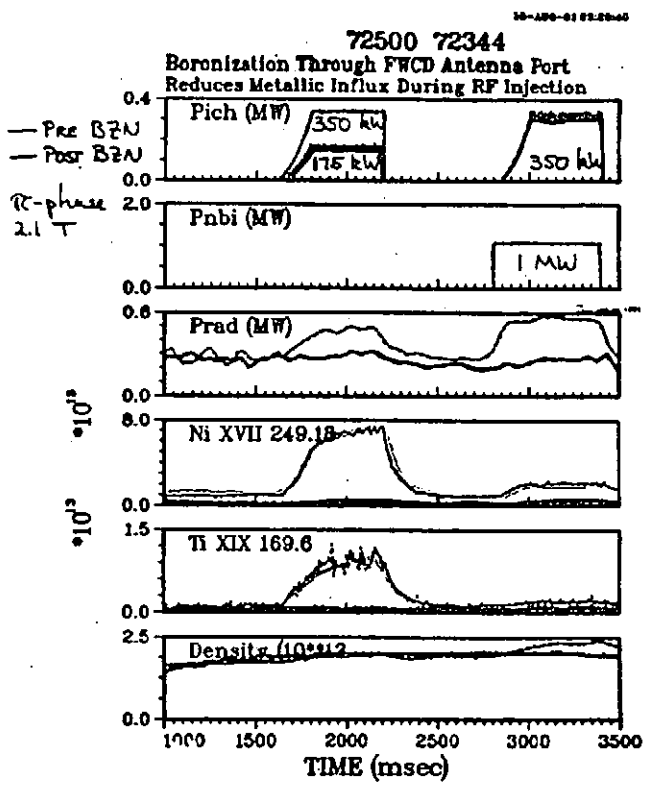

GENERAL ATOMICS

DIII-D FAST WAVE CURRENT DRIVE OPERATION

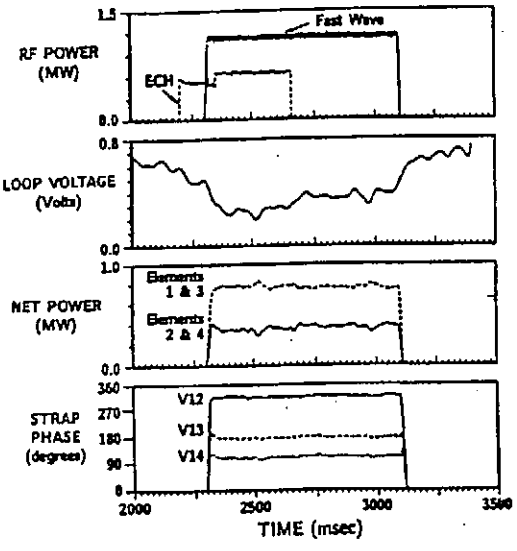

- Antenna phasing sustained
- Loop voltage drops more than electron heating
- Detailed modeling and analysis is ongoing

FAST WAVE CURRENT DRIVE DISCHARGE $\pi/2$ PHASING

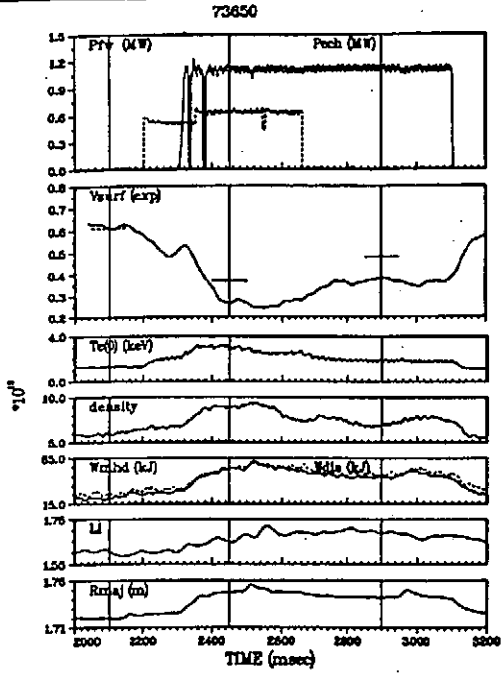

GENERAL ATOMICS

METHOD OF ANALYSIS

- During rf injection, I_p is held constant using feedback control and the rf power level is insufficient to drive all the toroidal current. Thus, the loop voltage during the current drive phase is non-zero; $V_\ell(\mathrm{rf}) \neq 0$.
- Under these conditions, and assuming steady state, the circuit equation becomes:

$$\mathrm{I_{rf}} = \mathrm{I_p} - \mathrm{I_{Boot}} - \frac{V_\ell(\mathrm{rf})}{\mathrm{R_p(rf)}}$$

in which I_{Boot} is the bootstrap current (Hirshman and Sigmar); R_p is the neoclassical resistance of the plasma.

- To calculate $\mathrm{R_p}$, a 1D numerical computation is performed using the measured profiles for $T_e(r)$, $n_e(r)$ and Z_{eff}.
- The validity of the analysis is tested in the Ohmic phase; generally, the measured V_ℓ is reproduced by this analysis to within 5 %.
- Experimental error bars are estimated by assuming a $\pm$ 30 mV error in $V_\ell(\mathrm{rf})$ and then calculating the resulting $\Delta \mathrm{I_{rf}}$.

GENERAL ATOMICS

KINETIC ANALYSES OF FWCD (1 T, 0.4 MA)

Shot/Time (msec)	P_{FW}/P_{ECH} (MW)	FW phasing	P_{OH} (MW)	P_{rad} (MW)	Z_{eff}	$T_e(0)$ (keV)	n_e (10^{13} cm^{-3})	V_ℓ (exp)	I_{Boot} (kA)	I_{CD} (kA)	% Non-inductive	$\frac{\delta_{FB} I_{FB}}{(P_{FW}+P_{ECH})}$
73679/2100	0/0	N.A.	0.24	0.09	2.7	1.5	0.61	0.60	21	0	5	N.A.
73650/2900	1.09/0	CO	0.15	0.47	3.6	2.1	0.70	0.37	41	81±20	31	0.08
73676/2950	0.93/0	CO	0.18	0.44	2.8	1.8	1.01	0.46	42	78±21	18	0.08
73650/2450	1.09/0.63	CO	0.10	0.50	4.6	3.6	0.89	0.26	43	116±27	40	0.08
73676/2500	0.94/0.76	CO	0.10	0.57	2.9	2.6	1.10	0.25	45	91±30	34	0.09
73686/2500	0.99/0.77	CTR	0.11	0.65	3.5	2.4	1.04	0.27	42	132±25	44	0.10

KINETIC ANALYSES OF FWCD (2 T, 0.8 MA)

Shot/Time (msec)	P_{FW}/P_{ECH} (MW)	FW phasing	P_{OH} (MW)	P_{rad} (MW)	Z_{eff}	$T_e(0)$ (keV)	n_e (10^{13} cm^{-3})	V_ℓ (exp)	I_{Boot} (kA)	I_{CD} (kA)	% Non-inductive	$\frac{\delta_{FB} I_{FB}}{(P_{FW}+P_{ECH})}$
73455/3000	0.58/0	CTR	0.36	0.18	3.0	2.6	1.85	0.46	46	92±40	18	0.4
73441/2800	1.05/0	CO	0.33	0.48	3.3	2.5	2.16	0.43	62	99±39	21	0.3
73442/2150	1.02/0.43	CO	0.29	0.62	2.8	2.9	2.40	0.37	78	18±58	12	0.2
73455/2675	0.60/0.68	CTR	0.25	0.75	2.6	4.0	1.79	0.32	58	80±58	18	0.2

GENERAL ATOMICS

EFFECT OF FWCD ON SAWTEETH SAME FOR FORWARD OR REVERSE PLASMA CURRENT

Forward Current

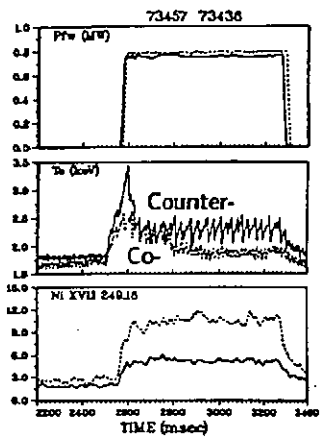

Reverse Current

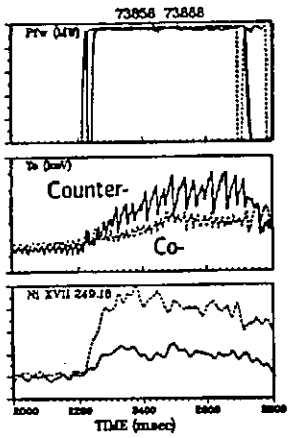

Conclusion: Antenna spectrum is directional

Tail formation (<40keV) during 2T FWCD experiment was observed clearly. Tail temperature for CO phasing is twice as large as CTR phasing.

#73860 (CTR) : P_{FW}=1.2MW, $\Delta\phi$=-105°, $Te(0)|_{2.7s}$=2.04keV, $Te(0)|_{2.0s}$=1.40keV

#73868 (CO) : P_{FW}=1.1MW, $\Delta\phi$=85°, $Te(0)|_{3.0s}$=1.70keV, $Te(0)|_{2.0s}$=1.45keV

X-ray : OH case Δt=1.75-2.15s, Te(0)=1.4keV
CTR case Δt=2.5-2.75s, T-tail~3keV
CO case Δt=2.75-3.0s, T-tail~6.6keV

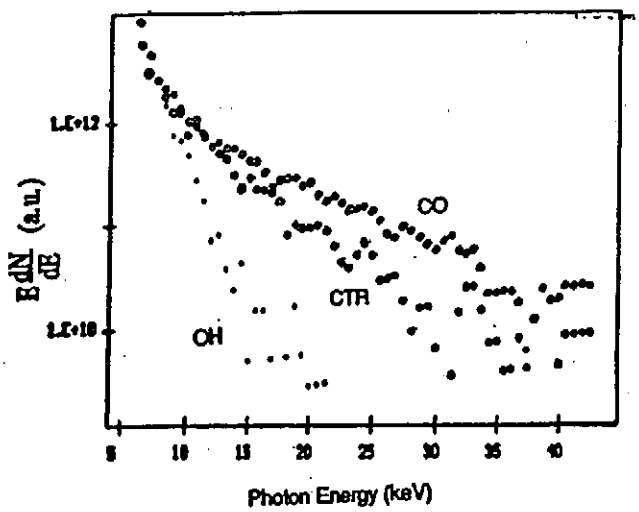

GENERAL ATOMICS

Summary of Status

- Absorption of FW exceeds single-pass damping, but target plasma temperature has to exceed some threshold.
- Direct FW electron heating can be highly efficient over a wide range of conditions.
- Efficient FWCD has been observed, but it is independent of directionality of antenna.

GENERAL ATOMICS

Future Focus

- Increase target plasma temperature to test strong single pass absorption regime.
- Reduce impurity level and control density rise. Boronization and new antenna will help.
- Raise FW transmitter output to 2 MW and explore fully noninductive current drive.

GENERAL ATOMICS

PLANS FOR FAST WAVE EXPERIMENTS

- During spring experimental run
  - — Test feasibility for ITER of FW heating without Faraday screen
  - — Improve single pass damping

- In late spring, install new Faraday shield to reduce impurities and improve the loading
  - — Tilted bars
  - — Low Z coating (B_4C)
  - — Single layer
  - — Current straps closer to plasma
  - — Insulating layer of B_4C around outside of frame of Faraday shield
  - — Reflectometer for measurement of local density profile

- Add a second 2 MW system and antenna at 60–120 MHz

Combined Current Drive of EC and LH Waves in WT-3

T. Maekawa, T. Maehara, T. Kishino
Y. Kishigami, K. Makino, T. Minami
K. Hanada, Y. Terumichi, S. Tanaka

Dept. of Phys., Kyoto Univ.

M. Nakamura
Osaka Inst. of Technology

WT-3 TOKAMAK
MAJOR RADIUS 65 cm
MINOR RADIUS 20 cm
TOROIDAL FIELD 1.75 T

LOWER HYBRID
KLYSTRON (2 GHz, 350 kW, 100 ms)
2 x 4 WAVE GUIDE LAUNCHER

ELECTRON CYCLOTRON
GYROTRON (56 GHz, 200 kW, 100 ms)
Vlasov Antenna + Elliptical Reflector

LHCD Flat-top Discharge with $I_p \simeq 80$ kA

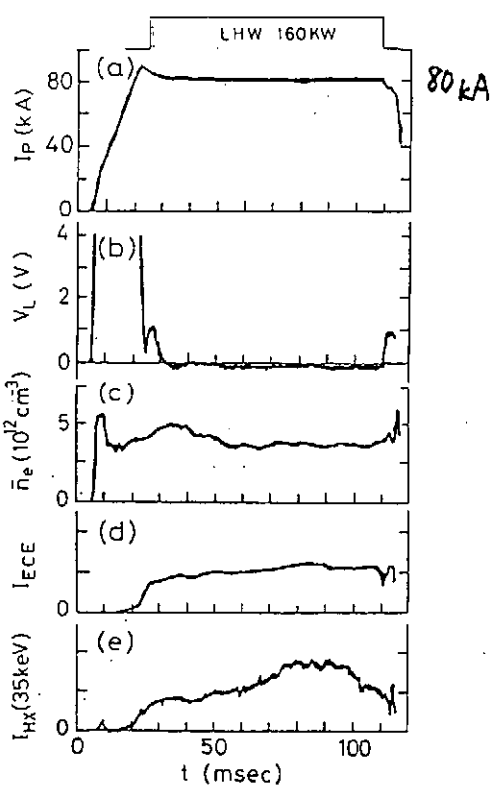

ECCD Flat-top Discharge with $I_p \simeq 70$ kA

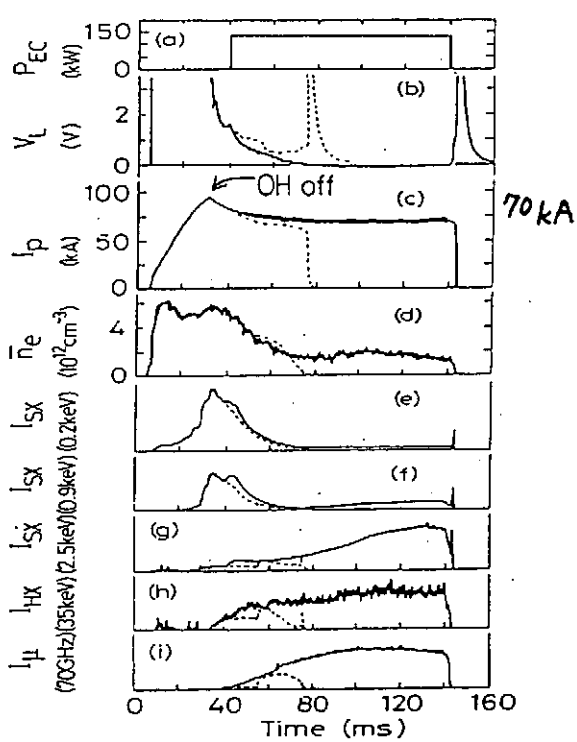

Motivation of Combined Current Drive

- Efficient ECCD by heating of fast electron tail in LHCD plasma
- Combined effect of the resonant interaction in momentum space

J/Pd in a relativistic plasma

[N.J. Fisch PHYS REV. A 24 (1981) 3245]

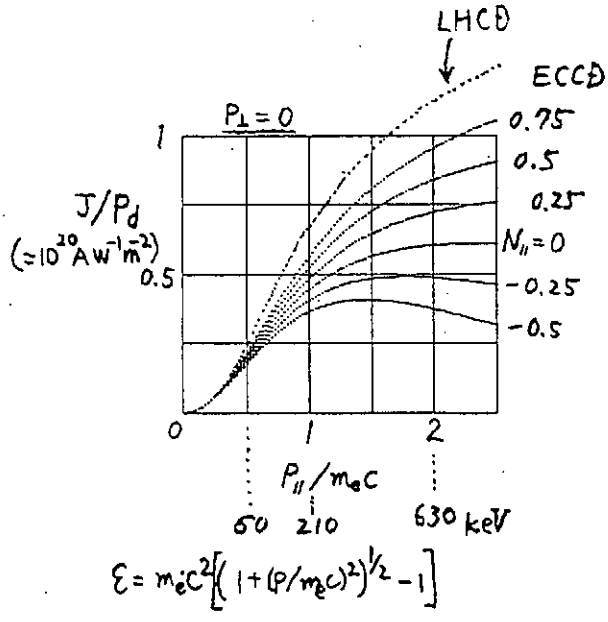

$$\mathcal{E} = m_e c^2 \left[\left(1 + (p/m_e c)^2 \right)^{1/2} - 1 \right]$$

Combined Current Drive (LH+EC)

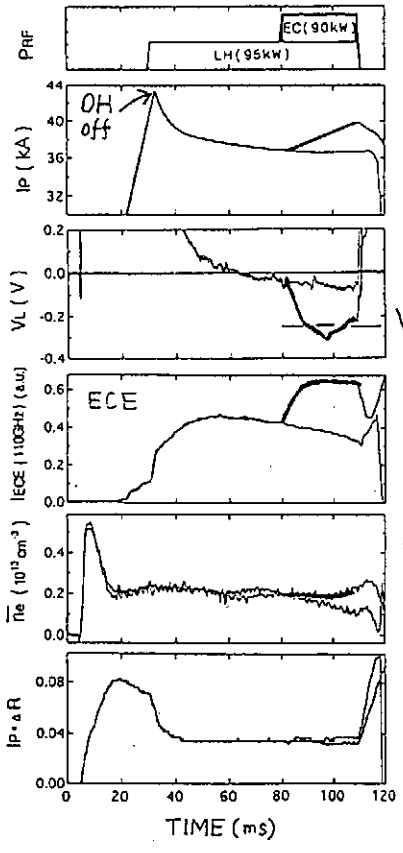

$\frac{dI_p}{dt} \simeq 100$ kA/s

37 kA → 40 kA during 30 msec

$V_L = -0.25$ V

$\bar{n}_e \leq 2 \times 10^{12}$ cm^{-3}

No bulk Electron Heating

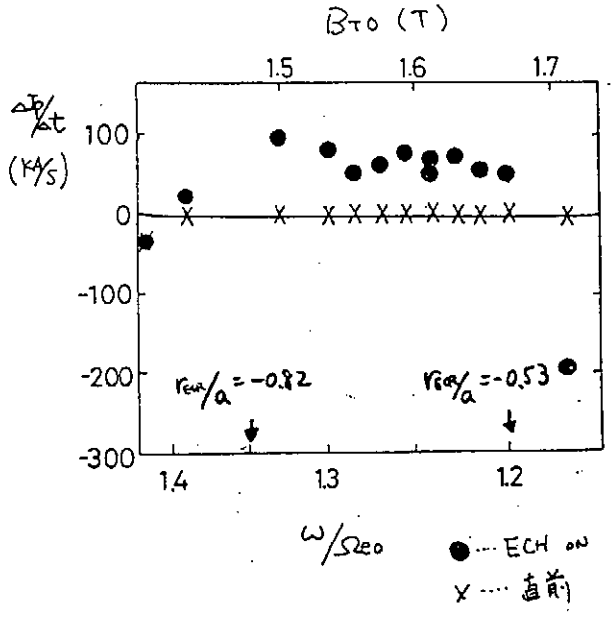

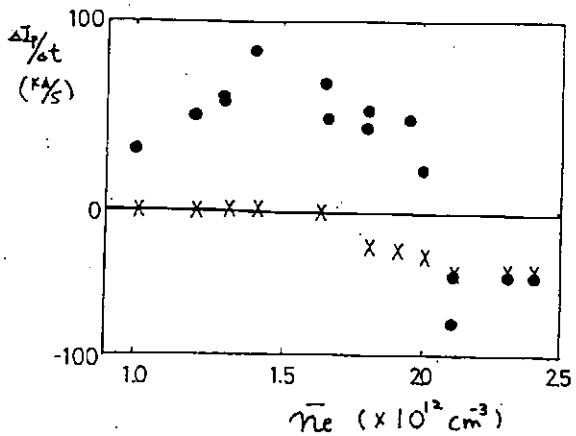

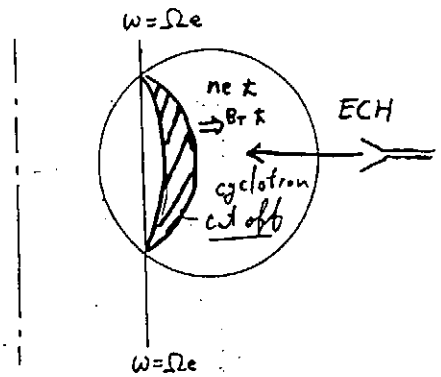

ECR Condition of Tail Electron

$\gamma = N_{\parallel} P_{\parallel} + \Omega_e/\omega$ (Fundamental)

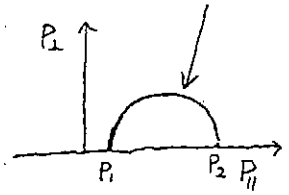

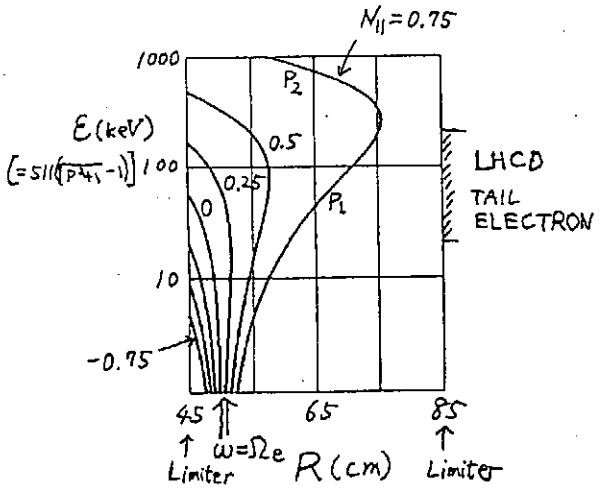

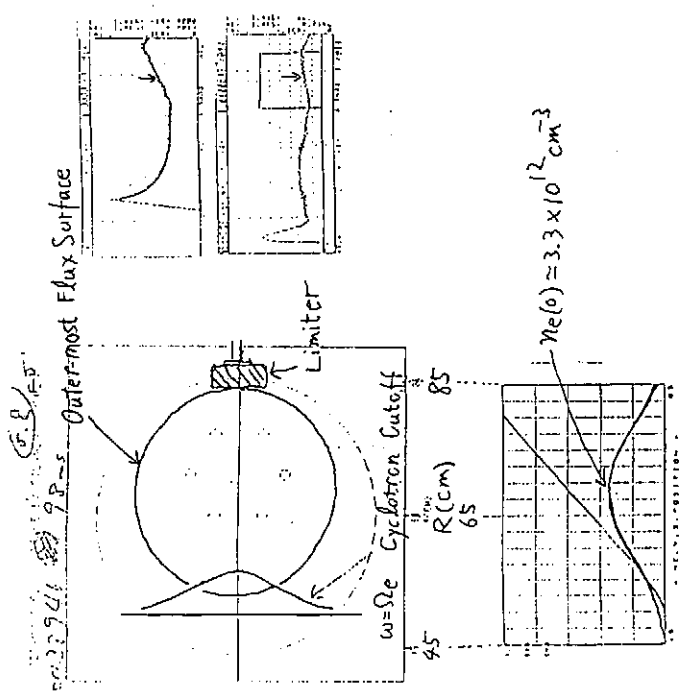

ECH Injection Antenna

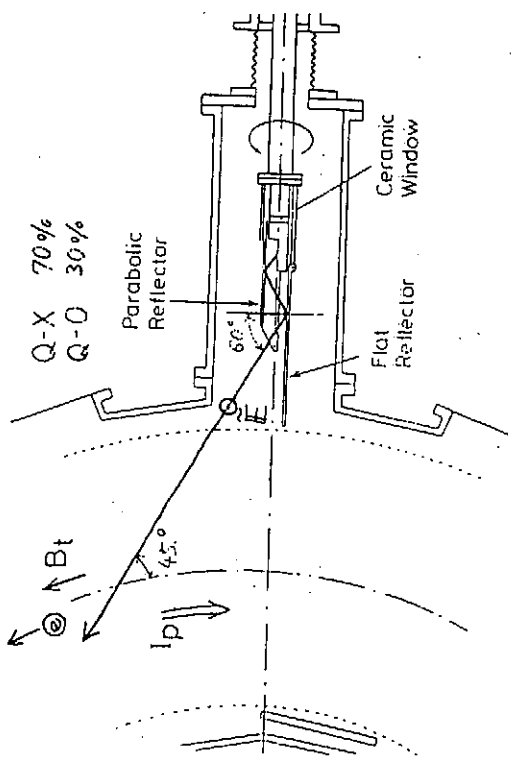

Increasing Rate of Poloidal Magnetic Energy

$$P_M = -V_L \cdot I_p + \frac{d}{dt}\int_{VESSEL}\left[B_\theta^2/2\mu_0\right] dV_{02}$$

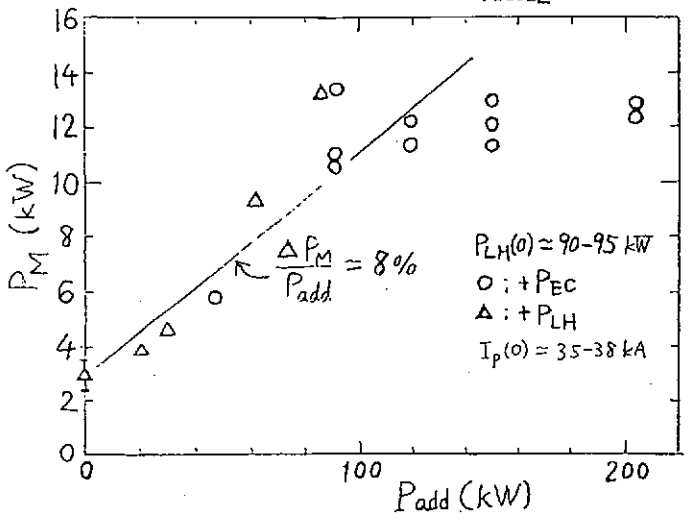

'91. 6/12 6/27

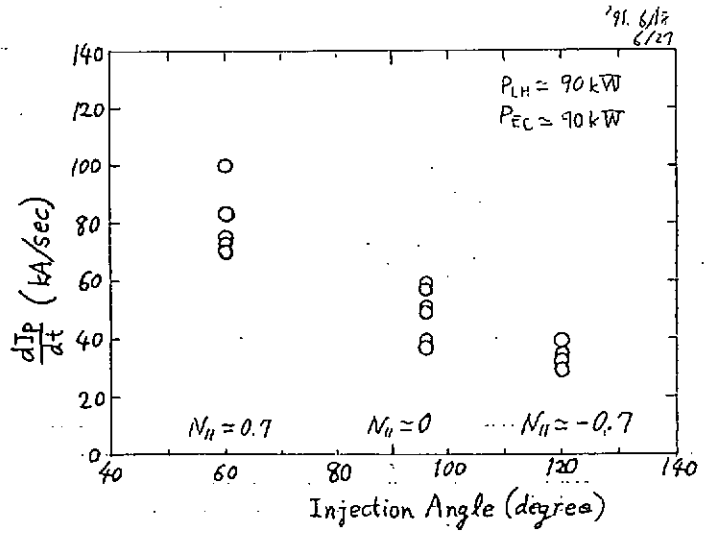

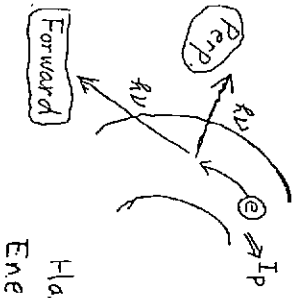

Hard X-ray Energy Spectra.

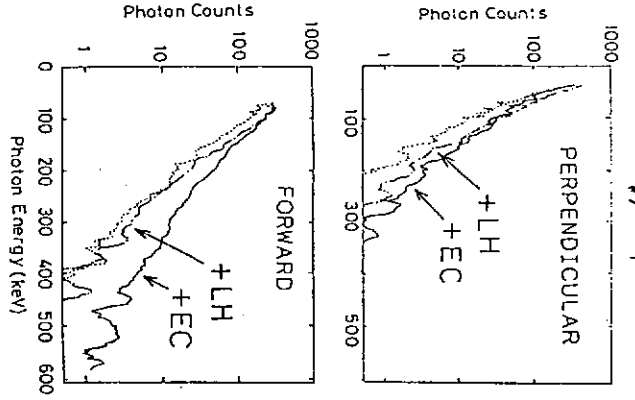

LH Step-Up Injection (LH+LH)

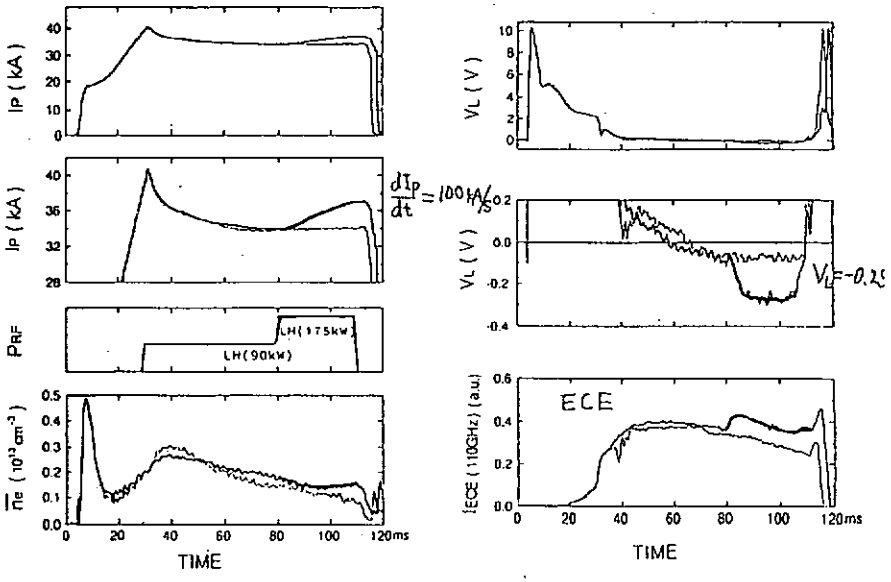

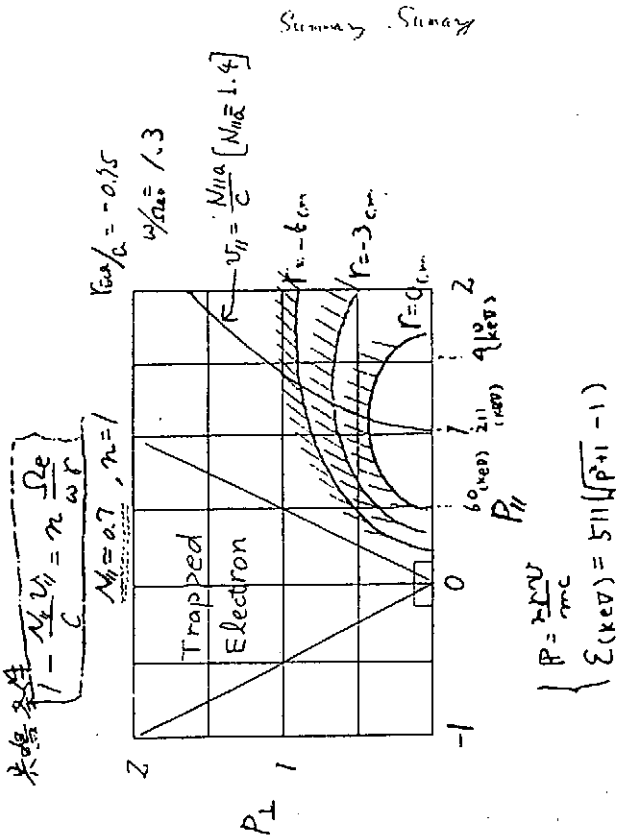

Parallel Momentum Input

	Loop Voltage	ECW
$\frac{\Delta P_{\parallel}}{\Delta \mathcal{E}}$	$\frac{eE}{e \cdot v_{\parallel} \cdot E} = \frac{1}{v_{\parallel}} \gtrsim \frac{1}{c}$	$\frac{k_{\parallel}}{\omega} = \frac{N_{\parallel}}{c}$
$\Sigma \Delta \mathcal{E}$	$\simeq V_L \cdot I_p \sim 10$ kW $V_L = -0.25$ V, $I_p = 40$ kA	$P_{EC} = 90$ kW $\alpha P_{EC} \sim 60$ kW $\alpha \simeq 0.7$ (O-X mode)
$\Sigma \Delta P_{\parallel}$	$\gtrsim \frac{10}{c}$	$\sim 60 \frac{N_{\parallel}}{c} \simeq \frac{40}{c}$ $N_{\parallel} = 0.7$

Summary

1. Current ramp-up by EC heating of fast electron tail in LHCD plasma
   Absorption of EC waves via fundamental resonance of oblique X-mode.
2. Ramp-up rate is similar to LH step-up injection case.
   $\Delta I_p / \Delta t = 100$ kA/s $\Delta P_M / P_{add} \simeq 8\%$
3. But, tail electron momentum distribution is different.
   - More energitic in parallel direction in EC case.
     - Parallel momentum input from EC waves
     - Combined diffusion

JAPAN-US WORKSHOP ON RF HEATING AND CURRENT DRIVE IN CONFINEMENT SYSTEM TOKAMAKS
NIFS, 18TH-21TH, NOV., 1991

PLANS OF RF HEATING AND RELATED R×D FOR LARGE HELICAL DEVICE

National Institute for Fusion Science
K.Akiba K.Masahara S.Kubo K.Kawamura T.Saroh
K.Sato F.Shibo T.Takita T.Watari

LARGE HELICAL DEVICE PROJECT

Large Helical Device project is being pursued in NIFS.

The LHD is a Heliotron/Torsatron type superconducting machine.

The basic design parameters of the device are:

poloidal pitch number of helical coil = 2
toroidal pitch number = 10
toroidal magnetic field =3T-4T
coil current = 7.8 MA
major radius = 3.9 m
plasma minor radius = 0.5-0.6m
heating power in plasma = 20 MW

PHSICAL OBJECT

To produce currentless steady state high temperature plasma

To conduct various experimental programs to develop helical fusion system as an alternative approach of tokamak

OBJECT OF ECH

* plasma production
* Transport analysis
* Electron root confiment
* Potential control
* Steady state heating

SPECIFICATION OF ECH SYSTEM

* Frequency 84(~112)GHz
* Power/Pulse 10 MW(10sec.)
  width 3 MW(CW)
* Gyrotron 10 tubes

OBJECT OF ICRF

* Heating profile control
* High Ti mode heating
* Energetic ion tail for Simulation of α particle
* Steady state heating

SPECIFICATION OF ICRF SYSTEM

* Frequency 25~100 MHz
* RF power 9 MW
* Pulse width 10 sec (9MW)
  CW (3MW)

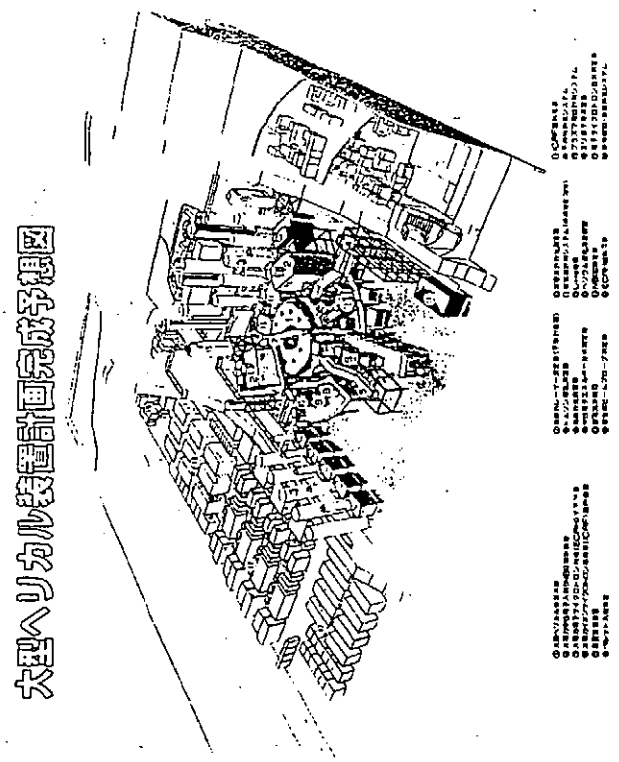
大型ヘリカル装置計画完成予想図

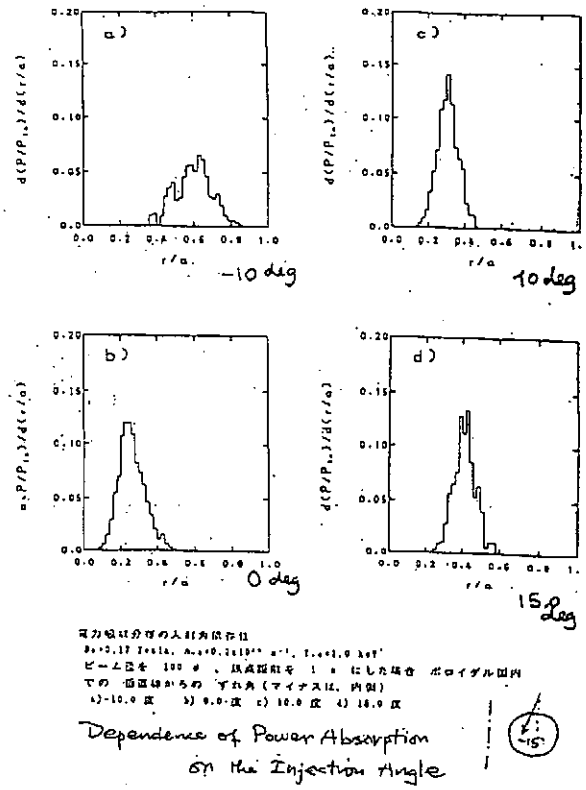
a)
b)
c)
d)
−10 deg
0 deg
10 deg
15 deg
Dependence of Power Absorption on the Injection Angle

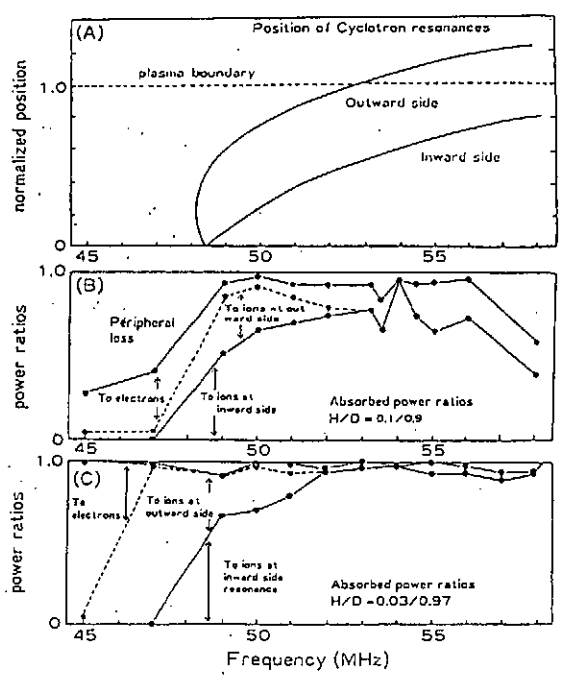
(A)
Position of Cyclotron resonances
plasma boundary
Outward side
Inward side
normalized position
(B)
Peripheral loss
To electrons
To ions at inward side
Absorbed power ratios H/D = 0.1/0.9
power ratios
(C)
To electrons
To ions at outward side
To ions at inward side resonance
Absorbed power ratios H/D =0.03/0.97
Frequency (MHz)

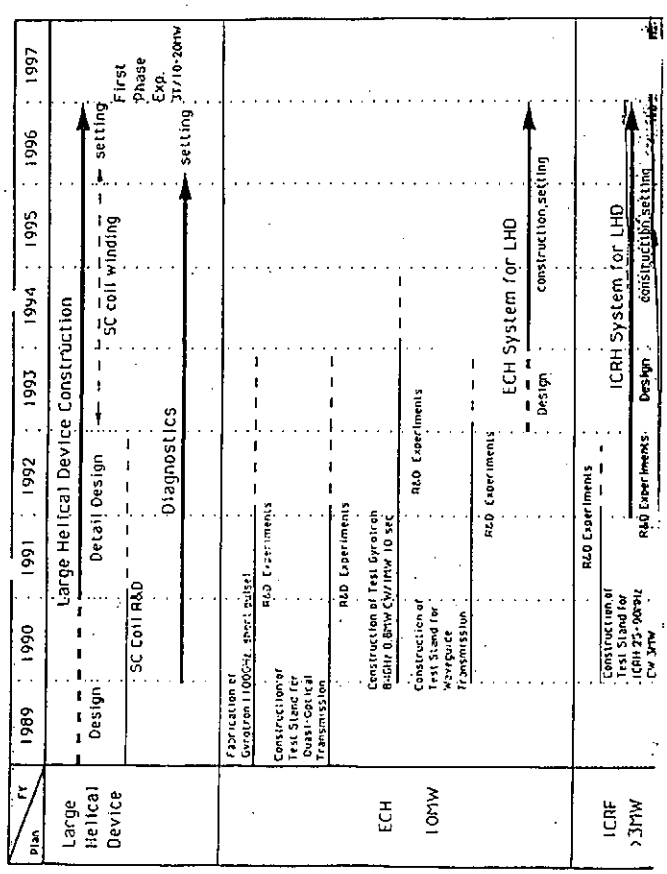
FY
Plan
1989
1990
1991
1992
1993
1994
1995
1996
1997
Large Helical Device
Design
Detail Design
Large Helical Device Construction
SC coil winding
setting
First Phase Exp.
SC Coil R&D
Diagnostics
setting
ECH
10MW
ECH System for LHD
ICRF
>3MW
ICRH System for LHD
R&D Experiments
Design
construction setting

R&D OF ICRF SYSTEM FOR LHD

* Antenna
  - Physical reserch in CHS, JIPPT-IIU and Heliotron-E
  - Theoretical analysis
    Conductor, Faraday shield. Feed-through designs
* Transmission Line
  - Fast response tuner
  - High power dummy Load
  - Cooling for transmission line
  - dc break

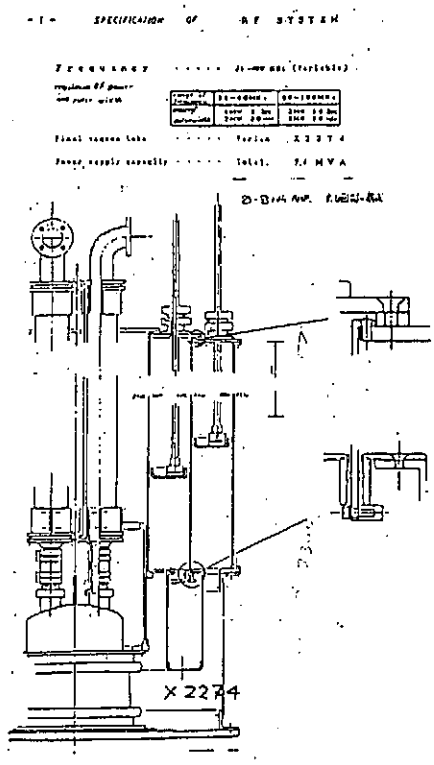

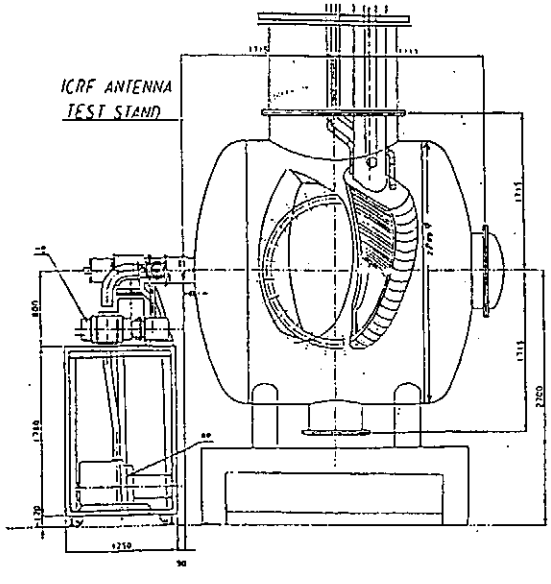

Feed-back Control Matching Circuit System

Frequency Modulation

- According to the change of the plasma loading resistance, the most relevant frequency, f + δf is selected to get the impedance matching.
  quick response

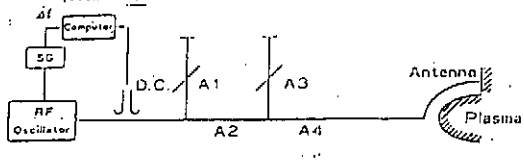

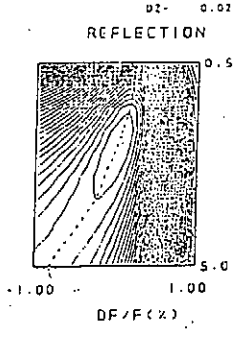

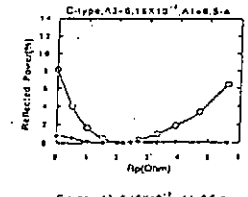

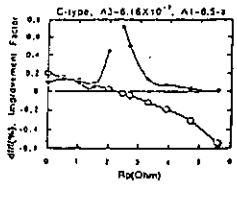

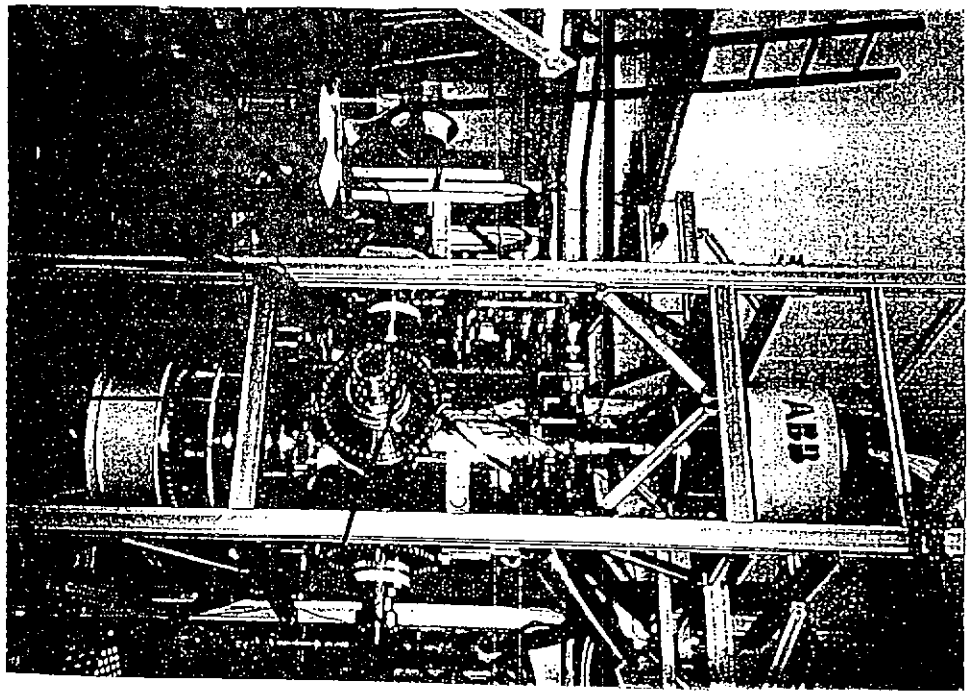

Temperature Increase of the Coaxial Cable in High Power Steady State Operation

$R = 0.0842 \cdot f^{1/2} / d$ (Ω/m)

f : frequency
d : diameter of the coaxial tube

dissipated power, $q = I^2 R$

transmitted power, $P = I^2 Z_0$

$q = P \cdot R / Z_0$

f = 42.5 MHz
d_{in} = 86.3 mm
d_{out} = 203 mm
Z_0 = 50 Ω
P = 3 MW

q_{in} = 373 W/m q_{out} = 162 W/m

In the impedance matching circuit for the plasma loading resistance, R_L = 4 Ω,

transmitted power, $P = I^2 R_L$

$q' = P \cdot R / R_L = q (Z / R_L)$

q'_{in} = 4860 W/m, q'_{out} = 2020 W/m

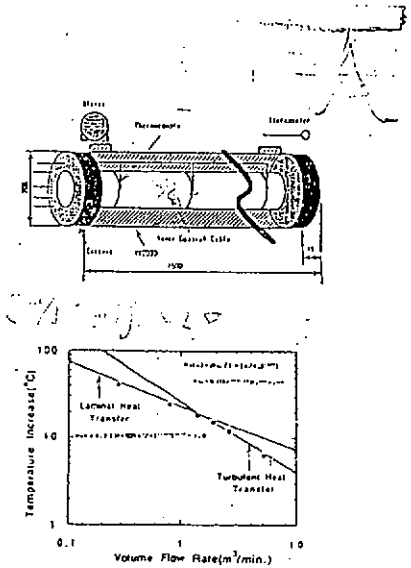

WHISPERING GALLERY GYROTRON

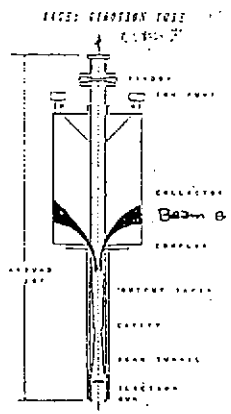

R&D OF 44GHz GYROTRON

TYPE	WHISPERING GALLERY MODE
GUN	MAGNETRON INJECTION
FREQUENCY	44GHz, 5GHz
OUTPUT MODE	TE.., WHICH BE MODE-TRANSFORMED TO TEM..
MODE PURITY	>95%
PULSE WIDTH	1MW 1MS DESIGN VALUE 0.8MW CW DESIGN VALUE
EFFICIENCY	30% MINIMUM
TYPE	MICROWAVE-BEAM SEPARATION
VOLTAGE	80KV, 81KV
BEAM CURRENT	62A MAXIMUM
SC MAGNET	3T-4T

R&D OF ECH SYSTEM FOR LHD

* Gyrotron

- Whispering gallery type (Varian/Toshiba)
- Quasi-optical type (ABB/CRPP)
- Power supply (Nissin Electric)

Power test will start in 1992 at the Toki-site

* Transmission Line

- Corrugated waveguide (Nitubishi Electric)
- Gaussian beam (Furukawa Electric)

Low power test is being carried out

TRANSMISSION LINES
FOR LHD

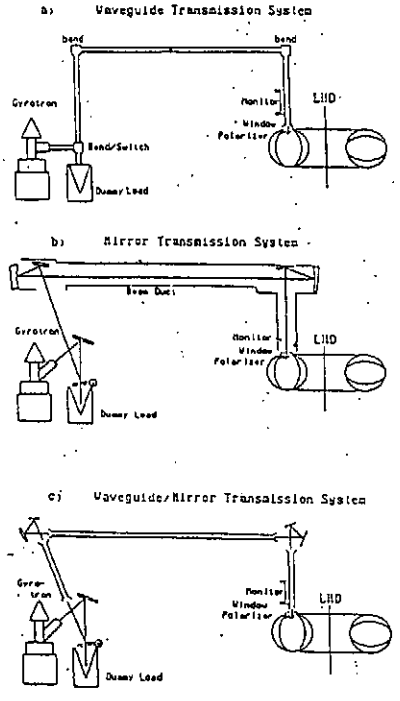

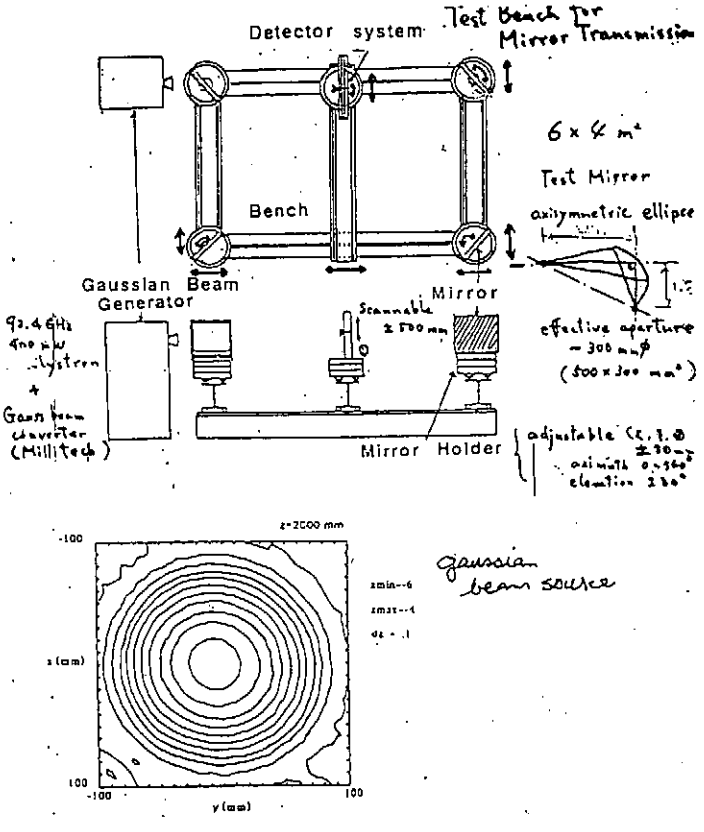

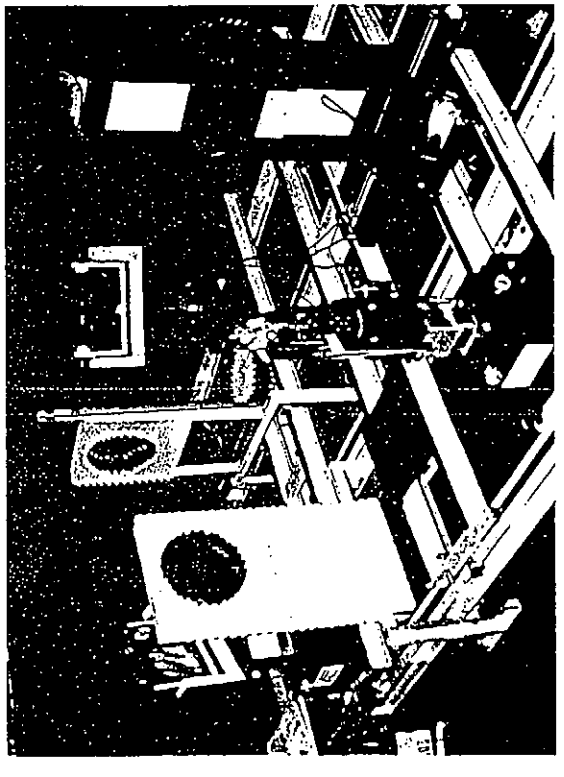

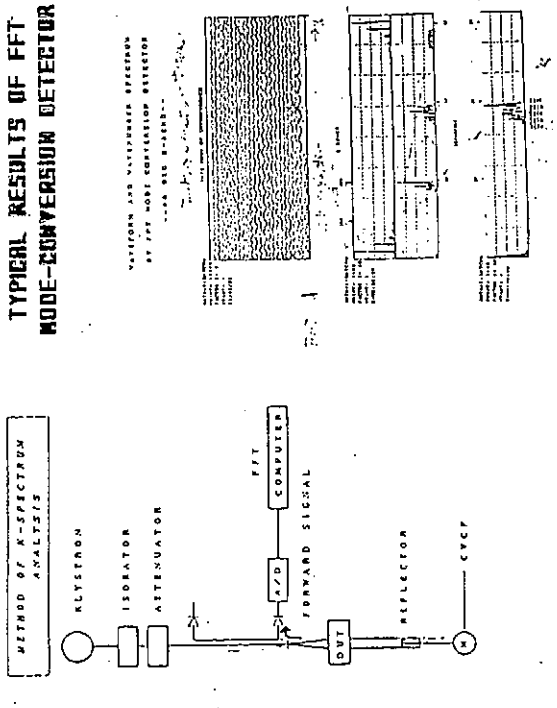

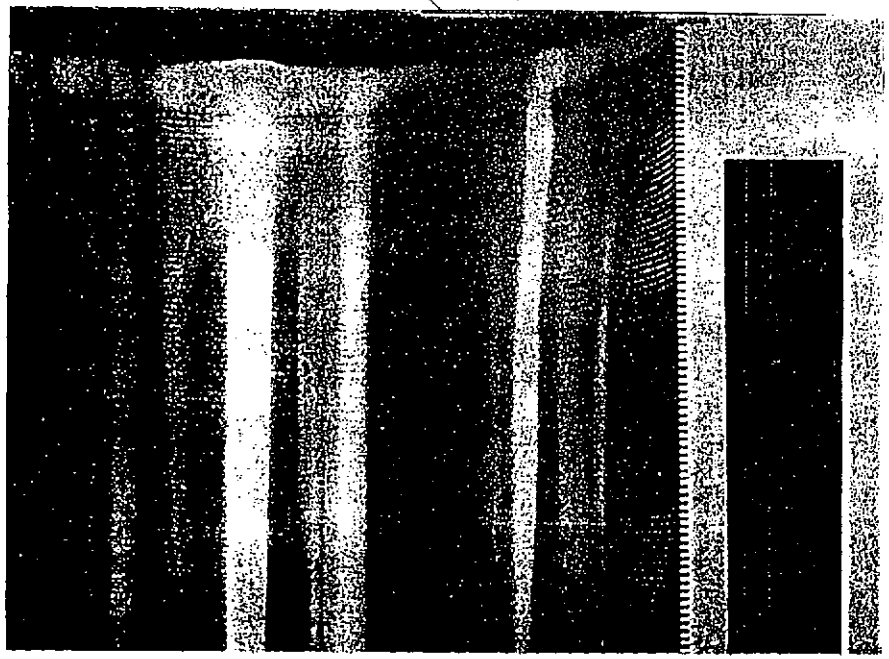

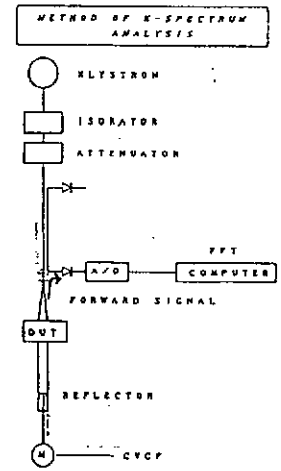

TYPICAL RESULTS OF FFT MODE-CONVERSION DETECTOR

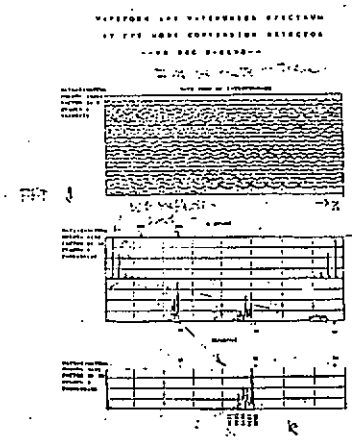

TAPER WAVEGUIDE SYSTEM FOR H11

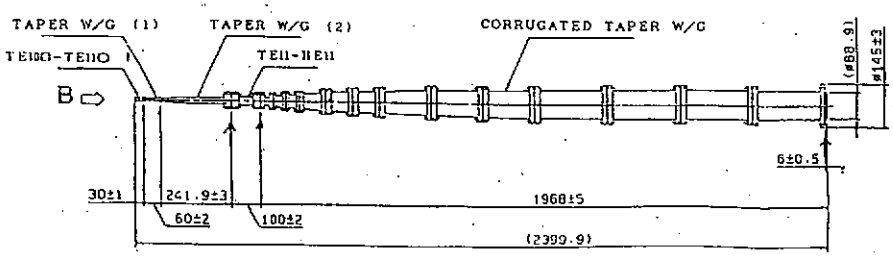

TEST STAND FOR R&D OF CORRUGATED WAVEGUIDE TRANSMISSION SYSTEM

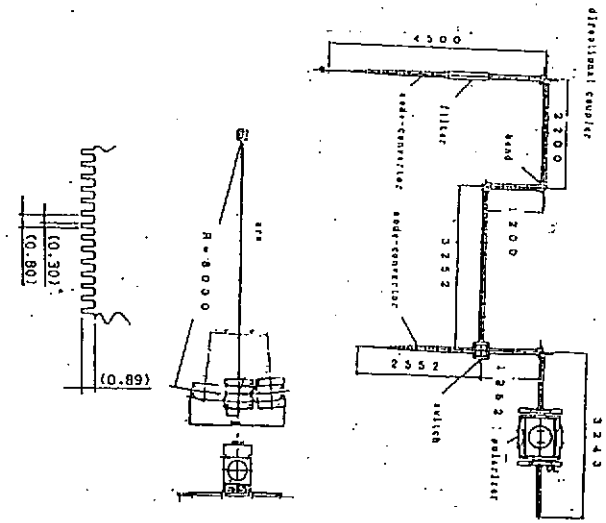

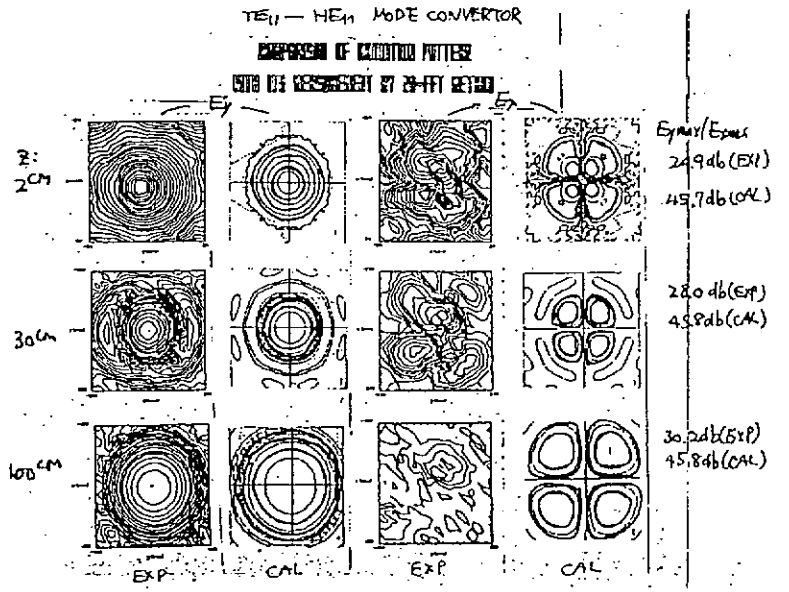
TE11 — HE11 MODE CONVERTOR
Ey
Ex
Z:
2CM
30CM
60CM
EXP
CAL
EXP
CAL
Eymax/Exmax
24.9db(EXP)
45.7db(CAL)
28.0 db(EXP)
45.8db(CAL)
30.2db(EXP)
45.8db(CAL)

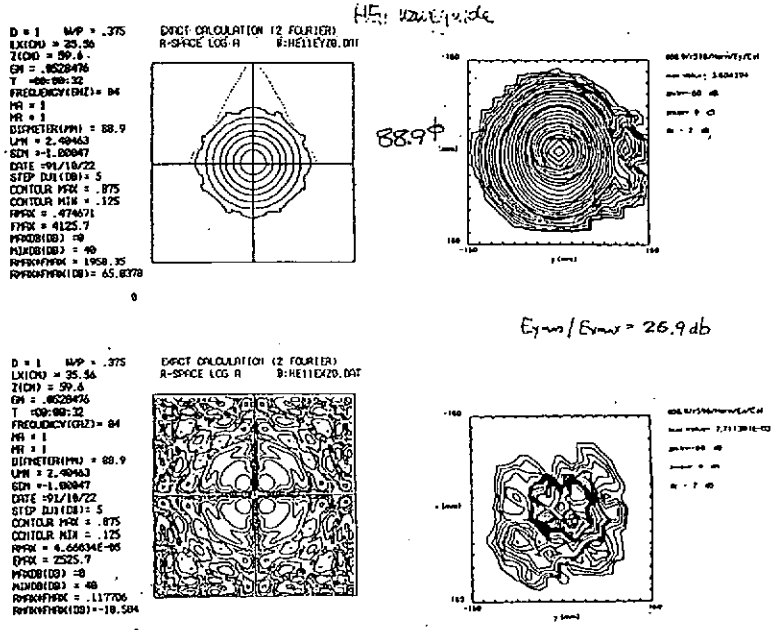
HE11 waveguide
D = 1 W/P = .375
LX(CM) = 35.56
Z(CM) = 59.6
EM = .0528476
T =00:00:32
FREQUENCY(GHZ)= 84
MX = 1
MR = 1
DIAMETER(MM) = 88.9
LMM = 2.49463
SDM =-1.00047
DATE =91/10/22
STEP DB(DB)= 5
CONTOUR MAX = .875
CONTOUR MIN = .125
MMAX = .474671
FMAX = 4125.7
MMAXDB(DB) =0
MMINDB(DB) = 40
RMAXAFMAX = 1958.35
RMAXAFMAX(DB)= 65.8378
0
EXACT CALCULATION (2 FOURIER)
R-SPACE LOG-R B:HE11EX20.DAT
88.9φ
Eymax / Exmax = 26.9 db
D = 1 W/P = .375
LX(CM) = 35.56
Z(CM) = 59.6
EM = .0528476
T =00:00:32
FREQUENCY(GHZ)= 84
MX = 1
MR = 1
DIAMETER(MM) = 88.9
LMM = 2.49463
SDM =-1.00047
DATE =91/10/22
STEP DB(DB)= 5
CONTOUR MAX = .875
CONTOUR MIN = .125
MMAX = 4.656634E-05
FMAX = 2525.7
MMAXDB(DB) =0
MMINDB(DB) = 40
RMAXAFMAX = .117706
RMAXAFMAX(DB)=-18.584
0
EXACT CALCULATION (2 FOURIER)
R-SPACE LOG-R B:HE11EX20.DAT

US-Japan Workshop on RF Heating and Current Drive in Confinement System Tokamaks, Nagoya, Nov. 18-21, 1991

FAST WAVE HEATING AND CURRENT DRIVE IN JT-60/60U

H. Kimura and T. Fujii

Naka Fusion Research Establishment
Japan Atomic Energy Research Institute

With acknowledgements to

M. Saigusa, S. Moriyama, M. Yamagiwa, K. Hamamatsu, Y. Kusama, K. Tobita, M. Nemoto, K. Nagashima, H. Takeuchi, M. Kuriyama, T. Imai, T. Yamamoto and A. Fukuyama*

* Faculty of Engineering, Okayama University

OUTLINE

1. Summary of JT-60 ICRF Experiments (120MHz, 13/MHz)
   - Power injection capability
   - Optimization of second harmonic heating
   - Third harmonic heating
   - Sawtooth stabilization
   - FWEH+LHCD
2. ICRF Experimental Plan on JT-60U
3. Analysis of FWCD Ability on JT-60U

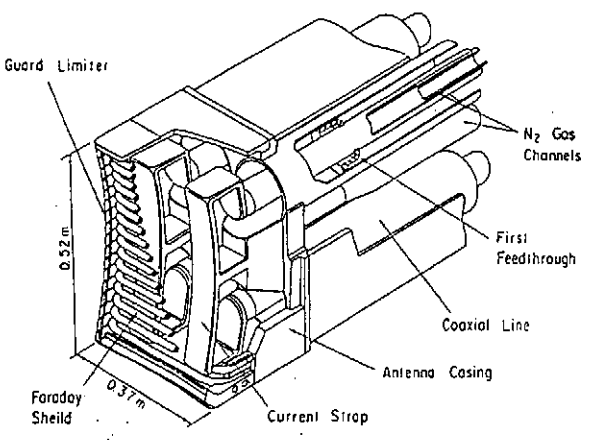

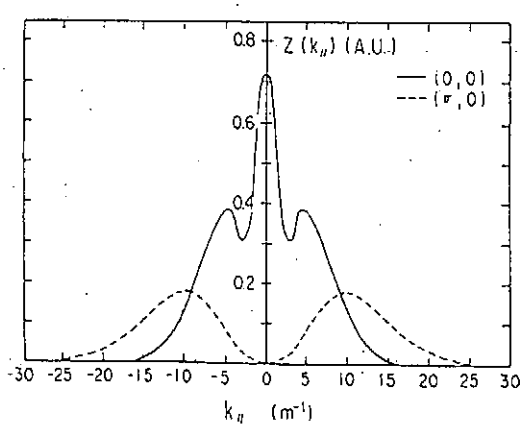

ANTENNA POWER DENSITY AT THE FARADAY SHIELD VS. INJECTION POWER PER ONE ANTENNA

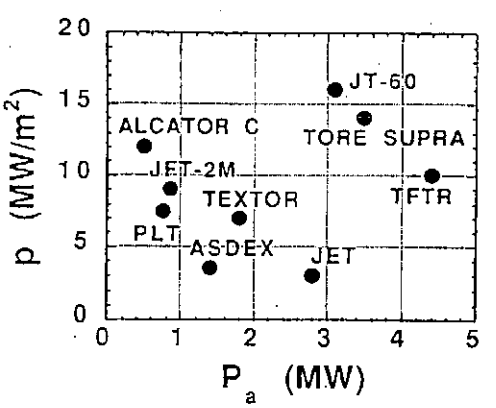

• The antenna power density at the Faraday shield reached 16MW/m² in JT-60, which is the highest value among the ICRF systems in the world.

POWER INJECTION CAPABILITY VS. ANTENNA-PLASMA DISTANCE

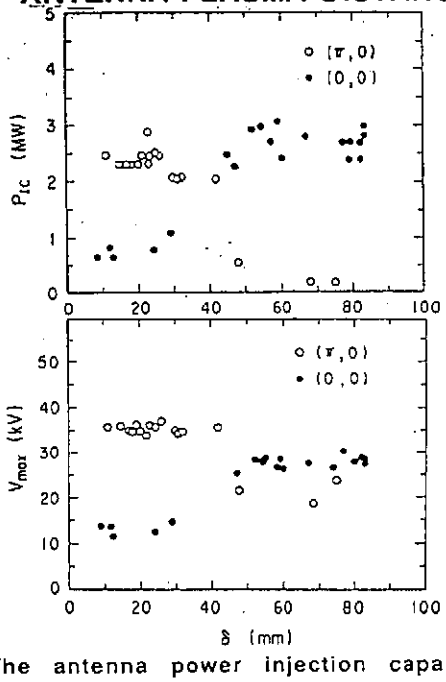

• The antenna power injection capability is inversely dependent on the antenna-plasma distance between in-phase (low-$k_{||}$) mode and out-of-phase (high-$k_{||}$) mode.

IN-PHASE MODE INJECTION

• Spectral line intensity of Ti increases significantly with small δ.

P_{IC} = 0.5 - 1.8 MW $\bar{n}_e$ = 1.9 - 3.4 x 10^{19} m^{-3}

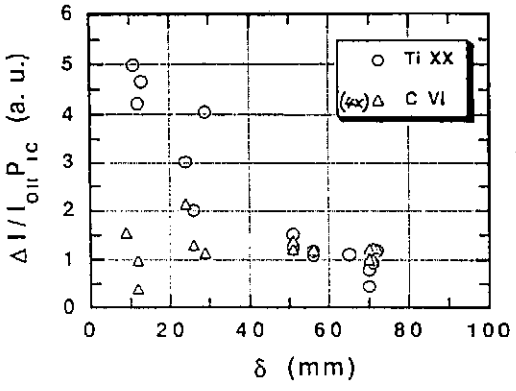

• Faraday Shield coating material; TiC

• Power limitation is due to the enhanced interactions between edge plasma and the Faraday Shield.

• The result may be explained by the RF sheath model.

FREQUENCY FEEDBACK CONTROL FOR AUTOMATIC ANTENNA IMPEDANCE MATCHING

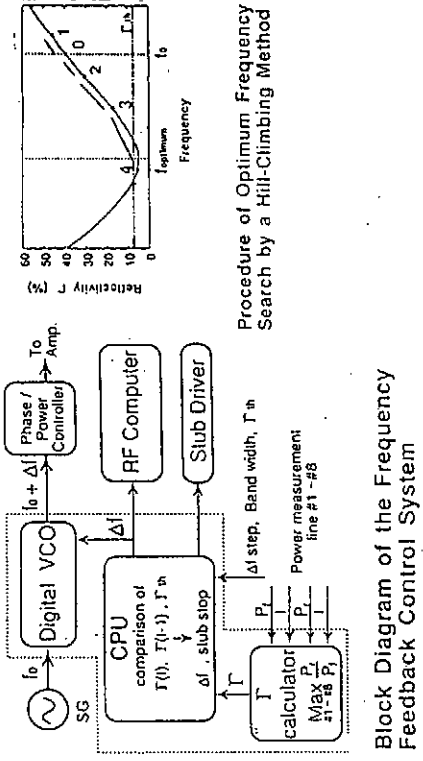

TYPICAL EXAMPLES OF FREQUENCY FEEDBACK CONTROL

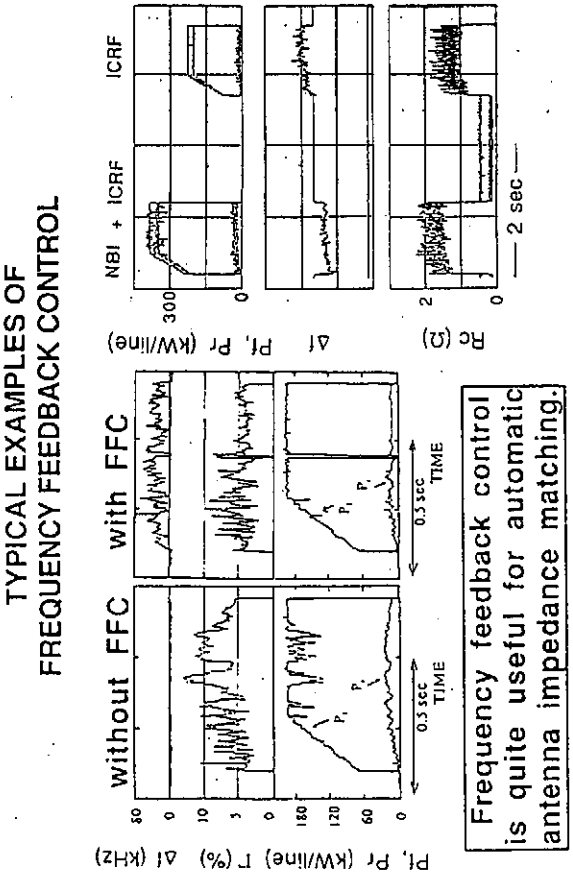

Frequency feedback control is quite useful for automatic antenna impedance matching.

SECOND HARMONIC HEATING RESULTS

- τ_E^{inc} of the out-of-phase (high-$k_{||}$) mode is about 50% better than that of the in-phase (low-$k_{||}$) mode.
- Minority hydrogen 2nd harmonic heating in helium discharges is found to be more effective in the wide electron density range.
- Efficient beam ion acceleration is observed in combined 2nd harmonic ICRF and NBI heating.

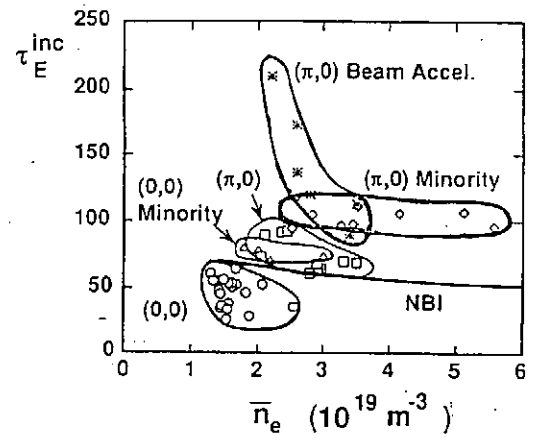

Hydrogen Minority Second Harmonic Heating in Helium Discharges

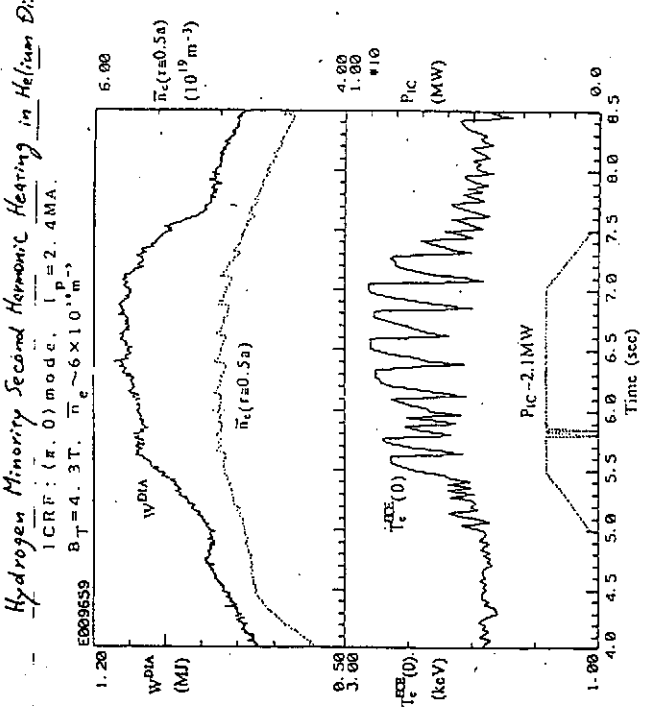

Beam Ion Acceleration by Second Harmonic ICRF Heating

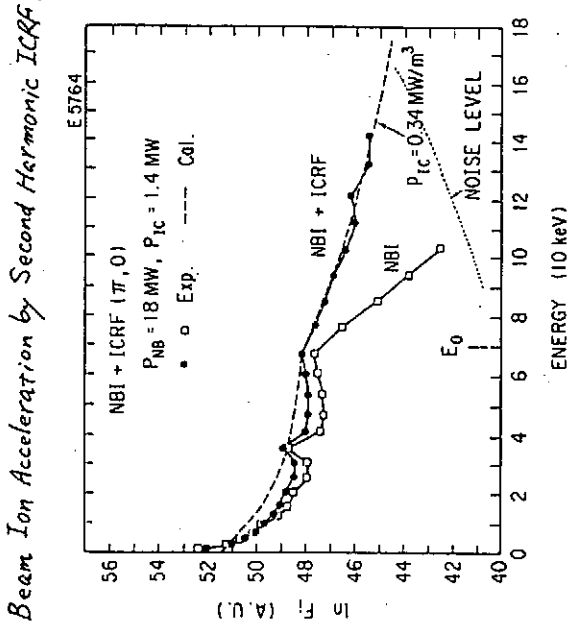

THIRD HARMONIC ICRF HEATING IN COMBINATION WITH NBI

(1) Strong Central Heating

(2) Giant Sawtooth
sawtooth period ~ 6 × τ_E

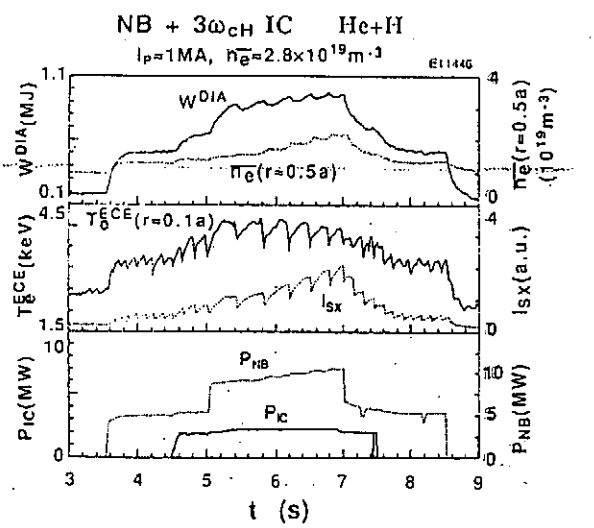

BEAM ION ACCELERATION BY THIRD HARMONIC ICRF WAVES

ICRF power density p_{IC} ~ 1MW/m³
power deposition radius Δr ~ 0.2m

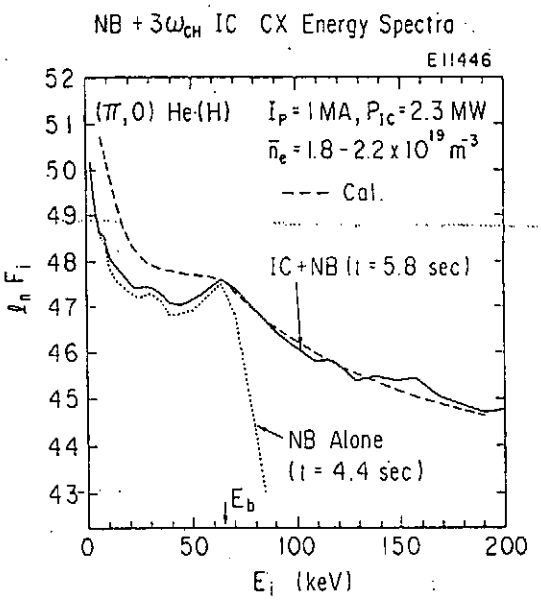

Enhancement of energ confinement can be explaine by fast ion stored energy.

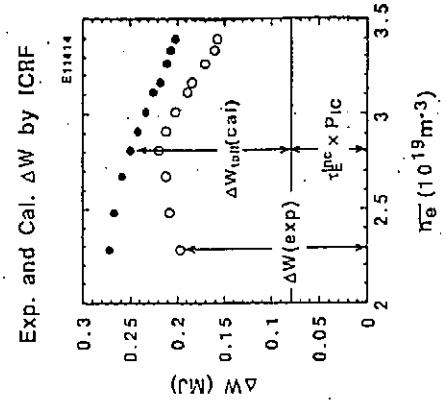

Energy Confinement Time of 3ω_CH ICRF + NBI Heating

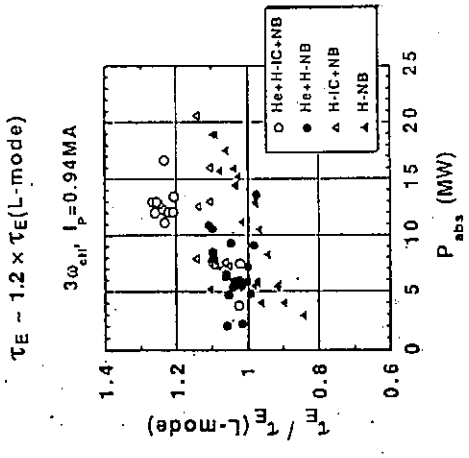

SECOND HARMONIC MINORITY HEATING

SAWTOOTH PERIODS VS. P_{IC}, $\bar{n}_e$

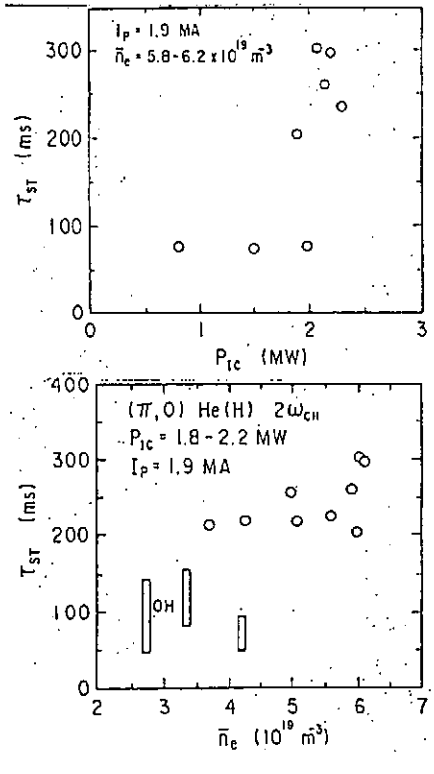

SAWTOOTH STABILIZATION STUDY BY SECOND HARMONIC MINORITY HEATING IN COMBINATION WITH NBI (70keV, H⁰beam)

HIGH DENSITY REGIME

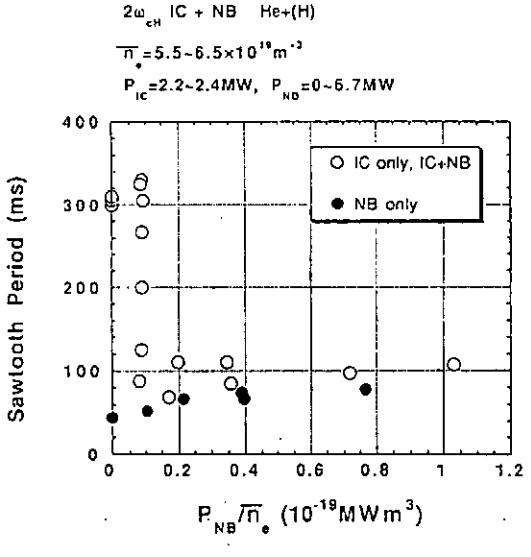

- Giant sawtooth is observed during ICRF heating only or combined heating with small NBI power.

SAWTOOTH PERIODS VS. FAST ION PRECESSION FREQUENCY

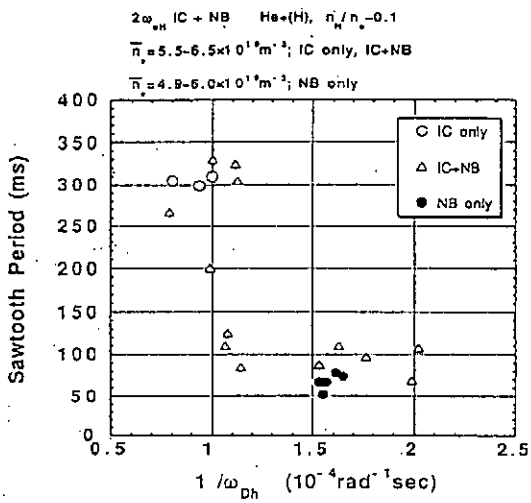

- Sawtooth period is critically dependent on the precession frequency of the fast ions.

COMPARISON AMONG ω_{cH}, $2\omega_{cH}$ AND $3\omega_{cH}$ HEATING

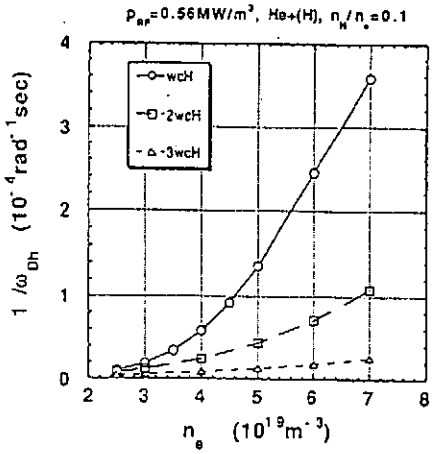

- Higher harmonic ICRF heating can keep the precession frequency to be high even at high electron density.

⇒ Suitable for sawtooth stabilization in high density plasmas with relatively small threshold power.

FWEH experiment in combination with LHCD on JT-60

fast wave frequency=131MHz

B_T=3.3T $\omega \sim 2.5\omega_{cH}$ $I_p \approx 1$MA

$T_{e0} \sim 3$keV, $n_{e0} \sim 2\times10^{19}m^{-3}$

$$\alpha \equiv \frac{\text{TTMP force } (v_\perp = v_{te})}{\text{total force}}$$

$$= \frac{\omega_{pi}^2}{\omega^2}\frac{T_e}{m_e c^2} \qquad \text{(D. Moreau)}$$

$$\approx 0.2$$

Landau Damping is dominant.

Absorption efficiency can be improved with LHCD (2GHz).

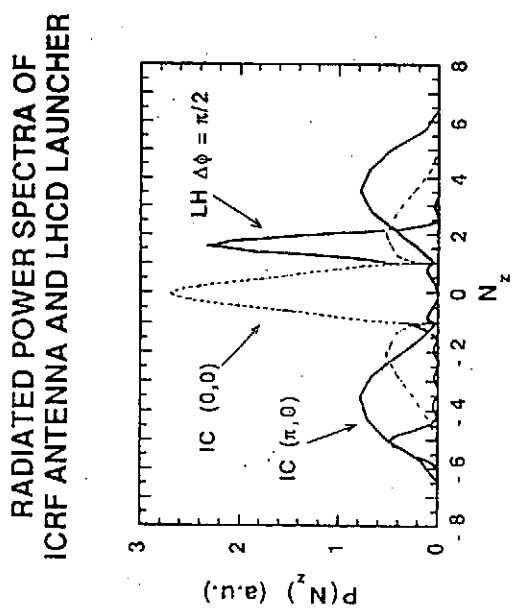

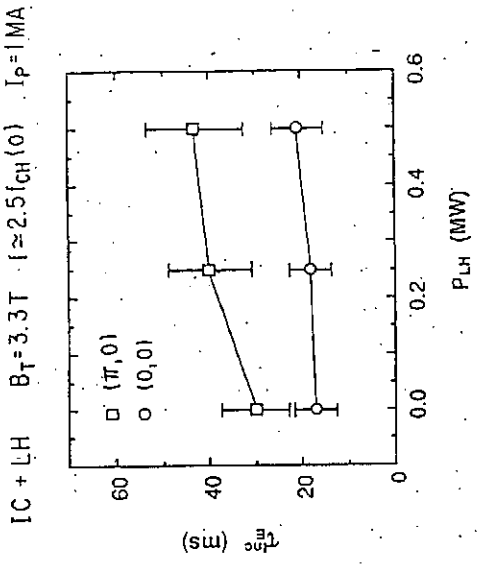

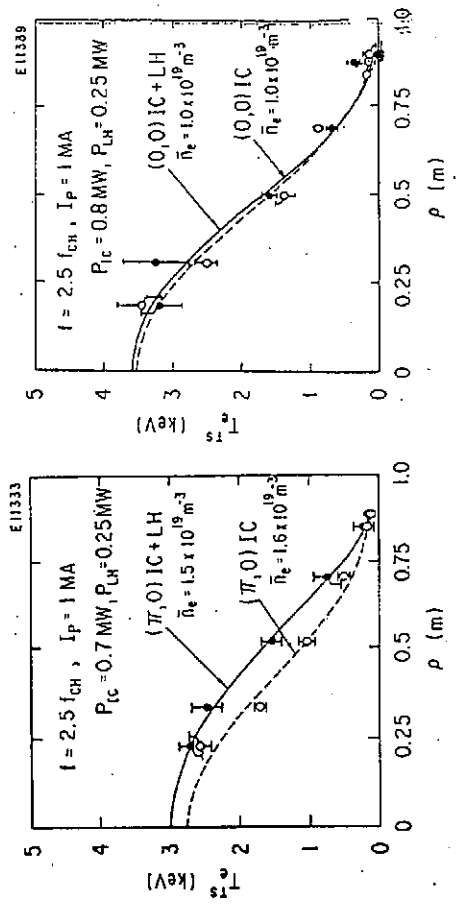

TRAJECTORY OF THE HARD X-RAY INTENSITY DURING LHCD ONLY AND SUBSEQUENT FWEH + LHCD PHASE

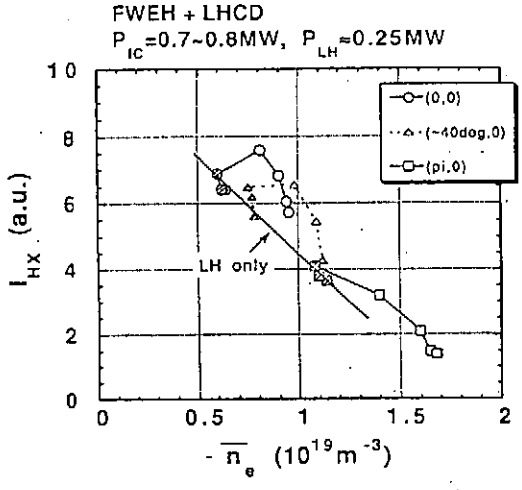

• Enhancement of the HX intensity by the fast wave is confirmed.

SYNERGETIC EFFECTS BETWEEN FWEH AND LHCD

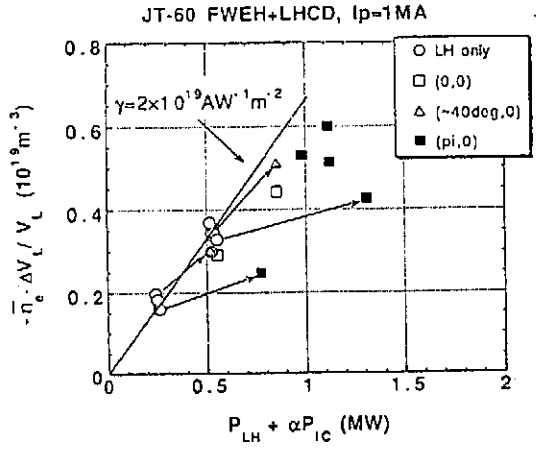

• LHCD efficiency may be improved by FWEH, since FWEH does not directly contribute current drive because of symmetrical phasing.

•Absorption efficiency of the fast wave is improved by LHCD.

SUMMARY

JT-60 ICRF Experiments

- Highest antenna power density of 16MW/m^2
- Enhanced interaction between edge plasma and Faraday shield is observed with in-phase mode with small antenna-plasma distance.
- Automatic antenna impedance matching by FFC
- Antenna phase control plays a key role in optimizing 2nd Harmonic Heating.
- 2nd Harmonic Minority Heating shows best result.
- Strong central heating by 3rd harmonic ICRF heating in combination with NBI
- Efficient beam ion acceleration by 2nd harmonic and 3rd harmonic ICRF heating
- Sawtooth stabilization in high density discharge with small ICRF power
- Synergetic effects between FWEH and LHCD

EXPERIMENTAL PLAN ON JT-60U (NEAR TERM)

- Two new antennas (P_{IC}~4.5MW)
- Higher harmonic heating with emphasis on the sawtooth stabilization in high density plasma.
- D-^{3}He fusion with 4th harmonic ICRF heating of ^{3}He beam in high density deuterium plasma.
- Local current profile control by uni-directional minority ion heating or beam ion acceleration in combination with tangential NBI.
- More systematic study on synergetic effects between FWEH and LHCD.

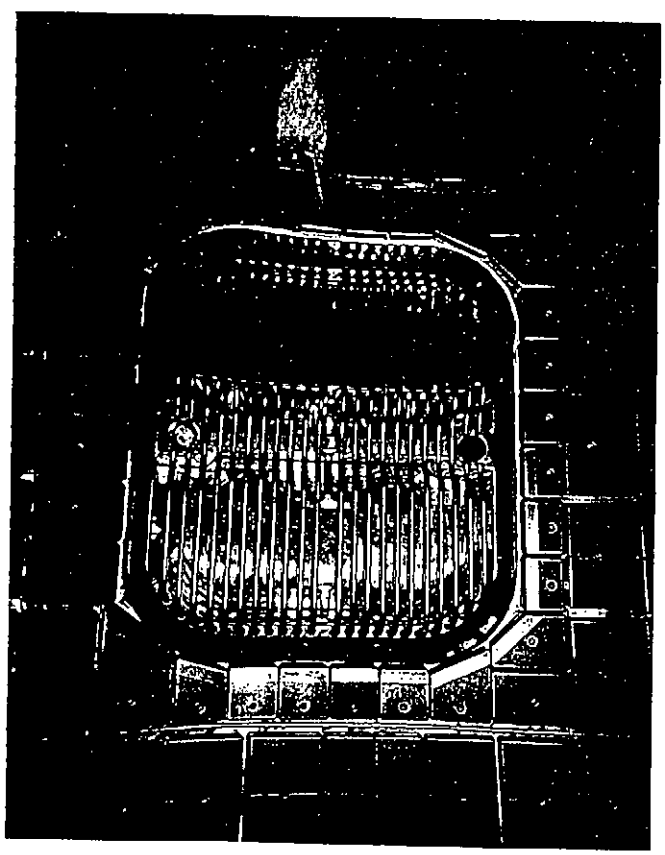

D-^{3}He FUSION YIELD WITH 4TH HARMONIC ICRF HEATING OF ^{3}He BEAMS

CONTOUR OF ΔQ

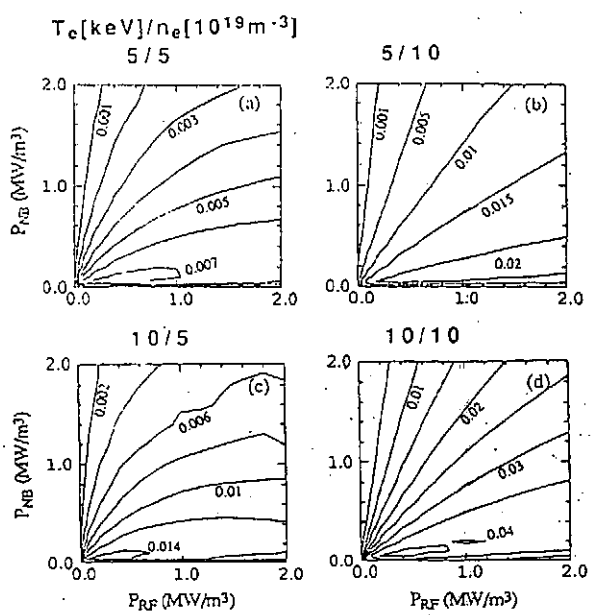

YAMAGIWA, M. and KIMURA, H., Nucl. Fusion, 31 (1991) 1519.

D-^{3}He FUSION YIELD WITH 4TH HARMONIC ICRF HEATING OF ^{3}He BEAMS

- Best Combination; $P_{RF} \sim 5 \times P_{NB}$
- $\Delta Q_{max} \sim 0.043(T_e[10keV])(n_e[10^{20}m^{-3}])^{1.5}$

Higher Harmonic Heating can enhance the fusion power more efficienctly than fundamental heating in high density discharge.

Fundamental Heating;

$$\Delta Q_{max} = \alpha(n_d/n_e)(W_{fast}/P_{RF}) \qquad \text{JET}$$

$$\propto T_e^{1.5} n_e^{-1}$$

FWCD Ability on JT-60U

- High frequency ICRF power source
  110-131MHz, 6MW (10MW planned)
  eight independent power units
- Large horizontal port for antenna
  0.9m in width
- Powerful other electron heating systems
  LH; 2GHz, 10MW
  NBi; 0.5MeV, 10MW (planned)
  EC; 110GHz, 4MW (planned)
- Two regimes consistent with EC central heating
  (1) $\omega \sim 2.5\omega_{cH}$ ($5\omega_{cD}$) with $B_T \sim 3.5$ T
  (2) $\omega \sim 4.5\omega_{cH}$ ($9\omega_{cD}$) with $B_T \sim 1.9$ T
- Intermediate regime between TTMP and ELD, but relatively strong damping can be expected especially in the low B_T regime.

Contents;

1. Antenna optimization
2. FWCD efficiency

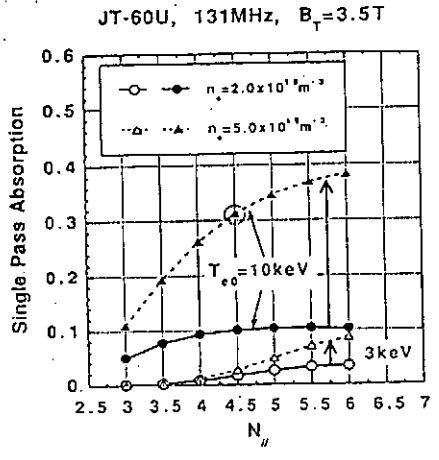

$$\eta_s = 1 - \exp\left(-2\int_{-a}^{a} k_{\perp z}^{(e)}\, dl\right)$$

$k_{\perp z}^{(e)}$ by S.C. Chiu (Nucl. Fusion 29 (1989) 2175)

$$n_e(r) = n_{e0}\left(1 - \left(\frac{r}{a}\right)^2\right)$$

$$T_e(r) = T_{e0}\left(1 - \left(\frac{r}{a}\right)^2\right)^{\frac{1}{2}}$$

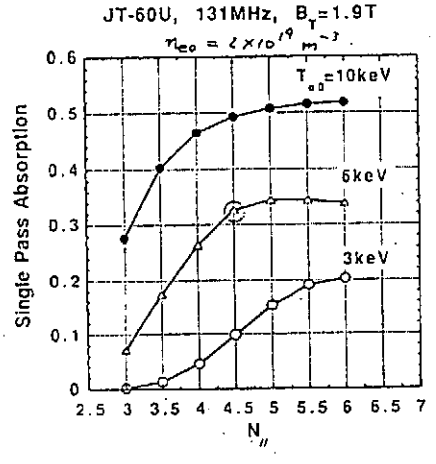

Desirable $N_{//}$-range;

$3 \leq N_{//}(\rho) \leq 6$

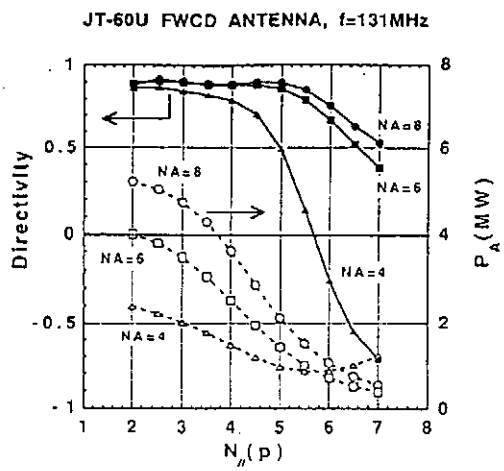

$N_A = 8$ is favourable and possible in JT-60U

Full width of main lobe ;

$$\Delta N_{//} = \frac{2c}{f\,W_A} = 5.4 < 10$$ (currently used FWCD antennas)

1D full-wave code high B_T case

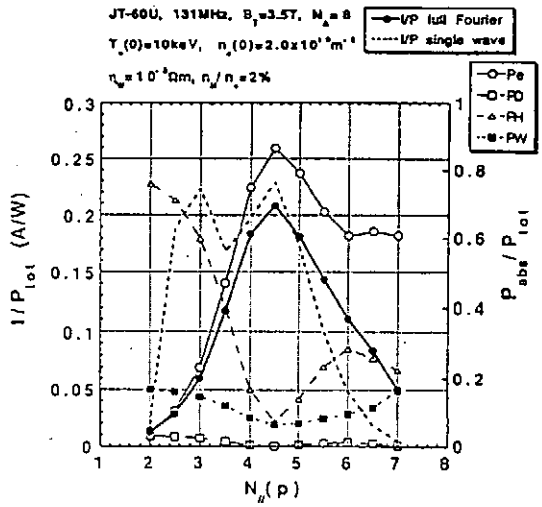

$n_H/n_e = 2\%$, $Z_{eff} = 2$, $\eta_w = 10^{-3}\Omega m$

$N_{//}$ control is difficult due to eigen mode effects in small η_s ($\lesssim 10\%$) regime.

low B_T case

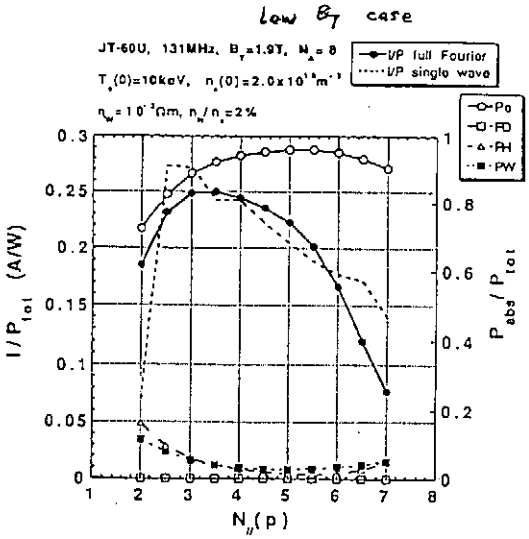

$N_{//}$ control is satisfactory with large η_s ($\gtrsim 30\%$).

high B_T case

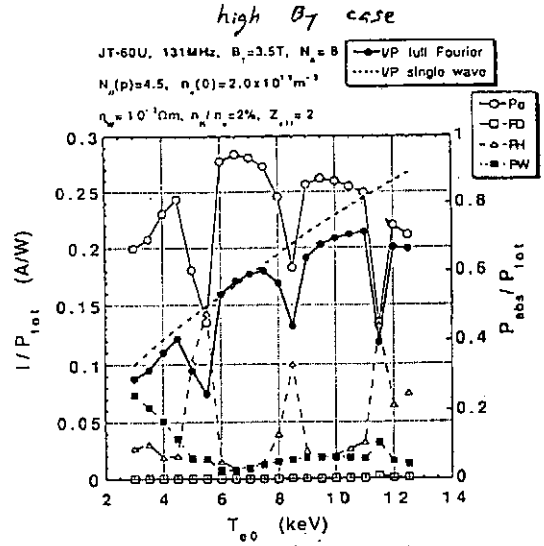

$I/P_{tot} \sim 0.21$ A/W

at $T_{e0} = 10$ keV, $n_{e0} = 2\times10^{19}\ m^{-3}$,

$N_{//}(p) = 4.5$

Dip in I/P_{tot} due to eigen mode effects.

low B_T case

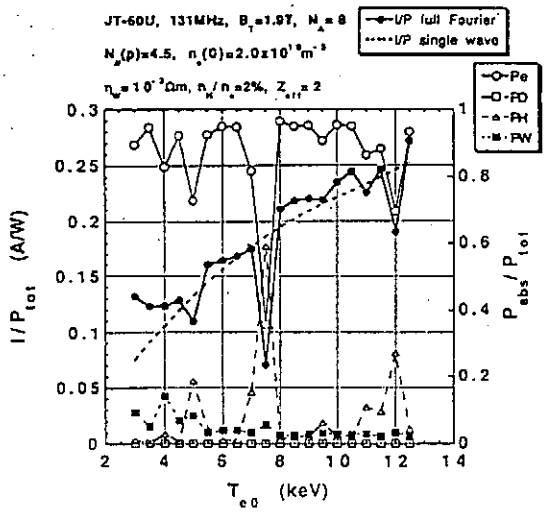

$I/P_{tot} \sim 0.24$ A/W

at $T_{e0} = 10$ keV, $n_{e0} = 2 \times 10^{19}\ m^{-3}$,

$N_{\parallel}(\rho) = 4.5$.

Eigen mode effects still appear in large η_s (≤ 0.6) regime.

SUMMARY

FWCD Analysis for JT-60U

- Desirable $N_{//}$-range is 3-6, which allows $\eta_s \geq$ 30% in both low field and high field regimes.
- Eight-loop antenna is favourable for keeping high directivity in the required $N_{//}$-range.
- Small $\Delta N_{//}$ (~ 5.4)
- Driven current of ~1MA with 4MW ICRF power
- Suitable for both physics and technology R&D for ITER
- Deleterious effects of the eigenmode even in large single-pass absorption regime ($\eta_s \leq 0.6$)

Wave Particle Interactions of Fast and Slow Waves in JIPP T-IIU

T. Seki, JIPP T-IIU group

National Institute for Fusion Science

○Review of recent RF experiments in JIPP T-IIU

1989 Construction of high frequency (130MHz) RF system

- preliminary trial of fast wave current drive
  - *coupling of wave and electrons was observed.
  - *n∥ parallel of wave was too small. ($n_{//,min}$ ~4.5 ⇒ ~20keV electron)
- higher (3rd) harmonic heating
  - *accomplished in combination with additional heating.

1990 Ion Bernstein Wave experiment

- core plasma heating
- increment of Fe impurity

Fast Wave Experiment

Feature of experiment

- four high-field loop antennas
- frequency~130MHz, B_t~3T, H/H+D~10%
- $3\Omega_H$ layer is located on center chord.
- four antenna phasings

(0, π, 0, π) ·····	$n_{//}$ ~4.5
(0, π/2, π, 3π/2) ···	$n_{//}$ ~2.3
(0, -π/2, -π, -3π/2) ··	$n_{//}$ ~-2.3
(0, 0, 0, 0) ·····	$n_{//}$ ~0

- competitive two heating regimes
  - electron heating regime ···fast wave current drive
  - ion heating regime ···3rd harmonic heating

Electron Heating Regime in Fast Wave

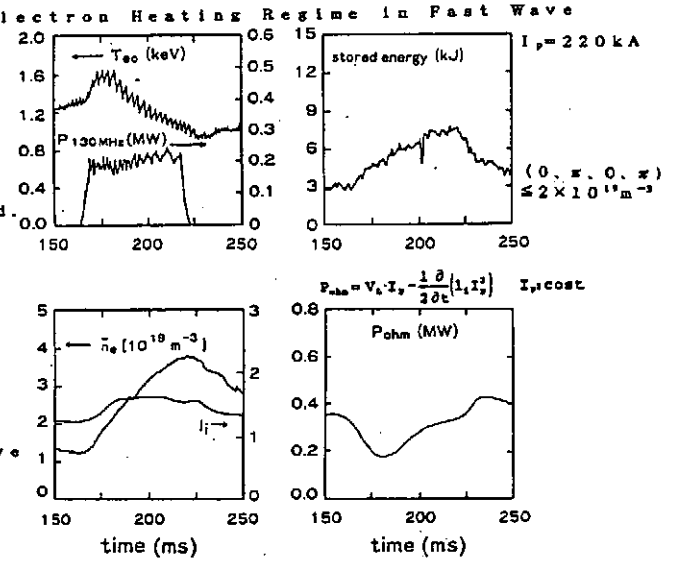

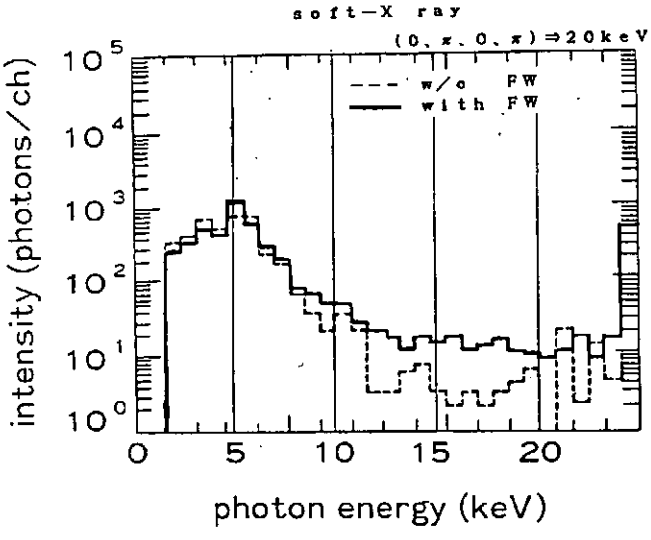

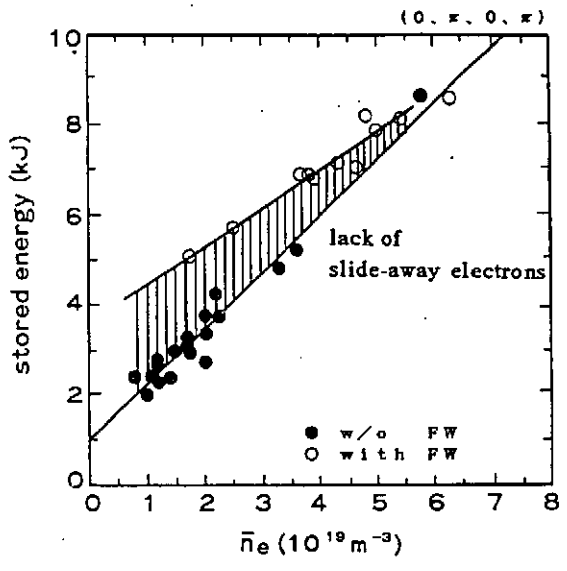

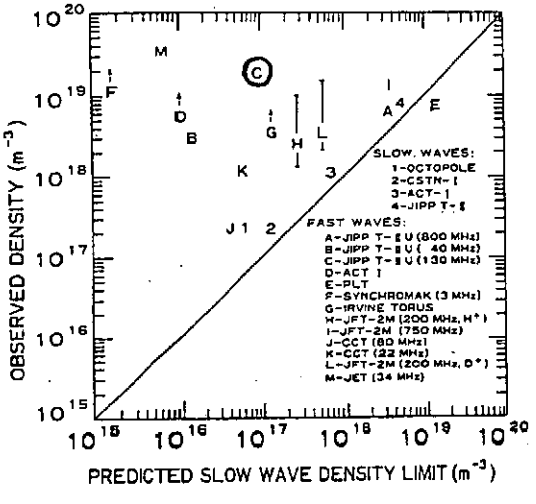

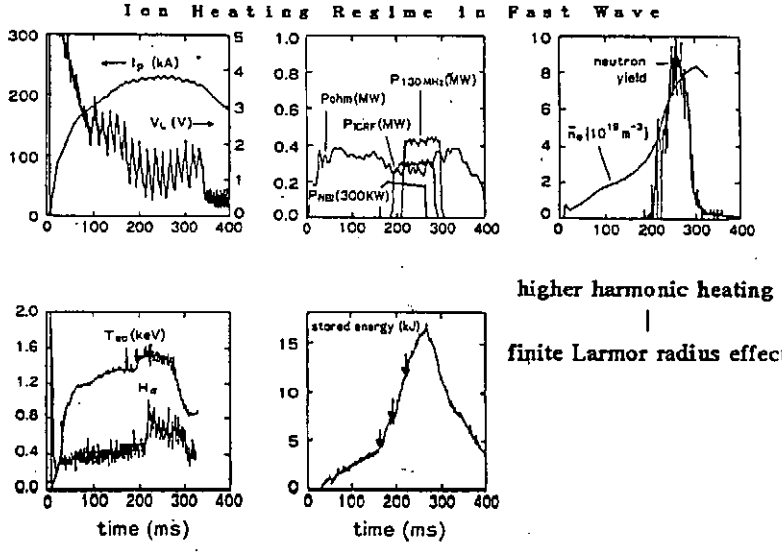

higher harmonic heating

|

finite Larmor radius effect

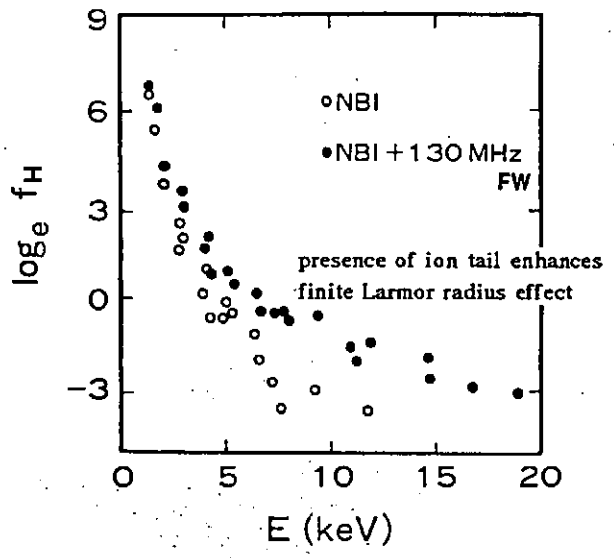

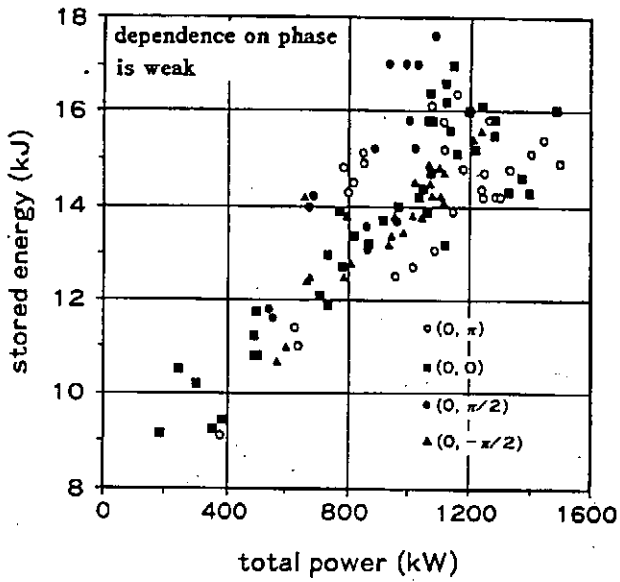

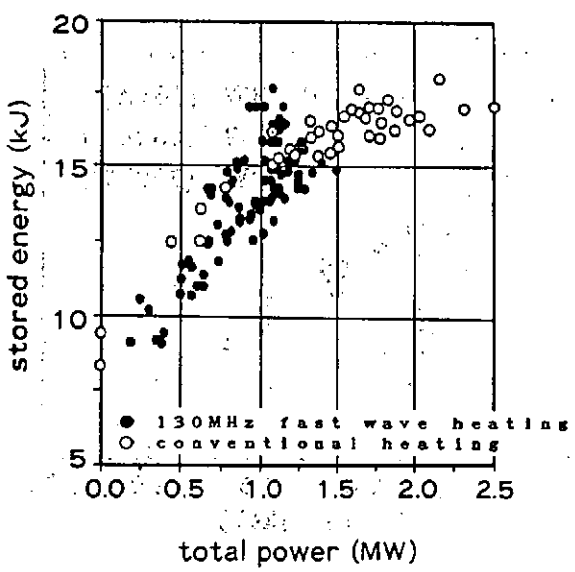

●Slow Wave (Ion Bernstein Wave) Experiment

Feature of experiment

- three low-field center-fed antenna
- frequency~130MHz, B_t~3T, pure H
- $3\Omega_H$ layer is located on center chord.
- two antenna phasings

  (0, π, 0) ··· $n_{//}$ ~4 (ion heating)

  (0, 0, 0) ··· $n_{//}$ ~8 (electron heating)

- highest frequency IBW experiment

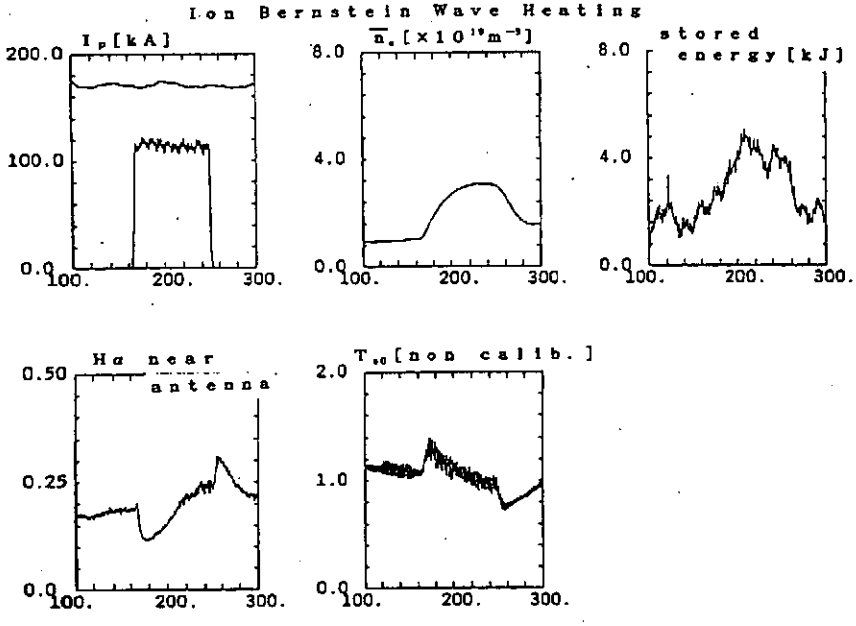
Ion Bernstein Wave Heating
I_p[kA]
$\bar{n}_e$[×10^{19}m^{-3}]
stored energy [kJ]
Hα near antenna
T_{e0}[non calib.]

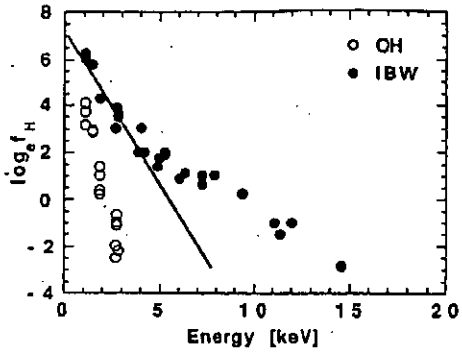
OH
IBW
$\log_e f_H$
Energy [keV]

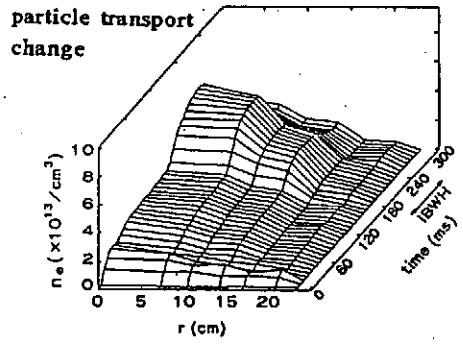
particle transport change
n_e(×10^{13}/cm^3)
r (cm)
time (ms)
IBW/H

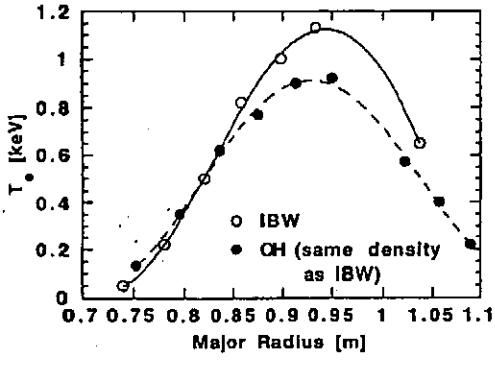
T_e [keV]
IBW
OH (same density as IBW)
Major Radius [m]

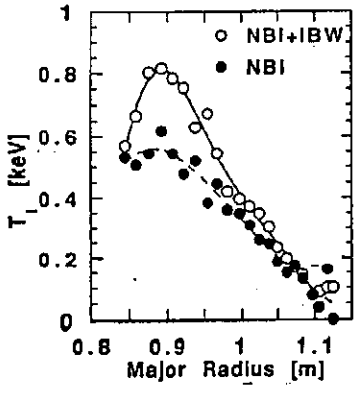
NBI+IBW
NBI
T_i [keV]
Major Radius [m]

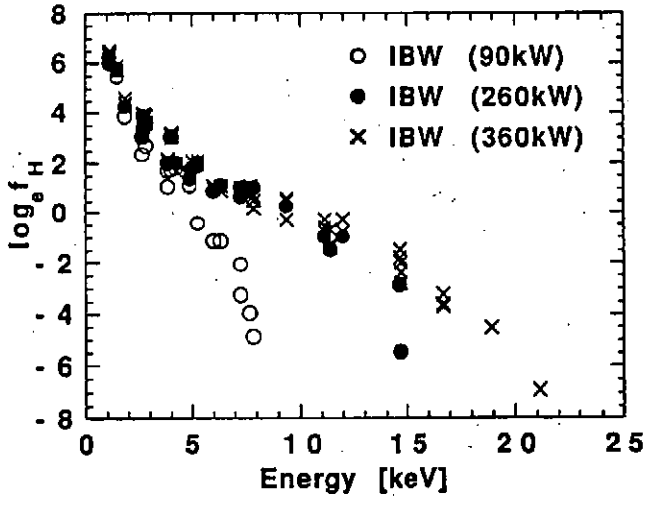
IBW (90kW)
IBW (260kW)
IBW (360kW)
$\log_e f_H$
Energy [keV]

Summary

- In fast wave experiment, there are two competitive heatimg regimes; the ion and electron heating regime.

- In the electron heating regime, the slide-away electrons interact with wave and the interaction is sensitive to the $n_{//}$ of wave.

- In the ion heating regime, the high energy ions enhance finite Larmor effect and the heating mechanism is independent of the $n_{//}$ of wave.

- In slow wave (IBW) experiment, wave interacts with particles at the plasma core region and the profiles of density and temperature are peaked.

- Different from the fast wave heating, the high energy ion tail shows non-runaway feature.

US-Japan Workshop on RF Heating and Current Drive in Confinement Systems Tokamaks
Nov. 18-21, 1991, NIFS, Nagoya, Japan

Wave Heating and Current Drive Experiments in JFT-2M

Y. Uesugi*, T. Yamamoto, H. Kawashima and JFT-2M Group

*Dept. of Electrical Engineering and Electronics
Nagoya University, Nagoya, 464-01, Japan
JAERI, Naka, 311-01, Japan

OUTLINE

1. Present Status of RF Heating and Current Drive in JFT-2M

2. 200 MHz Fast Wave Current Drive and Electron Heating Experiments

(1) Wave Excitation
- -Antenna loading
- -Phase control
- -Impurity problem

(2) Interaction with Electrons
- -Current drive in low density region
- -Electron heating in high density region

Recent Activities on RF Heating and Current Drive

1. ICRF -High Te plasma production for FWCD

2. FWCD -Antenna structure
- -Coupling
- -Current drive
- -Electron heating
- -Synergy with ECH and ICH

3. ECH -Plasma start up
- -High Te plasma production for FWCD
- -Current drive
- -MHD control(planned)
- -Sawtooth suppression(planned)

RF Systems in JFT-2M

1. ICRF

-frequency	10~40 MHz
-output power	1.5x3 MW(2.5 MW)
-pulse duration	0.5 sec.
-antenna	phased 3-loop high field side

2. FWCD

-frequency	200 MHz ($\omega \sim 10\,\omega_{ci}$)
-output power	200x4 kW(650 kW)
-pulse duration	0.5 sec.
-antenna	phased 4-loop low field side

3. ECH

-frequency	60 GHz
-output power	200x2 kW(250 kW)
-pulse duration	0.3 sec.
-antenna	conical horn low field side

Recent Activities on FWCD and FWEH

1. Antenna Coupling Low N_z and high N_z antennas
- -Loading characteristics(n_o, T_e, ϕ)
- -Wave excitation
- -Impurity generation

2. Fast Wave Current Drive
- -Density dependence
- @electron heating is dominant at high density
- @same as LHCD at low density
- -Phase dependence
- -Frequency dependence (f=200, 750 MHz)

3. Fast Wave Electron Heating
- -Absorption profile measurement
- @electron Landau damping
- @no ion absorption
- -Heating efficiency($\eta_{FW} \sim \eta_{ECH}$)
- -Confinement($\tau_{inc}^{FW} \sim \tau_{inc}^{NBI,ICH}$)

Direct absorption of electromagnetic fast waves by electron.
No mode conversion.

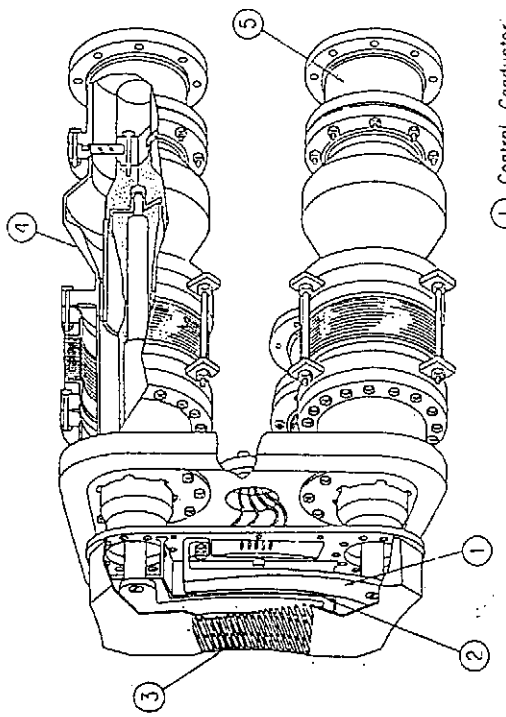

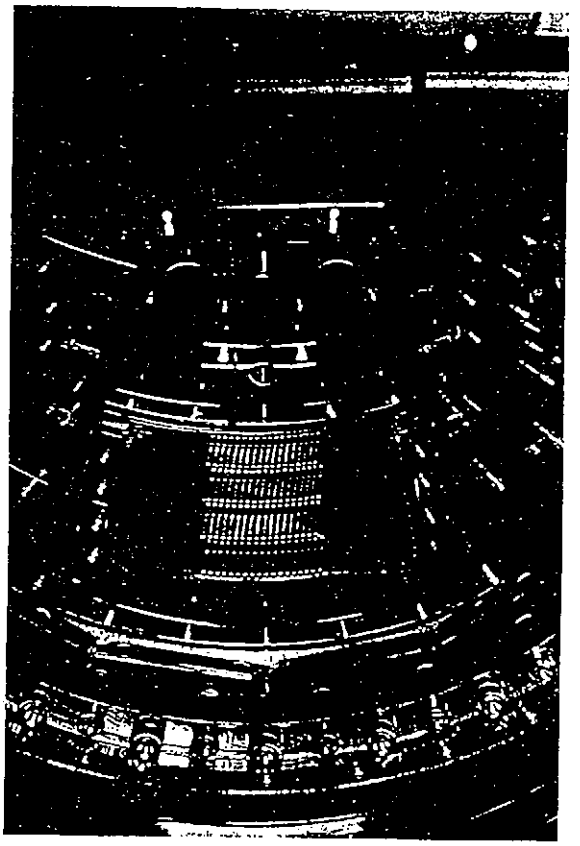

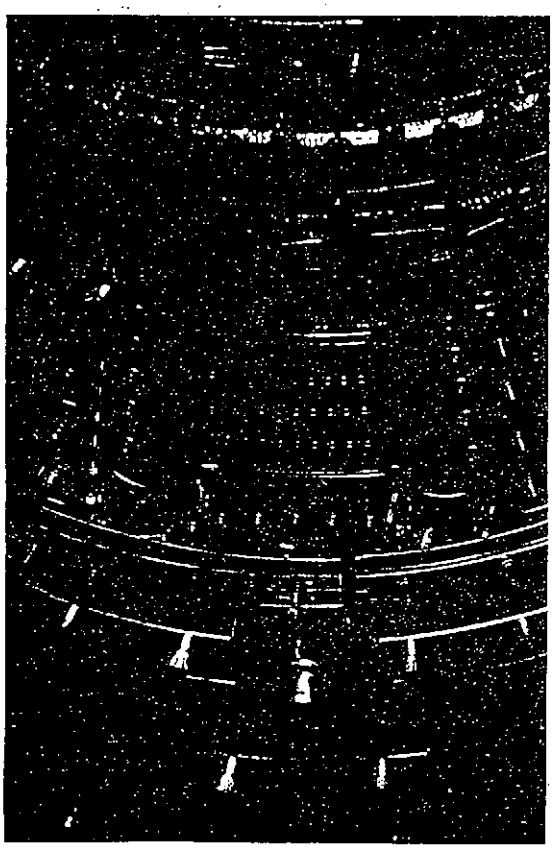

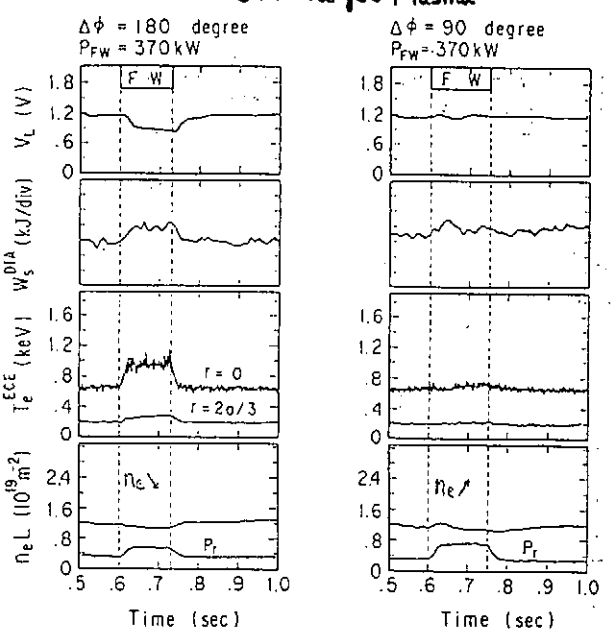

Fast Wave Electron Heating

- No ion absorption
- Density increase is small.
- Metal impurities. (T_i, F_e)

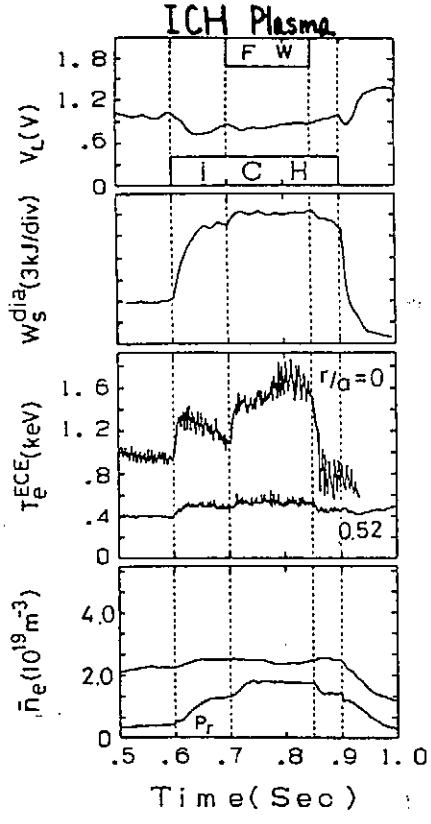

Density dependence of the plasma stored energy during ICH and FWEH

-D-shaped limiter discharge
-phased two-loop excitation
at $\Delta\phi=\pi$ for ICRF(P_{ICH}=450 kW)
-two ion hybrid heating(n_H/n_D~0.2)
-phased four-loop excitation
at $\Delta\phi=\pi$ for FWEH(P_{FW}=500 kW)
-τ_{inc}(ICH)=17~30 ms
-τ_{inc}(FWEH)~8 ms

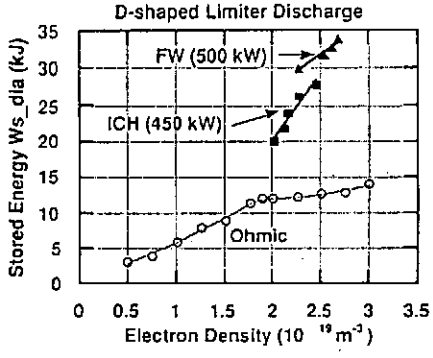

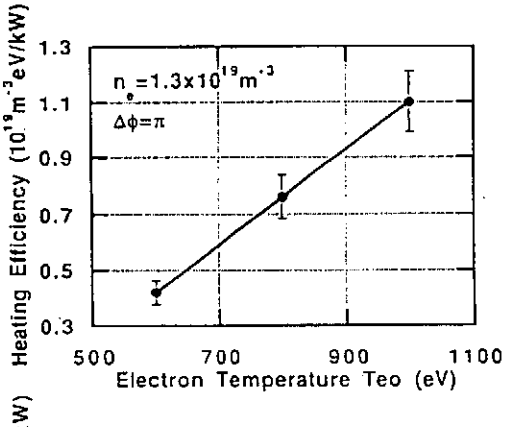

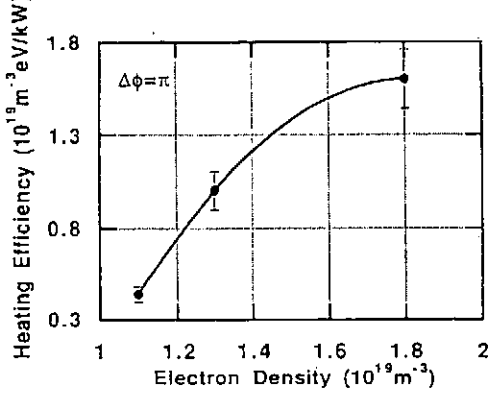

Phase Dependence of the Electron Heating Efficiency and Incremental Confinement Time

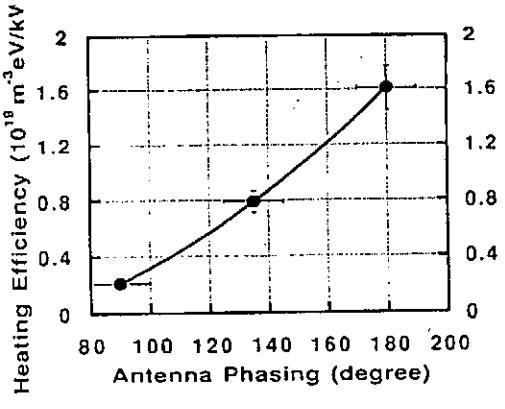

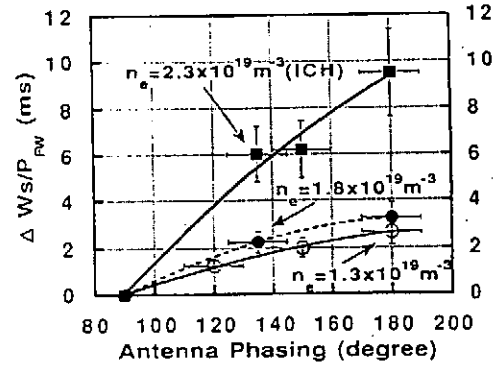

$v_{th}/v_{te} \lesssim 3-4$ for electron heating

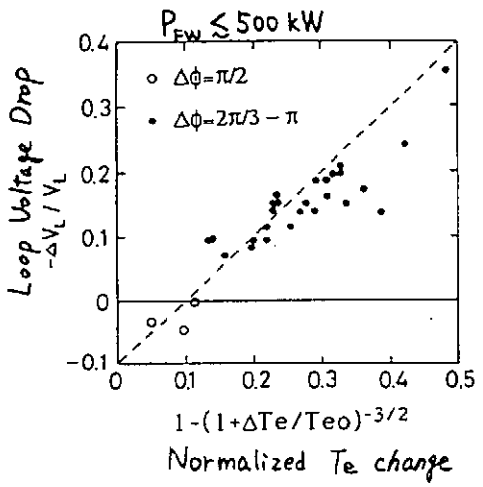

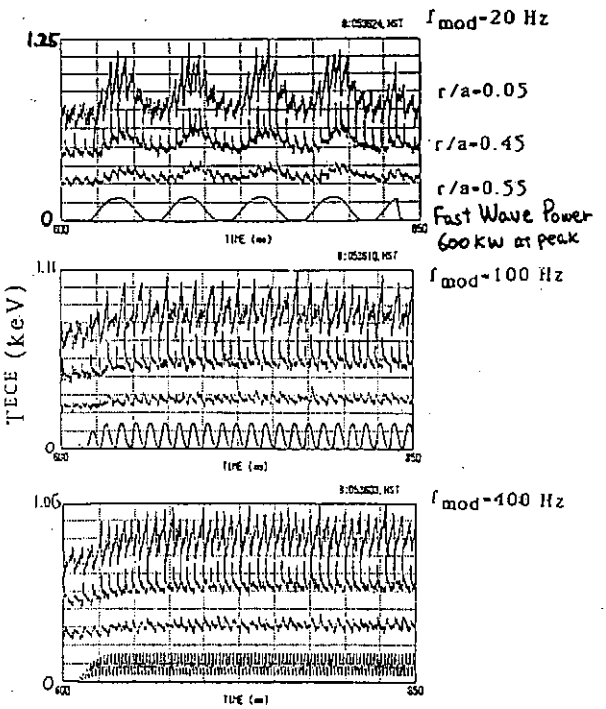

Time Traces of ECE Signals

$\bar{n}_e=2\times10^{19}m^{-3}$, P_{FW}=600 kW

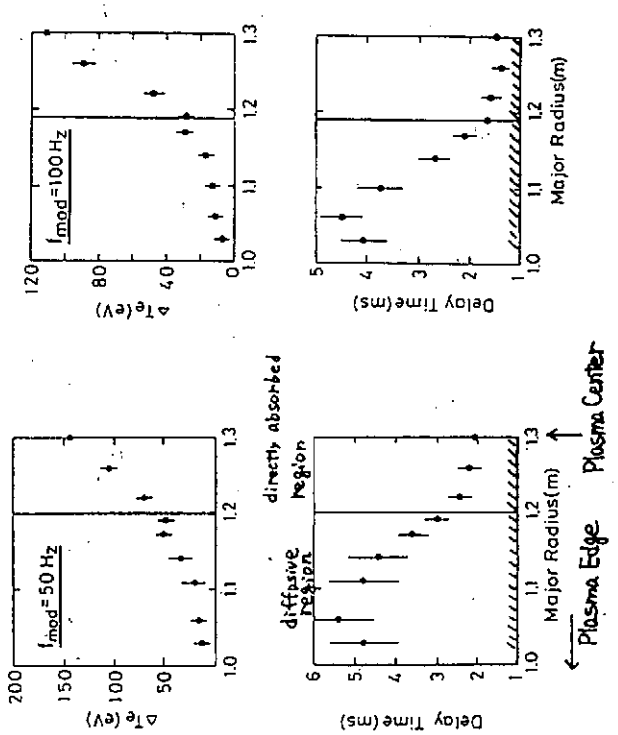

Absorption profile depends strongly on the electron temperature and density.

I_p=100 kA/$\bar{n}_e$=1x10^{19}m^{-3} --- T_{eo}=0.6 keV

I_p=230 kA/$\bar{n}_e$=1x10^{19}m^{-3} --- T_{eo}=1.2 keV

I_p=230 kA/$\bar{n}_e$=2x10^{19}m^{-3} --- T_{eo}=0.7 keV

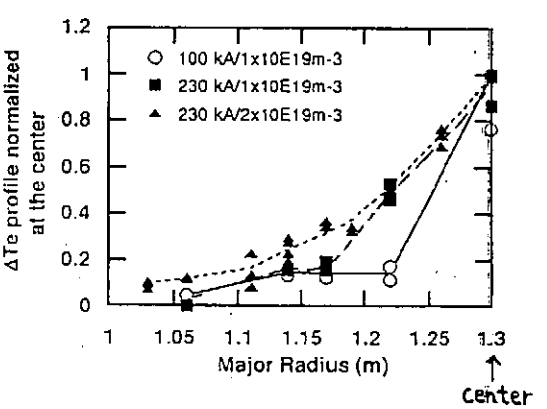

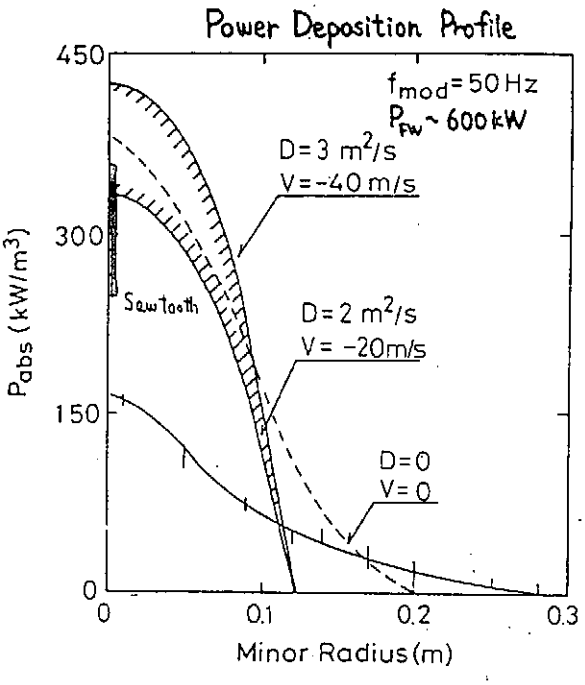

Experimental Result on Absorption Efficiency

$\bar{n}_e(10^{19}m^{-3})$	I_p(kA)	T_{eo}(keV)	η_{abs}
1	100	0.6	<0.05
1	230	1.2	0.05-0.1
2	230	0.7	0.3-0.4

$\longrightarrow \tau_{inc} = 8\sim10$ mS
$\eta_e = 4\sim5 eV \cdot 10^{19} m^{-3}/kW$

(1) $\Delta\phi=\pi$ (Nz~7.5), (2) Ohmic target plasma

$\bar{n}_e$ Increase ----> High Nz wave penetrates into the plasma.

T_e Increase ----> Absorption through ELD increases.

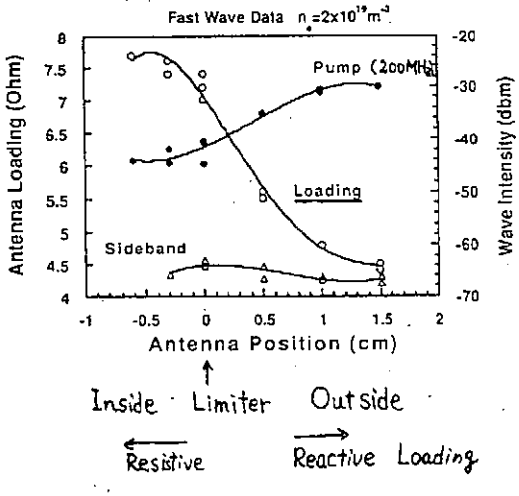

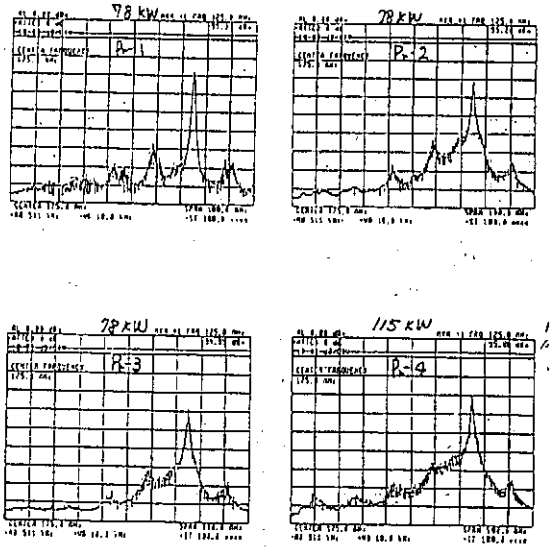

$\Delta\phi=0$

P_r-1	Toroidal	θ=22°
P_r-2	T	θ~90°
P_r-3	Poloidal	θ~180°
P_r-4	T	θ~180°

Far from Antenna

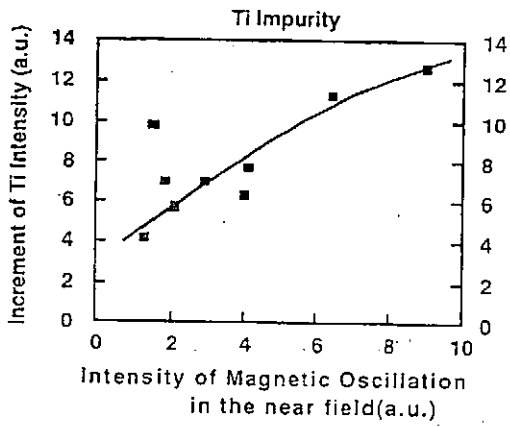

SUMMARY

1. Fast Wave Electron Heating
   - -electron Landau damping is dominant
   - -high heating efficiency as ECH
     $\eta_{FW} \sim 4 \times 10^{19} m^{-3} eV/kW \sim \eta_{ECH}$
   - -center electron heating
     $\tau_{inc}^{FW} = 8 \sim 10$ ms $\gtrsim \tau_{inc}^{NBI,ICH}$ in D-shaped limiter discharges.

2. Fast Wave Current Drive
   - -low density FWCD is quite similar to LHCD.
   - -high density FWCD requires high Te plasma and high Nz unidirectional fast wave, Te > 2keV and Nz~6 in JFT-2M.
   - -demonstration of high density FWCD is a near term objective.

US - Japan Workshop on
RF Heating and Current Drive in Confinement Systems Tokamaks
National Institute for Fusion Science
November 18-21, 1991

High - Density and Long - Pulse Operation by LHCD in TRIAM - 1M

Y. Nakamura, S. Kawasaki, E. Jotaki, T. Fujita
A. Nagao, K. Nakamura, S. Itoh

Advanced Fusion Research Center
Research Institute for Applied Mechanics
Kyushu University, Kasuga 816, Japan

LONG PULSE OPERATION

OUTLINE

(I) Long Pulse Operation by LHCD

- Detection of plasma current and position with Hall - effect sensors
- Plasma density control for steady - state discharges
- Impurity behaviour
- Damage of poloidal limiters

(II) High Density Operation by LHCD

- Extention of operational regime up to 1×10^{13} cm-3
- Improvement of current drive efficiency

(III) Next Operation Program in TRIAM - 1M

- High frequency (8.2 GHz) LHCD

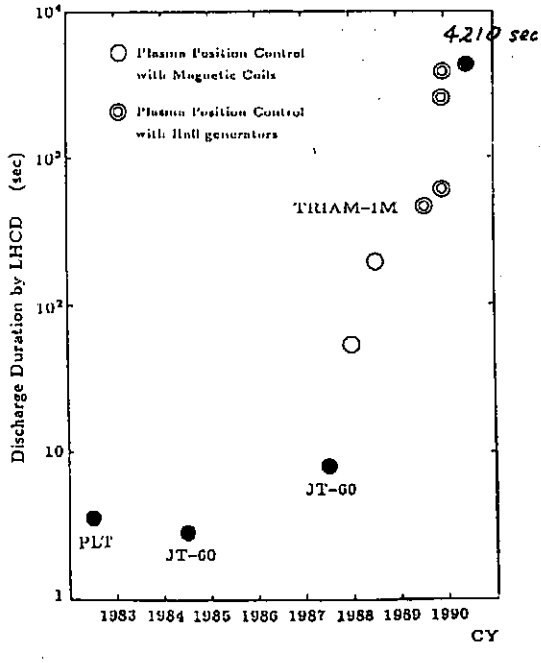

Plasma position detection system with magnetic coils

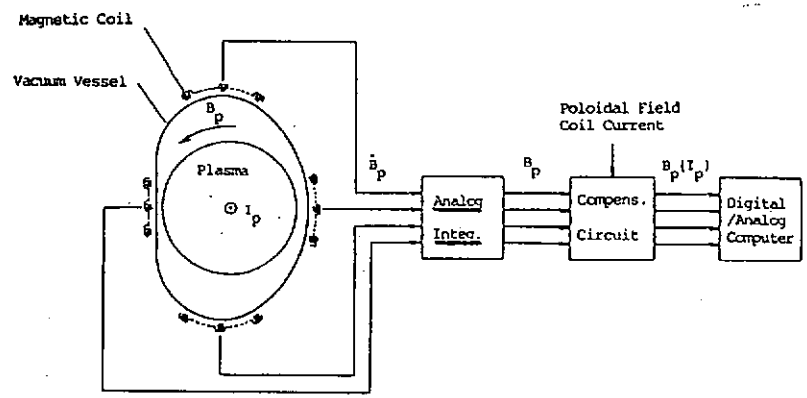

Longest-duration tokamak discharge

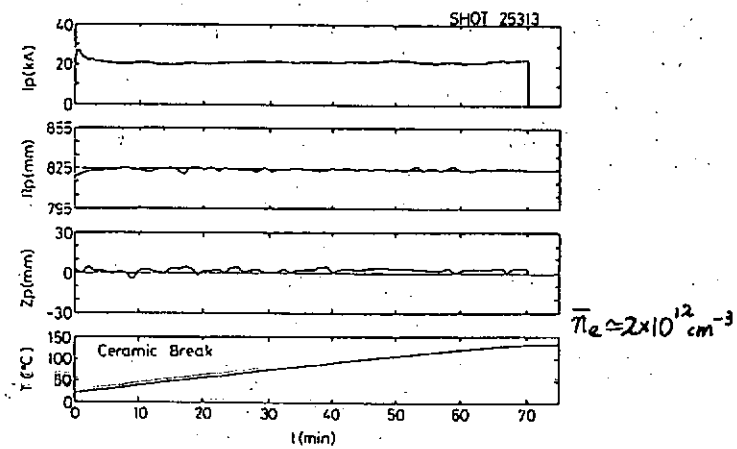

Plasma position detection system with Hall-effect sensors

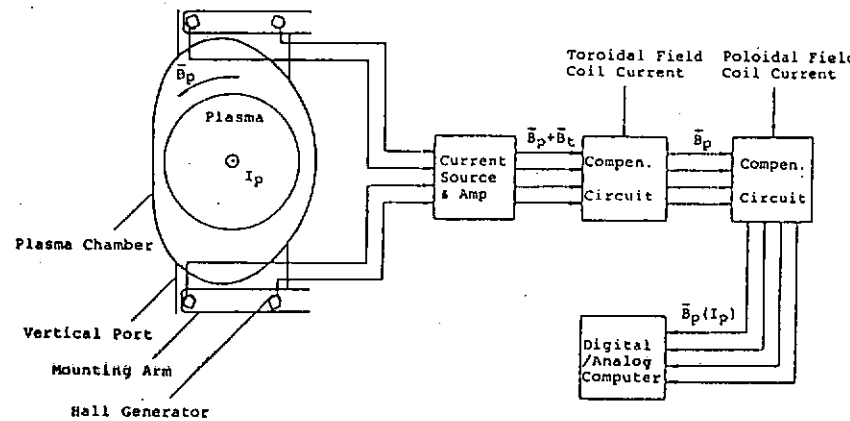

Coordinate systems of (r,θ) on the geometrical axis R_0

Poloidal magnetic field due to the plasma current

$$B_\theta = \frac{\mu_0 I_p}{2\pi\rho} - \frac{\mu_0 I_p}{4\pi R_0}\left(\ln\frac{8R_0}{\rho} - \left(A+\frac{1}{2}\right)\right)\frac{\rho_0^2}{\rho}\cos\theta + \frac{\mu_0 I_p}{2\pi\rho}\left(\frac{x_p}{\rho}\cos\theta + \frac{z_p}{\rho}\sin\theta\right)$$

ρ_0 : plasma minor radius

x_p : horizontal displacement

z_p : vertical displacement

Calculation for Hall element signals

$$S_p = B_{\theta out}^{up} + B_{\theta in}^{up} + B_{\theta out}^{down} + B_{\theta in}^{down} = \frac{2\mu_0 I_p}{\mu\rho_d}$$

$$S_z = B_{\theta out}^{up} + B_{\theta in}^{up} - B_{\theta out}^{down} - B_{\theta in}^{down} = \frac{2\mu_0 I_p}{\mu\rho_d}\frac{z_p}{\rho_d}\sin\theta_d$$

$$S_x = B_{\theta out}^{up} - B_{\theta in}^{up} + B_{\theta out}^{down} - B_{\theta in}^{down} = \frac{2\mu_0 I_p}{\mu\rho_d}\frac{x_p}{\rho_d}\cos\theta_d + f(\lambda,\rho_0)\cos\theta_d$$

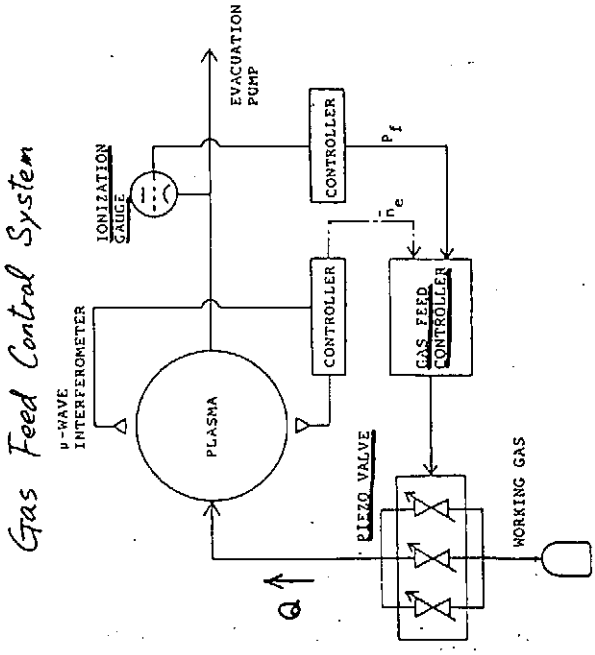
Gas Feed Control System
EVACUATION PUMP
IONIZATION GAUGE
CONTROLLER
CONTROLLER
GAS FEED CONTROLLER
μ-WAVE INTERFEROMETER
PLASMA
PIEZO VALVE
WORKING GAS
Q

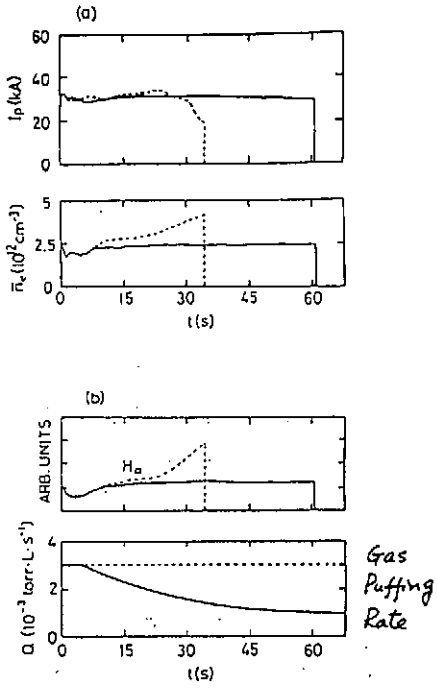
(a)
(b)
t(s)
ARB. UNITS
Gas Puffing Rate

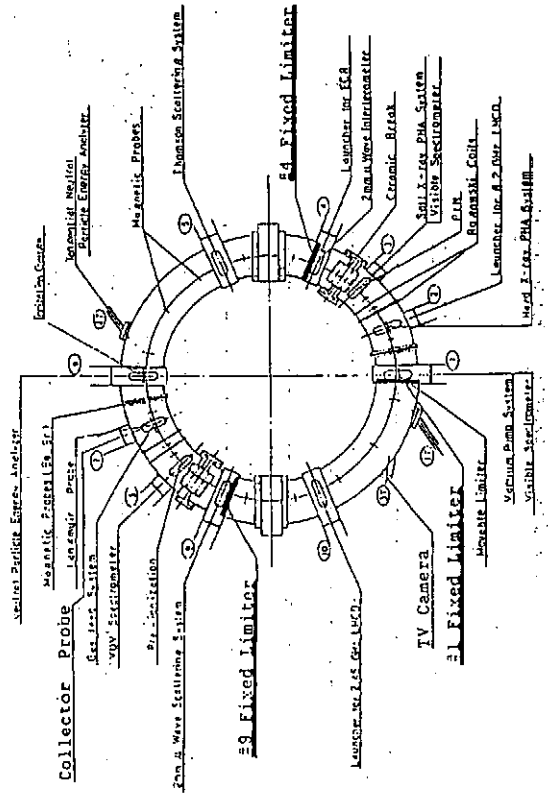
#4 Fixed Limiter
#9 Fixed Limiter
#1 Fixed Limiter
TV Camera
Collector Probe

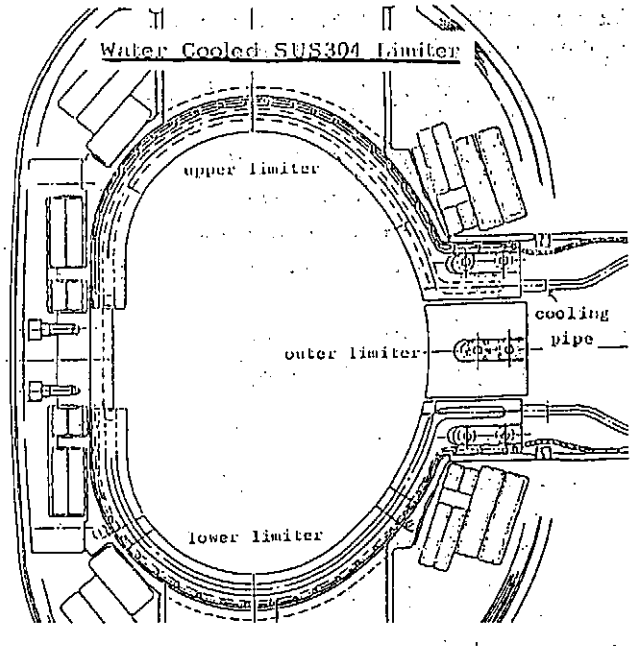
Water Cooled SUS304 Limiter
upper limiter
outer limiter
lower limiter
cooling pipe

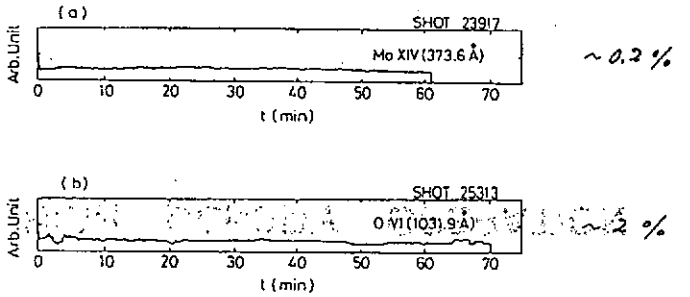

Impurity concentration

~ 0.2 %

~ 2 %

Mo Limiter mounted on water cooled SUS304 base

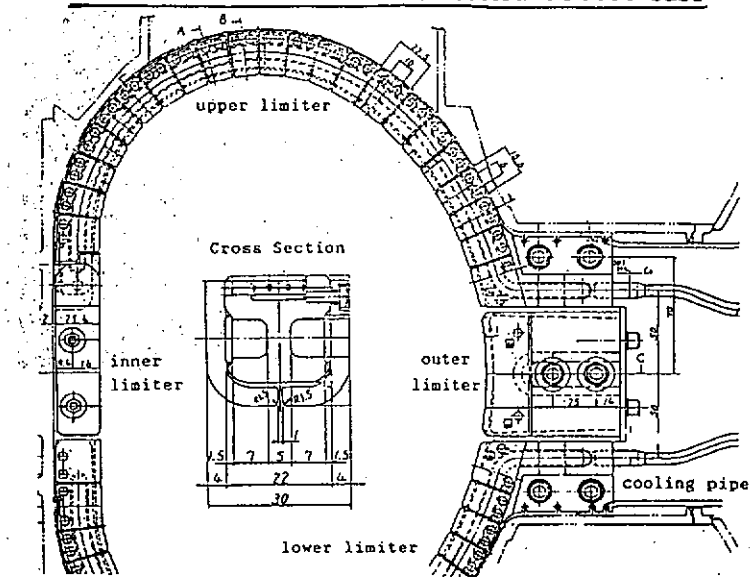

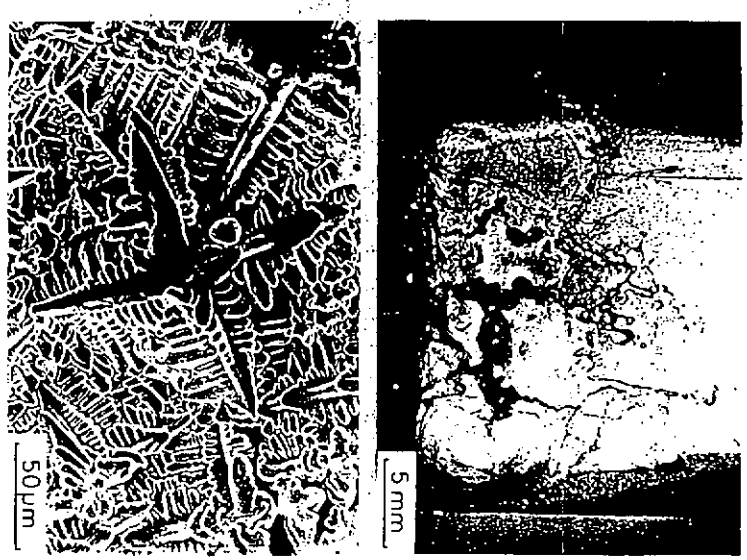

SUS304 #9 Lower Limiter

VUV spectrum

SUS304 limiter

Mo limiter

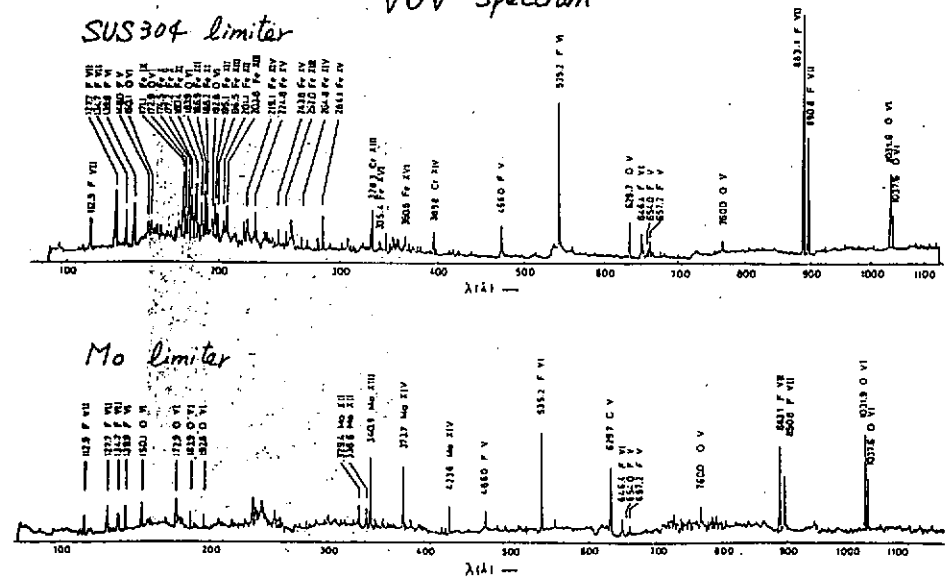

#9 Mo Limiter (inner ports)
(1992shots, 1990.4–7)

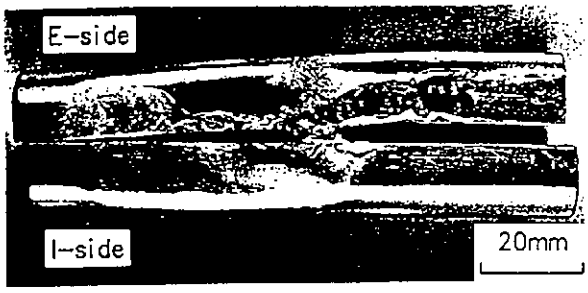

#4 Mo Limiter (outer ports)

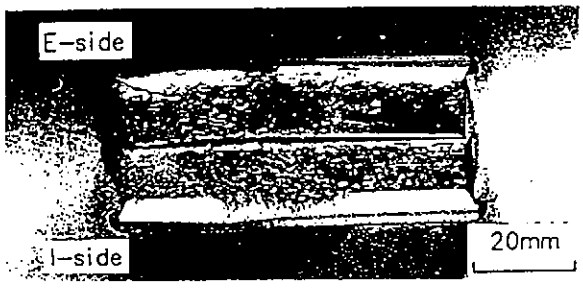

SUS304 #9
Lower Limiter,
Cross Section
long Pulse Rating
3~8 MW/m²

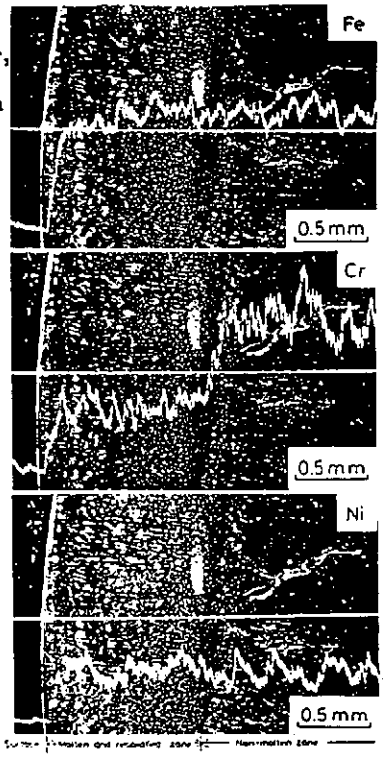

Long Pulse Operation in TRIAM-1M

(1) A new plasma position control system based on Hall-effect sensors was developed and plasma position was well controlled over one hour.

(2) Gas feed control is necessary to keep the plasma density constant and to obtain steady-state discharges.

(3) Main impurities were Mo from the limiters and O from recycling and desorption. Impurity accumulation was not observed during the long duration discharge. The impurity concentrations of Mo and O were 0.2 % and 2 - 3 %, respectively.

(4) Impurity influx into the plasma seems to be due to evaporation from the molten surface of the limiters.

(5) There is no essential problem in long pulse operation under our experimental conditions.

HIGH DENSITY OPERATION

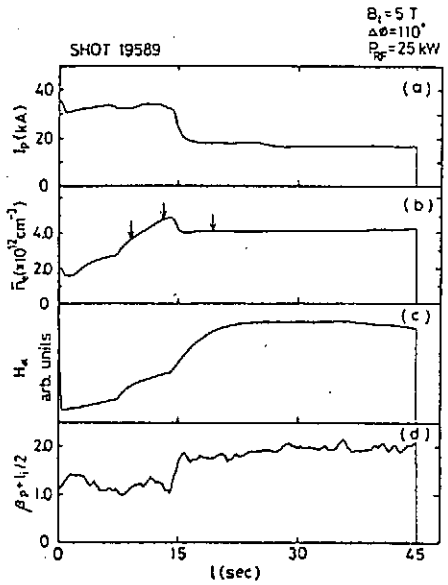

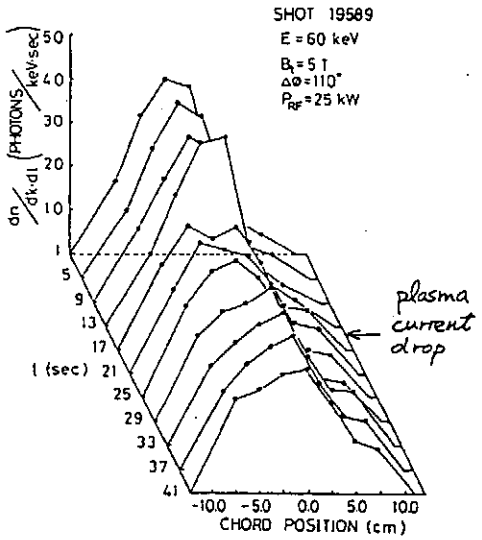

Maximum electron density in high density discharge

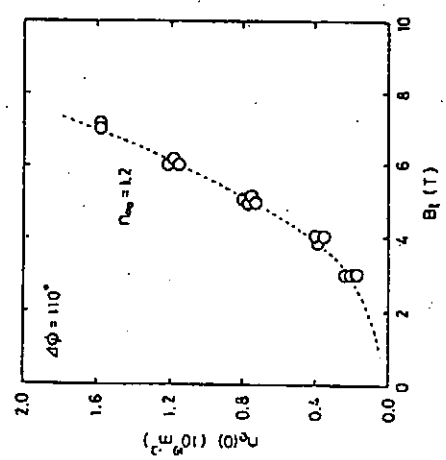

$N_{//}$ power spectra for 2.45 GHz launcher

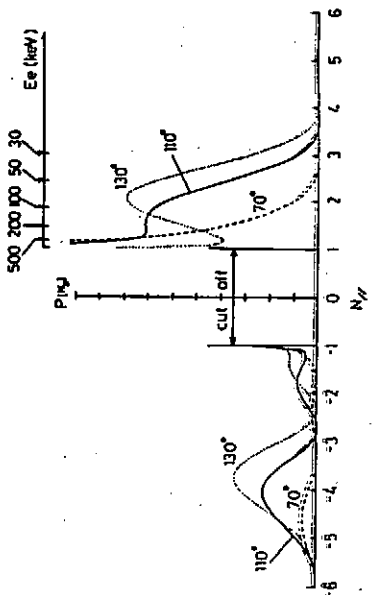

High Density Discharge

$\bar{n}_e = 1.0 \times 10^{13}\ cm^{-3}$

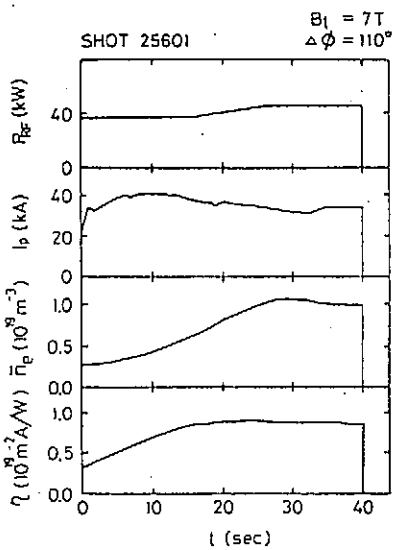

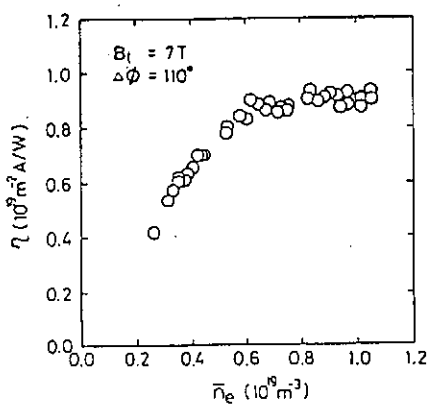

High density Operation in TRIAM-1M

(1) Long duration discharges with high plasma density were limited by the strong interaction of high energy electrons with the limiters.

(2) This density limit was due to the deterioration of the accesibility of the central plasma to LH waves.

(3) A high density current drive discharge with $\overline{Ne}$ =1.0 x 10^{13} cm^{-3} was obtained by improving wave accesibility at higher toroidal magnetic field.

(4) LH waves with sharp spectrum accesible to the central plasma will be required for higher density discharge.

(5) Current drive efficiency increased with the plasma density and reached up to 0.9 (10^{19} m^{-2} kA/kW).

(6) This density dependence can be ascribed to the improvement of confinement of high energy electrons.

HIGH FREQUENCY LHCD

Device Parameters of TRIAM-1M

Major Radius	0.8 m
Limiter Bore	0.24 x 0.36 m^2
Plasma Elongation	1.8
Toroidal Field	8 T
Plasma Current	0.5 MA
Discharge Duration	0.5 S

Main Parameters of RF System

Frequency (GHz)	2.45	8.2
Klystron	1	8
Output Power (kW)	50	200
Pulse Width	CW	CW
Launcher Waveguide Array	4 x 1	8 x 2
Launcher Waveguide Mouth (mm^2)	15 x 71	4 x 35

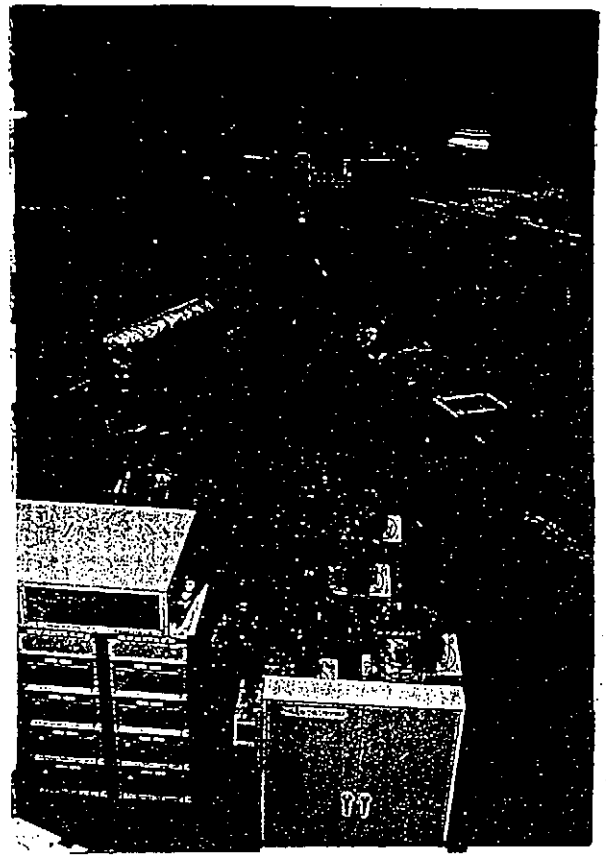

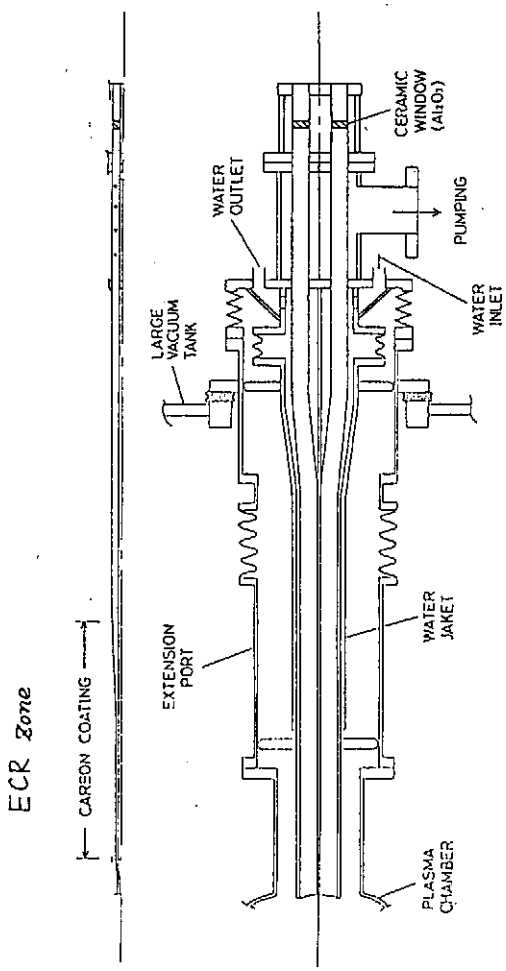

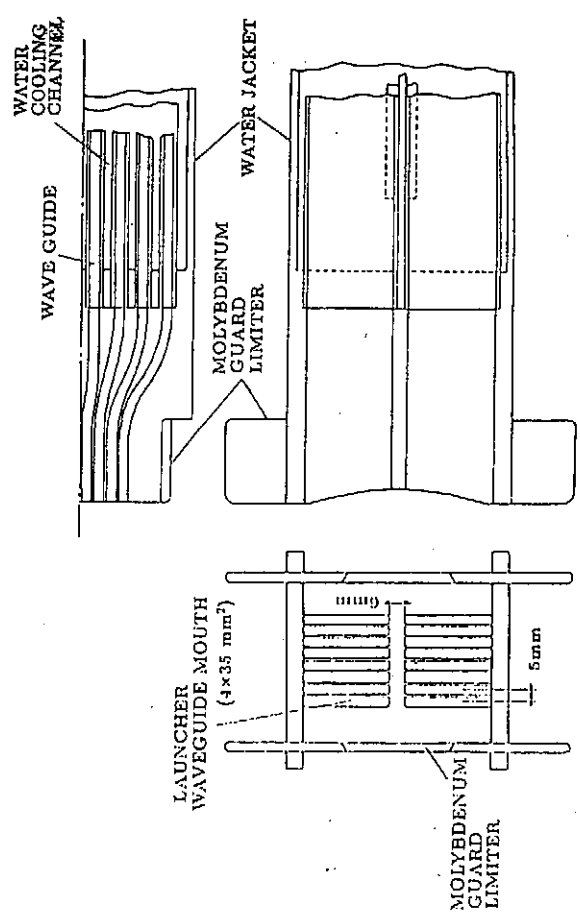

$N_{//}$ spectra for 8.2 GHz launcher

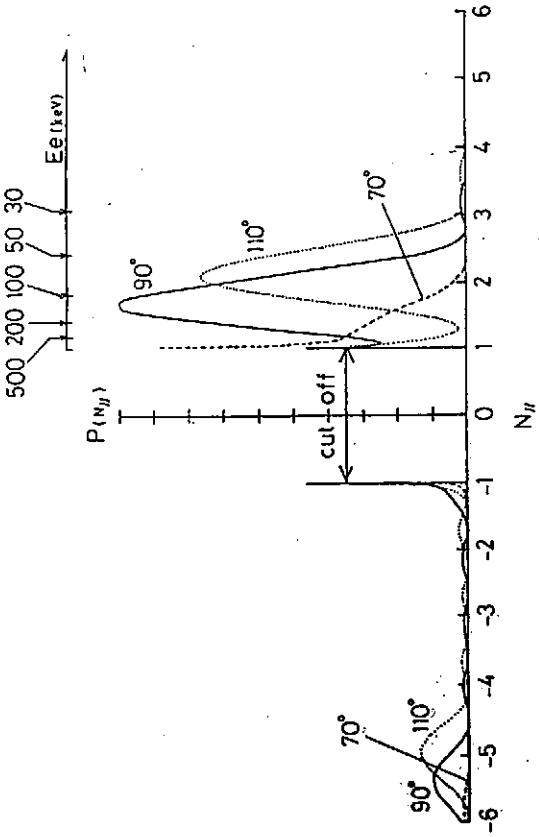

Operational regime of current drive discharge

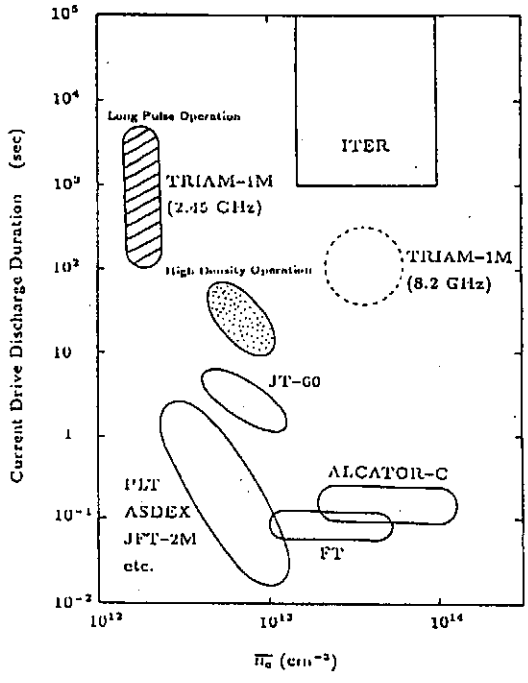

CURRENT PROFILE CONTROL WITH LOWER HYBRID WAVES IN ASDEX.

STEFANO BERNABEI

1. EXPERIMENTAL RESULTS AND COMPARISON WITH THEORY
2. APPLICATION TO THE FBX-M EXPERIMENT(1992) ON SECOND STABILITY

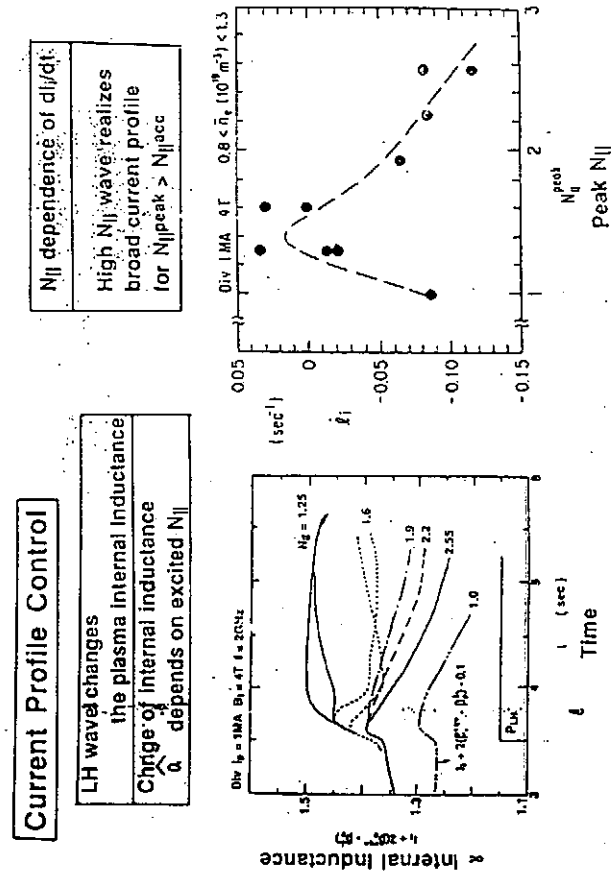

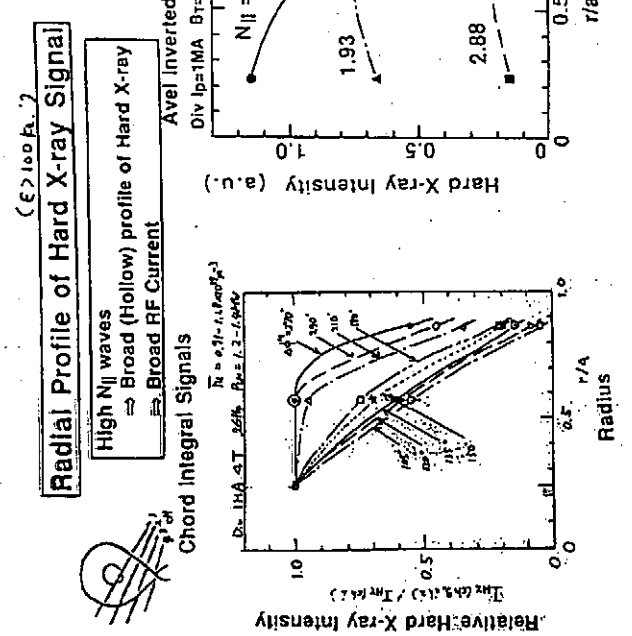

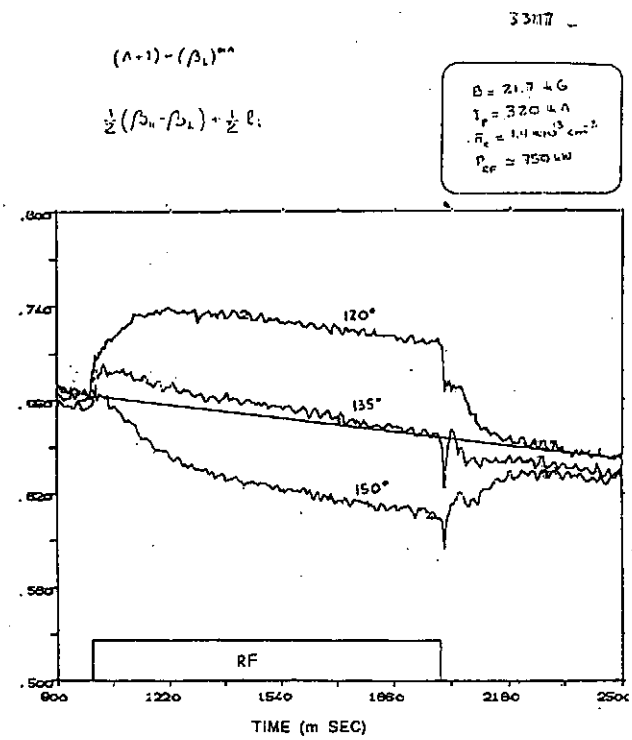

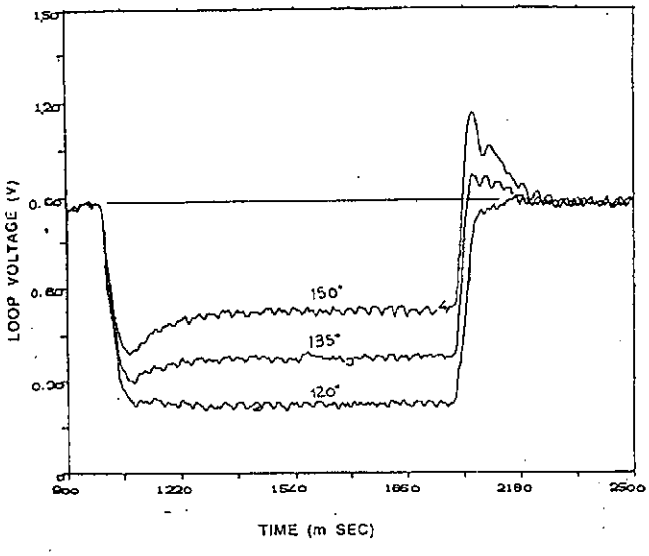

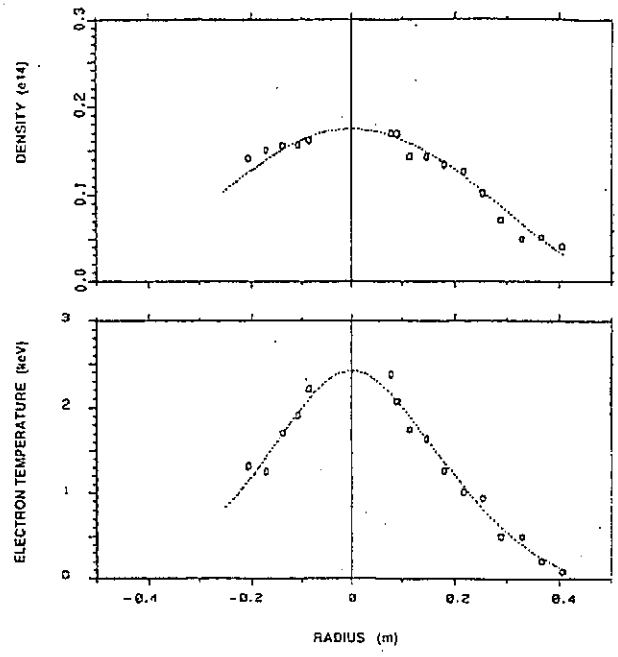

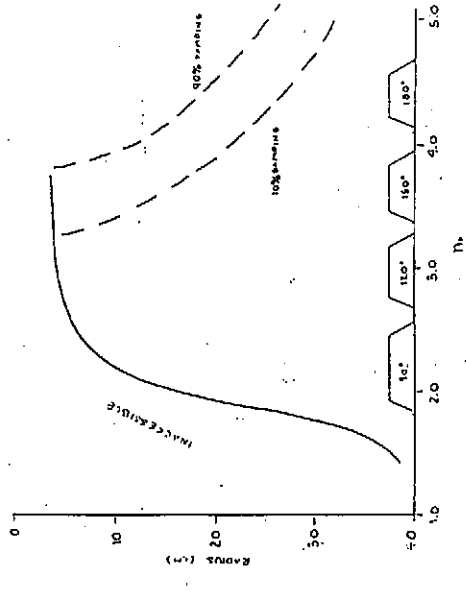

Accessibility and damping regions for a typical ASDEX plasma with $\bar{n}_e = 2 \times 10^{13}$ cm^{-3} and B_t = 21.7 kG. , FREQUENCY = 2.45 GHz

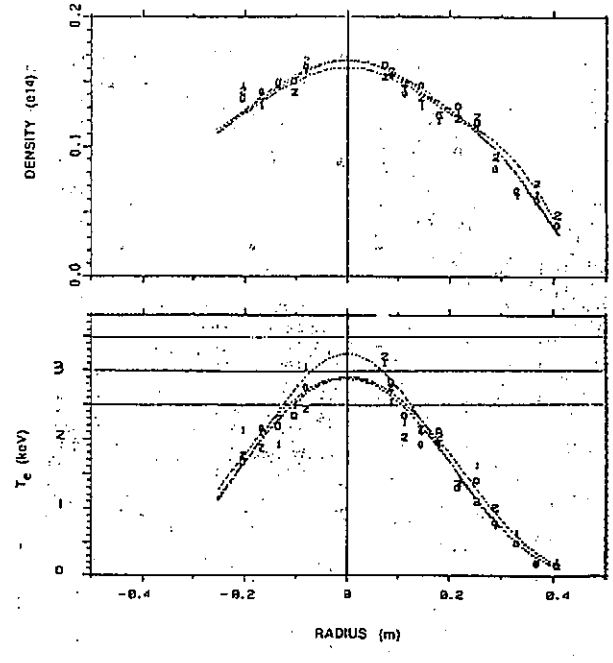

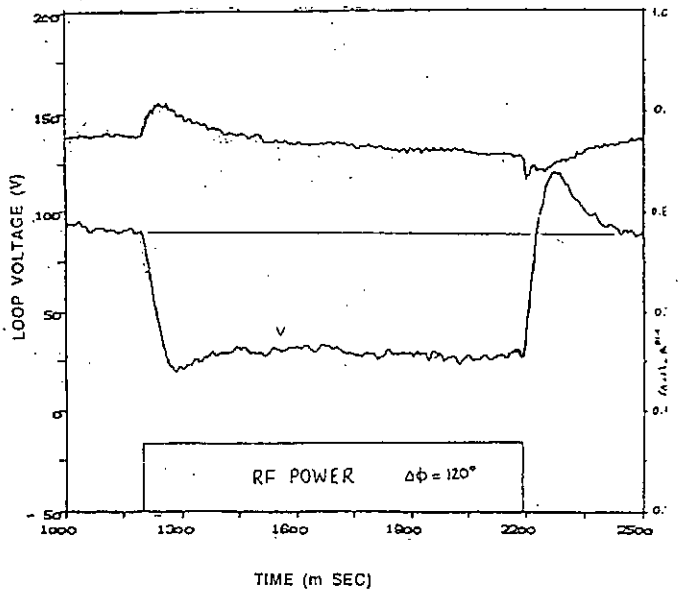
LOOP VOLTAGE (V)
TIME (m SEC)
RF POWER Δφ = 120°
V

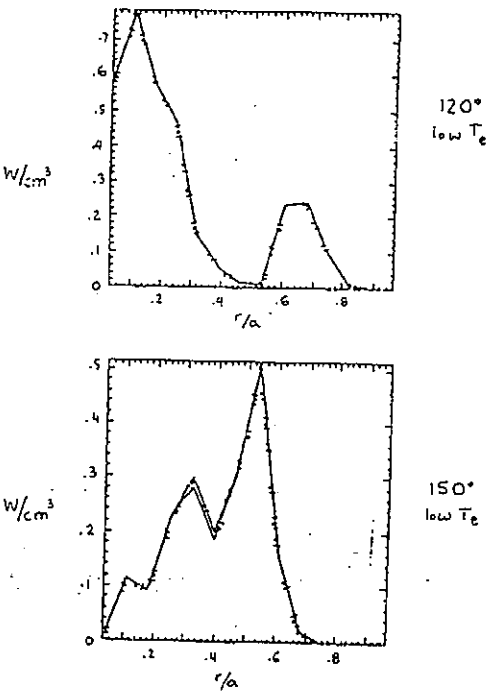
W/cm³
r/a
120° low T_e
150° low T_e

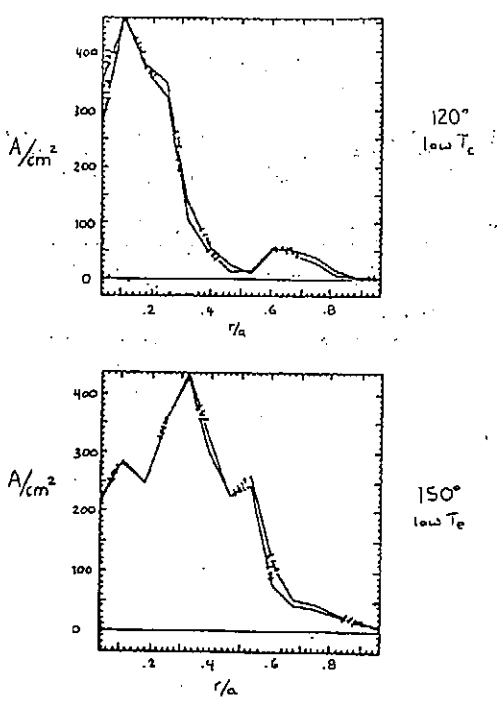
A/cm²
r/a
120° low T_e
150° low T_e

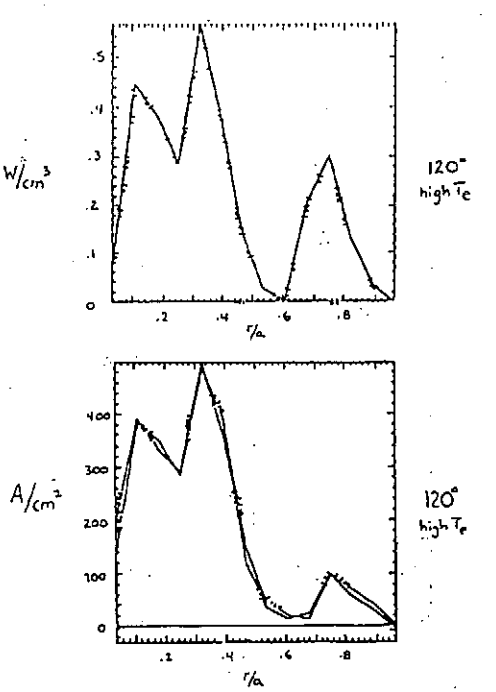
W/cm³
A/cm²
r/a
120° high T_e
120° high T_e

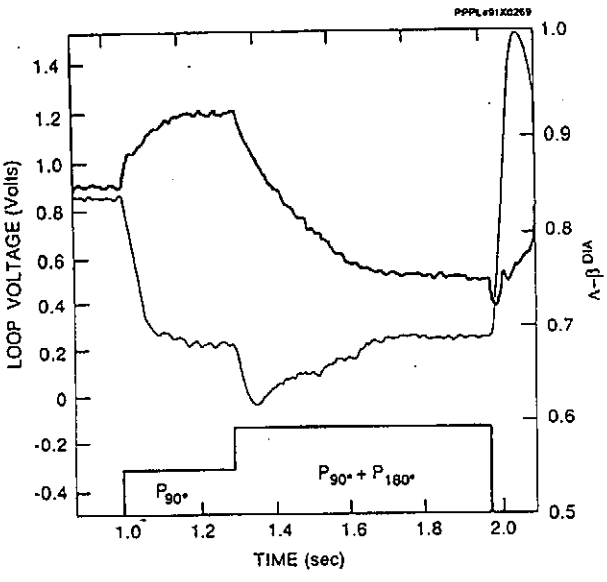

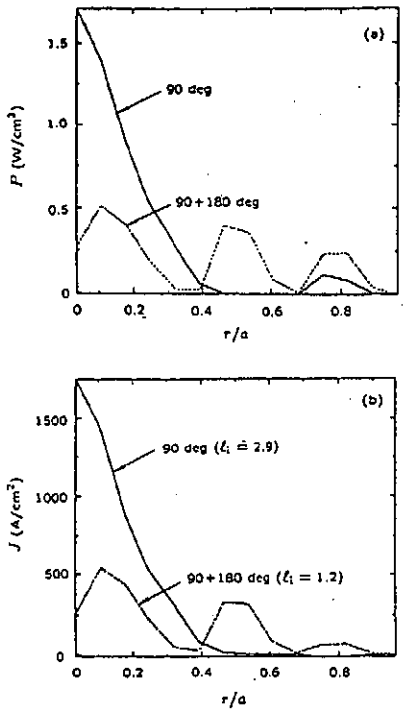

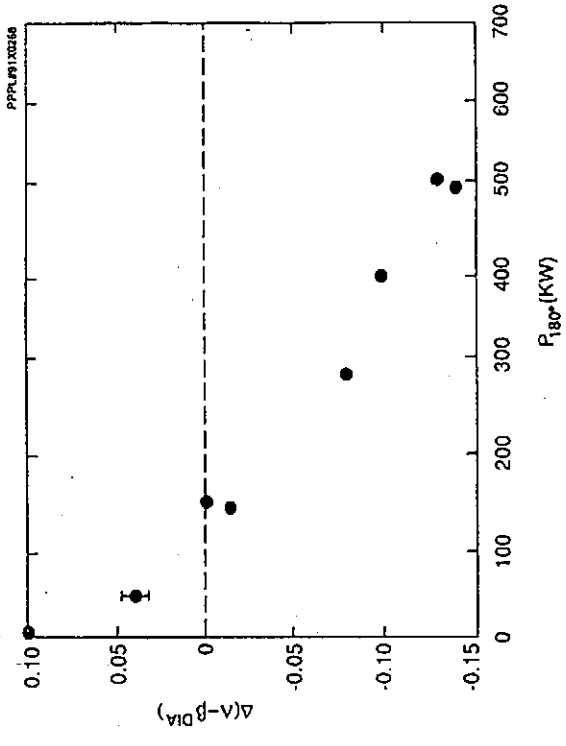

CONCLUSION

- Good degree of current profile control is possible using two $n_{\parallel}$ spectra: high $n_{\parallel}$ determines the damping location, low $n_{\parallel}$ provides most of the current.
- Excellent agreement between experiment and modelling code show that good degree of prediction can be achieved.
- The role played by the high $n_{\parallel}$ spectrum can be replaced by any other mean capable of producing a localized fast electron tail.

LOWER HYBRID PROGRAM FOR FY 92

SELECTED MILESTONES:

Complete final report on 1 MW LHCD experiment	Nov 92
Evaluation of current profile control for the achievement of plasma β in excess of Troyon limit	May 93
Commencement of 2 MW LHCD experiments to control the edge plasma current and q(0)	Nov 93

LOWER HYBRID PHYSICS

1. INITIAL TESTS AND COUPLING

   phase checking / power handling / conditioning / etc
   optimization of coupling in circular and bean plasmas

2. LHCD PHYSICS AND DIAGNOSTICS

   CD efficiency in circular plasma → comparison with TSC-LH code
   2D tangential X-ray imaging camera
   ω_{ce} diagnostic
   CD at high values of ω_{pe}/ω_{ce}

3. MODULATION EXPERIMENTS

   LHCD + pellet (ToreSupra results)
   diffusion of fast electrons (?)

CURRENT PROFILE MODIFICATION EXPERIMENTS

1. $n_{\parallel}$ VARIATION

   launch single - double spectrum (ASDEX results)
   study q-profile modification varying ohmic conditions with MSE diagnostic

2. LHCD + FAST PRIMARY OH RAMP

   study effect of electric field for edge current drive (vary $n_{\parallel}$, $\dot{i}_{oh}$, timing, P_{rf}/P_{oh} etc)

3. LHCD + IBWH

   IBWH can provide seed current for localization
   synergy?

4. PROFILE MODIFICATION AT LOW PLASMA CURRENT

   MIT proposal
   variation of plasma and wave parameters

5. LHCD + NEUTRAL BEAMS

   higher T_e plasma
   larger indentation

FY 93 CURRENT PROFILE MODIFICATION IN VIEW OF SECOND STABILITY REGIME

INCREASE POWER

LOWER HYBRID CURRENT DRIVE EXPERIMENT FY 92

RF SYSTEM

FREQUENCY	4.6 GHz
SOURCE POWER	250 kW x 4 = 1 MW
MAX PULSE LENGTH	0.5 sec
COUPLING	1 array with 32 waveguides
PHASE ADJUSTMENT	continuous 0° - 360° controllable in real time
POWER MODULATION	90% dc to kHz range

DIAGNOSTICS

2D HARD X-RAY TANGENTIAL IMAGING TUBE	damping location
POLARIMETRY (MSE)	q (r,t)
RELAXATION OF ω_{ce} EMISSION	f (v_e)

MODELLING

LH IN TSC CODE
- multiple LH rays
- quasi linear damping
- Karney-Fisch response function
- electric field

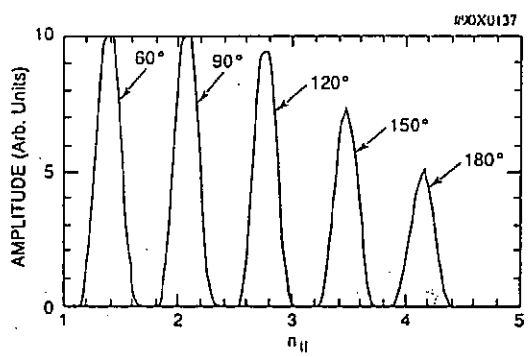

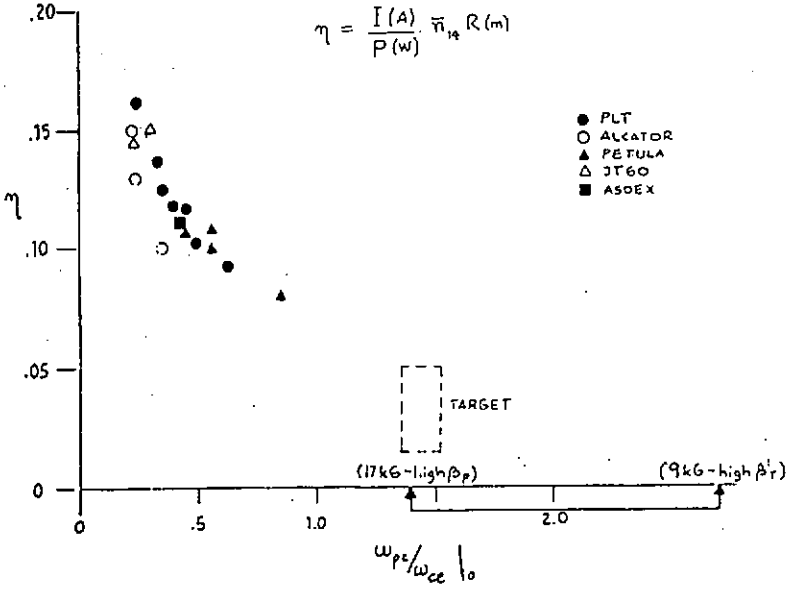
$\eta = \frac{I(A)}{P(W)} \bar{n}_{19} R(m)$
PLT
ALCATOR
PETULA
JT60
ASDEX
.20
.15
.10
.05
0
η
TARGET
(17kG-high β_p)
(9kG-high β'_T)
0
.5
1.0
2.0
$\omega_{pe}/\omega_{ce}|_o$

MODELLING DIII-D AND ITER FAST WAVE CURRENT DRIVE EXPERIMENTS WITH A FULL-WAVE CODE

P.T. Bonoli and M. Porkolab
MIT Plasma Fusion Center

Presented by P.T. Bonoli

I. INTRODUCTION

A. Current drive by ICRF fast waves is the leading alternate method for central current drive in the reactor regime [$n_e(0) \gtrsim 1 \times 10^{20} m^{-3}$; $T_e(0) \sim T_i(0) \gtrsim 20$ keV].

(1) Absorption mechanism is a combination of electron transit time magnetic pumping (TTMP) and electron Landau damping (ELD).

(2) Recent theoretical work has clarified the combined effects of electron TTMP and ELD for arbitrary wave phase speeds ($\omega/k_\parallel v_{te} \lesssim 1$). Two cases have been treated: (a) Maxwellian or bi-Maxwellian electron distribution function. (b) Electron distribution characterized by a tail component $\alpha_H = (2E_\parallel^H/m_e)^{1/2}$.

B. A toroidal full-wave code (FISIC) has been modified to incorporate these theoretical results for electron absorption.

(1) Full-wave results have been coupled to an ICRF current drive package.

(2) Code has been used to model the recent results of direct electron heating and current drive in the DIII-D tokamak.

II. ABSORPTION THEORY

A. Direct absorption of the magnetosonic wave in the ICRF regime by electrons:

Power Absorbed

$$P_{ABS} = -\frac{i\omega}{16\pi} \sum_{modes} \vec{E}^* \cdot \left(\vec{K} - \vec{\overline{1}}\right) \cdot \vec{E} + C.C. \qquad (1)$$

For electron Landau type of resonance, the following terms contribute:

Electron Landau Damping (ELD):

$$K_{zz} = 1 + \frac{1}{k_\parallel^2 \lambda_D^2} [1 + \zeta_e Z(\zeta_e)] \qquad (2)$$

Transit-Time Magnetic Pumping (TTMP)

$$K_{yy} = 1 + 2k_\perp^2 r_{ce}^2 \frac{\omega_{pe}^2}{\omega^2} \zeta_e Z(\zeta_e) \qquad (3)$$

Cross-Term: (CT)

$$K_{yz} = -K_{zy} = -i \frac{\omega_{pe}^2}{\omega \omega_{ce}} \frac{k_\perp}{k_\parallel} [1 + \zeta_e Z(\zeta_e)] \qquad (4)$$

where $\zeta = \omega/k_\parallel v_{te}$, $v_{te} = (2T_e/m_e)^{1/2}$, and $Z(\zeta_e)$ is the plasma dispersion function.

Damping Decrement

$$2k_{\perp_M} \simeq P_{abs}/S_\perp \qquad (5)$$

$$S_\perp = S_x \simeq \frac{cn_x}{8\pi} |E_y|^2 \xi_x \qquad (6)$$

$$\left(k_\parallel^2 \ll k_\perp^2 \equiv k_x^2\right)$$

$$P_{abs} = \frac{\zeta_e \omega}{4\pi^{1/2}} \frac{\omega_{pe}^2}{\omega^2} \left[\overset{A}{k_\perp^2 r_{ce}^2 |E_y|^2} - \overset{B}{\frac{\omega}{\omega_{ce}} \frac{k_\perp}{k_\parallel} |E_x||E_y|} + \overset{C}{\zeta_e^2 |E_x|^2} \right] e^{-\zeta_e^2} \qquad (7)$$

$A \equiv$ TTMP

$B \equiv$ Cross-Term

$C \equiv$ ELD

Polarization

$$\frac{E_x}{E_y} \simeq \overset{①}{\frac{n_\perp n_\parallel K_{xy}}{(K_{xx} - n_\parallel^2) K_{xx}}} - \overset{②}{\frac{K_{xy}}{K_{xx}}} \qquad (8)$$

① Adds to ELD ② Cancels TTMP

Damping Decrement (Cont.)

$$2k_{\perp_{IM}} = k_{\perp_{RE}} \left(\frac{\pi^{1/2}}{2}\right) \beta_e \zeta_e e^{-\zeta_e^2} \left[1 + \left(\frac{1}{\alpha}\right)^2\right] \quad , \tag{9}$$

$$\alpha = \left(\frac{T_e}{m_i c^2}\right) \left(\frac{\omega^2 - \omega_{ci}^2}{\omega_{pi}^2}\right) \left(S - n_\parallel^2\right) |K_{zz}| \quad . \tag{10}$$

$$S = 1 - \sum_j \omega_{pj}^2 / \left(\omega^2 - \omega_{cj}^2\right) \quad .$$

Cold Plasma Limit ($\zeta_e \gg 1$)

$$\left(\frac{1}{\alpha}\right)^2 \simeq \left(\frac{m_e c^2}{T_e}\right)^2 \frac{\omega^4}{\omega_{pi}^4} \quad . \tag{11}$$

III. FULL-WAVE ICRF CALCULATIONS

A. Model equations: /4/

$$\vec{\nabla} \times \vec{\nabla} \times \vec{E} = \left(\frac{\omega}{c}\right)^2 \left[\vec{E} + \frac{4\pi i}{\omega}\left(\vec{J}^{(0)} + \sum_i \vec{J}_i^{(2)} + \vec{J}_e^{(2)}\right)\right] \quad , \tag{12a}$$

$$\vec{E} + \frac{4\pi i}{\omega}\vec{J}^{(0)} = \hat{L}E_+\vec{e}_+ + \hat{R}E_-\vec{e}_- + \overleftarrow{\hat{P}E_\parallel\vec{e}_\parallel}^{\text{ELD}} \quad , \tag{12b}$$

$$\frac{4\pi i}{\omega}\vec{J}_e^{(2)} = -2\frac{c^2}{\omega^2}\vec{\nabla}_\perp \times \overbrace{\left[\hat{\lambda}_{0,e}\left(\vec{\nabla}_\perp \times \vec{E}_\perp\right)\right]}^{\text{TTMP}} +$$

$$i\frac{c^2}{\omega^2}\underbrace{\left\{\left(\vec{e}_\parallel \cdot \vec{\nabla}\right)\hat{\zeta}_{0,e}\left(\vec{\nabla}_\perp \times \vec{E}_\perp\right) + \vec{\nabla}_\perp \times \left[\left(\vec{e}_\parallel \cdot \vec{\nabla}\right)\hat{\zeta}_{0,e}E_\parallel\vec{e}_\parallel\right]\right\}}_{\text{CROSS-TERM}} \tag{12c}$$

(1) Plane Stratified Limit:

$$\hat{P} \to P = 1 - \frac{\omega_{pe}^2}{\omega^2}\zeta_{0,e}^2 Z'(\zeta_{0,e}) \quad , \tag{13a}$$

$$\hat{\lambda}_{0,e} \to \lambda_{0,e} = -\frac{1}{2}\frac{\omega_{pe}^2}{\omega_{ce}^2}\frac{v_{te}^2}{c^2}\zeta_{0,e}Z(\zeta_{0,e}) \quad , \tag{13b}$$

$$\hat{\zeta}_{0,e} \to \zeta_{0,e} = \frac{1}{2}\frac{\omega_{pe}^2}{\omega\omega_{ce}}\frac{v_{te}^2}{c^2}\zeta_{0,e}^2 Z'(\zeta_{0,e}) \quad . \tag{13c}$$

(2) Perturbative Formulation for $E_\parallel$:

Take limit in parallel component of wave equation (12a):

$$m_e/m_i \to 0;\ (\vec{e}_\parallel \cdot \vec{\nabla}) \to ik_\parallel;\ \hat{P} \to P;\ \hat{\zeta}_{0,e} \to \zeta_{0,e}$$

$$E_\parallel \approx -\frac{c^2}{\omega^2}\frac{ik_\parallel}{P}\left[i\zeta_{0,e}\vec{e}_\parallel \cdot \vec{\nabla}_\perp \times \vec{E}_\perp - \vec{\nabla} \cdot \vec{E}_\perp\right] \quad , \tag{14}$$

B. Numerical Solution of Wave Equation

(1) Semi-spectral expansion of $\vec{E}$ in Poloidal Fourier Modes:

$$\vec{E} = \sum_{m,n_\phi} \underline{\hat{E}}^{m,n_\phi}(\rho) e^{im\theta + in_\phi\phi} \quad . \tag{15}$$

- Each n_ϕ mode is treated separately.
- Variational form of wave equation is constructed based on the Spectral Anzatz (15).
- $\underline{\hat{E}}^{m,n_\phi}(\rho)$ are fit to cubic Hermite, interpolating polynomials.

(2) Rewrite $E_\parallel$:

$$E_\parallel \approx -ik_\parallel \frac{c^2}{\omega^2}\frac{\vec{e}_\parallel \cdot \vec{\nabla}_\perp \times \vec{E}_\perp}{P}\left|i\zeta_{0,e} - c_p\right| \quad , \tag{16}$$

$$c_p = \vec{\nabla} \cdot \vec{E}_\perp / \vec{e}_\parallel \cdot \vec{\nabla}_\perp \times \vec{E}_\perp \quad .$$

- The polarization ratio (c_p) is evaluated from the WKB form of the wave equation (12), assuming $\vec{k} = \vec{e}_x k_\perp + \vec{e}_z k_\parallel$ and $\vec{E} = (E_x, E_y, E_z)$.
- This simplification [Eq. (16)] eliminates the need to evaluate products of the form $(\vec{\nabla} \cdot \vec{E}_\perp)(\vec{e}_\parallel \cdot \vec{\nabla}_\perp \times \vec{E}_\parallel)$ in the variational solution.

(3) Retain 65 poloidal modes in spectral representation($m = -32 \to +32$).

- Use 80 points on "radial" (ρ)-grid.

IV ICRF CURRENT DRIVE EFFICIENCY

- Combined full-wave ICRF and Fokker Planck formulation

A. Current Drive Efficiency /5/

$$\left(\frac{J_{RF}}{S_{RF}}\right)_A = \frac{\int d^3p\vec{\Gamma}\cdot(\partial\chi/\partial\vec{p})}{\int d^3p\vec{\Gamma}\cdot\vec{v}} \quad , \tag{17}$$

- $\chi(\vec{p})$ is the Spitzer-Härm function which is found by solving the "adjoint" problem /5/

$$C(f_e\chi) = -qv_\parallel f_e \quad . \tag{18}$$

B. Wave Induced Flux ($\vec{\Gamma}$):

$$\vec{\Gamma} = -\overline{D}_{RF}\cdot\frac{\partial}{\partial\vec{p}}f_e \quad , \tag{19}$$

(1) Diffusion Tensor /2/:

$$\overline{D}_{RF} = \vec{e}_\parallel\vec{e}_\parallel D_W \quad , \tag{20a}$$

$$D_W = \frac{\pi}{2}\left(\frac{e}{m_e}\right)^2\left(\frac{k_\parallel}{\omega}\right)^2|\Theta_0 v_\perp|^2 \quad , \tag{20b}$$

$$|v_\perp\Theta_0|^2 = \frac{1}{4}\left(\frac{k_\perp}{\omega_{ce}}\right)^2|E_y|^2\left|v_\perp^2 - v_{te}^2 - 2\frac{\omega_{ce}c^2}{\omega}\frac{iK_{xy}}{(S-n_\parallel^2)K_{xx}}\right|^2 \quad . \tag{20c}$$

- $E_y(\rho, k_\parallel^{m,n\phi})$ is known for each n_ϕ mode from the full-wave solution.

B. RF Current Density:

$$J_{RF}(\rho) = \left(\frac{J_{RF}}{S_{RF}}\right)_A \cdot S^{\mathcal{E}}_{abs}(\rho) \quad , \tag{21}$$

- $S^{\mathcal{E}}_{abs}(\rho)$ is the profile of electron absorption (TTMP + ELD) which is known from the full-wave code.
- Present calculation uses parameterization for $(J_{RF}/S_{RF})_A$ due to Ehst and Karney /6/

$$G \equiv \left(\frac{J_{RF}}{S_{RF}}\right)_A = G(Z_{eff}, \epsilon, \zeta_e, \theta) \quad . \tag{22}$$

V. MODEL RESULTS FOR DIII-D

A. Parameters for Electron Heating Regime

60 MHz	$(0-\pi-0-\pi)$ phasing
$k_{\parallel peak} \approx 12.7m^{-1}$	$(n_\parallel \approx 10)$

(Shot #72750)	(Shot #72685)
$a = 0.628$ m	$a = 0.48$ m
$R = 1.71$ m	$R = 1.86$ m
$B_T = 1.99$ T	$B_T = 2.10$ T
$I_p = 998$ kA	$I_p = 308$ kA
$\kappa = 1.99$	$\kappa = 1.42$
$n_e(0) = 2.7 \times 10^{19}m^{-3}$	$n_e(0) = 2.6 \times 10^{19}m^{-3}$
$T_e(0) = 2.43$ keV	$T_e(0) = 2.13$ keV
$T_i(0) = 1.33$ keV	$T_i(0) = 0.6$ keV
$n_H/(n_H+n_D) = 2\%$	$n_H/(n_H+n_D) = 2\%$

B. Parameters for Current Drive Regime

(1) RF Parameters

60 MHz		$(0-\pi/2-0-\pi/2)$ Phasing
$k_\parallel^{peak} \simeq 7m^{-1}$	for	forward direction ($k_\parallel > 0$)
$k_\parallel^{peak} \simeq 20m^{-1}$	for	reverse direction ($k_\parallel < 0$)

(2) Plasma parameters similar to electron heating regime.

(3) Experimental finding of DIII-D Current Drive Experiments:

- Decrease in loop voltage with reverse phasing is greater than or equal to loop voltage decrease with forward phasing.

RAY TRACING RESULTS (ACCOME) FOR DIII-D
CURRENT DRIVE REGIME

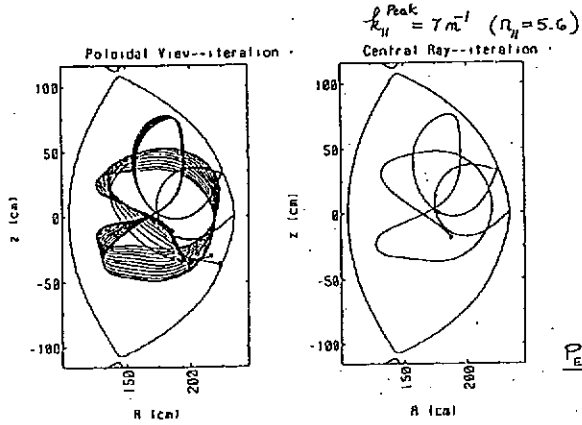

$P_{ELD} = 40\%$

$B_o = 1T$; $I_p = 600$ kA ; $T_e(0) = 1.5$ keV ; $n_e(0) = 3\times10^{19} m^{-3}$

RAY TRACING RESULTS (ACCOME) FOR DIII-D
CURRENT DRIVE REGIME

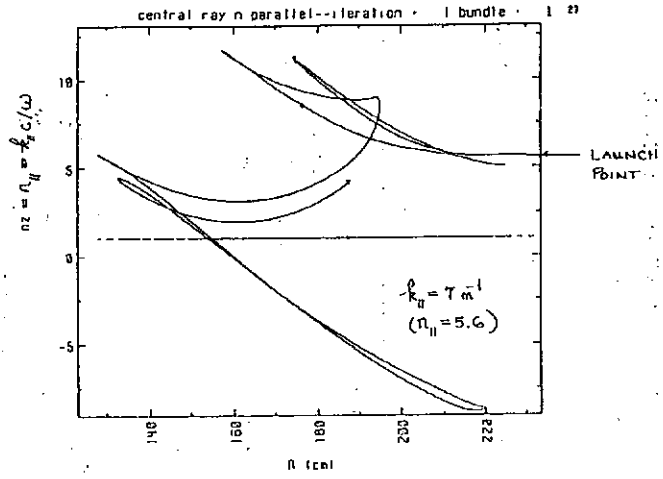

$B_o = 1T$; $I_p = 600$ kA ; $T_e(0) = 1.5$ keV ; $n_e(0) = 3\times10^{19} m^{-3}$

FULL-WAVE RESULTS FOR DIII-D ELECTRON HEATING

SHOT #72685 $\quad a = 0.48$ m $\quad B_T = 2.10$ T

$I_p = 308$ kA $\quad T_e(0) = 2.13$ keV

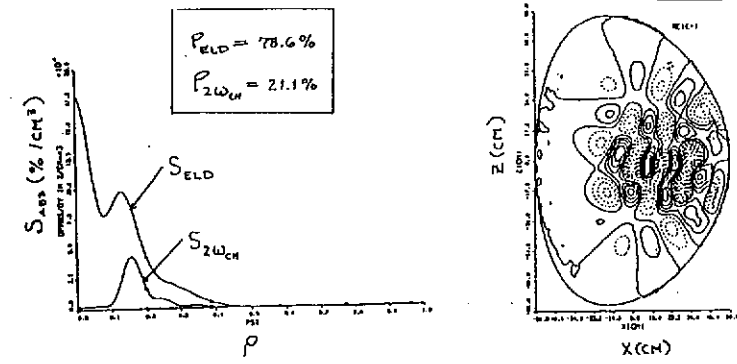

$(k_{\parallel} = 12.6\,m^{-1}$; $n_+ = 30)$

FULL-WAVE RESULTS FOR DIII-D ELECTRON HEATING

SHOT #72750 $\quad a = 0.628$ m $\quad B_T = 1.97$ T

$I_p = 998$ kA $\quad T_e(0) = 2.43$ keV

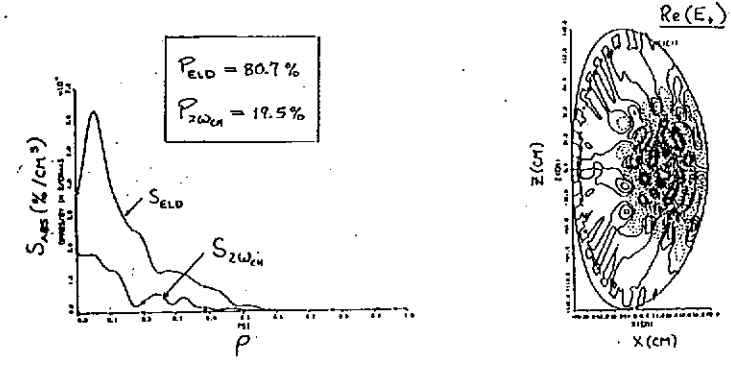

$(k_{\parallel} = 12.7\,m^{-1}$; $n_+ = 30)$

FULL-WAVE RESULTS FOR DIII-D CURRENT DRIVE REGIME

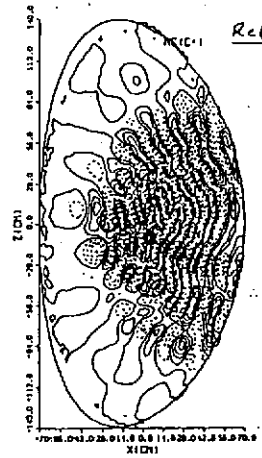

$k_{\parallel} = 7\ m^{-1}$

$B_T = 1.99\ T$

$I_p = 998\ kA$

$T_e(0) = 2.43\ keV$

$n_e(0) = 2.7 \times 10^{19}\ m^{-3}$

FULL-WAVE RESULTS FOR DIII-D CURRENT DRIVE REGIME

$k_{\parallel} = 7\ m^{-1}$ $\quad B_T = 1.99\ T$ $\quad T_e(0) = 2.43\ kA$

$I_p = 998\ kA$ $\quad n_e(0) = 2.7 \times 10^{19}\ m^{-3}$

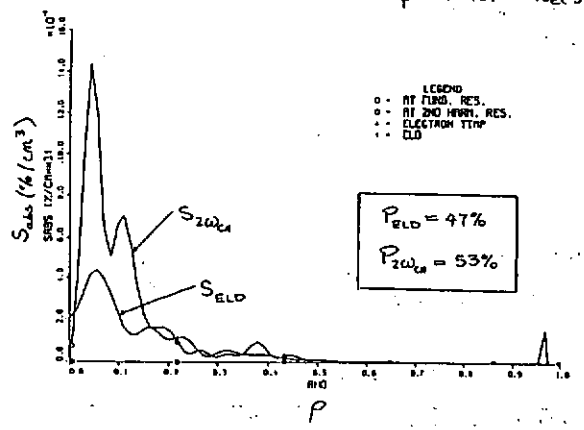

$P_{ELD} = 47\%$

$P_{2\omega_{CH}} = 53\%$

DIII-D ICRF CURRENT DRIVE RESULTS

(FULL-WAVE PLUS FOKKER PLANCK)

$B_T(T)$	$T_e(0)$(keV)	α_N^*	$k_{\parallel_0}(m^{-1})$	$J_e(0)$	I/P (A/W)	P_{ELD} (%)	$P_{2\omega_{CH}}$ (%)
2	2.43	1.16	7	1.30	0.096	47.0	53.0
2	2.43	0.5	20	0.37	0.259	99.6	0.3
1	1.50	1.16	7	1.65	0.175	89.8	6.6
1	1.50	0.5	20	0.59	0.134	100.0	0

* $n_e(\rho) = [n_e(0) - n_e(a)](1-\rho^2)^{\alpha_N} + n_e(a)$

PARAMETERS SIMILAR TO SHOT # 72750

$Z_{eff} = 2.0$

$J_e(0) = \omega / k_{\parallel_0} V_{te}(0)$

FULL-WAVE RESULTS FOR DIII-D CURRENT DRIVE REGIME

$k_{\parallel} = 7\ m^{-1}$ $\quad B_T = 1.99\ T$ $\quad T_e(0) = 2.43\ keV$

$I_p = 998\ kA$ $\quad n_e(0) = 2.7 \times 10^{19}\ m^{-3}$

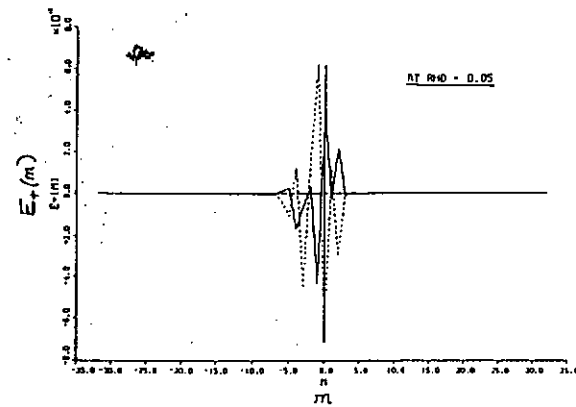

——— $Re(E_+)$ $\quad$ – – – $Im(E_+)$

FULL-WAVE RESULTS FOR DIII-D CURRENT DRIVE REGIME

$k_\parallel = 20\ m^{-1}$ $\quad B_T = 1.99\ T$ $\quad T_e(0) = 2.43\ keV$

$I_p = 998\ kA$ $\quad n_e(0) = 2.7 \times 10^{19}\ m^{-3}$

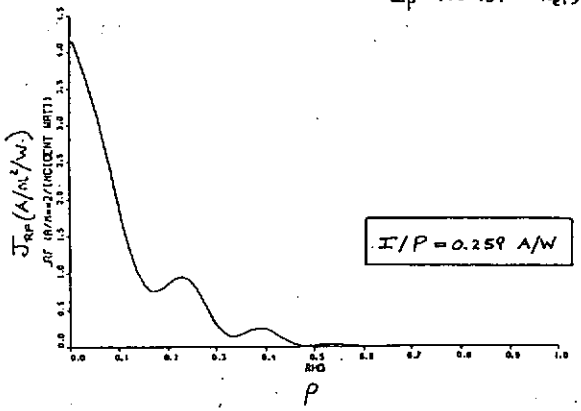

$I/P = 0.259\ A/W$

FULL-WAVE RESULTS FOR DIII-D CURRENT DRIVE REGIME

$k_\parallel = 7\ m^{-1}$ $\quad B_T = 1.99\ T$ $\quad T_e(0) = 2.43\ keV$

$I_p = 998\ kA$ $\quad n_e(0) = 2.7 \times 10^{19}\ m^{-3}$

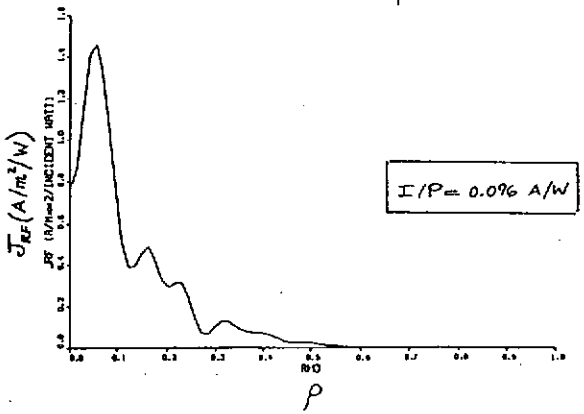

$I/P = 0.096\ A/W$

FULL-WAVE RESULTS FOR DIII-D CURRENT DRIVE REGIME

$k_\parallel = 7\ m^{-1}$ $\quad B_T = 1.0\ T$ $\quad T_e(0) = 1.5\ keV$

$I_p = 400\ kA$ $\quad n_e(0) = 2.7 \times 10^{19}\ m^{-3}$

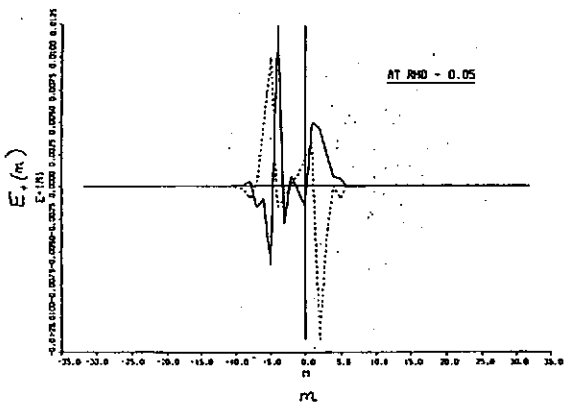

—— $Re(E_+)$ $\quad$ – – – $Im(E_+)$

FULL-WAVE RESULTS FOR DIII-D CURRENT DRIVE REGIME

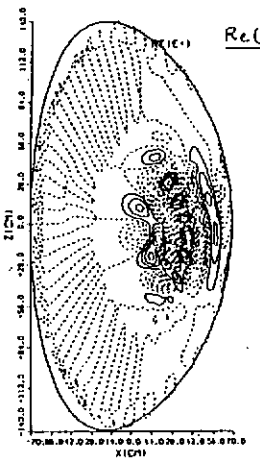

$B_T = 1.99\ T$

$I_p = 998\ kA$

$T_e(0) = 2.43\ keV$

$n_e(0) = 2.7 \times 10^{19}\ m^{-3}$

FULL-WAVE RESULTS FOR DIII-D CURRENT DRIVE REGIME

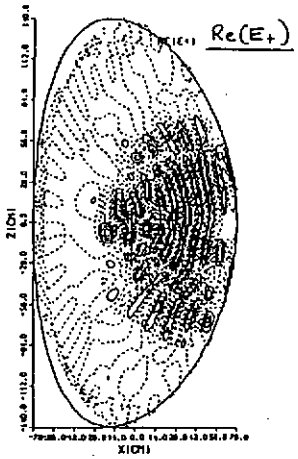

$k_{\parallel} = 20\ m^{-1}$

$B_T = 1.0\ T$
$I_P = 400\ kA$
$T_e(0) = 1.5\ keV$
$n_e(0) = 2.7 \times 10^{19}\ m^{-3}$

FULL-WAVE RESULTS FOR DIII-D CURRENT DRIVE REGIME

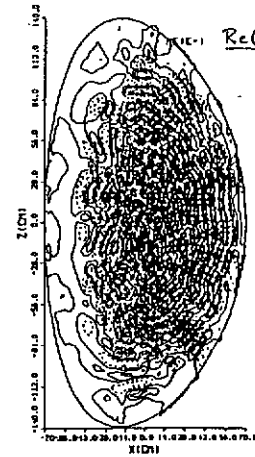

$k_{\parallel} = 7\ m^{-1}$

$B_T = 1.0T$
$I_P = 400\ kA$
$T_e(0) = 1.5\ keV$
$n_e(0) = 2.7 \times 10^{19}\ m^{-3}$

FULL-WAVE RESULTS FOR DIII-D CURRENT DRIVE REGIME

$k_{\parallel} = 20\ m^{-1}$ $B_T = 1.0\ T$ $T_e(0) = 1.5\ keV$
$I_P = 400\ kA$ $n_e(0) = 2.7 \times 10^{19}\ m^{-3}$

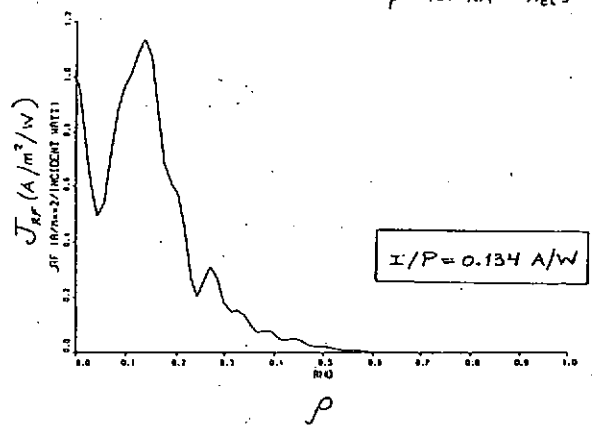

I/P = 0.134 A/W

FULL-WAVE RESULTS FOR DIII-D CURRENT DRIVE REGIME

$k_{\parallel} = 7\ m^{-1}$ $B_T = 1.0\ T$ $T_e(0) = 1.5\ keV$
$I_P = 400\ kA$ $n_e(0) = 2.7 \times 10^{19}\ m^{-3}$

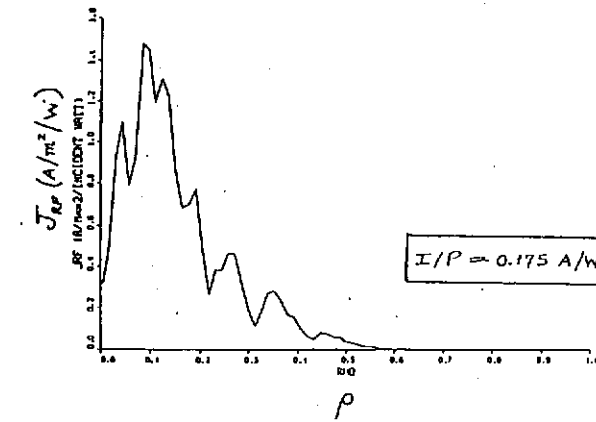

I/P = 0.175 A/W

VI. CONCLUSIONS FOR NUMERICAL MODELLING

A. DIII-D Electron Heating Regime

(1) Direct electron heating by ICRF waves is predicted by a full-wave analysis with multiple passes of the ICRF wave front.

(2) Typically $P_{ELD} \simeq 80\%$, $P_{2\omega_{CH}} \simeq 20\%$ for $B_T = 2T$ and $f_0 = 60$ MHz.

(B.) DIII-D Current Drive Regime

(1) Sign reversal of $k_\parallel \simeq 7m^{-1}$ is predicted by a ray tracing analysis. However, electron absorption is only found for $k_\parallel > 0$.

(2) Full-wave analysis shows that broadening of the $E_+(m)$ spectrum near $\rho = 0$ is not enough to cause large negative values of $k_\parallel$.

(3) Reverse power at $k_\parallel = 20m^{-1}$ is found to couple and damp strongly (ELD) if $n_e(\rho)$ is made flat enough $[n_e \alpha (1-\rho^2)^{1/2}]$.

(4) Combined Fokker Planck and full-wave analysis of ICRF current drive experiments in DIII-D predict:

- $I/P \simeq (0.1 - 0.18)A/W$ for $k_\parallel = 7m^{-1}$
- $I/P \simeq (0.13 - 0.26)A/W$ for $k_\parallel = 20m^{-1}$
- Higher I/P for $k_\parallel = 7m^{-1}$ occurs at $B = 1$ T because $2\omega_{CH}$ absorption is cut-off and ELD is increased.

REFERENCES

/1/ M. Porkolab, GA Memo D3DPM No. 8813, March 24, (1988); GA Memo D3DPM No. 8817, Nov. 11, (1988).

/2/ S.C.Chiu et al., Nucl. Fusion 29, 2175 (1989).

/3/ M. Porkolab, "On the Physics of Magnetosonic Wave Damping on Electrons" to be published in the Proc. of the Ninth Topical Conf. on RF Power in Plasmas, Charleston, S.C. (1991).

/4/ M. Brambilla and T. Krücken, Nucl. Fusion 28, 1813 (1988).

/5/ C.F.F. Karney and N.J. Fisch, Phys. Fluids 28, 116 (1985).

/6/ D.A. Ehst and C.F.F. Karney, Argonne National Laboratory Report ANL/FPP/TM-247 (1990).

US-Japan Workshop
RF Heating and Current Drive
NIFS, 1991/11/18-21

Helicity Injection and Current Drive by RF Waves

A. Fukuyama, K. Hamamatsu[1], K. Itoh[1] and S.-I. Itoh[1]

Faculty of Engineering, Okayama University, Okayama 700
[1]Japan Atomic Energy Research Institute, Naka, Ibaraki 311-01
[1]National Institute for Fusion Science, Nagoya 464-01

CONTENT

RF Helicity Injection
Averaged Force by RF Waves
Non-Resonant Current Drive
1-D Full Wave Analysis
Parameter Dependence
Summary

Original Concept of RF Helicity Injection

Current drive by wave helicity injection

[Ohkawa et al., IAEA Nice, 1988]

Circularly polarized waves have magnetic helicity.

$\langle A_1 \cdot B_1 \rangle$ $\qquad B_1 = \nabla \times A_1$

$E_1 = -\nabla \phi_1 - \partial A_1 / \partial t$

Magnetic helicity conservation

$$\frac{\partial H}{\partial t} + \nabla \cdot Q_H = -2 E_0 \cdot B_0 - 2 \langle E_1 \cdot B_1 \rangle$$

Helicity density: $H = A_0 \cdot B_0 + \langle A_1 \cdot B_1 \rangle$

Helicity flux:

$$Q_H = A_0 \times \frac{\partial A_0}{\partial t} + \left\langle A_1 \times \frac{\partial A_1}{\partial t} + 2 \phi_1 \cdot B_1 \right\rangle$$

Absorption of wave helicity: $2 \langle E_1 \cdot B_1 \rangle$

↓

Compensation of DC helicity: $2 E_0 \cdot B_0 = 2 \eta J_0 \cdot B_0$

- Current drive efficiency J/P is independent of density.
- J/P can be comparable to ohmic for collisional damping.

Approach in terms of Averaged Force

Averaged force by RF waves

[Fukuyama et al.; JPSJ 51 (1982) 1010]

- Resonant force (conventional current drive)
- Non-resonant force (ponderomotive force)
  - Conservative force
  - Non-conservative force (helicity injection)

In a uniform and stationary plasma

$$F = q \langle n_1 E_1 + \Gamma_1 \times B_1 \rangle$$

$$= \omega \varepsilon_0 \Big[\frac{k}{\omega} \mathrm{Im} \left(E_1^* \cdot \bar{\chi}_A \cdot E_1 \right) \quad \text{non-resonant force} \quad \mathbb{k}$$

$$+ \frac{k}{2\omega} \frac{\partial}{\partial r} \cdot \left(E_1^* \cdot \frac{\partial \bar{\chi}_H}{\partial k} \cdot E_1 \right) \quad \text{dispersive force} \quad \mathbb{k}$$

$$- \frac{1}{2\omega} \frac{\partial}{\partial r} \left(E_1^* \cdot \bar{\chi}_H \cdot E_1 \right) \quad \text{ponderomotive force} \quad \frac{\partial}{\partial r}$$

$$+ \frac{1}{\omega} \frac{\partial}{\partial r} \cdot \left(\bar{\chi}_H \cdot E_1 E_1^* \right) \Big] \quad \text{non-conservative force} \quad \mathbb{E}_1^T$$

$\bar{\chi}$: Electric susceptibility $\quad \bar{\varepsilon} = \bar{1} + \sum_s \bar{\chi}_s$

COLLISIONAL DAMPING CASE [Taylor, PRL, 1986]

$$F^R = \omega \epsilon_0 \left[\frac{k}{\omega} \mathrm{Im} \left(E_1^* \cdot \overleftrightarrow{\chi}_A \cdot E_1 \right) \right]$$

$$F^{NR} = \omega \epsilon_0 \left[\frac{1}{2\omega} \frac{\partial}{\partial r} \left(E_1^* \cdot \overleftrightarrow{\chi}_H \cdot E_1 \right) \right]$$

$$\chi_A \sim -i \frac{\nu}{\omega} \chi_H$$

$$\frac{\partial}{\partial r} \sim -\frac{\nu}{\omega} k$$

$$\therefore F^{NR} = -\frac{1}{2} F^R$$

F^{NR} $\quad$ F^{NR}

F^{NET}

Non-Resonant Current Drive

Evaluation of averaged force

Slab plasma $B_0 = (0, 0, B_z)$

$k = (k_x, 0, k_z)$

$$F = q\left(n_1^* E_1 + \Gamma_1^* \times B_1\right)$$

$$= \frac{n_0 q}{i\omega}\left(-(\nabla \cdot v_1^*) E_1 - v_1^* \times (\nabla \times E_1)\right)$$

$$F_z = \frac{n_0 q}{i\omega}\left(\underbrace{v_1^* \cdot \frac{\partial E_1}{\partial z}}_{\text{Resonant force } F^R} - \underbrace{\frac{\partial}{\partial z}(v_{1z}^* E_{1z})}_{\text{Conservative force}} - \underbrace{\frac{\partial}{\partial r}(v_{1r}^* E_{1z})}_{\text{Non-conservative force } F^{NR}}\right)$$

If $E_{1z} = 0$, non-conservative force vanishes.

$\omega \ll \omega_c$

$v_{1x}^* \sim \frac{E_{1y}^*}{B_0}$

$\frac{\partial E_{1y}}{\partial x} \sim -i\omega B_{1z}$

$F_{NR} \sim 2 n_0 q \frac{E_{1y}^* B_{1z}}{B_0}$

Evaluation of driven current

$$J_{//}^R = \frac{q}{m}\tau\left(\frac{\omega}{k_{//} v_{Ts}}\right) f_{tp}^R\left(\frac{\omega}{k_{//} v_{Ts}}\right) F^R$$

$$J_{//}^{NR} = \frac{q}{m}\tau_c \quad f_{tp}^{NR} \quad F^{NR}$$

f_{tp} : trapped particle effect

f_{tp}^R : fitting formula (Ehst et al.)

f_{tp}^{NR} : neoclassical resistivity

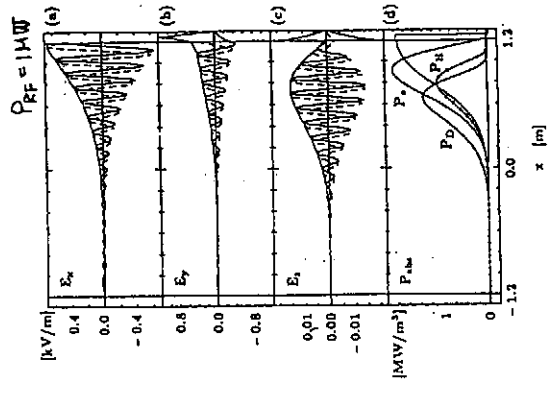

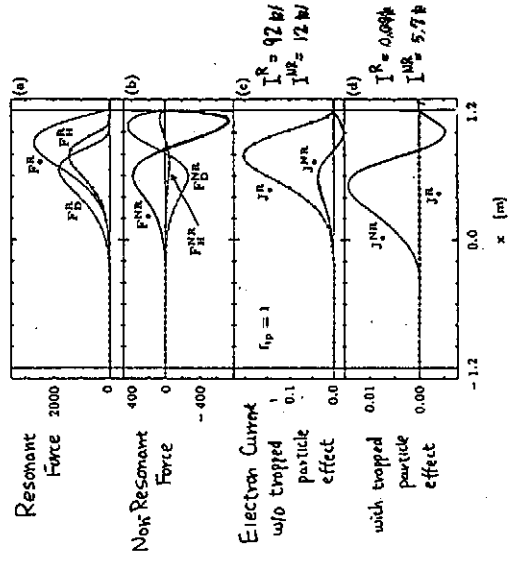

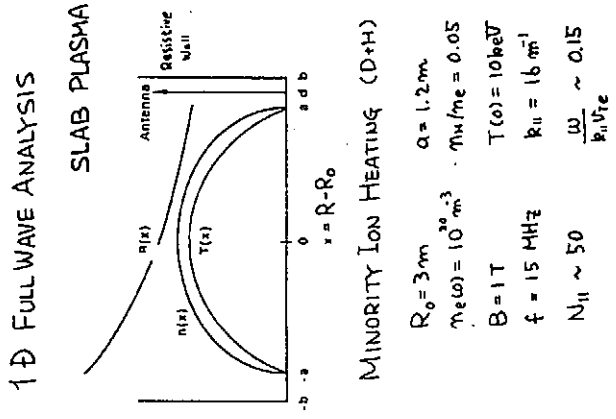

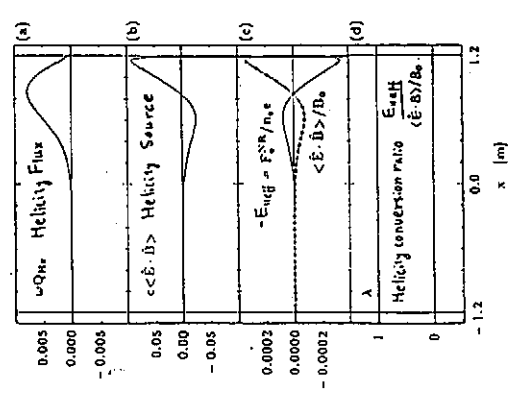

JET (B=1T n=1 (=15MHz)

WAVE NUMBER DEPENDENCE

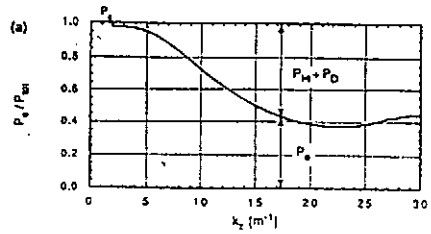

POWER ABSORBED BY ELECTRONS

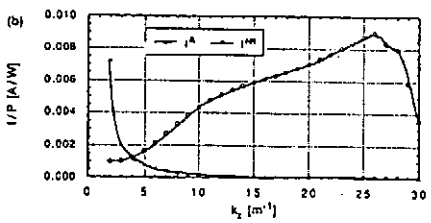

CURRENT DRIVE EFFICIENCY

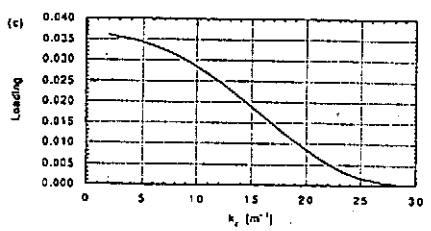

LOADING RESISTANCE

Current Drive Efficiency

Local analysis

Without trapped particle effect

$Z_{eff} = 1$

[Chan et al.: PF B2 (1990) 944]

$$\frac{I_{CD}\,R}{P_{abs}} \approx 0.0043\,\frac{N_{//}\,T_{10kev}^{5/2}}{B_T}\ [\mathrm{Am/W}]$$

independent of n_{20}

Numerical example:

$N_{//} \approx 50,\ T_{10kev} \approx 0.8,\ B_T \approx 1$

$$\frac{I_{CD}\,R}{P_{abs}} = 0.123$$

$Z_{eff} = 2$ and cancellation ⟶ 0.0354

Trapped particle effect ⟶ 0.0170

PARAMETER DEPENDENCE [$k_{//} = 20\,m^{-1}$]

LOCAL ESTIMATE $\frac{I_{CD}}{P} \propto T^{5/2}$ $\propto n^{0}$ $\propto n(0)^{-0.8}$

GLOBAL RESULT $\frac{I_{CD}}{P} \propto T(0)^{1.8}$ $\propto B^{-3}$ $\propto B^{-2}$

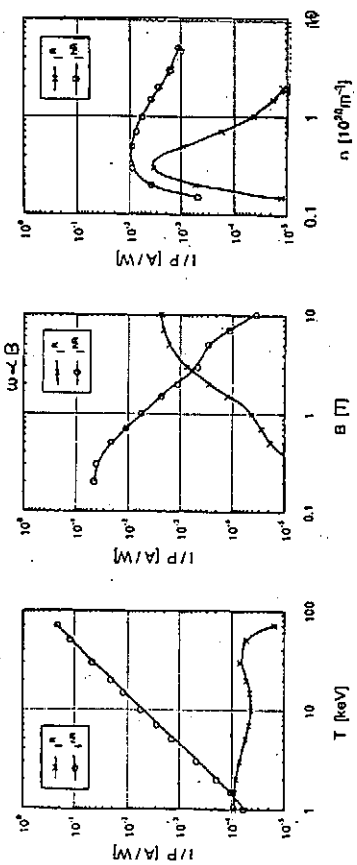

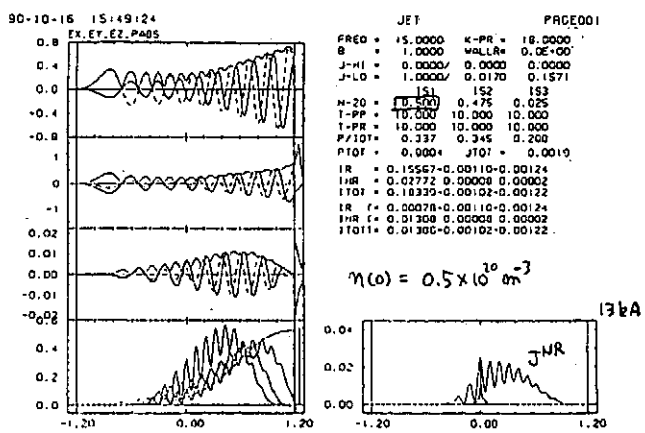

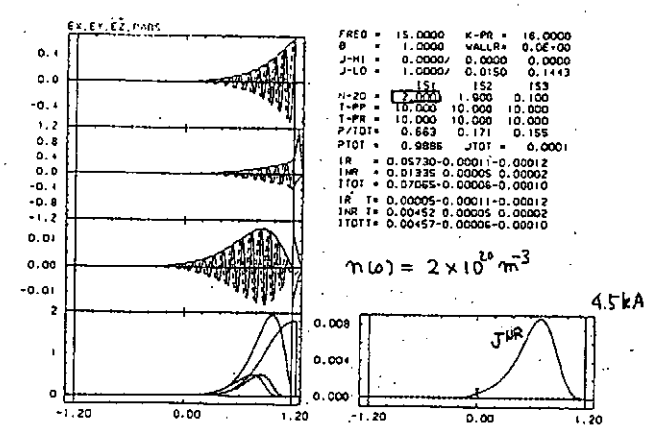

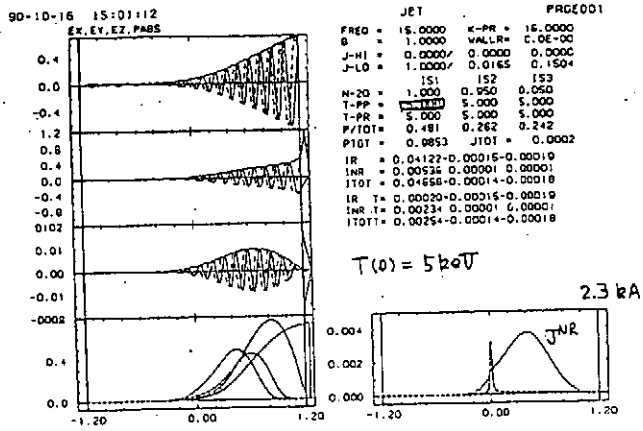

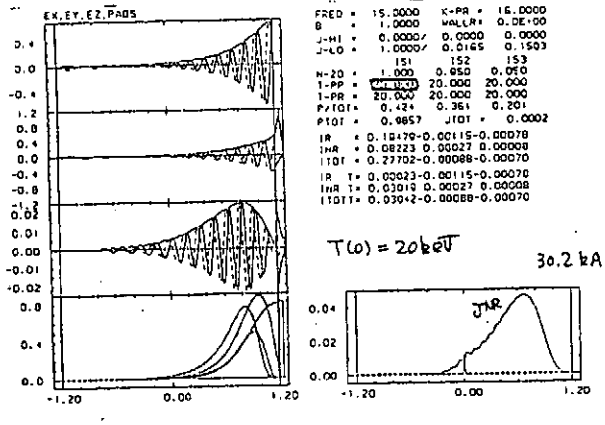

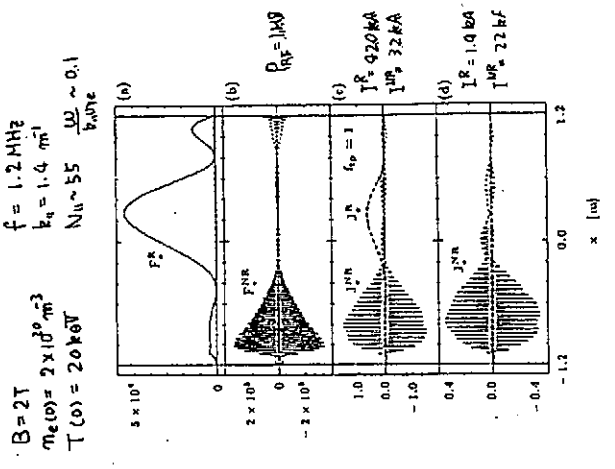

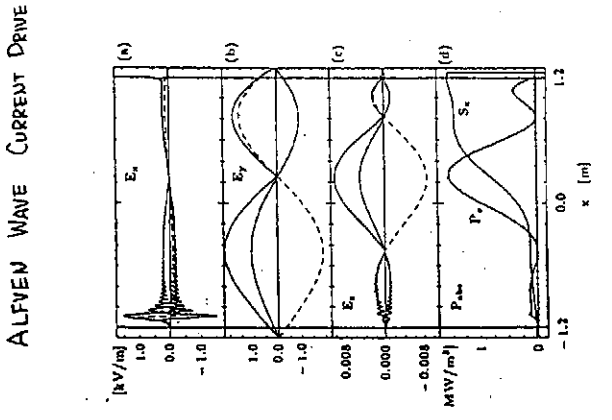

B=2T f=1.2 MHz

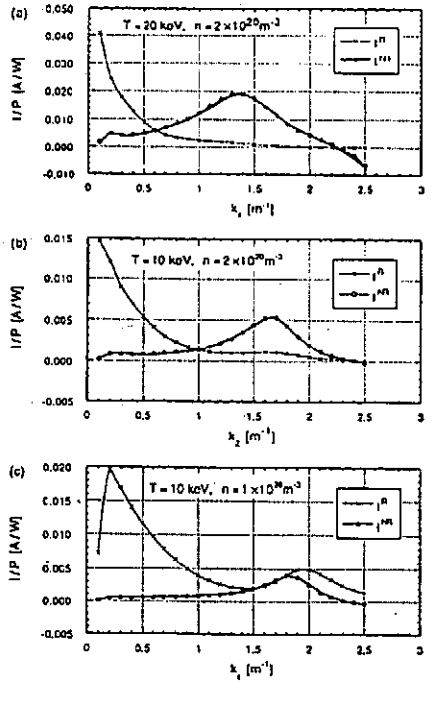

Summary

- Mechanism of current drive by non-resonant RF force was analyzed.
  - Force resulting from spatial inhomogeneity of the wave amplitude.
  - Net momentum input from wave is quite small.
  - $E_{//}$ is necessary to derive non-conservative force.
  - Wave helicity is completely converted to DC helicity.
  - Trapped particle effect is relatively weak.

- Global analysis using 1-D full wave code was carried out.
  - Cancellation due to the change of current direction reduces the drive efficiency.
  - Local estimate gives maximum drive efficiency.

$$\frac{I_{CD}\,R}{P_{abs}} \approx 0.0043\,\frac{N_{//}\,T_{10keV}^{3/2}}{B_T}\ [\mathrm{Am/W}]$$

  - Parameter dependence of the current drive efficiency is strongly affected by the location of absorption region.
  - The upper limit of $N_{//}$ is determined by poor antenna coupling and excitation of the kinetic Alfven wave.

GENERAL ATOMICS

Improved Confinement and Stability Through Current Profile Modification

T.S. Taylor
General Atomics

U.S.–Japan Workshop
on RF Heating and Current Drive
in Confinement System Tokamaks

MOTIVATIONAL
FOR
CURRENT DRIVE

- STEADY STATE TOKAMAK OPERATION
  → TRIAM-1M (Y. NAKAMURA)
- CURRENT PROFILE CONTROL
  → ASDEX (S. BERNABEI)

⇒ IMPROVED TOKAMAK PERFORMANCE
- STABILITY, BETA
- CONFINEMENT
- REACTIVITY

GENERAL ATOMICS

INTRODUCTION

- The maximum achievable volume average beta increases with peaking of the current density profile (high ℓ_i)
- Stability to high n ballooning improves with increasing magnetic shear (first regime stability) and low magnetic shear (second regime stability)
- We propose that improved confinement results from operation far from stability limits [$\tau \propto (\beta_{crit}/\beta)$]
  - Consistent with global scalings
  - Consistent with current ramp and dynamic shaping experiments

GENERAL ATOMICS

⟹ CURRENT PROFILE CONTROL CAN LEAD TO HIGH BETA REGIMES AND IMPROVED CONFINEMENT REGIMES

- High ℓ_i → improved first regime stability
- Negative central shear → second stable core plasmas
- High edge current density (and lower ℓ_i)
  → second stable edge

GENERAL ATOMICS

PROFILES AND THE BETA LIMIT OVERVIEW

- Maximum volume average beta increases with peaking of the current density profile (high ℓ_i) and with broad pressure profiles
- $\beta_{max}^{exp}(\%) \lesssim 4\ \ell_i\ I/aB$ MA/m/T
- ℓ_i (and beta) is limited by the onset of internal kinks
- $n = 1$ kink stability
  - Low ℓ_i → external and global modes become unstable
  - High ℓ_i → internal modes become unstable
  - Finite edge current reduces β-limit at all ℓ_i's
- Ballooning ($n \to \infty$) stability
  - Circular

$$\beta_{crit} \propto \frac{(\ell_i - 0.5)}{q_*}\ \frac{I}{aB}$$

  - Shaped plasmas β_{crit} shows weaker dependence on ℓ_i
- The beta limit in bootstrap dominated discharges is substantially reduced, as a consequence of broader current density profiles.

GENERAL ATOMICS

THE DIII-D OPERATIONAL BETA LIMIT IS NOT FULLY DESCRIBED BY $\beta_{MAX} = C\ I/aB$

- Many discharges reach a normalized beta

$$\beta_N = \frac{\beta}{I/aB} = 3.5 \quad (\%, MA, m, T)$$

- Some discharges reach normalized beta as high as
  - $\beta_N = 5$ (elongated divertor discharges)
  - $\beta_N \sim 6$ (low elongation limiter discharges)

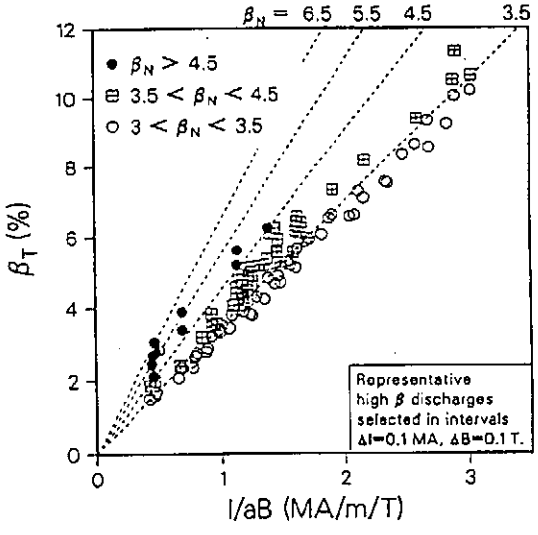

GENERAL ATOMICS

THE DIII-D OPERATIONAL BETA LIMIT FITS THE EMPIRICAL SCALING

$\beta_{MAX} = 4\ \ell_i\ I/aB$ (%, MA, m, T)

- The highest values of $\beta_N = \frac{\beta}{I/aB}$ are achieved with strongly peaked current profiles (high ℓ_i) produced by negative plasma current ramps.

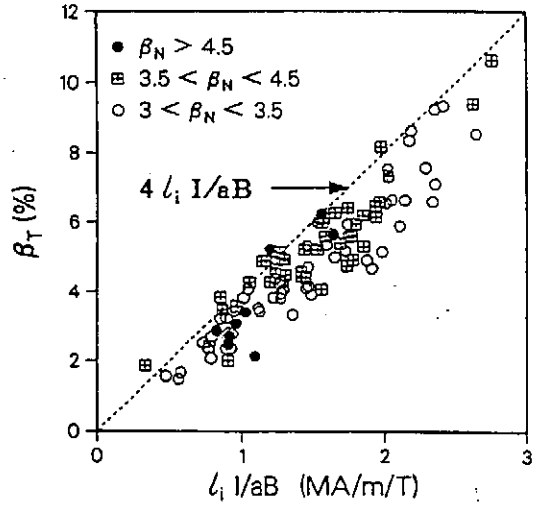

GENERAL ATOMICS

β_N GREATER THAN 6 REACHED BY INCREASING ℓ_i

- Strong negative current ramp raises ℓ_i above 2.
- β_N decays on the time scale of the current profile (ℓ_i) relaxation, longer than τ_E.
- Near-circular, limiter discharge.

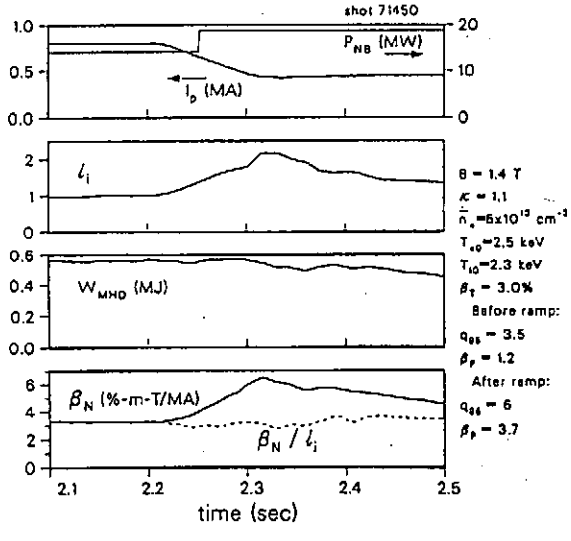

GENERAL ATOMICS

CALCULATED KINK MODE LIMIT INCREASES WITH ℓ_i FOR DIII-D SINGLE-NULL DIVERTOR DISCHARGES

- The kink mode limit lies below the ballooning mode limit, for most cases.
- Kink mode limit increases with ℓ_i, for optimized pressure profiles.
- $q = 3.2$, $\kappa = 1.9$, $A = 2.7$

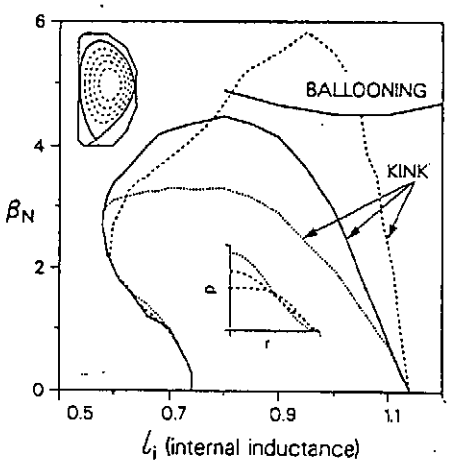

(GA-A19953, W.Howl, et al., submitted to Phys. R.)

GENERAL ATOMICS

FINITE EDGE CURRENT REDUCES β_N AND THE ACCESS TO HIGH ℓ_i

- Finite J_s reduces β_N and the high ℓ_i accessible space.

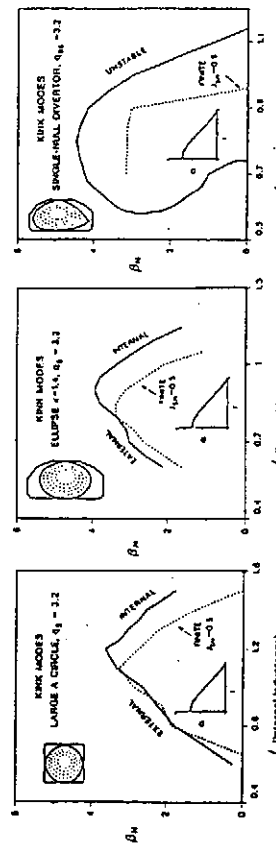

GENERAL ATOMICS

n = 1 STABILITY IS ENHANCED WHEN THE REGION OF HIGH PRESSURE GRADIENT OCCURS IN A REGION OF HIGH SHEAR

$\ell_i \downarrow$, $\frac{\langle J(x)\rangle}{J} \downarrow \Longrightarrow$ increases central shear (peaked pressure profile stable)

$\ell_i \uparrow$, $\frac{\langle J(x)\rangle}{J} \downarrow \Longrightarrow$ increases edge shear (broad pressure profile stable)

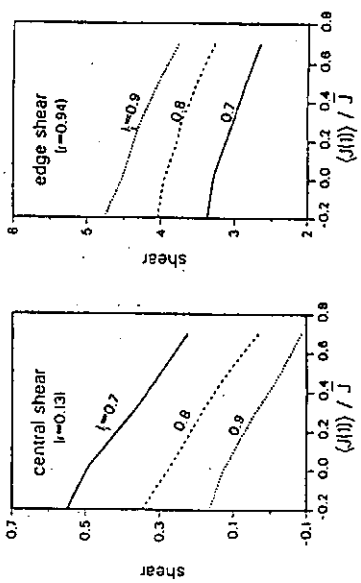

GENERAL ATOMICS

ANALYTICAL STUDY

- Assuming plasma is at marginal stability against the high n ideal ballooning modes, for infinite aspect ratio circular geometry $\alpha \simeq C_P S$, $C_P \simeq 0.6$, and

$$\beta_C = \frac{C_P}{A}\int_0^1 \frac{x^3 q'(x)}{q^3}dx, \quad \ell_i = \frac{1}{2} + q_S^2\int_0^1 \frac{x^4 q'(x)}{q^3}dx$$

- $\beta_{NC} = \beta_C / I_N$ increases approximately linearly with ℓ_i and may be expressed as

$$\beta_{NC} = \frac{20 C_P}{q_S C_q}(\ell_i - \frac{1}{2})$$

— $I_N = I_P/(aB_{T_A})$, β_{NC} is in units of (% m-T/MA)

— C_q is a weak function of ℓ_i and q_S

$$C_q = \int_0^1 \frac{x^4 q'(x)}{q^3}dx \Big/ \int_0^1 \frac{x^3 q'(x)}{q^3}dx$$

GENERAL ATOMICS

FOR MODERATELY SHAPED PLASMAS β_{NC} INCREASES APPROXIMATELY LINEARLY WITH ℓ_i

- For strongly shaped plasmas β_{NC} is less sensitive to ℓ_i.

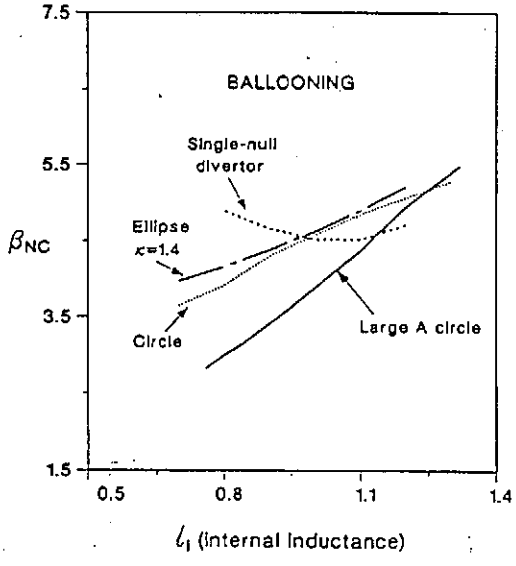

GENERAL ATOMICS

FOR PLASMAS WITH STRONGLY SHAPED POLOIDAL CROSS SECTIONS, S DOES NOT RELATE LINEARLY TO α

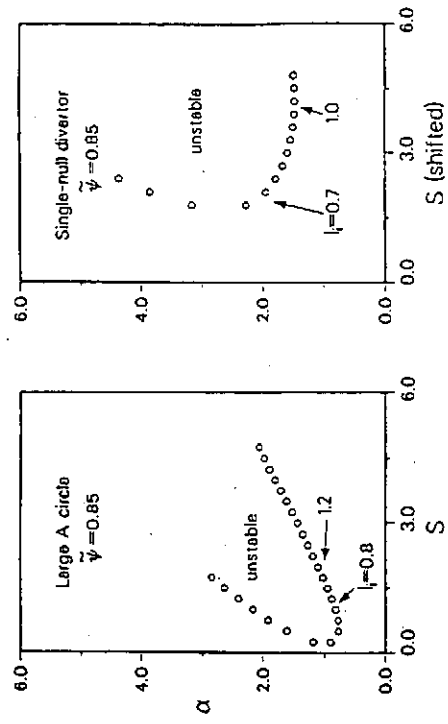

GENERAL ATOMICS

As β_N increases, the measured pressure gradient approaches, then saturates at the value which is marginally stable to the ballooning mode

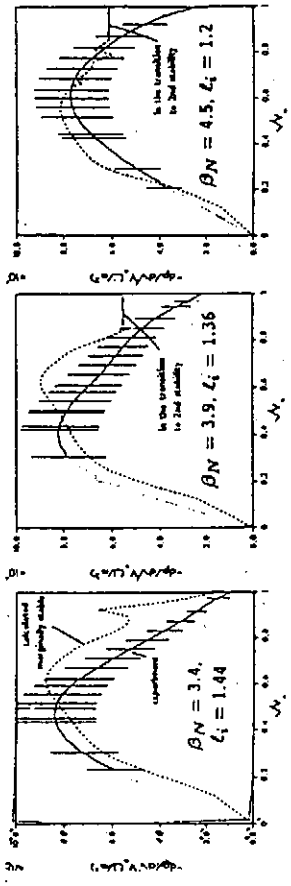

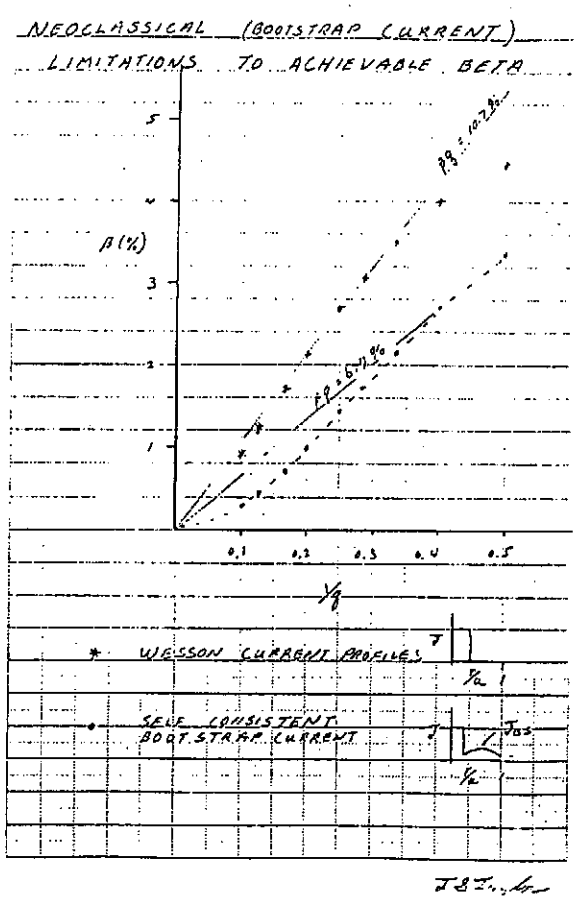

GENERAL ATOMICS

BOOTSTRAP CURRENT LARGE ASPECT RATIO CIRCLE

FROM BICKERTON

$$J_{BS} \sim \frac{\sqrt{\epsilon}}{a}\frac{\sqrt{x}}{B_\theta}\left(\frac{-dP}{dx}\right)$$

$$\frac{1}{B_\theta} = \frac{1}{\epsilon x}\frac{1}{B_T}$$

FROM WESSON

$$\frac{-dP}{dx} \sim 0.8\frac{B_T^2}{2\mu_o R_o}\left(\frac{a}{q^2}\right)\frac{x}{q}\left(\frac{dq}{dx}\right)$$

$$\Longrightarrow J_{BS} \lesssim \frac{0.15}{\sqrt{\epsilon x}}\left(\frac{2B_T}{\mu_o R_o q_o}\right)\frac{q_o}{q}\left(\frac{x}{q}\right)\frac{dq}{dx}$$

SET $J_{BS}(a) = J(a)$

$$\frac{0.15}{\sqrt{\epsilon}}\left(\frac{J_o q_o}{q_o}\right) S_a = \frac{J_o q_o}{q_o}\left(1 - \frac{S_a}{2}\right)$$

$$\Longrightarrow S_a = \frac{2}{1+\frac{0.3}{\sqrt{\epsilon}}}$$

ϵ	S_a
0.36	4/3
0.25	5/4
0.16	8/7
0.09	1.0

$$\Longrightarrow \frac{J_{BS}(a)}{(J)} = \frac{\frac{0.3}{\sqrt{\epsilon}}}{1+\frac{0.3}{\sqrt{\epsilon}}}$$

GENERAL ATOMICS

BETA LIMIT IN JT-60 WITH LARGE BOOTSTRAP CURRENT

$A = 4.5 \Longrightarrow S(a) \sim 0.9\text{–}1.0$

FOLLOWING WESSON

$$q(x) = q_a x^2 \qquad x > x_0$$

$$q(x) = q_0 = 1 \qquad x \le x_0 \qquad x_0 = 1/q_a$$

$$\beta_{MAX} = \frac{0.3\epsilon}{q_a}\left(\frac{2}{q_a}\right)\left(1 - \frac{1}{q_a}\right)$$

(WESSON)

$$\frac{0.3\epsilon}{q_a}\left(\frac{4}{q_a}\right)(\sqrt{q_a} - 1)$$

$$\epsilon/q = \frac{1}{5}\, I/aB \text{ MA/m-T}$$

$$\Rightarrow \beta_{NC} = \frac{\beta_{MAX}}{I/aB} = 0.06\,\frac{2}{q_a}\left(1 - \frac{1}{q_a}\right)$$

$q = 12$

$\Rightarrow \beta_{NC} = 1.5$

GENERAL ATOMICS

SUMMARY - BETA LIMIT SCALING

We have taken the next step beyond the simple I/aB scaling in describing the experimentally observed beta limit and comparing it to theory.

- The operational beta limit in DIII-D increases with internal inductance.

  The scaling $\beta = 4\ell_i I/aB$ provides a good description of DIII-D experimental data.

- Ideal MHD stability calculations predict a beta limit which increases with ℓ_i.
  - — Elongated discharges: n=1 kink
  - — Low elongation: kink and ballooning
- Beta greater than 6 I/aB has been achieved with high ℓ_i produced by strong negative current ramping.
- The accessible range of ℓ_i depends on q.

GENERAL ATOMICS

APPROACH

We propose that transport in tokamaks is the result of two or more diffusive processes, Goldston *et al.*

$$\chi = \chi_0 + \chi_\beta$$

Where χ_0 is the diffusive process which is dominant at vanishingly low beta; and χ_β is the increased transport as a result of an increase in the pressure gradient or beta. The exact form of these diffusivities is not critical, but as long as they have the correct limits the main features of confinement scaling will be produced.

- The limits are:
  - — χ_0 is $\chi_{OH} \approx \chi_{NA}$ for low density ohmic discharges.
    - * χ_{NA} is the diffusivity consistent with neo-Alcator confinement
  - — $\chi_\beta \longrightarrow 0$ as $p' \longrightarrow 0$
  - — $\chi_\beta \longrightarrow \infty$ as $p' \longrightarrow p'_{crit}$

H-MODE CONFINEMENT SCALING
OPEN DIVERTORS
ITER H-MODE DATABASE
DIII-D

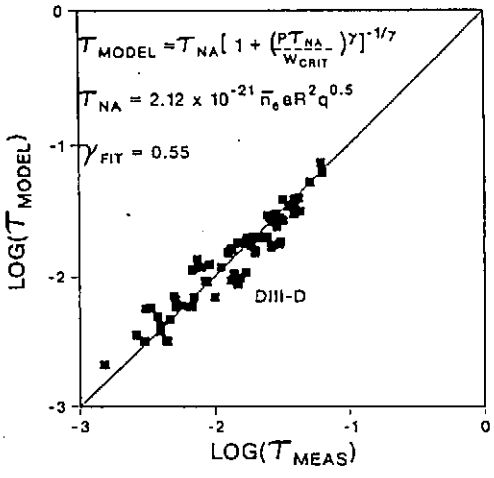

H-MODE CONFINEMENT SCALING
OPEN DIVERTORS
ITER H-MODE DATABASE
JET, DIII-D, and JFT2M

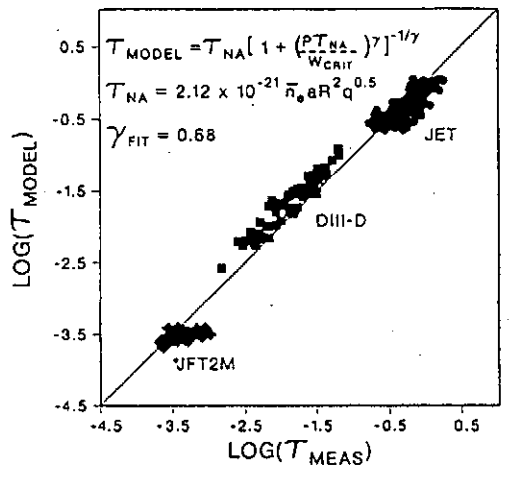

GENERAL ATOMICS

In DIII-D near-circular discharges, confinement does not follow L-mode current scaling in the period just after a rapid negative current ramp

- These results can be explained qualitatively in the context of the theory of transport linked to pressure gradient driven turbulence.
- The rapid current ramp increases the internal inductance (ℓ_i) resulting in an increase in confinement that offsets the decrease in current.
- A test of this explanation is to repeat this experiment in a double-null divertor discharge. In diverted discharges the effect of an increase in ℓ_i is expected to be weaker.

GENERAL ATOMICS

The stored energy decrease does not match the decrease in current until after the current profile relaxes

- L-mode, $\kappa = 1.2$, $P_{beam} = 10MW$, inside wall limiter discharge.
- The current ramp duration is $3\tau_E$.

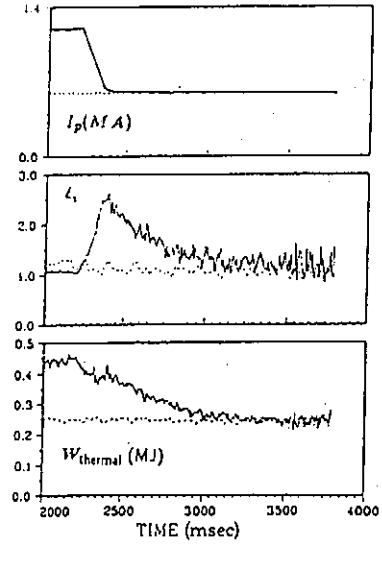

GENERAL ATOMICS

A change in the local shear can result in a change in the critical P' for pressure gradient driven modes

- We propose that theories that link pressure gradient driven turbulence to transport can be used to explain the scaling of confinement with ℓ_i and current that is observed in these experiments (see T.S. Taylor, 8T18).
- Suppose that $\tau \propto (\beta_{crit}/\beta)^{\gamma}$. $\beta \propto \tau P$ so $\tau \propto (\beta_{crit}/P)^{\gamma/(\gamma+1)}$.

GENERAL ATOMICS

β_{crit} and $\tau_{thermal}$ have similar time evolution, consistent with $\tau \propto \beta_{crit}$

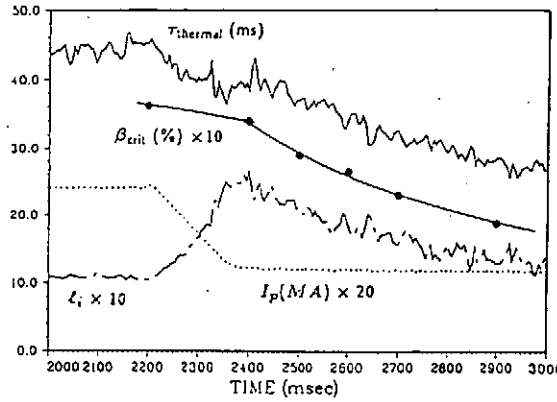

GENERAL ATOMICS

Confinement time in L-mode discharges scales with ℓ_i.

- The best confinement is comparable to H-mode as defined by the DIII-D/JET H-mode scaling.

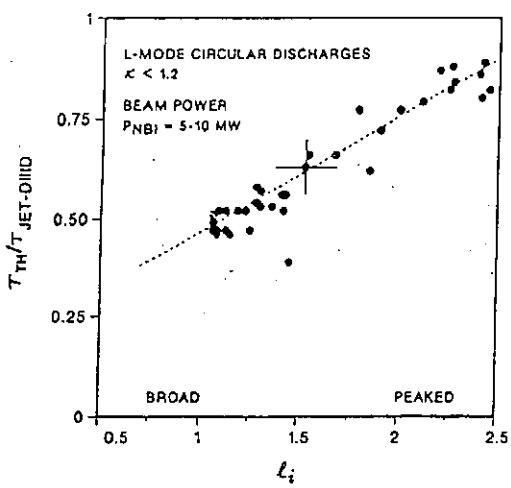

GENERAL ATOMICS

ELONGATION RAMP EXPERIMENT

- κ dynamically raised from 1.3 to $\geq$ 1.8 in 200 ms, ℓ_i changed from 1.1 to > 1.7
- H-mode plasmas obtained for final target κ > 1.8, $\tau_{TH}/\tau_{JET-DIIID} \sim 1.8$
  - energy confinement improves strongly with ℓ_i
  - plasma stored energy then decays slowly as ℓ_i relaxes
  - $\tau_{TH}/\tau_{JET-DIIID}$ remains high in ELMing phase
- Plasmas remain in L mode for final target κ < 1.8
  - energy confinement improves weakly with ℓ_i

GENERAL ATOMICS

ELONGATION RAMP EXPERIMENT

- Peaked current density profile obtained by rapidly elongating the plasma poloidal cross section to trap the current channel in the plasma center region
  - — κ 1.3 → 2.0 in 200 ms
  - — ℓ_i 1.1 → 1.8
  - — H mode, $\tau_{TH}/\tau_{JET-DIIID} \sim 1.8$

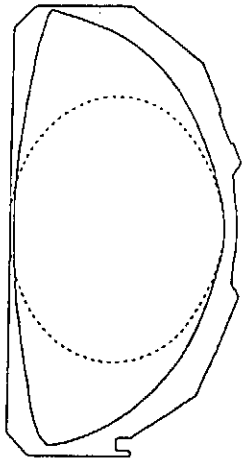

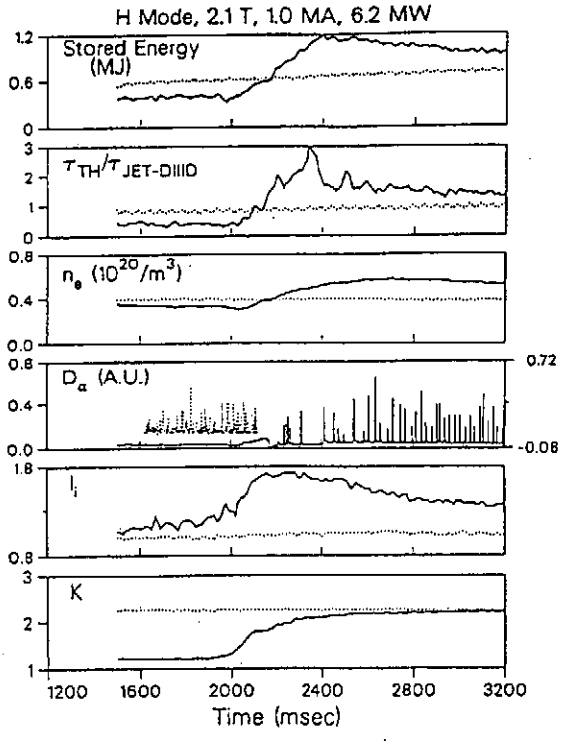

ENERGY CONFINEMENT INCREASES WITH ℓ_i AND STRONG SHAPING

- $\tau_{JET-DIIID} = 0.11 P_L^{-0.48} I_P^{1.03} R^{1.48}$, H-mode scaling

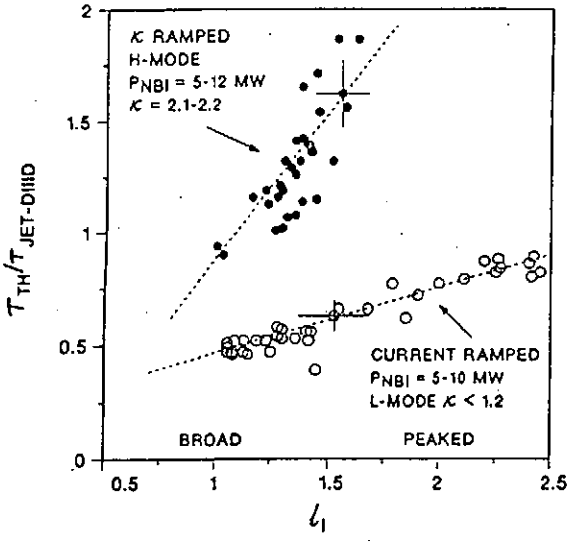

GENERAL ATOMICS

SUMMARY

- Theoretical study suggests that high normalized beta and high energy confinement may be obtained with optimized pressure and current density profiles and proper shaping in the poloidal cross section
  - — peaked current density profile
  - — low edge current density
  - — broad pressure profile
- High normalized beta ($\beta_N > 5.5$) and high energy confinement ($\tau_{TH}/\tau_{JET-DIIID} > 1.5$) have been transiently obtained in DIII-D by peaking the current density profile using current ramp, elongation ramp, and current ramp plus NBCD technique

GENERAL ATOMICS

SECOND STABLE REGIME ACCESS OVERVIEW

- Access to the second stable regime is afforded by low magnetic shear
  - — High ℓ_i and/or high central q → low or negative shear in the plasma center
  - — Low ℓ_i and/or high edge current density → low shear near the plasma boundary
- Strong shaping improves the access to the second stable regime
- Neutral beam current drive and bootstrap current can contribute to the formation of central negative shear
  - — J_{NB} and $J_{BS} \propto \sqrt{\rho/R}$
- DIII-D discharges with a second stable regime plasma core have achieved $\beta(0) > 40\%$ with $\beta_T = 11\%$
- Low collisionality H-mode discharges (high edge P') have substantial edge bootstrap current and are calculated to be in the second stable regime near the boundary, $\rho \gtrsim 0.85$–0.9

GENERAL ATOMICS

SYMMETRIZED RECONSTRUCTION OF SHOT 69608 (1417 ms)

$\beta_T = 11\%$

$\beta(0) = 44\%$

$\beta^* = 15\%$

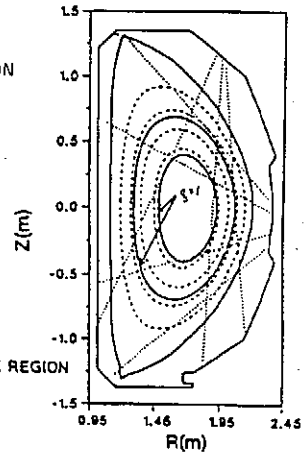

CORE PLASMA IN SECOND STABLE REGION

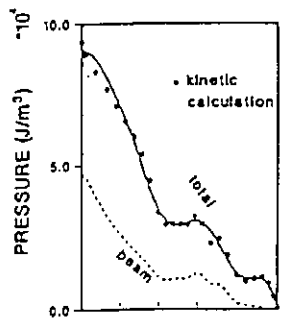

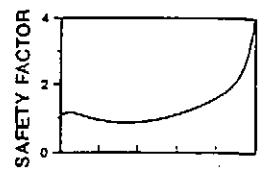

GENERAL ATOMICS

SECOND STABILITY DIII-D CORE WITH 44% BETA

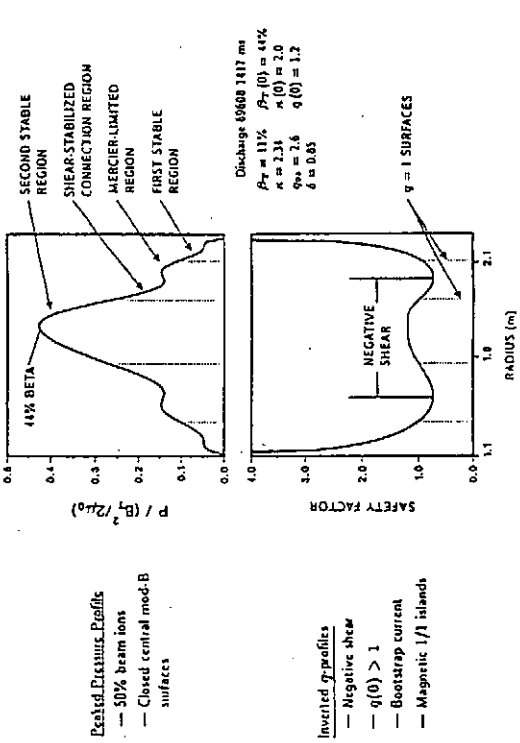

GENERAL ATOMICS

MANY VH-MODE DISCHARGES EXHIBIT A CHANGE IN CONFINEMENT TIME DURING THE ELM-FREE PHASE

In conjunction with this change:

- Bootstrap current increases, particularly in the region $0.7 < \rho < 0.9$
- χ_{eff} is reduced
- Electric field shear is shifted inward
- Initial fluctuation data indicates $(\tilde{n}/n)$ are reduced a factor of roughly 2 compared to H-mode

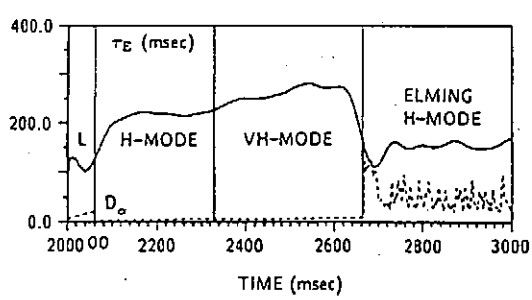

GENERAL ATOMICS

VH-MODE AND SECOND STABILITY

A possible explanation of the improved confinement in VH-mode is that a significant portion of the plasma near the boundary has entered the second stable region to ballooning modes.

- Boronization has allowed discharge operation with high power NBI with:
  - — Low radiated power
  - — Low density
  - — Low recycling
- These conditions lead to low $n_e(a)$ and high $T_e(a)$, which give low collisionality near the edge.
- The low collisionality at the edge and the high pressure gradient near the boundary in H-mode give a large bootstrap current near the boundary.
- The large bootstrap current produces low shear and and in the high triangularity DND, access to the second regime of stability.

GENERAL ATOMICS

A SIGNIFICANT FRACTION OF THE VH-MODE EDGE PLASMA IS CALCULATED TO BE IN THE SECOND BALLOONING STABILITY REGIME

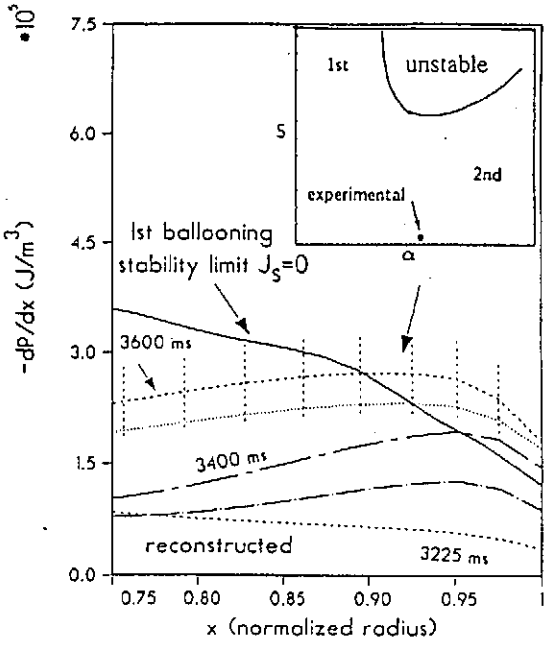

GENERAL ATOMICS

INCREASING EDGE CURRENT DENSITY IS CORRELATED WITH AN INCREASING FRACTION OF THE PLASMA VOLUME ENTERING SECOND STABILITY

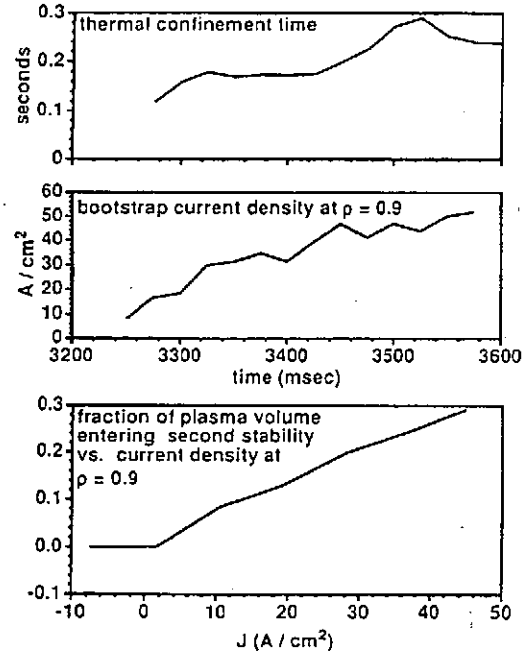

SUMMARY

- $\beta \leq 4 l_i \; I/aB$
  - — EXPERIMENTALLY OBSERVED
  - — CONSISTENT WITH KINK STABILITY
  - — CONSISTENT WITH BALLOONING STABILITY
- $\gamma_E \propto l_i$
  - — SAME DEPENDENCE AS β-LIMIT
  - — CONSISTENT WITH $\gamma_E \propto \frac{A_{CRIT}}{\beta}$
- SECOND STABLE CORE OBTAINED WITH NEGATIVE CENTRAL SHEAR
  - $-\beta(0) = 44\%$
  - $-\langle\beta\rangle = 11\%$

  $\langle\beta^2\rangle^{1/2} = 15.2\%$
- ENHANCED CONFINEMENT REGIME, VH-MODE, MAY BE A CONSEQUENCE OF SECOND REGIME ACCESS OF THE PLASMA BOUNDARY REGION
  - — τ INCREASES AS β INCREASES
  - — HIGH BOOTSTRAP CURRENT IS CALCULATED.

- INCREASED REACTIVITY IS OBTAINED IN TETR WITH NEGATIVE CURRENT RAMP

- CURRENT DRIVE HAS THE POTENTIAL OF PROVIDING STEADY STATE

  HIGH BETA

  HIGH CONFINEMENT

  HIGH REACTIVITY

TOKAMAK OPERATION!

US-Japan Workshop on "RF heating and Current Drive in Confinement System Tokamak", Nagoya, 18-21, Nov. 1991

Profile Control by Lower Hybrid Wave Application

K. Ushigusa and the JT-60 Team

Japan Atomic Energy Research Institute
Naka Fusion Establishment
Naka-machi, Naka-gun, Ibaraki-ken,
Japan

OUTLINE

1. Current Profile Control and Sawtooth Suppression by LHCD (in JT-60)
2. Preliminary Results on Profile Control in JT-60U
3. Summary

Current Profile Control and Sawtooth Suppression by LHCD (JT-60 experiments)

LHCD with low $N_{\parallel}$ (<1.7) wave does not change l_i so much.

LHCD with high $N_{\parallel}$ (>2.3) wave decreases l_i.

Sawteeth are suppressed by both high and low $N_{\parallel}$ injection, however we found some differences.

- Time delay until sawtooth suppression from onset of LH pulse
  - High $N_{\parallel}$ wave ⇒ > 1.5 s
  - Low $N_{\parallel}$ wave ⇒ < 0.5 s
- ST Reappearance time after LH pulse
  - High $N_{\parallel}$ wave ⇒ ~ 0.5 - 1 s
  - Low $N_{\parallel}$ wave ⇒ < 0.2 s
- Midium $N_{\parallel}$ (= 1.9 - 2.3) does not suppress ST in the same condition.

• Change in Sawtooth Period

Current Profile Control by LHCD (JT-60 experiments)

- High $N_{\parallel}$ wave decreases the internal inductance
- Low $N_{\parallel}$ wave does not change or increases l_i
- Broad RF current is formed by high $N_{\parallel}$ injection and low $N_{\parallel}$ makes peaked RF current.

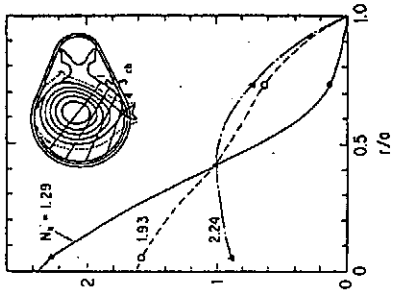

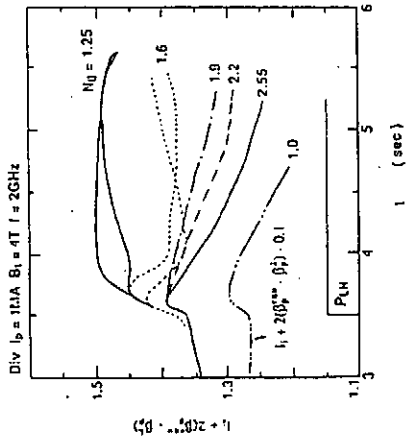

Sawtooth Suppression with various $N_{\parallel}$

- q_{eff} ~ 4.1
- n_e ~ 1 - 1.25 x 10^{19} m^{-3}
- P_{LH} ~ 1.4 MW

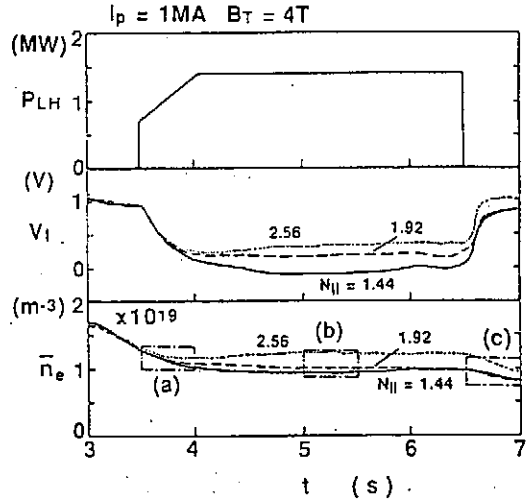

No measurement of SX signal in this series of experiment unfortunately !!

Two regimes are characterized by

high hard X-ray signal & high $l_i + 2(\beta_p^{equ} - \beta_p^{dia})$

low hard X-ray signal & low $l_i + 2(\beta_p^{equ} - \beta_p^{dia})$

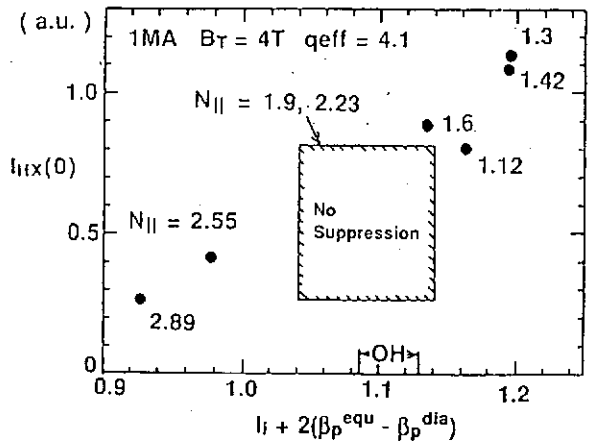

	$N_{\parallel} = 1.44$	$N_{\parallel} = 1.92$	$N_{\parallel} = 2.56$
Sawtooth Period	increase	increase and decrease	increase and decrease
Disappeared timing from LH onset	~ 0.35 s	no suppress	~ 1.8 s
Reappearance time after LH pulse	~ 0.1 s	no suppress	~ 0.4 s

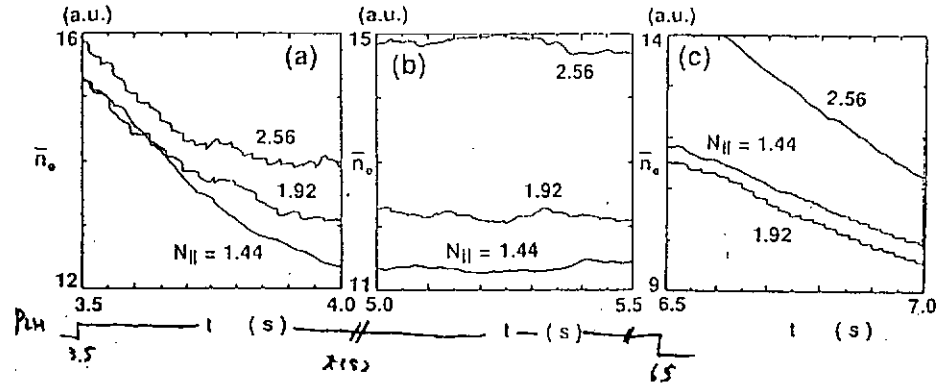

Sawteeth disapperace time (○) and reappearance time(●)

$N_{\parallel}$ regime is clearly separated into two.

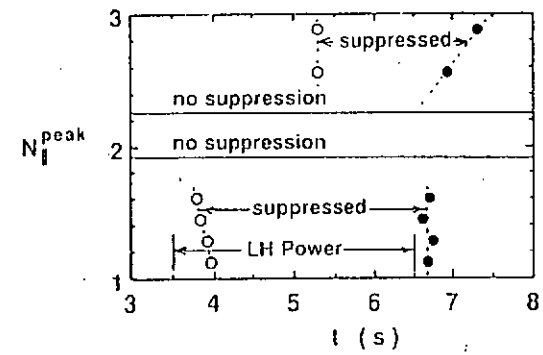

Sawtooth Suppression by LHCD in JT-60
with fixed parameters

LH power	~ 1.4 MW
density	~ 1 - 1.25 x 10^{19} m^{-3}
qeff	~ 4.1

High $N_{\parallel}$ ⇒ current profile broadening

Low $N_{\parallel}$ ⇒ different from high $N_{\parallel}$ cases

kinetic effect of high energy electrons
modification of local current profile(?)

LH experiments in JT-60U ~ 1.5 weeks in this year including conditioning time

Preliminary Results on Profile Control in JT-60U

$P_{LH} < 1.5$ (due to less Ajis) MW, $n_e < 0.5$-0.75×10^{19} m^{-3},
$q_{eff} \sim 8.5$, $I_p = 1.2$MA, Hydrogen

Low $N_{||}$ ⇒ similar results as OH case in JT-60

High $N_{||}$ ⇒ Various MHD activities during decreasing phase of l_i are observed.

Sawtooth is disappeared

Edge MHD instability which is accompanied by the loss of high energy electrons

Sawtooth Oscillation at $q \fallingdotseq 1$ surface

high m mode

m/n = 3/1 mode

Low $N_{||}$ case with NB heating

l_i is roughly constant

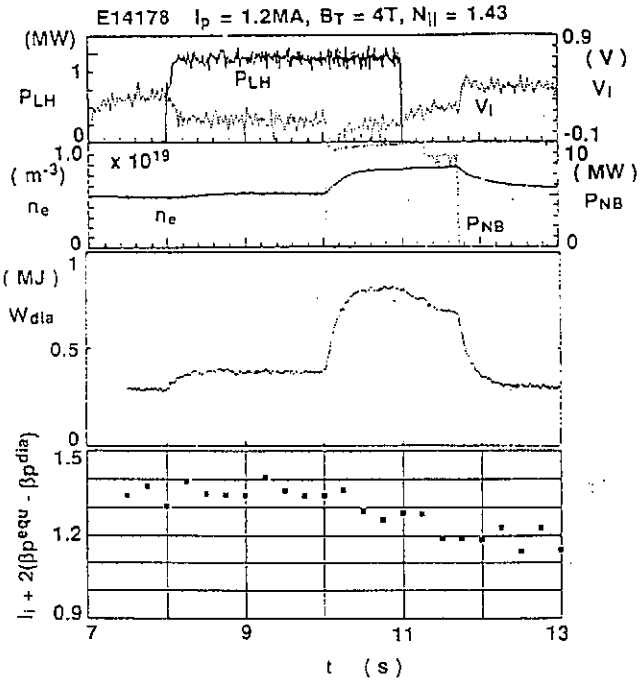

Soft X-ray signal
Sawteeth before LH injection
Suppression quickly by LH injection

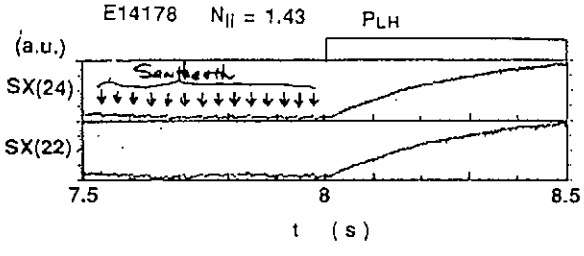

Sawtooth does not appear in NB heating phase and reappears at ~0.25s after LH pulse

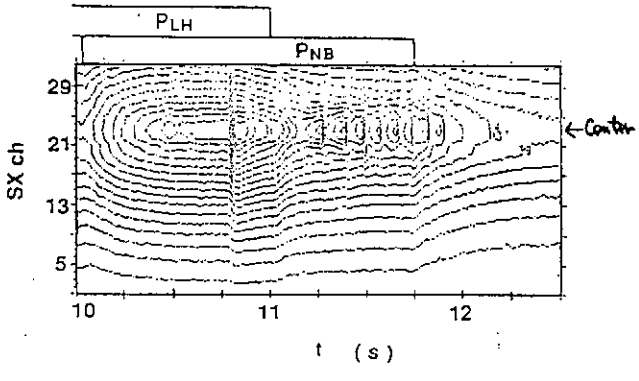

High $N_{||}$ case with NB heating

decrease in $l_i \sim 0.4$

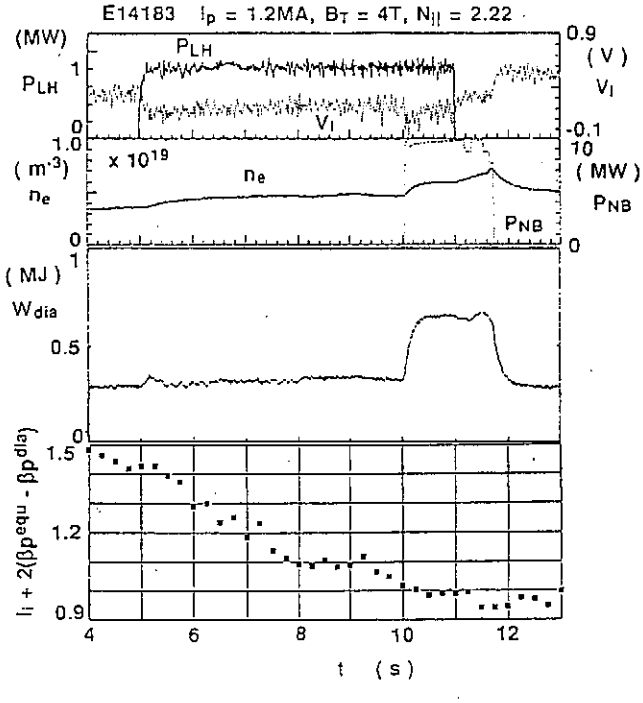

Time evolution of Soft X-ray signal at r/a ~ 0.23

Slow Oscillations in SX signal
a period of ~ (0.1 - 0.2) s
containes small crashes

After slow oscillations, fast oscillations are growing

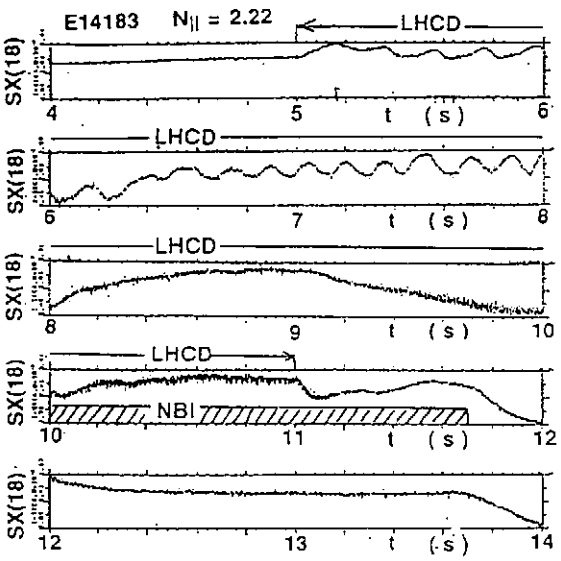

Comparison of SX and hard X-ray signals

Slow oscillation of SX signal correlates to HX signal

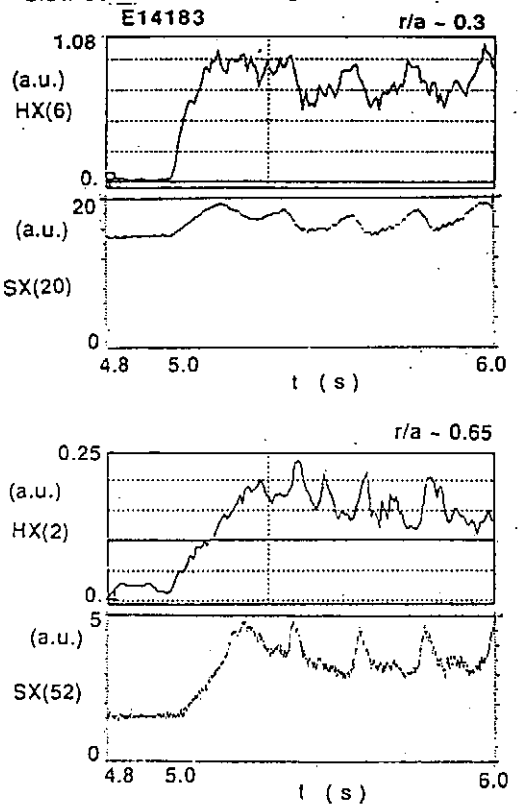

Two arrays of soft X-ray detector
top array 32 ch
bottom array 32 ch
ch 59 - ch 64 views divertor plate

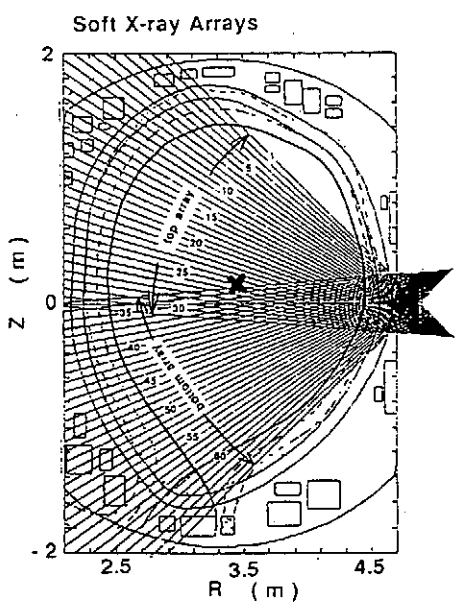

Contour plot of SX signal for slow oscillations

SX pulse propagates outward and reaches to the divertor plates
(Usually SX signals of ch 59-64 can not be detected.)

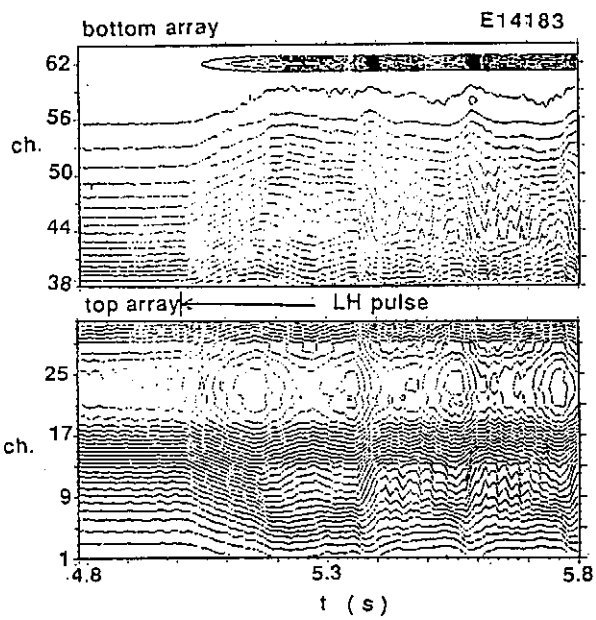

Inversion radius of sawtooth-like crashes occurs at just inside region of the release of high energy electrons and tends to move inside.

The crash disappears at t > 7.4 s
Other inversion of SX signal at edge is observed.

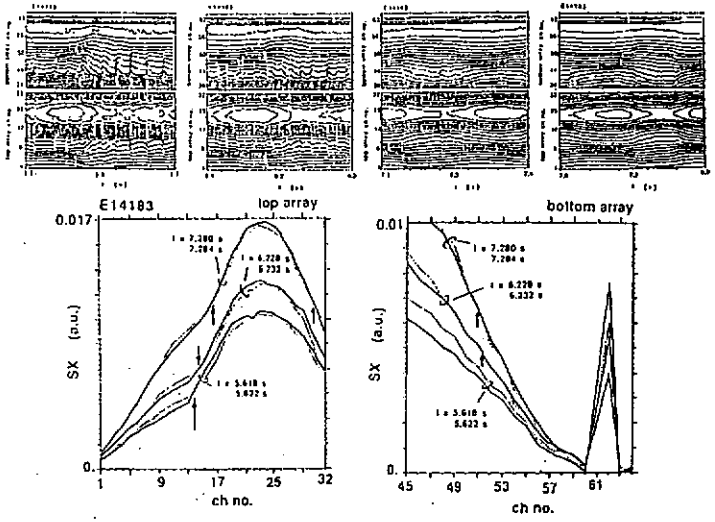

Energetic electrons at ~ half radius are released and reaches divertor plates with the time delay of ~ 30ms.

(ch 8 ~ ch 13 ⇒ r/a≈0.35 ~ 0.6)

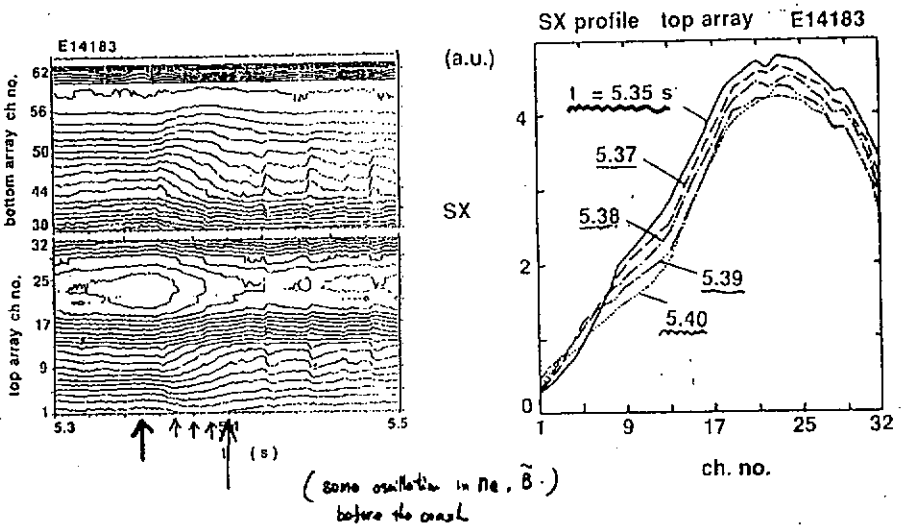

In NB heating phase, m/n = 3/1 mode is dominant.

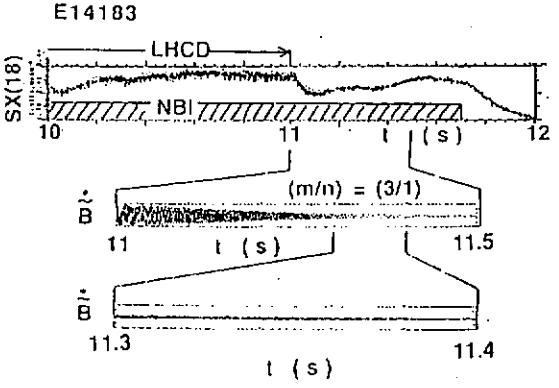

The release of high energy electron are observed in high $N_{//}$ injection with high power, low density plasma.

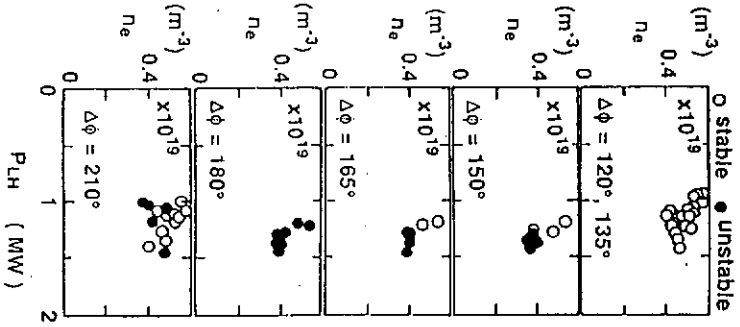

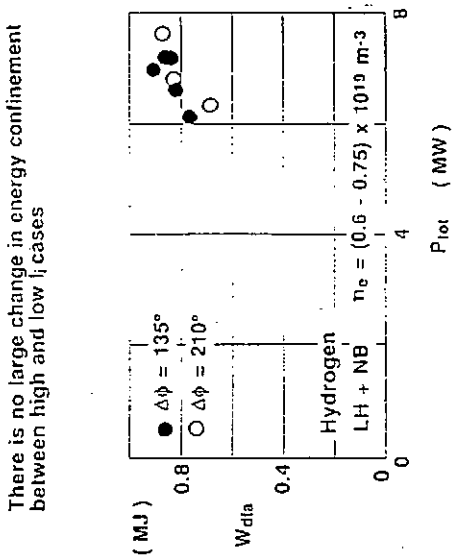

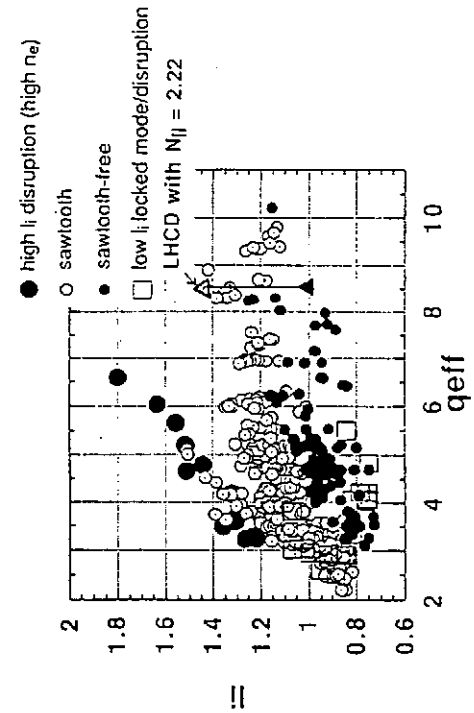

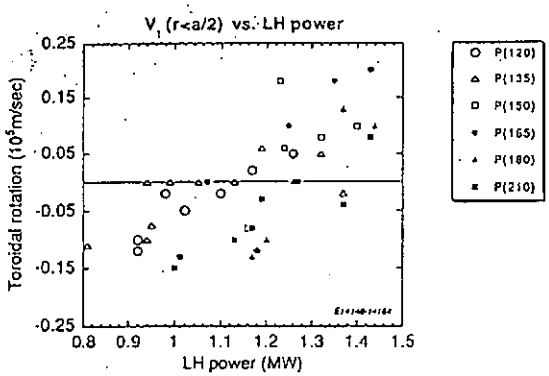

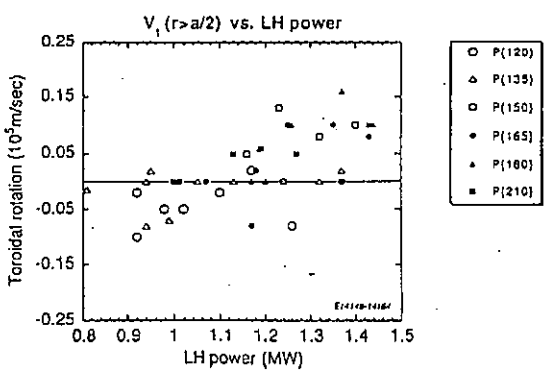

Summary

- LHCD can change the internal inductance, which is one of most important parameter to characterize MHD activities (and confinement).
- We observed indeed various changes in MHD activities by changing activ... l_i with LHCD
- Rotation of plasma also can be controlled by LHCD*

  * see ... on ... management

- Further studies of profile control by non-inductive current drive will be studied in JT-60 program to understand the role of profiles on confinement, stability ..... and finally to find out best profile for nuclear fusion reactor.

Sawtooth Stabilization by ECH near q=1 surface in WT-3

presented by K.Hanada (Kyoto Univ.)

T.Maekawa, Y.Kishigami, T.Kishino, T.Maehara, M.Makino, T.Minami, M.Nakamura, Y.Terumichi and S.Tanaka

Contents

1. Experimental Apparatus
2. Sawtooth Stabilization by ECH applied near q=1 surface
3. Sawtooth Excitation by ECH
4. Theoretical Explanation
5. Summary

Top View of WT-3

WT-III Toroidal Device

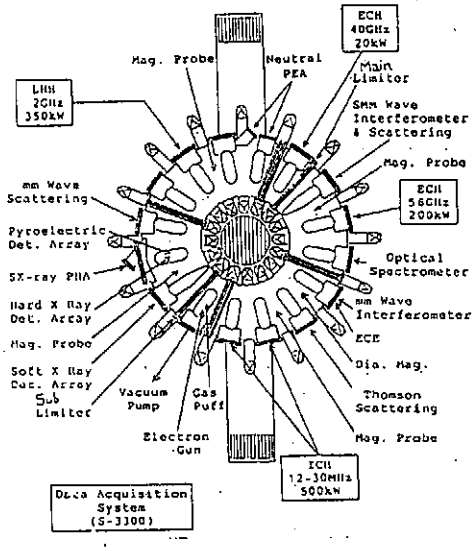

Major radius R = 65 cm
Minor radius a = 20 cm
Maximum Bt = 1.75 T
Maximum Ip = 150 kA

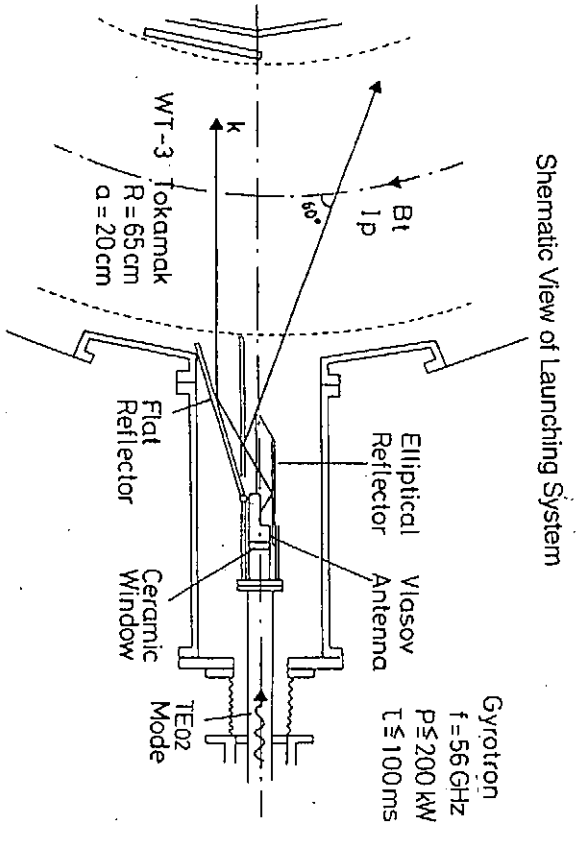

Shematic View of Launching System

Typical Effect of ECH at $q_L = 3.5$

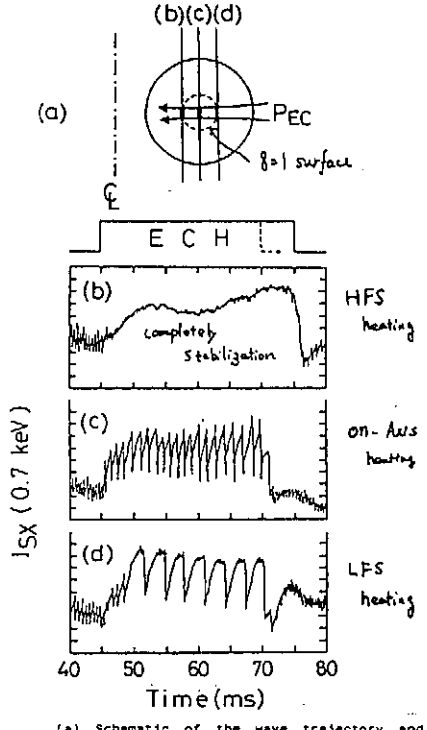

(a) Schematic of the wave trajectory and ECH layers shown as vertical lines for the three cases (b), (c), and (d) shown below. The q=1 surface is shown as a dashed circle. Evolution of soft-X-ray signal I_{sx}(0.7keV) for (b) ECH at q=1 on the high-field-side (B_t=0.93T), (c) on-axis heating (B_t=1.02T), and (d) on the LFS of q=1 (B_t=1.08T), in the range from q_L=3.7 to 3.4, I_p=79-100 kA, and P_{EC}=213 kW.

Typical Waveforms for Stabilization of Sawtooth

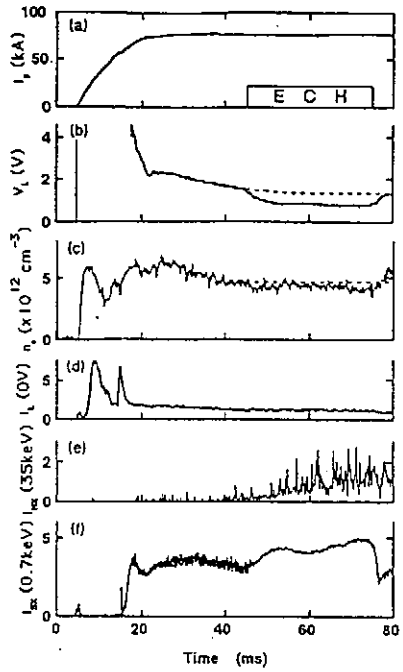

Typical waveforms of (a) plasma current I_p, (b) loop voltage V_L, (c) line-averaged electron density n_e along the vertical chord at R=65 cm, that is, the center of vacuum vessel, (d) intensity of OV line IL(OV), (e) intensity of hard X-ray more than 35 keV, (f) intensity of soft-X-ray emitted from bulk plasma. Solid curves are for operation with P_{EC}=220 kW, τ=30ms, and dotted ones without P_{EC}. The toroidal field B_t is 0.93T and the resonance zone locates at R=80.3 cm on the high-field-side. The safety factor at limiter q_L is 3.7.

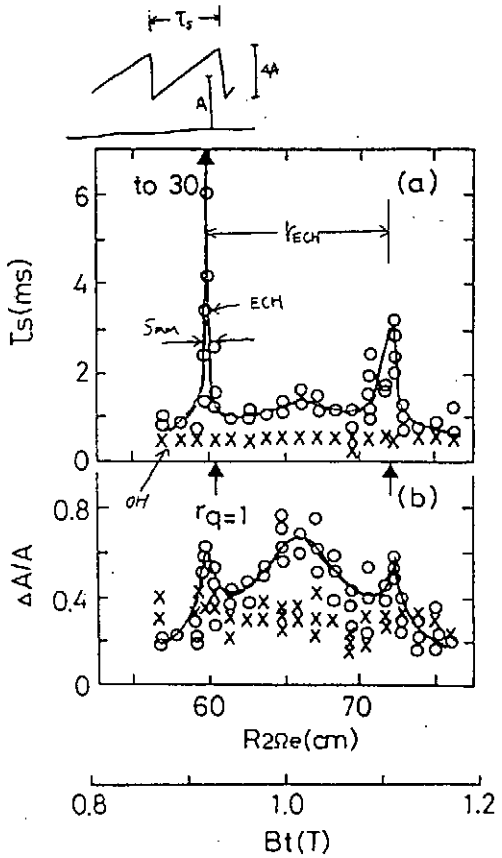

Dependence of Sowtooth Periodson P_{EC}/P_{OH} at $q_L = 3.5$

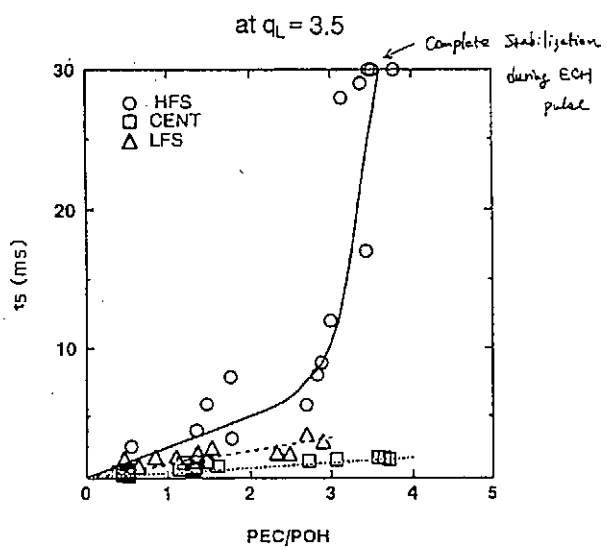

τ_s vs normalized ECH power, P_{EC}/P_{OH}, for the q=1 surface on the HFS (open circles), LFS (triangles), and for on-axis heating (squares) in the range from q_L=3.8 to 3.4, and at n_e=0.5x10^{13} cm^{-3}. Note that the complete suppression of STO, that is, τ_s=30ms is attained when the heating is on HFS.

Typical Effect of ECH at q_L= 5.0

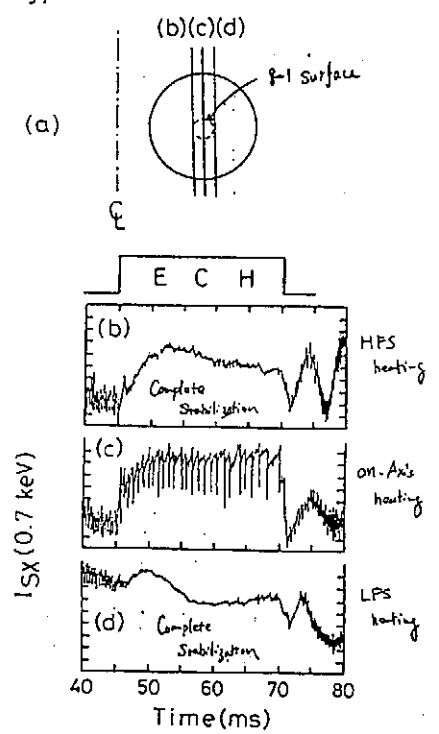

(a) Schematic of the ECH layers shown as vertical lines for the three cases (b), (c), and (d) shown below. The q=1 surface is shown as a dashed circle. Note that the radius of a dashed circles is smaller than that in Fig. 5(a) corresponding to decreasing of q_L. Evolution of soft-X-ray signal I_{sx}(0.7keV) for (b) ECH at q=1 on the high-field-side (B_t=0.89T), (c) on-axis heating (B_t=0.98T), and (d) on the low-field-side of q=1 (B_t=1.155T), in the range from q_L=4.6 to 5.0, I_p=52-55 kA, and P_{EC}=223 kW.

Dependence of Sawtooth periods on P_{EC}/P_{OH} at $q_L = 5.0$

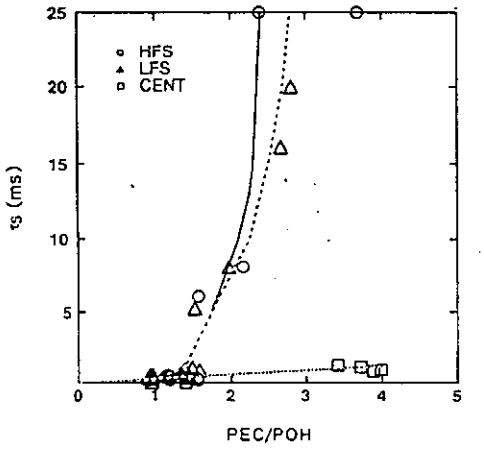

τ_s vs normalized ECH power, P_{EC}/P_{OH}, for the q=1 surface on the HFS (open circles), low-field-side (triangles), and for on-axis heating (squares) in the range from q_L=4.8 to 5.2, and at n_e=0.5x10^{13} cm^{-3}. Note that the complete suppression of STO, that is, τ_s=30ms is attained except the on-axis heating.

Stability Diagram with resprct to q_L and P_{EC}/P_{OH}

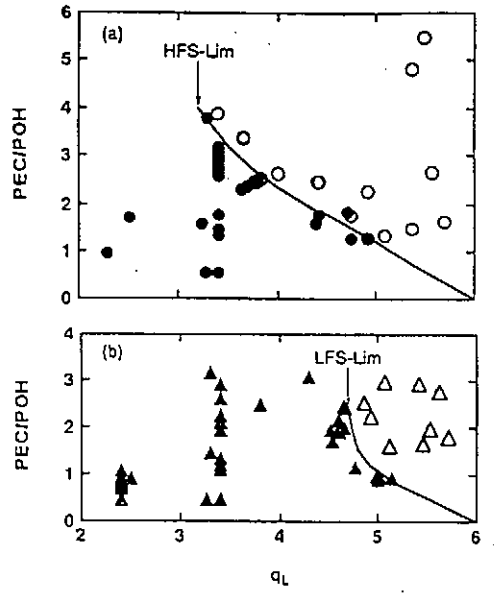

Stability diagram for STO, with respect to qL and normalized P_{EC}. (a) Solid line shows the suppression limit on q_L-normalized P_{EC} diagram when the ECH is applied at the HFS. (b) Solid line shows the suppression limit on q_L-normalized P_{EC} diagram when the ECH is applied at the LFS. Open symbol shows the achieving of suppression due to ECH, while closed symbol shows the remaining with STO during the whole ECH pulse.

$q_L = 6.4$ ($q_L = 6.0$ no STO in OH plasma)

Typical Effect of ECH on Excitation of Sawtooth

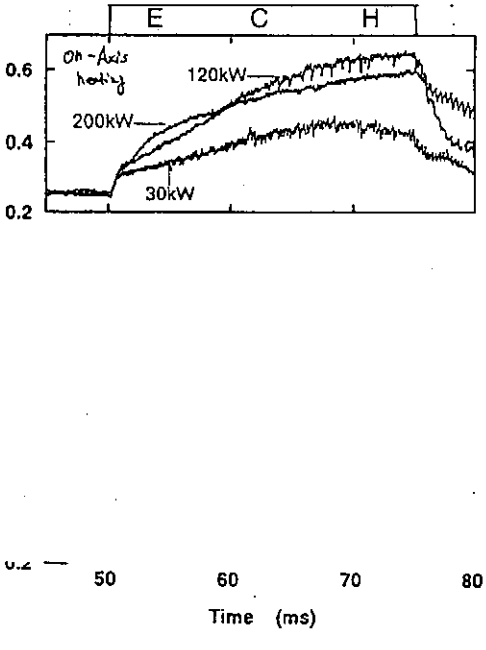

The typical waveforms of the SXR signal for excitation of STO at (a) B_t=1.03T, $R_{q=1}$=67.1cm, (b) B_t=1.07T, $R_{q=1}$=69.4cm, (c) B_t=0.95T, $R_{q=1}$=61.4cm. The other major plasma parameters are q_L=6.4, n_e=0.5x10^{13}cm^{-3}, I_p=45-51 kA.

Stability Diagram for m/n=1/1 Mode

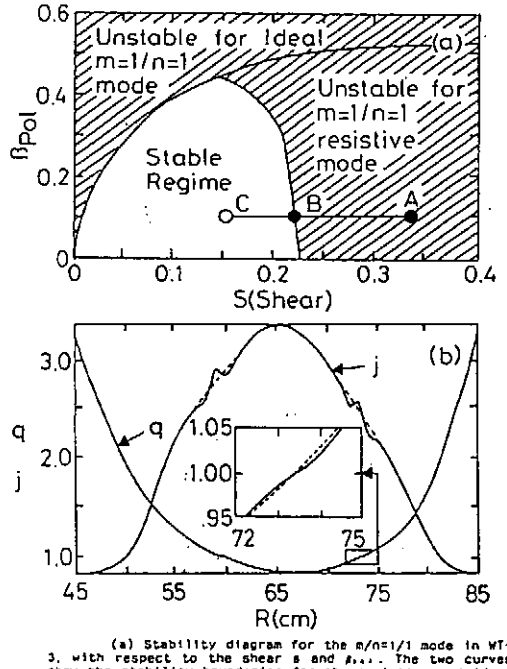

(a) Stability diagram for the m/n=1/1 mode in WT-3, with respect to the shear s and β_{pol}. The two curves show the stability boundaries for the resistive and ideal instability. As the ECH power is increased the shear is reduced and the plasma moves from an unstable point (A) without ECH, to a marginal point (B) with ECH at threshold power, to a stable point (C) with substantial ECH power. (b) The current density j and q profiles across the plasma midplane without ECH (dashed curves) and with ECH (solid curves). Inset: A magnification of the q=1 region to show the reduction of the shear when the ECH was in use.

Major difference ; ECH on HFS and LFS

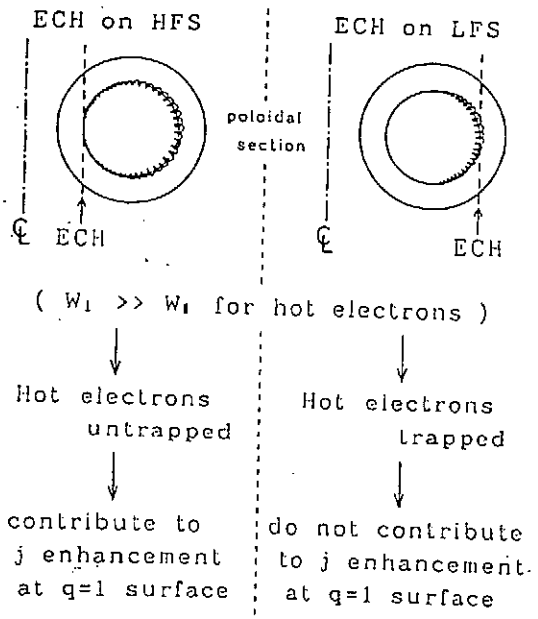

Evidence for Local ECH ovserved on Te Profile

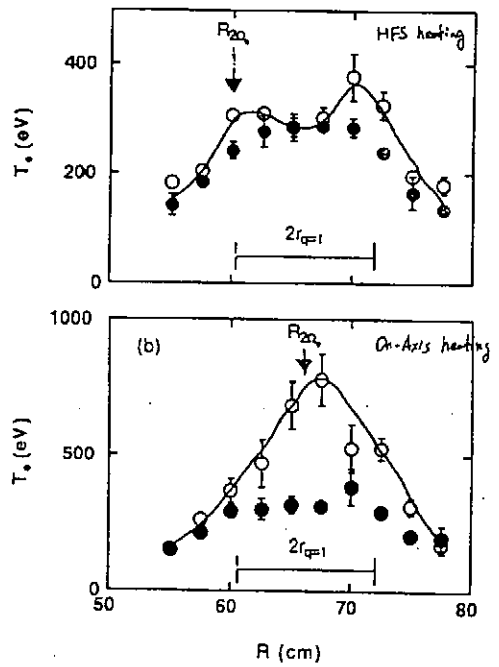

Radial T_e profiles measured by Thomson scattering with (open circles) and without (solid circles) ECH (a) near the q=1 region and (b) on-axis. Magnetic axis is at R=66cm and ECH is at (a) R=60cm and (b)R=66cm.

$$\gamma_{m=1} \cong S^{2/3} \tau_A^{-2/3} \tau_R^{-1/3}$$

Damping of Growth Rate of Precursor

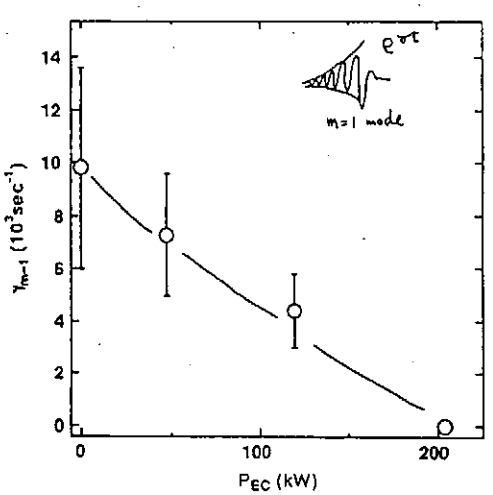

The growth rate of precursor oscillations consisting of m/n=1/1 structure are plotted as the function of PEC when the ECH is applied at $r_{...}$ on the HFS. The data point at $P_{\perp}$=204KW, $r_{...}$=0 shows the stabilization of STO.

Summary

1. A significant effect of stabilization of STO due to ECH when it is applied near the q=1 surface. This effect is much stronger when the ECH is applied on the high-field side and it is consistent with our theoritical model. There is a power threshold above which complete stabilization is obtained; below that the sawtooth period increases linearly.

2. The stabilization is attributable to a local reduction of the shear near the q=1 surface. These results also suggest that STO may be controlled effectively with ECH at the q=1 surface, especially by application on the HFS.

3. In higher qL = 6 - 7, where STO does not exist in the Ohmically heated tokamak, the excitation of STO can be obtained when the ECH applied [redacted]. The injected ECH power increasing, the excitation of STO is not observed when ECH is applied near the magnetic axis.

4. These observations for the excitation of STO cannot be explained by the most conventional theory that STO is controlled by the change of q(0). Our experimental results suggested that STO is partially controlled by the value of local shear at q=1 surface.

Nov. 19. 1991

ITER
Current Drive
Requirement

H. Kimura
(JAERI)

Results of CDA

ITER CURRENT DRIVE AND HEATING SYSTEMS

REFERENCE: SYSTEM	POWER	ROLE ($\gamma \approx 0.45 - 0.5$)	REMARKS
NB (1.3MeV)	75MW	Current Drive (central region) Heating to Ignition Burn Control	$V_b \gtrsim V_\alpha$? beam penetration ?
LH (5GHz)	50MW	Current Drive (outer region) Current Ramp-up Assist ~ 20 V/s by $\gamma \approx 0.5$ at $\langle n_e \rangle \gtrsim 4 \times 10^{19}\,m^{-3}$	divertor heat load ?
EC (120GHz)	20MW	Plasma Start-up Assist Current Drive (q=2 surface)	trapped electron ?

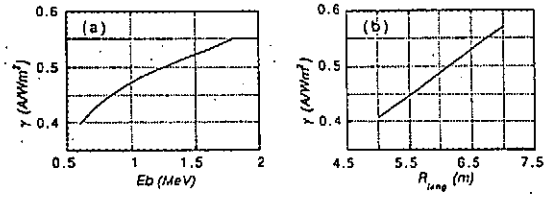

FIG. 5-3 Figure of merit for NB current drive efficiency, γ, is plotted for ITER technology phase plasmas and NB configuration, based on MS formula [5.61].

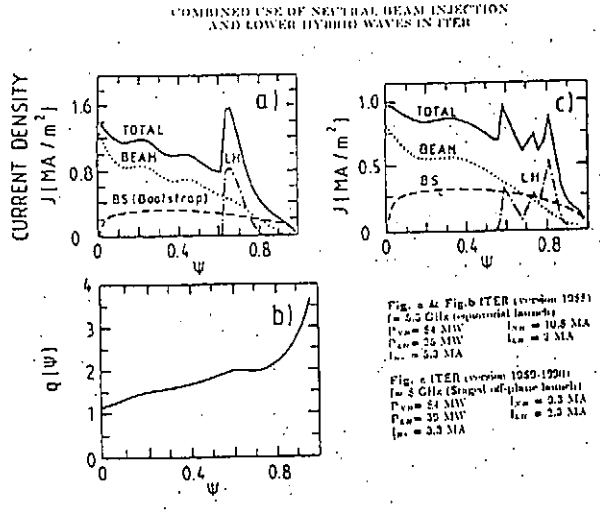

FIG. 5-2 Combined use of Neutral beam injection and LHW in ITER [5.17].
(Caption is expanded)

Results of CDA

ITER CURRENT DRIVE AND HEATING SYSTEMS

ALTERNATE:

SYSTEM	POWER	ROLE	REMARKS
IC (15-80MHz)	130MW	Current Drive (central region) Heating to Ignition Burn Control	data base ? $k_\parallel$-upshift ? eigenmode
LH (5GHz)	50MW	Current Drive (outer region) Current Ramp-up Assist	divertor heat load ?
EC (120GHz)	20MW	Plasma Start-up Assist Current Drive (q=2 surface)	trapped electron ?

ICRF Scenarios for [redacted] ITER

IC Resonance on axis	Damping	Function	
none ($\omega<\omega_{cT}$)	electrons (TTMP)	Current Drive highest γ (~ 0.3)	ITER
ω_{cD} ω_{cHe4}	D ($n_D/n_T>0.2$) He^4	Central Ion Heating ignition approach	ITER
ω_{cHe3} $2\omega_{cT}$	He^3 T	Central (ion) Heating burn control sawtooth stabilization D-He^3 burn	FER
none ($\omega>2\omega_{cT}$)	electrons (TTMP) - higher damping per pass	Current Drive γ = 0.2 ~ 0.25	FER
ω_{cH} $2\omega_{cD}$ $2\omega_{cHe4}$	H D He^4	Central (ion) Heating burn control sawtooth stabilization heating of hydrogen plasma	FER

ITER: 15-80 MHz, FER: 50-80 MHz

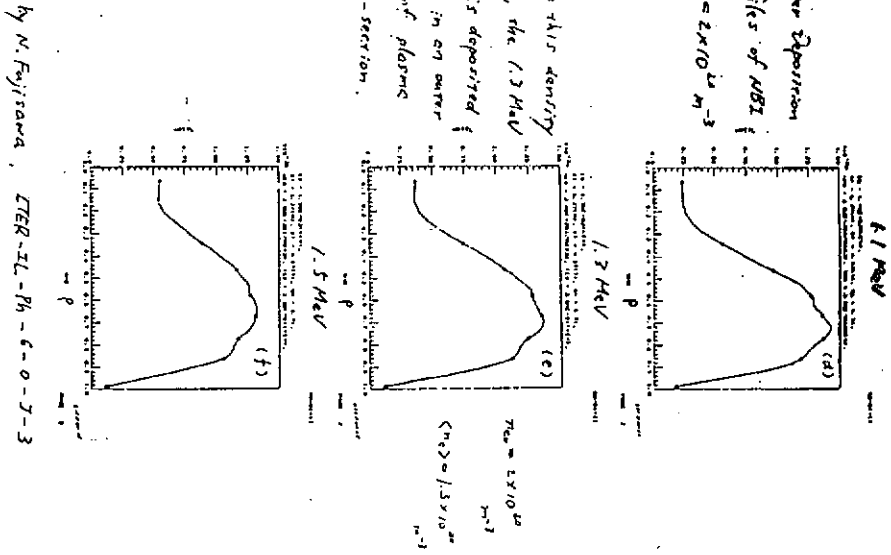

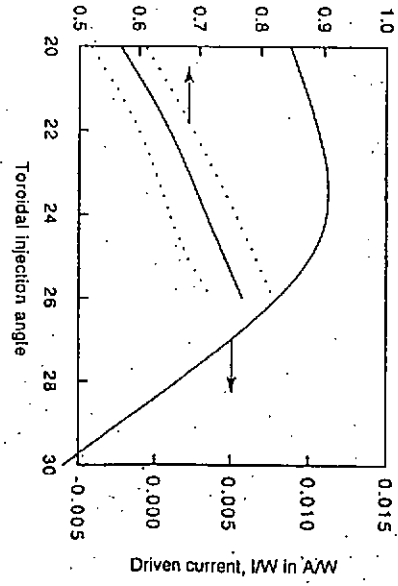

FIG. 5-7 Band of localization and total driven current as a function of toroidal injection angle ϕ for wave frequency f = 123 GHz [5.97].

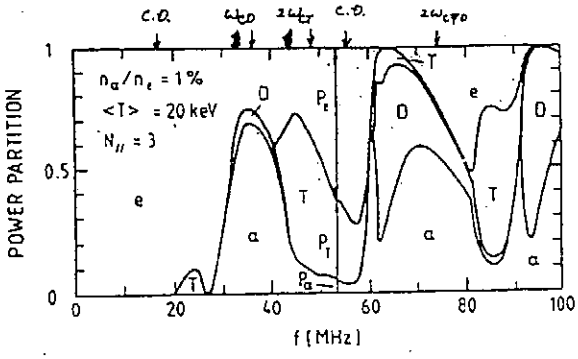

FIG. 5-4 The fraction of fast wave power absorbed by various ions species vs. frequency [5.68].

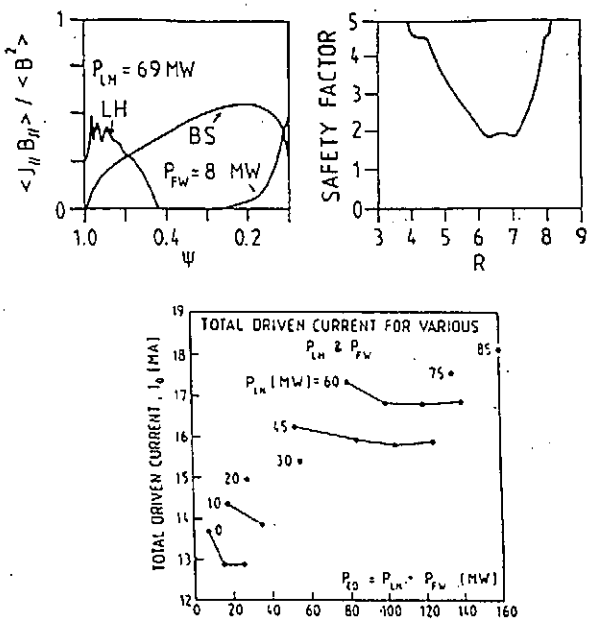

FIG. 5-6 MHD equilibrium with large bootstrap fraction using ICW (8 WM) and LHW (60 MW) [5.33].

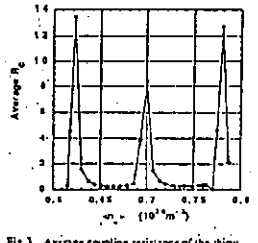

Fig.3 Average coupling resistance of the thirty antennas with $N_{//}(p)$=1.5 against the electron density.

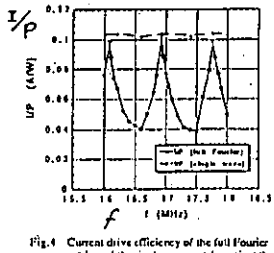

Fig.4 Current drive efficiency of the full Fourier mode and the single wave mode against the wave frequency for $N_{//}(p)$=1.5.

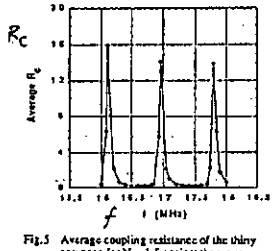

Fig.5 Average coupling resistance of the thirty antennas for $N_{//}$=1.5 against the wave frequency for $N_{//}(p)$=1.5.

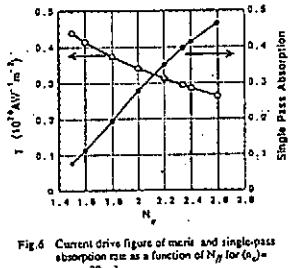

Fig.6 Current drive figure of merit and single-pass absorption rate as a function of $N_{//}$ for (n_e)= 0.7×10^{20} m^{-3}, (T)=20keV and Z_{eff}=2.26.

H. Kimura et al. IAEA FWCD TCM, Arles, 1991

CURRENT DRIVE EXPERIMENTS ON CDX-U: HELICITY INJECTION AND PRESSURE DRIVEN CURRENTS

Presented by
C. B. Forest
and the CDX-U Team
Princeton University

US-Japan Workshop on Current Drive
November 18-21, 1991

OUTLINE

- Motivation
  - Trapped Particles
  - Toroidal Field-Aligned Currents
- A Toroidal Trapped Particle Configuration
- Observations
  - Large Toroidal Currents
  - Magnetics Analysis
  - 2-D Density Profiles
  - Probe Data
  - Isolated Limiter Data
- Explanations
  - Currents generated by Charge Separation
  - Currents generated by Toroidal Precession
  - Bootstrap Currents?
- The FUTURE

A LOW ASPECT RATIO TOKAMAK[3]

Features:

- Low cost reactor due to small size.
- Very large I_p for a given q_a.

$$I_p(MA) = \frac{5aB_t\epsilon}{q_a}\left(\frac{C_I}{(1-\epsilon^2)^2}\right)\left(\frac{1+\kappa^2}{2}\right) \quad (1)$$

High aspect ratio:

$$I_p(MA) = \frac{5aB_t}{q_a}\epsilon \quad (2)$$

- High β, first stability equilibria are possible because of large I_p.

$$\beta_c = .033 \times \frac{I_p}{aB_t} \quad (3)$$

- $f_{trapped} \propto \epsilon^{\frac{1}{2}} \beta_p$

Problems:

- Difficult to engineer.
- Very difficult to drive current.
  - Small area for ohmic flux core.
  - High β makes RF current drive difficult.

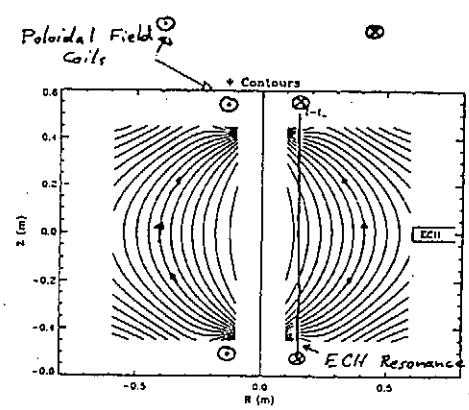

TRAPPED PARTICLE CONFIGURATION

- Provide particle confinement in the absence of toroidal current.
- Electrons have banana orbits.
- ECH resonance is located at R=15 cm to heat banana tips.
- B_t= 875 Gauss at R=15 cm. $B_t \propto \frac{1}{R}$, $\frac{B_{max}}{B_{min}} = 6$
- $B_t \sim$ 10 Gauss at R=35 cm.

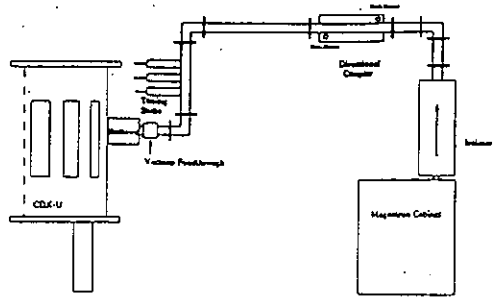

ECH HEATING SYSTEM

- Power = 4.5kWatts $X\,2 = 9\ KW_{atts}$
- Pulse length= 25 mSecs
- Launching antenna is a simple unterminated waveguide
- $\vec{E}_{rf} \parallel \vec{B}$
- No preferred $n_{\parallel}$

Total Plasma Current Measured By Rogowski Coil

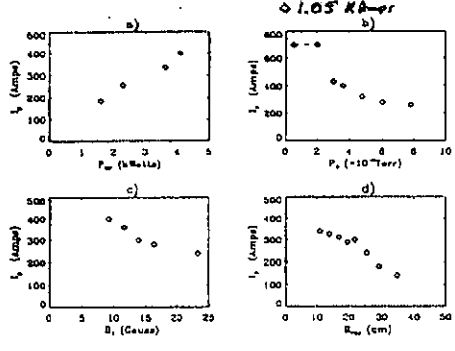

Variation with external variables.

Field Direction	B_t: +	B_t: -
B_{pf}: up	+	+
B_{pf}: down	-	-

Direction of current

– Current adds to the imposed field on the outside

$\uparrow\downarrow \odot \uparrow\uparrow B_{coils}$

I_p

I_p $\qquad$ B_v at $z=0$ cm, $R=10$ cm

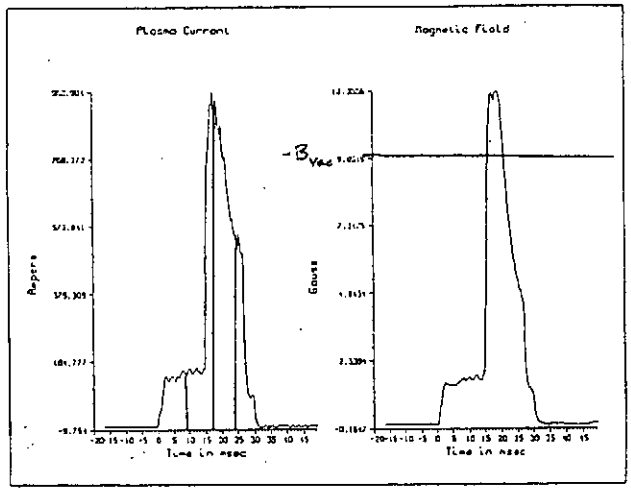

Plasma Current Decrease Correlates with Density Increase

CDX-U Magnetics Arrangement

(Pick-up Coils and Voltage loops)

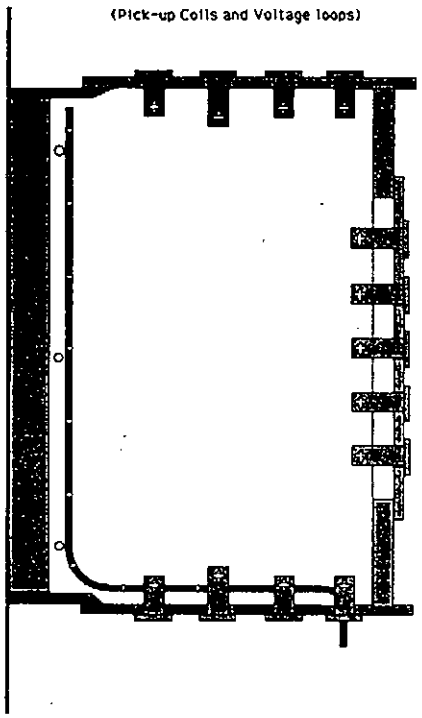

Current Density Reconstruction Example

(Finite Element Methode)

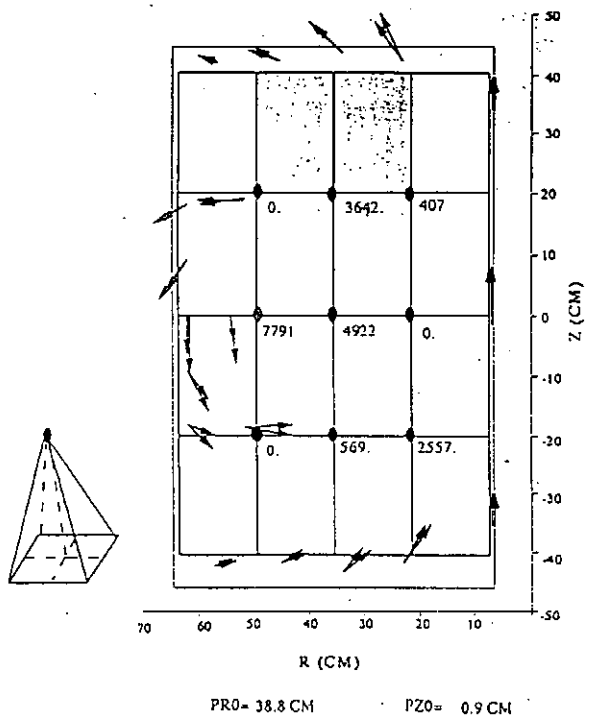

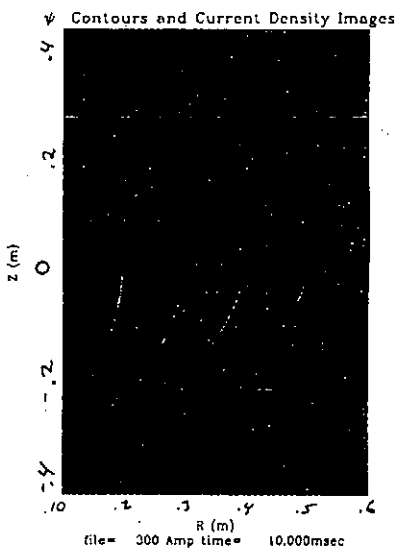

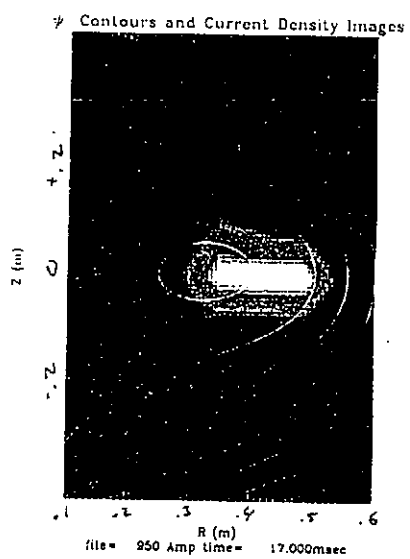

- Flux surfaces have formed
- 5 msec Duration (many magnetic Diffusion times)
- X point outside vacuum vessel

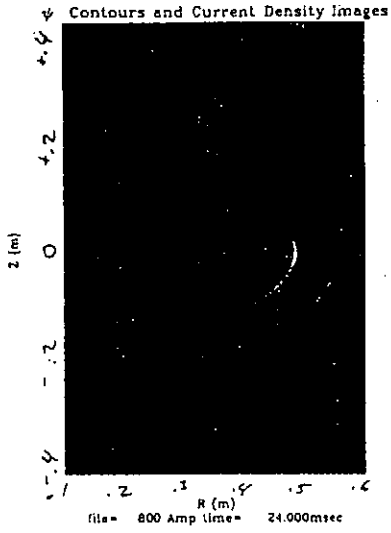

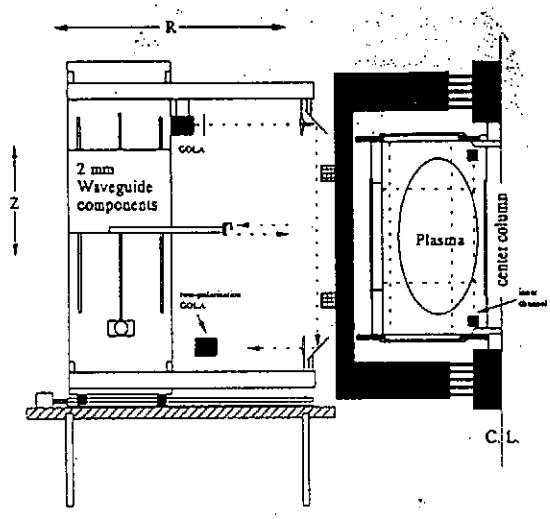

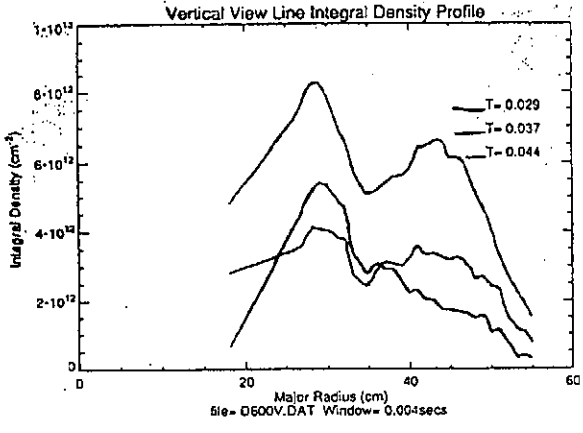

NEUTRAL PRESSURE EFFECTS

Standard Current:

Total plasma current during a shot in which the neutral pressure is increasing during the shot.

He

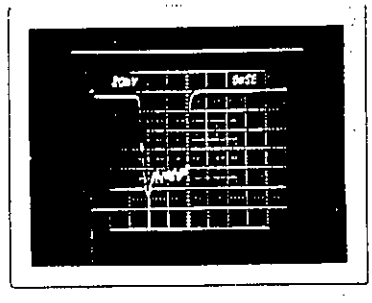

Wall Pumping:

Total plasma current during a shot in which the neutral pressure is dropping due to wall pumping.

H

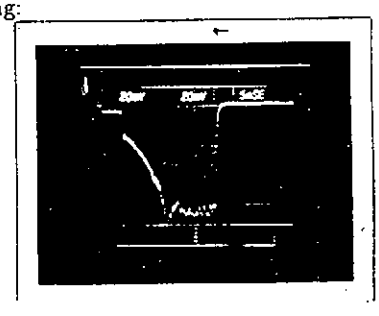

CURRENTS ARE INTERNAL

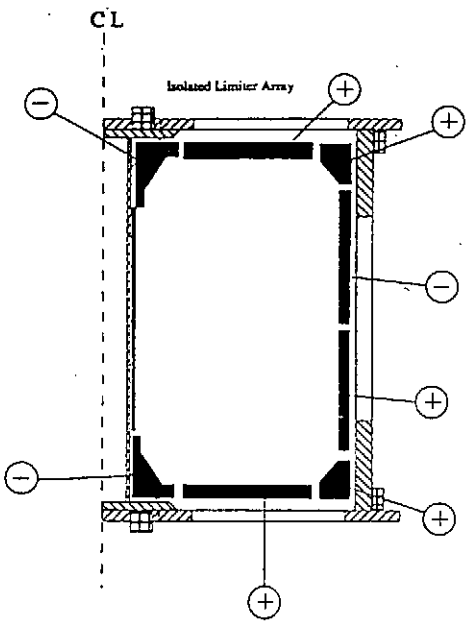

All currents are less than .5 Amps

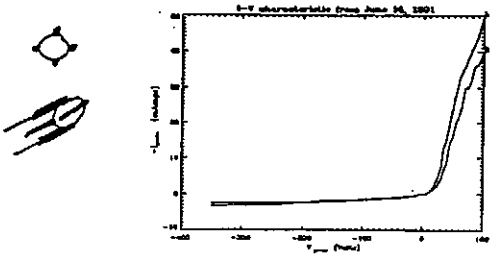

ELECTRON TEMPERATURES AND ION FLOWS

MACH Probe[6] data shows toroidal electron and ion flow in the direction opposite of the current. Edge probe meausurements show:

- $T_e \sim 10$ - 20 eV, with indications of a higher energy (200 eV) tail.
- $\phi_{float} \sim 0$ Volts, $\phi_{plasma} \sim 3\ T_e$.
- A net toroidal flow is observed.
- No poloidal flow is observed.

$J_\parallel$ Generation

- Any time the ∇B drift is across a constant pressure surface, parallel currents must flow to maintain steady state conditions. [2]
- Parallel flows determine equilibrium and transport properties.
- Three toroidal examples:
  - Simple toroidal field + vertical field.
  - Tokamak field - bootstrap currents and Pfirsch-Schüter currents.
  - Trapped particle configuration.

[2] This was recognized very early by Birkeland (1908) for magnetospheric currents, and Pfirsch and Schüter in toroidal geometries.

FIELD-ALIGNED CURRENTS

Currents flow: (Single Particle Drifts + Magnetization Current)

$$\vec{J}_\perp = \frac{\nabla P \times \vec{B}}{B^2} \qquad (3)$$

Consider a pure toroidal field: $\nabla \cdot \vec{J} \neq 0$

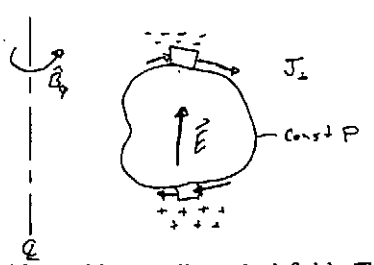

Now add a small vertical field: $\nabla \cdot \vec{J}$ can $= 0$

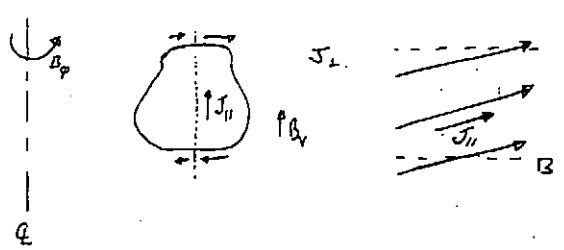

EXAMPLE

Given P(Z) and $\vec{B} = B_t\hat{\phi} + B_z\hat{z}$, $B_z << B_t$, $B_t = \frac{B_0 R_0}{R}$

Then

$\vec{J}_\perp \approx \frac{1}{B_t}\frac{dP}{dZ}\hat{R}$

$\nabla \cdot \vec{J}_\perp = \frac{1}{RB_t}\frac{dP}{dZ}$

Constrain $\nabla \cdot \vec{J} = \nabla \cdot \vec{J}_\parallel + \nabla \cdot \vec{J}_\perp = 0$

but,

$\nabla \cdot \vec{J}_\parallel = \nabla \cdot \frac{J_\parallel}{B}\vec{B}$

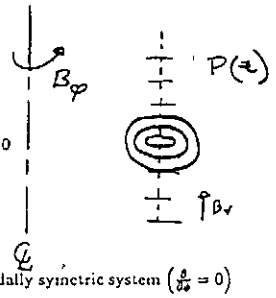

and since we are considering a toroidally symetric system $\left(\frac{\partial}{\partial\phi} = 0\right)$

$\nabla \cdot \vec{J}_\parallel = B_z\frac{d}{dz}\left(\frac{J_\parallel}{B}\right) = -\frac{1}{RB_t}\frac{dP}{dZ}$

Which shows,

$$J_\parallel = J_\parallel(Z) = \frac{2}{RB_0}P(Z) + C$$

- C= 0 for an open field line in a mirror,
- C= "the bootstrap current" on a closed field line.
- Current = Pressure

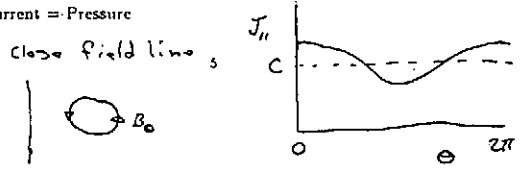

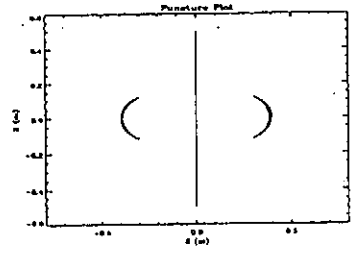

PRECESSIONAL DRIFT CURRENTS

- Banana orbits precess toroidally.
- Currents a similar in magnitude to Pfirsch-Schlüter currents.
- Single particle orbit code has been written to predict currents due to this effect.
  - E=40 eV, $\frac{v_\parallel}{v} = .5$, I_p=500 amps, $n_e \sim 10^{11}$ cm^{-3}.
  - V_{prec}=6.5×10^6 cm·sec^{-1}.
  - τ_{bounce}= 27 μsecs,

I_{prec} = 200 Amps

- Flux Surface Formation may have some Beatstrap currents.

FIELD ALIGNED CURRENTS

- Pfirsch-Schlüter currents from equilibrium,[5]

$$J_\perp = \frac{\vec{B} \times \nabla P_\perp}{B^2} + (P_\parallel - P_\perp)\frac{\vec{B} \times \nabla B}{B^3} \quad (4)$$

Charge neutrality,

$$\nabla \cdot \vec{J}_\perp = -\nabla \cdot \vec{J}_\parallel \quad (5)$$

This equation can be rewritten as

$$B\frac{\partial}{\partial s}\frac{J_\parallel}{B} = -\nabla \cdot \vec{J}_\perp. \quad (6)$$

- For $P(R,Z) = P_0 \cdot exp(\frac{(R-R_0)^2+Z^2}{\delta P})$, $n_0 = 10^{11}$ cm^3, T_e=40 eV, δP=15 cm,

I_{PS} = 400 Amps

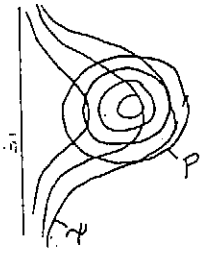

- Anisotropy allows $P \neq P(\psi)$
- Specify $P_\perp(R,Z)$
- Integrate $J_\parallel$

CURRENTS FLOW IN THE "RIGHT" DIRECTION

Field Aligned Currents

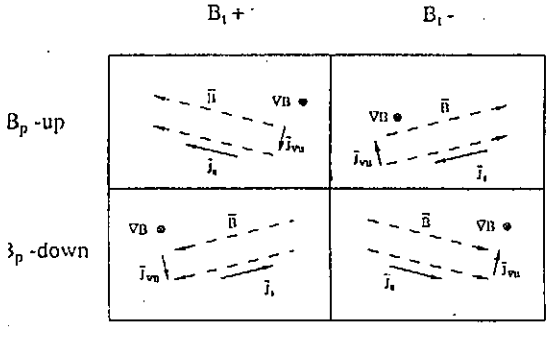

Precessional Drift Currents

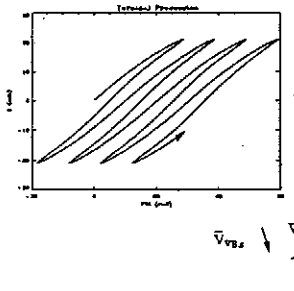

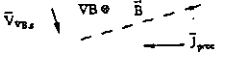

SUMMARY

- A new, toroidal confinement configuration is introduced and tested in the CDX-U vessel.
- Large toroidal currents are observed to spontaneously occur, resulting in flux surface formation.
- A preliminary diagnosis of the plasma is presented.
- These currents are toroidal, pressure driven currents which may provide the seed current required for a purely bootstrap driven tokamak.

DC - Helicity Current Drive

* Low voltage DC- power is efficient compared to RF.
* Theoretical current drive efficiency from helicity balance is high.

Objectives on CDX-U

* Extend the parameters toward more fusion relevant regimes(larger current, plasma size, magnetic Reynolds number, etc).
* Investigate the physics of current transport.

Future Plans

* Increase the plasma current toward 10 - 30 kA range (q(a) ≈ 3-5).
* Improve poloidal field control.
* Improve plasma current density profile diagnostics.
  - Faraday rotation measurements.
  - 2-D scanning magnetic probe systems.
* Magnetic fluctuation measurements for helicity transport studies.

DC - Helicity Current Drive

* Low voltage DC- power is efficient compared to RF.
* Theoretical current drive efficiency from helicity balance is high.

Objectives on CDX-U

* Extend the parameters toward more fusion relevant regimes(larger current, plasma size, magnetic Reynolds number, etc).
* Investigate the physics of current transport.

Recent Results on CDX-U

* Plasma current as high as 6 kA obtained.

* Current multiplications 25 - 30 observed in high current regimes.

* Aspect ratio ≈ 2
  Edge safety factor ≈ 10
  Poloidal $\beta \approx 1$ (estimated from equilibrium)
  $n_e(0) \approx 5.e+12\ cm^{-3}$

* Evidence of inward current diffusion and tokamak formation obtained by magnetics.

* Tokamak equilibrium is satisfied within experimental uncertainties.
  - I_p vs. B_v
  - Higher B_v moves plasma inward.
  - Lower B_v moves plasma outward.

Future Plans

* Increase the plasma current toward 10 - 30 kA range (q(a) ≈ 3-5).

* Improve poloidal field control.

* Improve plasma current density profile diagnostics.
  - Faraday rotation measurements.
  - 2-D scanning magnetic probe systems.

* Magnetic fluctuation measurements for helicity transport studies.

US-Japan Workshop
18-21 Nov. 1991
NIFS

Model of Divertor Biasing and SOL Plasma Response

K. Nagasaki
(Plasma Physics Laboratory of Kyoto Univ.)
K. Itoh and S. I. Itoh
(NIFS)

Introduction

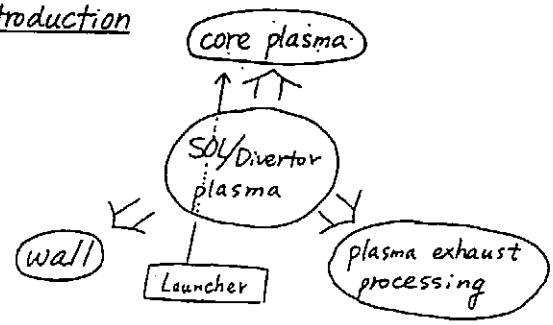

SOL/Divertor plasma
- Effect on core plasma confinement
  improved mode like H-mode
- Consistent fullfilment of technological constraints
  heat load, sputtering, impurity

Control method of boundary plasma
gass puffing, baffling, ...

Recently divertor bias experiments have been performed in DIII-D, JFT-2M, TdeV and so on.

Observation of SOL current

DIII-D

H.J. Schaffer and B.J. Leikind
Nucl. Fusion 31 (1991) 1750

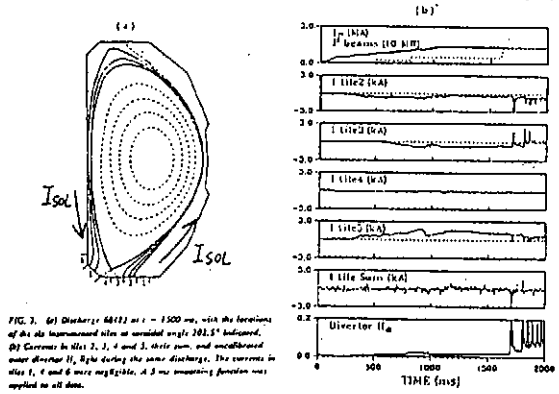

A prototype tile current array was installed.
- $I_{SOL} \sim 1$ kA in L-mode phase
- I_{SOL} decreases at the onset of the H-mode.
- I_{SOL} increases with core plasma current and ELMs
- In single null plasmas, the sum of the measured tile current is close to zero.

The SOL current must be flowing poloidally around the confined plasma.

Driving Mechanism
- toroidal loop voltage
- magnetic helicity
- thermoelectric potential
- bootstrap effect

Purpose

We investigate the controllability of heat load and plasma parameters such as n_e, T_e in both SOL and divertor plate region by using the divertor bias method.

1. Model and equations
   - Staebler model is extended.
   - Slab geometry and fluid approximation
   - Sheath condition
2. Linear response
   - the case of floating divertor plate
   - Applied voltage necessary for equalizing the temperature or sheath potential of in and outer divertor plate.
3. Numerical results.

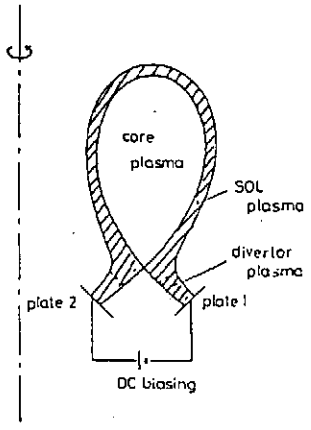

Schematic view

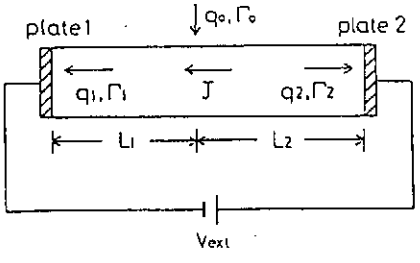

Slab geometry

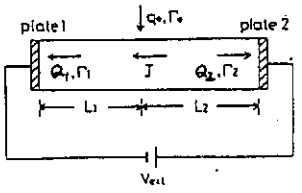

- Conductive heat flux $\vec{q}_{//} = -K_e \nabla_{//} T - C\alpha T \vec{J}_{//}$
- SOL current $J_j = e\Gamma_j \{1 - \exp(\phi - \phi_j)\}$
- pressure balance $n_j T_j = \frac{1}{2} n_0 T_0$
- heat flux to plate $q_j = e\Gamma_j T_j \{2 + \phi_j + 2\alpha \exp(-\phi_j)\}$
- particle flux to plate $\Gamma_j = A n_j T_j^{1/2}$
- Kirchhoff's law $J_1 = -J_2 = J_{//}$
- Circuit equation $V_{ext} = \int \eta_0 J\, dz + \Phi_1 - \Phi_2 + (\sigma_p - \delta_2)(T_1 - T_2)$

where

$\Phi_j = \phi_j T_j$

$\phi = \ln\{(1-\gamma)\alpha\}$

$A = (2e/m_i)^{1/2}$

$\alpha = (m_i/4\pi m_e)^{1/2}$

γ: secondary electron emission coefficient

γ_p: presheath effect $\simeq 0.5$

γ_t: thermoelectric effect $\simeq 0.7$

Conservation relation

- Distance between two plates

$$L_1 + L_2 = 2L$$

- Particle flux

$$\Gamma_1 + \Gamma_2 = G\Gamma_0$$

- Total energy

$$\nabla \cdot \vec{Q} = \eta J^2, \quad \vec{Q} = \vec{q}_{cond} - \frac{5}{2}\vec{J}_{//} T$$

SOL layer width

If $E_{//}$ is zero,

$$\Delta_k = (2\pi)^{3/11} \left(\frac{\eta}{4\pi}\right)^{4/11} (aR)^{7/11} \left(\frac{L}{R}\frac{B_p}{B_t}\right)^{4/11} P^{-3/11} \kappa_0^{7/11} \kappa_e^{-4/11}$$

If $E_{//}$ is <u>not</u> zero,

$$K_0' = \left(1 + \delta \frac{16}{\beta} \left|\frac{e\Phi}{T_0}\right| \frac{\Delta}{a}\right) K_0$$

$$\Delta = \left(1 + \delta \frac{16}{\beta} \left|\frac{e\Phi}{T_0}\right| \frac{\Delta}{a}\right)^{7/11} \Delta_k$$

where $\delta = -1$: inward flow
$\delta = +1$: outward flow

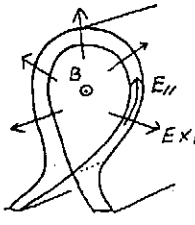

$\delta = -1$: counter-current
$\delta = +1$: co-current

$$\frac{\Delta}{\Delta_k} = \left(1 + \delta \frac{16}{\beta} \left|\frac{e\Phi}{T_0}\right| \frac{\Delta_k}{a} \frac{\Delta}{\Delta_k}\right)^{7/11}$$

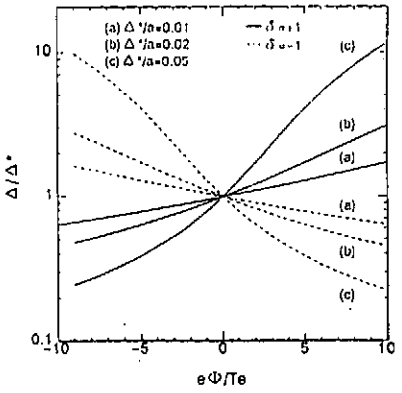

Linear response

If the source position of the particle and heat flux is a little shifted from the mid-point,

$$Q_j = \bar{Q} \pm \tilde{Q}, \quad n_j = \bar{n} \pm \tilde{n}$$
$$\Gamma_j = \bar{\Gamma} \pm \tilde{\Gamma}, \quad T_j = \bar{T} \pm \tilde{T}$$
$$\phi_j = \bar{\phi} \pm \tilde{\phi} \qquad (j = 1, 2)$$

where

$$\bar{Q} = \frac{1}{2} q_0, \qquad \tilde{Q} = e\bar{\Gamma}\bar{T}\left\{\left(\frac{1}{2} f D_{21} - \frac{1+\gamma}{1-\gamma}\phi D_{11}\right)x + \left(\frac{1}{2} f D_{22} - \frac{1+\gamma}{1-\gamma}\phi D_{12}\right)y\right\},$$

$$\bar{\Gamma} = \frac{1}{2}\Gamma_0, \qquad \tilde{\Gamma} = -\bar{\Gamma}(D_{21}x + D_{22}y),$$

$$\bar{n} = \frac{f^{1/2}(\Gamma_0)^{1/2}}{2A q_0^{1/2}}, \qquad \tilde{n} = -\bar{n}(D_{21}x + D_{22}y),$$

$$\bar{T} = \frac{q_0}{f\Gamma_0}, \qquad \tilde{T} = \bar{T}(D_{21}x + D_{22}y),$$

$$\bar{\phi} = \ln\{(1-\gamma)\alpha\}, \qquad \tilde{\phi} = \bar{\phi}(D_{11}x + D_{12}y),$$

$$\tilde{J} = e\bar{\Gamma}\tilde{\phi}(D_{11}x + D_{12}y),$$

$$\tilde{\Phi} = \tilde{\phi}\bar{T} + \bar{\phi}\tilde{T}$$

$$x = \frac{\tilde{q}}{e\bar{\Gamma}\bar{T}}, \qquad y = \frac{V_{ext}}{\bar{\phi}\bar{T}}$$

$$D_{11} = \frac{2\left(1 + \frac{\Gamma_s - \Gamma_f}{\bar{\Gamma}}\right)}{D}, \qquad D_{12} = -\frac{f}{2D}$$

$$D_{21} = -\frac{2 + \frac{e\bar{\Gamma}C_{f0}(0)L}{\bar{T}}}{D}, \qquad D_{22} = \frac{1-\gamma}{2(1-\gamma)}\frac{\gamma}{D}$$

$$D = \frac{3-\gamma}{1-\gamma}(\bar{\phi} + \Gamma_f - \Gamma_s) - \frac{1}{2} f\left(2 + \frac{e\bar{\Gamma}C_{f0}(s)L}{\bar{T}}\right)$$

If divertor plates are floating,

$$\tilde{J} = 0, \quad \tilde{\phi} = 0$$

Potential difference between two divertor plates

$$\frac{V_{ext}}{\bar{\phi}\bar{T}} = \frac{4\left(1 + \frac{\Gamma_s - \Gamma_f}{\bar{\Gamma}}\right)}{f}\frac{\tilde{q}}{e\bar{\Gamma}\bar{T}}$$

Perturbed terms

$$\tilde{n} = \frac{D_{11}D_{22} - D_{12}D_{21}}{D_{12}}\frac{\tilde{q}}{e\bar{\Gamma}\bar{T}}\bar{n}$$

$$\tilde{T} = -\frac{D_{11}D_{22} - D_{12}D_{21}}{D_{12}}\frac{\tilde{q}}{e\bar{\Gamma}\bar{T}}\bar{T}$$

$$\tilde{\Gamma} = \frac{1}{2}\frac{D_{11}D_{22} - D_{12}D_{21}}{D_{12}}\frac{\tilde{q}}{e\bar{\Gamma}\bar{T}}\bar{\Gamma}$$

$$\tilde{Q} = \tilde{q}$$

For example, when we use typical parameters,

$$\bar{q} = 10 \text{ MW/m}^2, \quad \bar{\Gamma} = 10^{24} \text{/m}^2\text{s}, \quad L = 30 \text{ m},$$

then

$$T_0 = 47.6 \text{ eV}$$
$$\bar{T} = 9.6 \text{ eV}$$
$$V_{ext} = 8.8 \text{ V} \quad (\text{if } \tilde{q}/\bar{q} = 0.1).$$

At the plate where larger heat flux flows,

$$\tilde{n} \searrow \quad \tilde{T} \nearrow \quad \tilde{\Gamma} \searrow \quad \tilde{\Phi} \nearrow$$

Condition for $\tilde{Q} = 0$

$$V_{ext} = \frac{2 - 5\phi D_{11}}{5\phi D_{12}}\frac{\tilde{q}}{e\bar{\Gamma}\bar{T}}\phi\bar{T}$$

Perturbed terms

$$\tilde{n} = -\frac{2D_{22} - 5\phi(D_{11}D_{22} - D_{12}D_{21})}{5\phi D_{12}}\frac{\tilde{q}}{e\bar{\Gamma}\bar{T}}\bar{n}$$

$$\tilde{T} = \frac{2D_{22} - 5\phi(D_{11}D_{22} - D_{12}D_{21})}{5\phi D_{12}}\frac{\tilde{q}}{e\bar{\Gamma}\bar{T}}\bar{T}$$

$$\tilde{\Gamma} = -\frac{1}{2}\frac{2D_{22} - 5\phi(D_{11}D_{22} - D_{12}D_{21})}{5\phi D_{12}}\frac{\tilde{q}}{e\bar{\Gamma}\bar{T}}\bar{\Gamma}$$

$$\tilde{\Phi} = \frac{2(D_{12} + D_{22}) - 5\phi(D_{11}D_{22} - D_{12}D_{21})}{5\phi D_{12}}\frac{\tilde{q}}{e\bar{\Gamma}\bar{T}}\phi\bar{T}$$

$$\tilde{J} = \frac{2}{5}\frac{\tilde{q}}{e\bar{\Gamma}\bar{T}}e\bar{\Gamma}$$

External power into the plasma is needed.

For typical parameters ($\bar{q} = 10 \text{ MW/m}^2$, $\bar{\Gamma} = 10^{24}\text{/m}^2\text{s}$, $L = 30 \text{ m}$)

$$\frac{2D_{22} - 5\phi(D_{11}D_{22} - D_{12}D_{21})}{5\phi D_{12}} = 0.05$$

$$V_{ext} = 22.3 \text{ V} \quad (\text{if } \tilde{q}/\bar{q} = 0.1)$$

Numerical Results

- We investigate the plasma parameters in the SOL/Divertor region as a function of the external voltage.
- Plasma parameters

Density	n_s, n_{d1}, n_{d2}
Temperature	T_s, T_{d1}, T_{d2}
Sheath potential	Φ_{d1}, Φ_{d2}
Heat flux	Q_{d1}, Q_{d2}, Q_{s1}, Q_{s2}
Particle flux	Γ_{d1}, Γ_{d2}
Current density	$J_\parallel$

- Imbalance of heat and particle fluxes are made by the length of field lines.
- Effect of the electric field on the SOL width is not included in numerical calculations yet.

Temperature

$q_0 = 50\ MW/m^2$
$\Gamma_0 = 1.2\times10^{23}\ /m^2s$
$L_1 = 20\ m$
$L_2 = 30\ m$

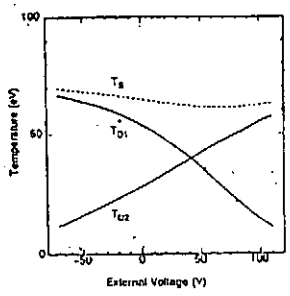

Sheath potential

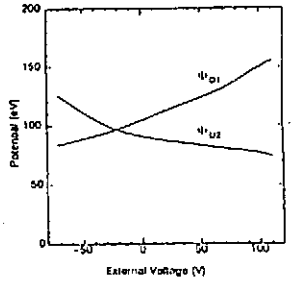

Heat flux (conductive + convective)

$q_0 = 50\ MW/m^2$
$\Gamma_0 = 1.2\times10^{23}\ /m^2s$
$L_1 = 20\ m$
$L_2 = 30\ m$

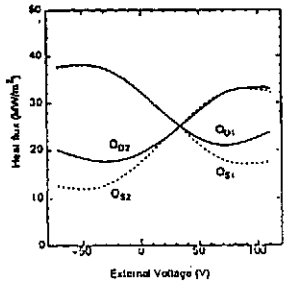

Particle flux

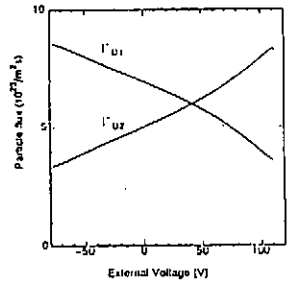

$q_0 = 50\ MW/m^2$
$\Gamma_0 = 1.2\times10^{23}\ /m^2s$
$L_1 = 20\ m$
$L_2 = 30\ m$

Vext vs. $J_\parallel$

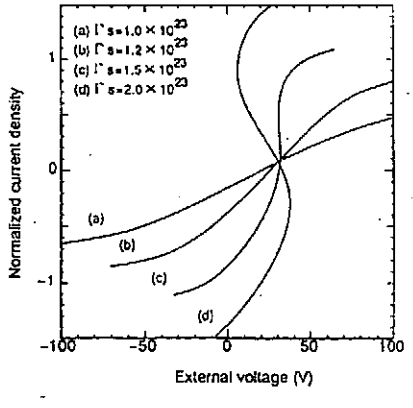

Summary

- Effects of the divertor biasing on the SOL/Divertor plasma was investigated theoretically. We use a simple slab geometry and one fluid approximation.
- Plasma parameters, especially in divertor regions can be controlled by the external applied voltage. The imbalance of divertor plasma parameters between in- and outer divertor plates is able to controlled. On the other hand, the SOL width and SOL plasma parameters remains to be corrections of the order of 10 %.
- Convective flow is important in the parallel transport in the presence of the parallel SOL current.

GENERAL ATOMICS

BIASED DIVERTOR EXPERIMENTS ON DIII-D

by

M. J. Schaffer, N. Brooks, D. Buchenauer,* D. N. Hill†
A. Hyatt, T. Jarboe,§ C. Klepper,‡ L. L. Lao, S. Lippmann
M. A. Mahdavi, D. Orvis,§ T. Osborne, T. Petrie, G. Porter†
M. Rensink,† J. Smith, G. Staebler, R. Stambaugh

*Sandia National Laboratory, Livermore CA
†Lawrence Livermore National Laboratory, Livermore CA
‡Oak Ridge National Laboratory, Oak Ridge TN
§University of Washington, Seattle WA

PRESENTED BY R. STAMBAUGH AT US-JAPAN WORKSHOP ON RF HEATING AND CURRENT DRIVE IN CONFINEMENT SYSTEMS TOKAMAKS

~~Presented at the~~
~~APS Division of Plasma Physics Annual Meeting~~
~~Tampa, FL~~
~~1991 Nov 4-8~~
NAGOYA, JAPAN
11-19-91

GENERAL ATOMICS

DIII-D RING ELECTRODE AND PUMPING PLENUM

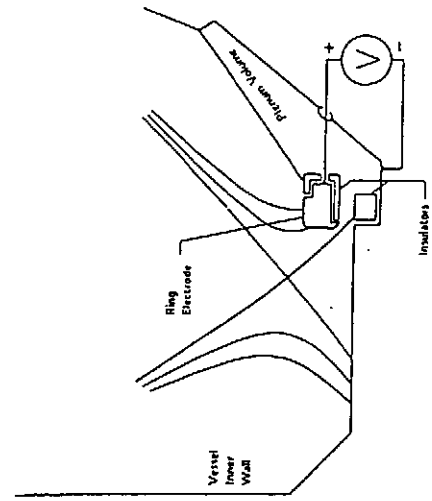

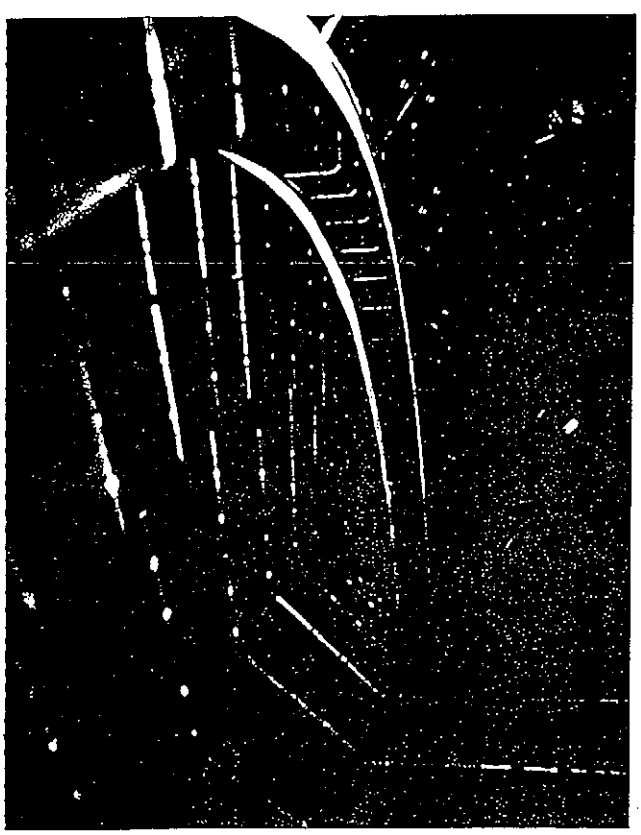

GENERAL ATOMICS

DRIVEN E x B DRIFTS IN SCRAPE-OFF LAYER

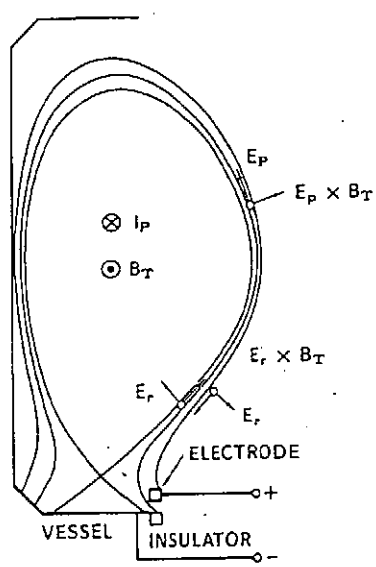

GENERAL ATOMICS

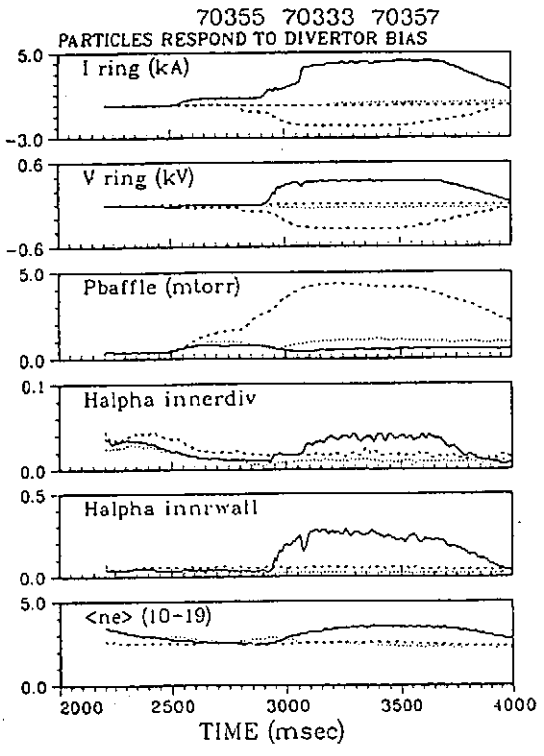

GENERAL ATOMICS

PLENUM GAS PRESSURE RAISED AND LOWERED BY DIVERTOR BIAS

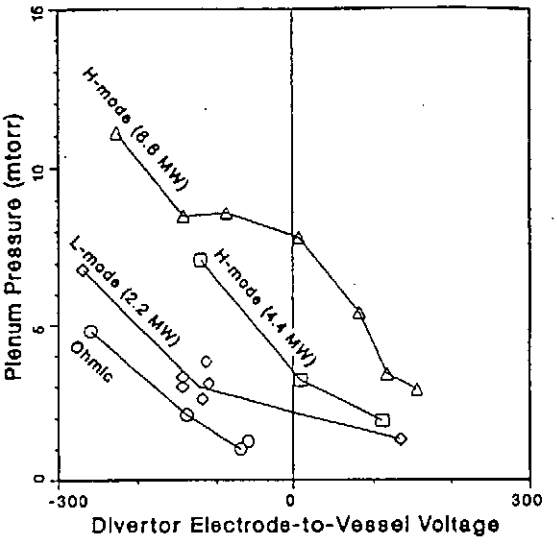

NEGATIVE DIVERTOR BIAS DURING H-MODE REDUCES DENSITY AND INCREASES TEMPERATURE

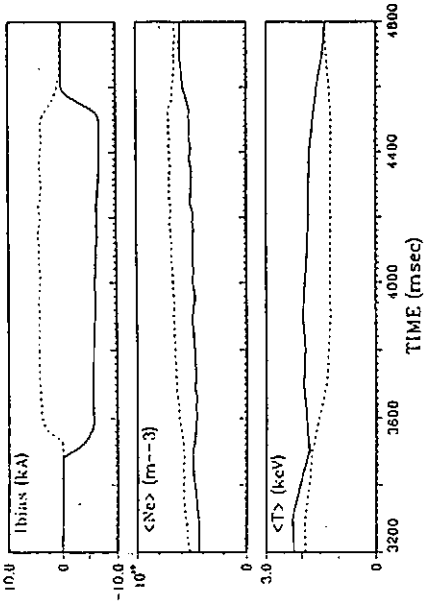

GENERAL ATOMICS

E x B PLASMA PUMP

Consider a potential U applied across one dimension of an aperture:

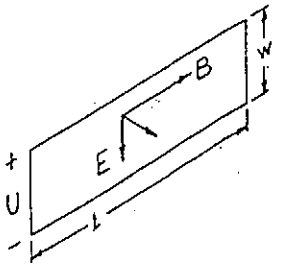

The E × B pumping speed through the aperture is then:

$$S = \int\int E/B \, dx dy = \ell U/B$$

Example: DIII-D biased divertor

$\ell = 2\pi R_0 \approx 10\text{m}$

$U/B \approx 200$ V/2 T ≈ 100 m^2/s

$S \approx 10^3$ m^3/s

GENERAL ATOMICS

BIAS YIELDS LARGE PLENUM PRESSURE, EVEN WITH SEPARATRIX FAR ON ELECTRODE

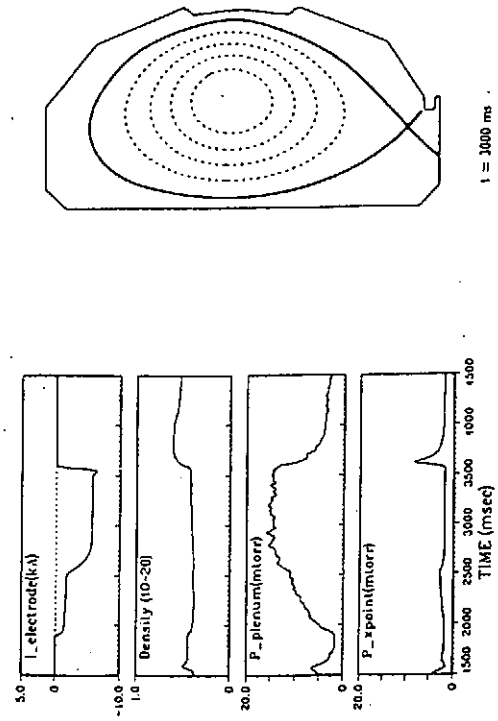

GENERAL ATOMICS

DIVERTOR BIAS OVERCOMES SENSITIVITY OF PRESSURE TO SEPARATRIX POSITION

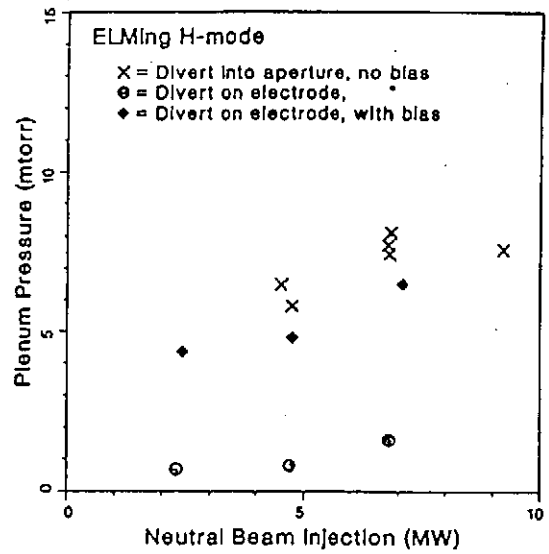

GENERAL ATOMICS

HELICITY INJECTION CURRENT DRIVE (COMPOSITE OF 72022 AND 72023)

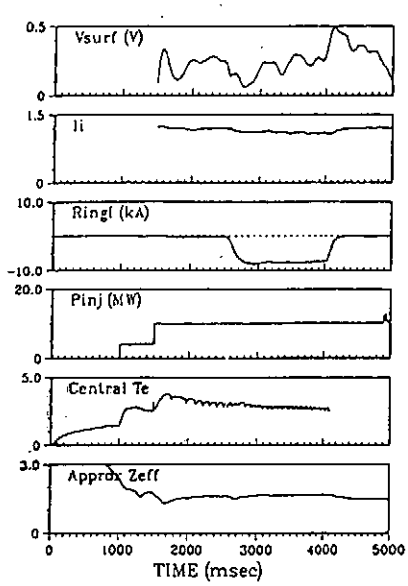

GENERAL ATOMICS

REFERENCE CASE 72014

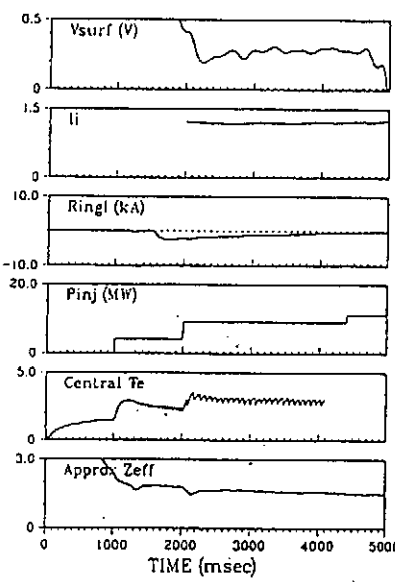

GENERAL ATOMICS

CONCLUSIONS

- Scrape-off layer plasma flows are driven by $E \times B_{Tor}$ "pump".
- $E \times B$ "pump" can be made geometry insensitive.
- Control of H-mode density appears feasible.
- Some evidence for current profile modification and helicity current drive.
- Divertor bias has little effect on:
  - Energy confinement
  - Impurity accumulation
  - Edge instabilities.
- Future plans:
  - Improve electrode insulation.
  - Install cryo pump.

GENERAL ATOMICS

OUTLINE

- Introduction
  - ADP experimental arrangement
  - SOL Electric field pattern and current paths
- Results of power threshold studies
  - H-mode power threshold is a strong function of the bias voltage with a minimum, for either polarity of the toroidal field.
  - The minimum is at a bias voltage of $\simeq$ 70 Volts, for grad-B drift direction towards the X-point, and in the range of 0 to 80 Volts, for the opposite direction of the toroidal field.
- Speculations on how divertor biasing affects H-mode transition power threshold
  - comparison with experimental observations.
- Summary and conclusions

- Papers on other aspects of ADP:
  - 3E11 M. Schaffer, 3E10 C. Klepper, 9T10 J. Hogan, 8S10 L. Owen

GENERAL ATOMICS

EFFECTS OF EDGE CURRENTS AND ELECTRIC FIELDS ON THE H-MODE TRANSITION

By

M.A. Mahdavi

in collaboration with

R.J. Groebner, D.N. Hill,* A.W. Hyatt, A.W. Leonard, T.H. Osborne, M.J. Schaffer, G. Staebler, R.D. Stambaugh, and E.J. Strait

General Atomics

*Lawrence Livermore National Laboratory.

Presented at

The American Physical Society

33rd Meeting of the Division of Plasma Physics

Tampa, Florida

November 4-8, 1991

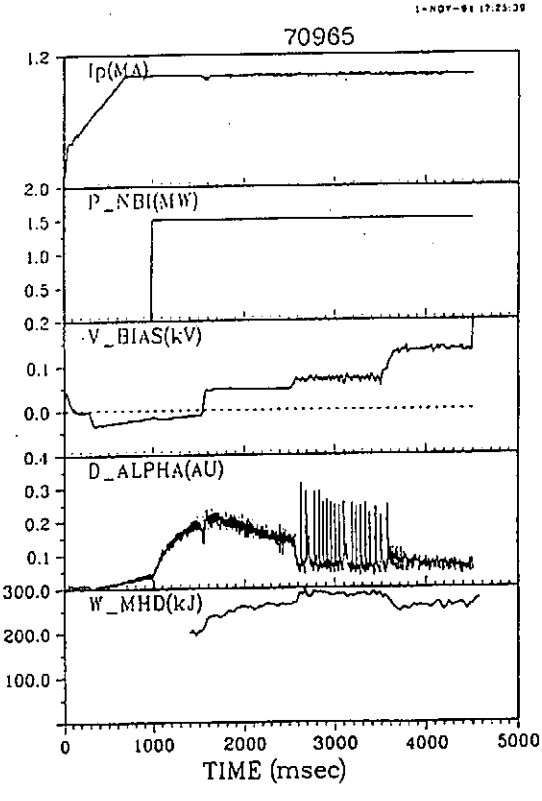

H--MODE POWER THRESHOLD HAS A MINIMUM AT +75 VOLTS GRAD-B DRIFT TOWARDS X-POINT

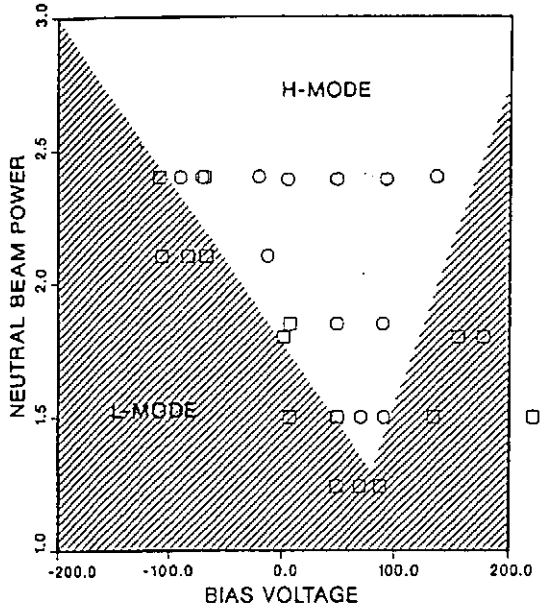

H--MODE POWER THRESHOLD HAS A MINIMUM AT +75 VOLTS GRAD-B DRIFT TOWARDS X-POINT

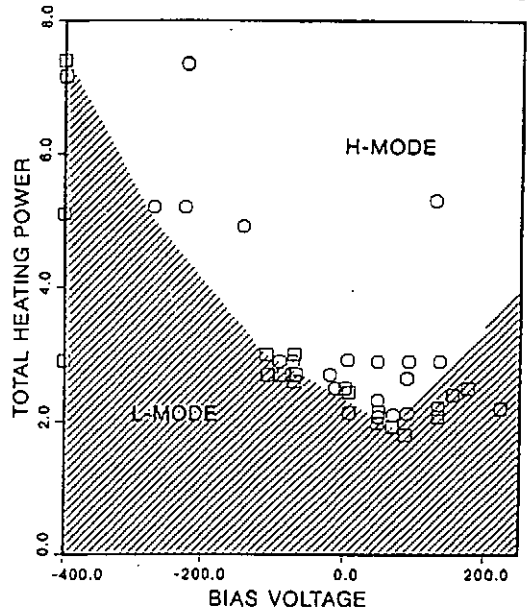

BIAS ON BEFORE H-MODE GRAD-B DRIFT AWAY FROM X-POINT

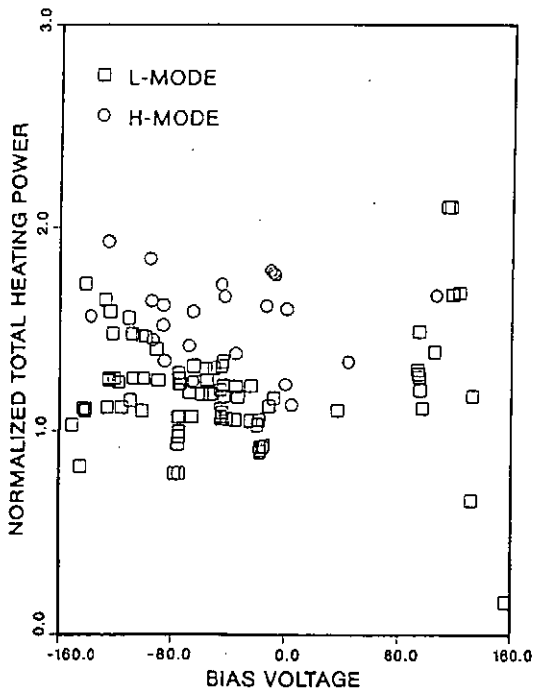

GENERAL ATOMICS

HOW DOES DIVERTOR BIASING INFLUENCE THE H-MODE POWER THRESHOLD?

The existence of a minimum in the power threshold and its off axis location could be due to one or a combination of several physical effects. In the following, postulated physical effects are tested against the experimental results.

- Modification of heat flux across the separatrix by $E_P \times B$ flows, or changes in recycling do not explain the off axis location of the minimum.
  - With Grad-B drift towards the X-point and positive biasing, heat flow associated with the $E_P \times B$ drifts is outwards, which should increase the power threshold, in the experiment power threshold decreased.
  - With the polarity of the electric field for which the minimum in the H-mode power threshold is observed, the core recycling is enhanced. According to the conventional wisdom, this should increase the power threshold

GENERAL ATOMICS

HOW DOES DIVERTOR BIASING INFLUENCE THE H-MODE POWER THRESHOLD?

- Enhancement of shear in edge rotation can not be ruled out as a possible cause for the reduced power threshold at low positive potentials.
  - — The direction of $E_r \times B$ rotation, due to the external fields, relative to the usual H-mode poloidal rotation is independent of the B_T direction.
  - — There is a significant difference between rotation profiles of two shots with opposing biasing polarities.
- Toroidal currents, driven by biasing, could explain existence of a minimum in power threshold but not its off axis locations.
  - — A current driven instability in SOL is plausible since SOL toroidal current density can approach several percent of the peak value.
  - — Our data do not indicate a preferred finite edge current density since the direction of the toroidal SOL current depends on the direction of the B_T; whereas, the location of the minimum power threshold is at a positive bias for either polarity of B_T.

H-MODE RADIAL E-FIELD PROFILES
POSITIVE BIASING
GRAD-B DRIFT AWAY FROM X-POINT

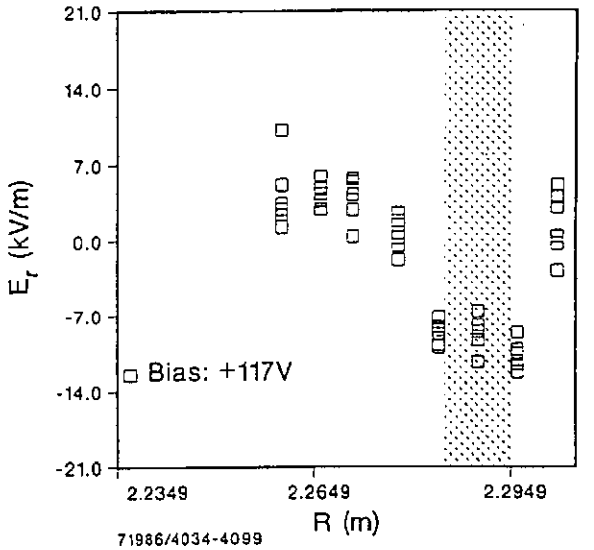

71986/4034-4099

H-MODE RADIAL E-FIELD PROFILES
NEGATIVE BIASING
GRAD-B DRIFT AWAY FROM X-POINT

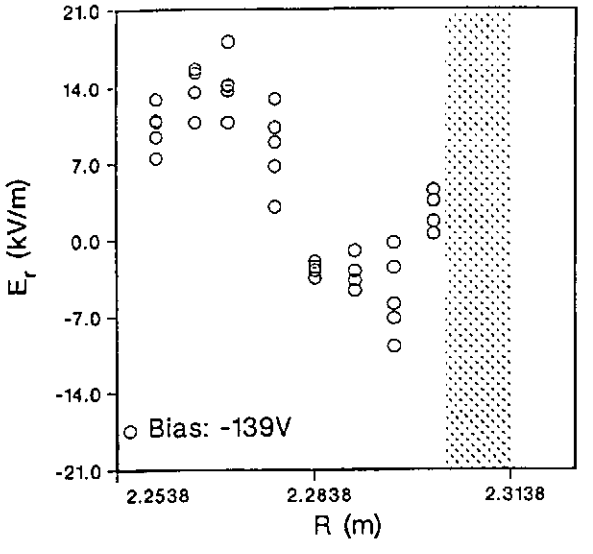

72012/2236-2300

GENERAL ATOMICS

SUMMARY AND CONCLUSIONS

- SUMMARY OF OBSERVATIONS:
  - — H-mode power threshold is a strong function of the bias voltage with a minimum which with either polarity of the toroidal field occurs in the range of 0 to +80 volts.
  - — Biasing has no significant effect on confinement of the H-mode plasmas.
  - — During biasing, SOL current density can approach several percent of the peak core value
  - — There is a measurable difference between the edge rotation characteristics of positively and negatively biased plasmas.
- CONCLUSIONS:
  - — $E_P \times B$ drift effects, either due to changes in particle recycling or heat transport, are not good candidates for explaining either the existence or the off axis location of the minimum in the power threshold.
  - — Enhanced shear in the edge plasma rotation can not be ruled out as the cause of the reduced H-mode power threshold at small positive bias potentials.
  - — A current driven instability is a plausible candidate for explaining the observed increase in P_{th} at high SOL currents.

1991/11/15
NIFS
US-Japan Workshop on
"RF Heating and Current Drive in Confinement Systems"

Divertor Biasing and Helicity Injection

K. ITOH
(NIFS)

This work is in collaboration with
S.I. Itoh (NIFS)
A. Fukuyama (Okayama)

Motivations

① In many theories/models, current (driven near edge by helicity drive) is assumed to be transported to the core.

② Questions:

mechanism for current transport

What is the expense for this current rearrangement?

Double tearing
magnetic braiding
⋮

③ Solve current profile in the presence of current diffusion
(do not depend on relaxation phenomena)
Evaluate shape

Constraint on the thermal transport coeffient

④ "Pure" Bootstrap state

Such as Bellan et al.

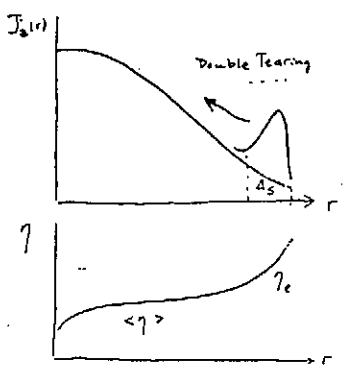

Resistive skin depth

$$\Delta_s = \sqrt{\eta_e/\omega\mu_0}$$

Injected helicity
(in the phase of ①)

$$\int \tilde{B}_t \tilde{E}_t = \boxed{2\pi a \Delta_s \tilde{E} \tilde{B}_t}$$

Dissipated in core

$$\int B_t E_t = \pi a^2 E B_t$$
$$= \boxed{\langle\eta\rangle I_p B_t}$$

If current is transferred to core such that helicity is conserved

$$I_p = \frac{2\pi a \Delta_s \tilde{E}}{\langle\eta\rangle}$$

Injection power $P = (2\pi a \Delta_s)\frac{(\tilde{E})^2}{\eta_e} 2\pi R$

$$\frac{P}{2\pi R I_p} = \left[\frac{a\langle\eta\rangle}{\Delta_s \eta_e}\right] \frac{\langle\eta\rangle I_p}{a^2}$$

Improvement

Steady State by Divertor Current Drive

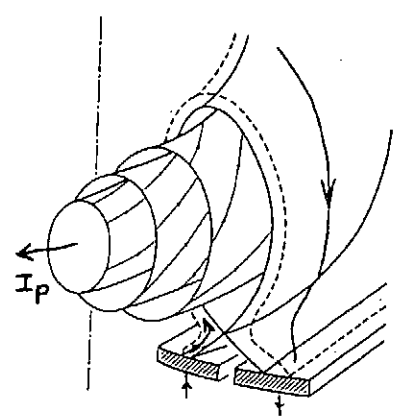

Schaffer
US-J ws
San Diego
('90, Sept.)

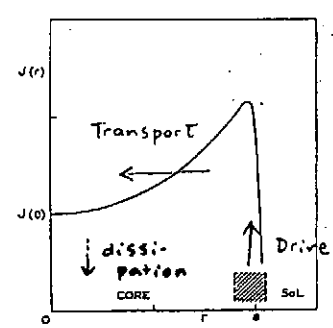

Scheme to sustain steady state

Sustain J by current diffusion

$$E + v \times B = \eta J - \lambda \Delta J$$

Not relaxation process,
Continuous transport

Stationary Solution $E, v = 0$

$$J = J_0 \cdot I_0\left(\sqrt{\frac{\eta}{\lambda}}\, r\right) \qquad \text{cylinder model}$$

parameter $\Lambda = a\sqrt{\frac{\eta}{\lambda}}$

large $\eta \rightarrow$ Large $\Lambda \rightarrow$ Hollow profile $\rightarrow$ Low ℓ_i

Λ must be $O(1)$ ($\lesssim 2$)
for MHD stability

$$\ell_i = 1 - \frac{I_0(\Lambda) I_2(\Lambda)}{I_1^2(\Lambda)}$$

Stationary Solution is obtained.

Current diffusivity & Ohm's Law

Example: Magnetic diffusion Kaw '79 ... et al.

$$\frac{\partial f}{\partial t} + v \cdot \partial f + \frac{q}{m}(E + v \times B) \cdot \partial_v f = \frac{\partial}{\partial z}(|v_z| D_M)\frac{\partial f}{\partial v_z} + C(f)$$

multiply $\int \frac{1}{2} m v^2 \, dv \rightarrow$ energy eq.

$$\chi_e = \frac{3}{\pi} v_{te} D_M$$

multiply $\int \frac{q v_z}{|v_z|} dv \rightarrow$ Current eq.

$$E_z + (v \times B)_z = \eta J_z - \underbrace{\frac{2}{\sqrt{\pi}} \frac{T D_M}{\int q^2 |v_z| f_M d^3v}}_{\lambda} \frac{\partial}{\partial z} J_z$$

$$\lambda = \frac{\sqrt{\pi}}{2}\left(\mu_0 \frac{c^2}{\omega_p^2}\right) v_{te} D_M$$

Internal Inductance $\Lambda \lesssim 2$ for stability

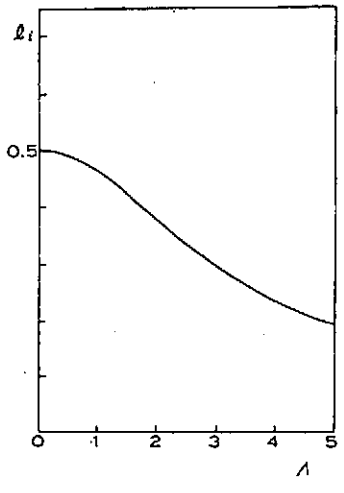

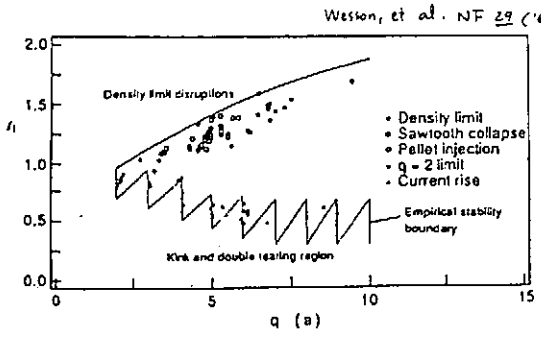

Relation with Thermal Transport

$$\lambda = \frac{\mu_0 c^2}{\omega_p^2} \mu_e \qquad \mu_e : \text{electron shear viscosity}$$

$$\mu_e / \chi_e \sim O(1)$$

For instance: Microscopic Magnetic Braiding ← Current-rearrangement with helicity conservation

$$\mu_e / \chi_e = \pi/6$$

$$\lambda = \frac{\sqrt{\pi}\, c^2 \mu_0}{2\omega_p^2} v_{te} D_M$$

$$\chi_e = \frac{6 \omega_p^2 a^2 \eta}{\pi c^2 \mu_0} \frac{1}{\Lambda^2} \qquad \text{if } \Lambda < 2 \text{ then}$$

$$\chi_e > \frac{3 \omega_p^2 a^2 \eta}{2\pi c^2 \mu_0}$$

$$\chi_e \gtrsim \frac{1}{2} a_m^2 n_{20} T_{kev}^{-3/2} \times 10^5 \quad (m^2/s)$$

This value is too large to apply to experiments.

"Bootstrap" steady state without Seed Current

Bootstrap Current [Bickerton, et al., Galeev & Sagdeev]

Electromotive Force by diffusion

$$-B_p D \frac{1}{n}\frac{dn}{dr} \qquad (D \sim \frac{1}{\epsilon^{3/2}} \nu \rho_i^2 \text{ for banana regime})$$

Ohm's law without Electric Field

$$\eta J_{\parallel} = -B_p D \frac{1}{n}\frac{dn}{dr}$$

Necessity of the Seed Current If $J_\parallel \xrightarrow{\text{Ampere}} B_p \xrightarrow{\text{Bootstrap current}}$

$$\eta J_{\parallel} = -D\mu_0 \frac{1}{n}\frac{dn}{dr}\frac{1}{r}\int_0^r r\,dr\, J_{\parallel}$$

Homogeneous Equation

$J_\parallel = 0$ if $J_\parallel$ should be regular at $r = 0$

Let $J_\parallel = J_{\parallel b} + J_{seed}$; then

$$\eta J_{\parallel b} - D\mu_0 \frac{1}{n}\frac{dn}{dr}\frac{1}{r}\int_0^r r\,dr\, J_{\parallel b} = \boxed{-D\mu_0 \frac{1}{n}\frac{dn}{dr}\frac{1}{r}\int_0^r r\,dr\, J_{seed}}$$

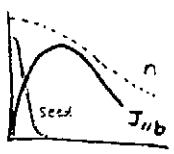

Finite Current Drive Power is necessary to Generate Seed Current

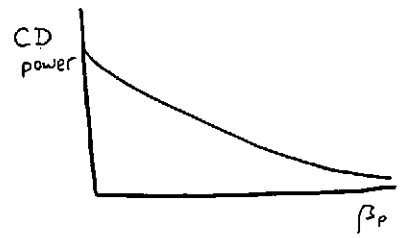

Diffusion of Current supplies seed current

Purely Bootstrap steady state is possible !

(Academic interest , but ....)

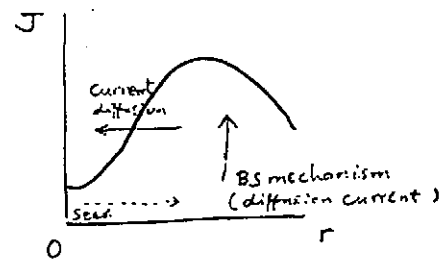

Ohm's Law in the presence of current diffusion

$$\boxed{\eta J_{\parallel} - \lambda \Delta J_{\parallel} = -D\mu_0 \frac{1}{n}\frac{dn}{dr}\frac{1}{r}\int_0^r r\,dr\, J_{\parallel}}$$

In the vicinity of the axis

$$\eta J_{\parallel} - \lambda \Delta J_{\parallel} = C\, s^{-1/4}\int_0^s J_{\parallel}\, s\, ds \qquad (\sqrt{s}\, J_\parallel(0) \text{ near axis})$$

$$s = r/a$$

$$C = \nu\rho^2\mu_0 \left(\frac{R}{a}\right)^{3/2}$$

Let $s \to 0$ then $(\frac{n'}{n} = -as + \cdots)$

$$\eta J_{\parallel} - \lambda \Delta J_{\parallel} = 0$$

$$J_{\parallel} = J_{\parallel}(0)\, I_0\left(\sqrt{\frac{\eta}{\lambda}}\, s\right)$$

medium s : $\left(|\lambda \Delta J_\parallel| \ll \left|\eta J_\parallel - C s^{-1/4}\int_0^s J_\parallel s\, ds\right| \right)$

$$J_{\parallel} \sim \bar{J}_{\parallel}(0)\, \frac{1}{s\sqrt{s}} \exp\left(\frac{2C}{\eta}\sqrt{s}\right)$$

Connection is possible $\frac{C}{\eta} \gtrsim 1$

or $\beta_e \gtrsim (a/R)^{3/2}$

- Homogeneous solution can be regular at $r = 0$
- If $\lambda \Delta J_\parallel \le 0$ at edge, no supply (external) is required

Model Example

$\frac{n'}{n} = -s(1-s^2)$ η, λ const. in space

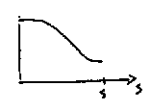

Power Balance

$$\lambda J \frac{\partial J}{\partial s} = \int \lambda (\nabla J)^2 r\,dr + \int \eta J^2 r\,dr - \int J \cdot (\text{source}) r\,dr$$

($\lambda J \frac{\partial J}{\partial s}$: input)

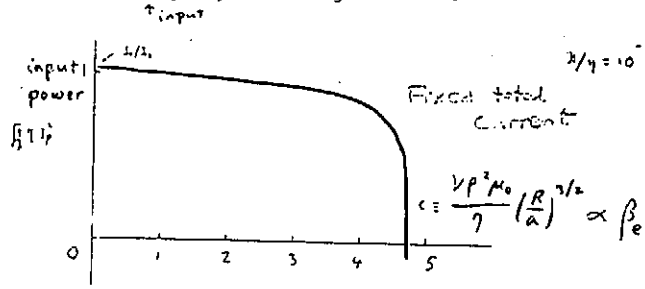

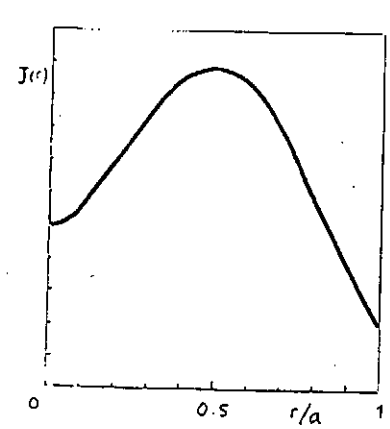

$\lambda/\eta = 10^{-2}$

$C = 4.795$

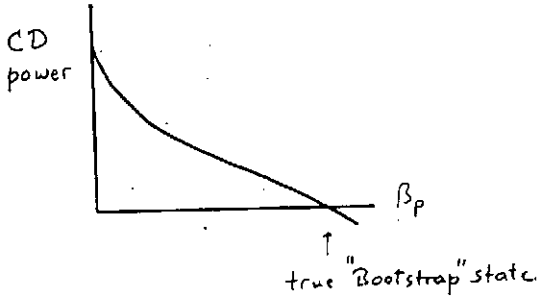

- Bootstrap state without need current is possible
- Possibility of Igniting Steady State Tokamak
- Stability Analysis necessary

Summary

1. Steady state with dc helicity injection near edge is studied.

   Current diffusion works to sustain the steady state.

   MHD stability limits lower boundary of internal inductance.

   This limits the lower boundary of $\chi_\perp$
   → too large for experimental application

   "Flux rearrangement via helicity conservation" is a violent process from the view point of plasma confinement

2. Bootstrap state without seed current is found to be possible.

   This may allow steady state ignition in tokamaks.

3. Future study is required since current rearrangement process may have large impact.

US-Japan Workshop on "RF Heating and Current Drive in Confinement System Tokamak", Nagoya, 18-21, Nov. 1991

Initial Results of LHCD in JT-60U and Limitation of the LHCD Application

T. Imai and JT-60 Team

Japan Atomic Energy Research Institute

Contents

1. LHCD Program in JT-60U
   1) Plan
   2) Initial Results
2. Power Balance and Limitation of LHCD Application
   -Effects of Fast Electrons on First Wall-

JT-60U LHCD Launcher Installation Plan

1991~ 24x4wgs. MJ Launcher ~3 MW Exp.
1993~ + 48x4wgs. MJ Launcher ~10 MW Exp.

Phase 1 (1991 ~ 92)

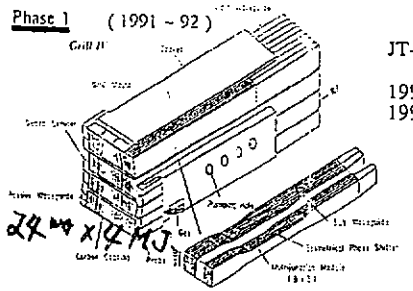

Phase 2 (1993 ~)

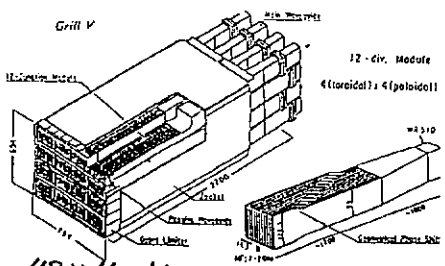

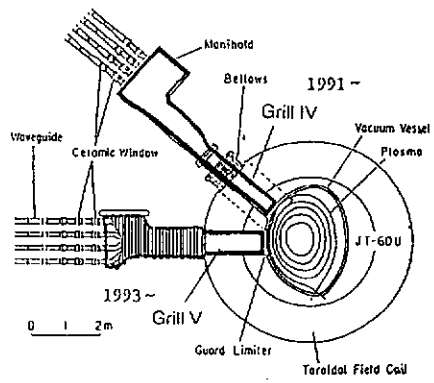

CURRNET DRIVE EXPERIMENTS in JT-60 & 60U

1985	1986	1987	1988	1989	1990	1991	1992	1993	1994	1995
First Plasma	2 MALHCD			M.J. Launcher		*High Ip(6MA)*			*500keV NBCD*	
	First LHCD			~80% BS Current		*~3MWLHCD*		*~10MWLHCD*		
				LHCD H-mode			*120keV NBCD*		*ECCD/ FWCD*	
							JT-60Upgrade			

LHCD in JT-60U

1. High Performance LHCD with ~ 10MW. (η_{CD}, I_{CD}, Profile Control)
2. Confirm Engineering Feasibility (Thermal Load, Coupling)
3. LHCD Physics

Progress of the JT-60 LHCD

1) The η_{CD} of 0.34×10^{20}m^{-2}A/W by the multi-junction launcher, well approaching the necessary value for ITER (0.5×10^{20}m^{-2}A/W).

2) The progress by one order of magnitude in the *CDP* – 1.25×10^{20}m^{-2} MA.

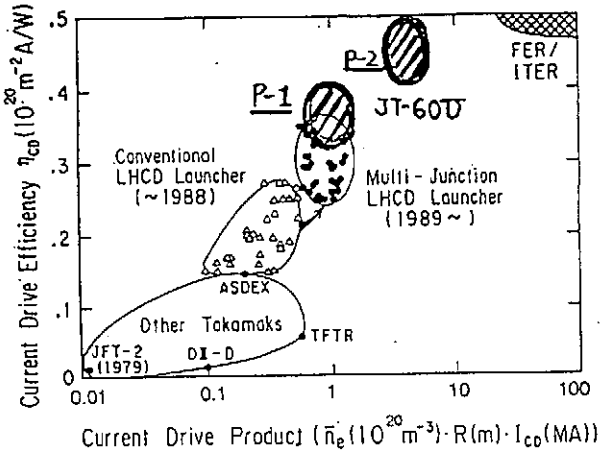

LHCD in JT-60U

	P_{LH} (MW)	η_{CD} (10^{20}m^{-2}A/W)	CDP (10^{20}m^{-2}A)
P-1	2–3	0.3–0.4	~1
P-2	~10	0.4~0.5	~5

Initial Results of LHCD in JT-60U

< 2 Weeks Experiment
P_{LH} < 1.5 MW

1) ~ 2 MA Current Drive in Low Density Plasma

2) Current Drive Efficiency VS $N_{\parallel}$

3) Sawtooth Suppression & MHD ---> by K. Ushigusa

4) Rotation of LHCD Plasma (---> by K. Ushigusa)

5) LHW Dispersion

6) Divertor Heat Load/Fast Electron Loss ---> Next Topic

2 MA Current Drive in JT-60U

B_t= 4 T, $\bar{n}_e$ = 3×10^{18}m^{-3}, P_{LH}= 1.1 MW

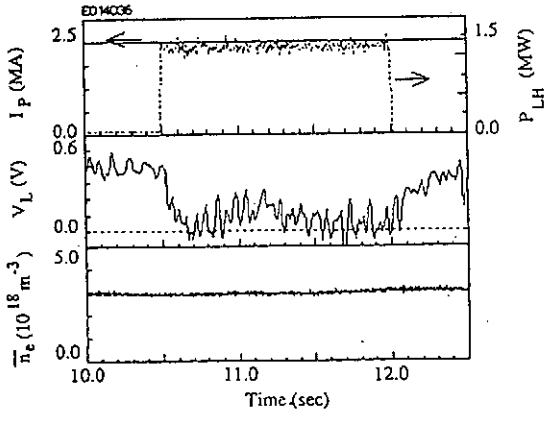

$N_{\parallel}$ Dependence of Current Drive Efficiency

$N_{\parallel peak}$ is varied from 1.3 to 1.9 ($\Delta\phi^m$=120°–180°)
Dependence qualitatively agrees with Theory

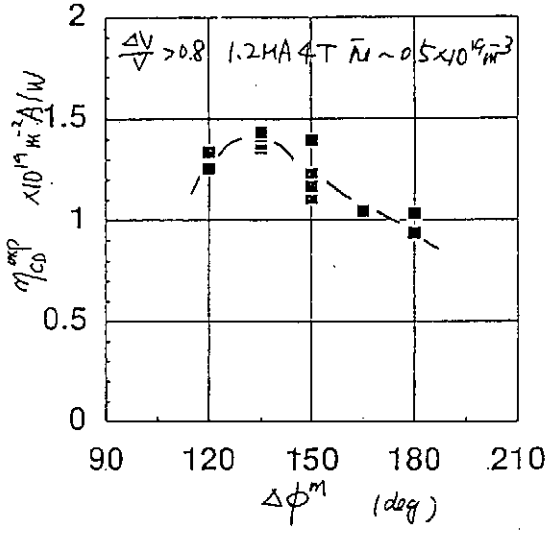

$N_{//}$ Dependence of Current Drive Efficiency

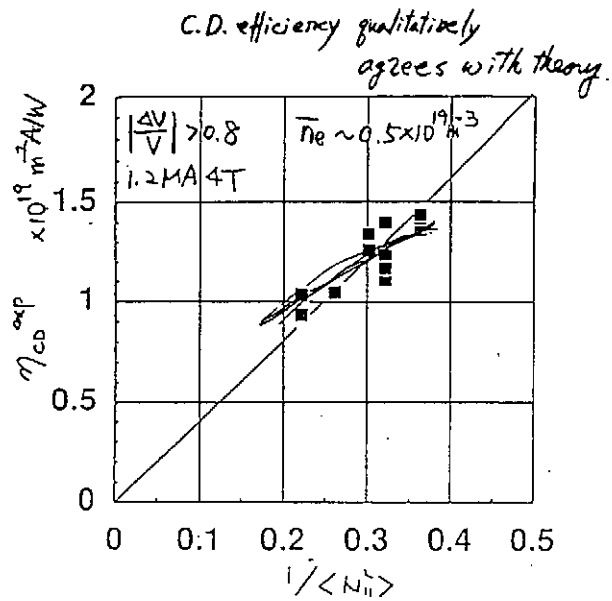

$$\frac{1}{\langle N_{//}^2\rangle} \equiv \frac{\int_{N_{min}}^{\infty} \frac{P(N_{//})}{N_{//}^2}\,dN_{//} - \int_{-\infty}^{-N_{max}} \frac{P(N_{//})}{N_{//}^2}\,dN_{//}}{\int P(N_{//})\,dN_{//}}$$

interaction of LHW with ions

dispersion relation of LHW

$$\frac{\omega^2}{\omega_{LH}^2} = 1 + \frac{1}{\frac{m_e}{m_p}\left(\frac{k_\perp}{k_{//}}\right)^2 \cdot \gamma} \qquad \gamma = \frac{1}{n_e}\sum_{ions}\frac{Z_i^2 \cdot n_i}{A_i}$$

electorns interact with $k_{//}$

ions interact with $k_\perp$

$$\left(\frac{k_\perp}{k_{//}}\right)^2 = \frac{m_B}{m_e}\cdot\frac{F_2^2 \cdot T_e}{E_B}$$

change E_B = 40–90 keV

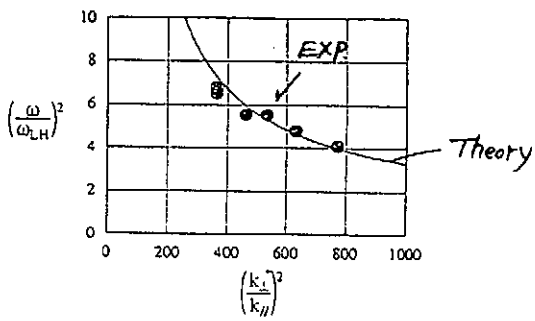

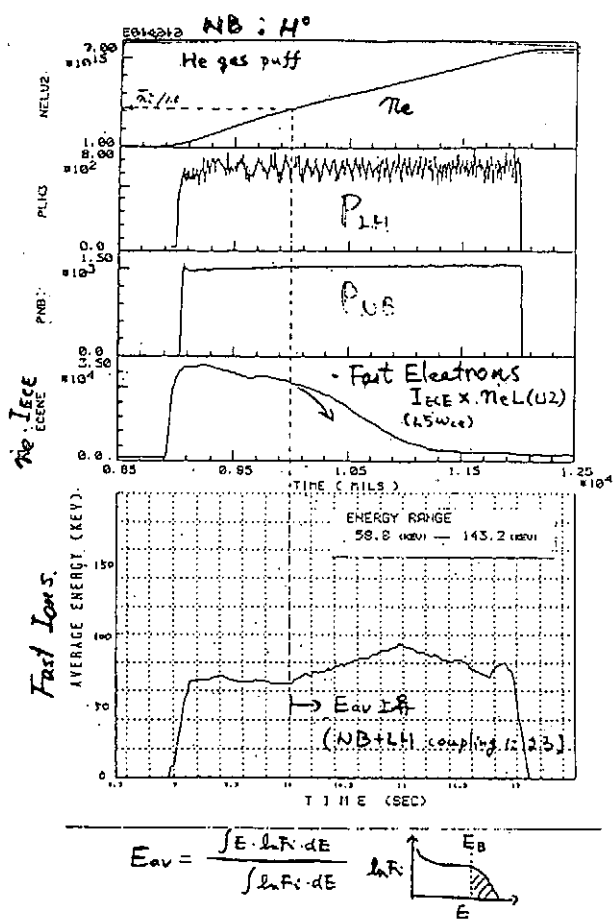

$$E_{av} = \frac{\int E \cdot h_F \cdot dE}{\int h_F \cdot dE}$$

Power Balance and Limitation of LHCD Application

No Large Difference between LHCD and NBI Plasmas in Medium Density (> $1\times10^{19}m^{-3}$)

Direct Loss of Fast Electrons / Localized Heat Load / Hot Spot Phenomena seem to occur in case of very Low Density, Disalignment of First Wall or Error Field

1) Example of the High Power LHCD
   Power Loss to the Divertor and Radiation Loss

2) Divertor Heat Load Profile of LHCD Plasma

3) Direct Power Loss of Fast Electrons to the Divertor
   Preliminary Results from JT-60U

4) Example of Hot Spot in JT-60
   due to the Disalignment

5) Heat Load to the Launcher Head

NO INHERENT BAD EFFECTS on DIVERTOR due to FAST ELECTRONS in HIGH POWER LHCD

1. LARGE *CDP* ~ 12x10^{19}m^{-2}MA, P_{LHCD} ~4.2 MW
2. POWER to DIVERTOR ~1.8 MW, RADIATION~1.9 MW

similar to NBI/OH Plasma

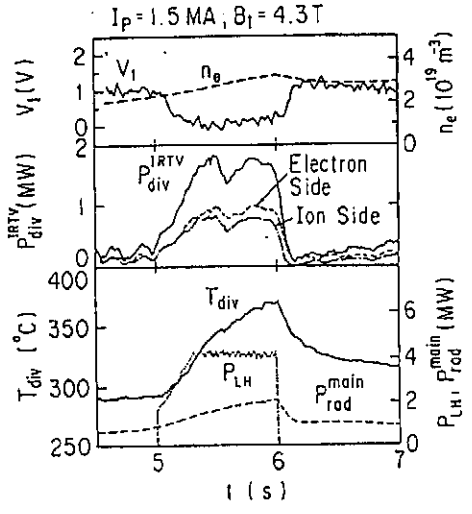

Profile of Heat Flux

- Width of Heat Flux : ~4cm
- No Large Difference of Heat Flux on Electron and Ion Side

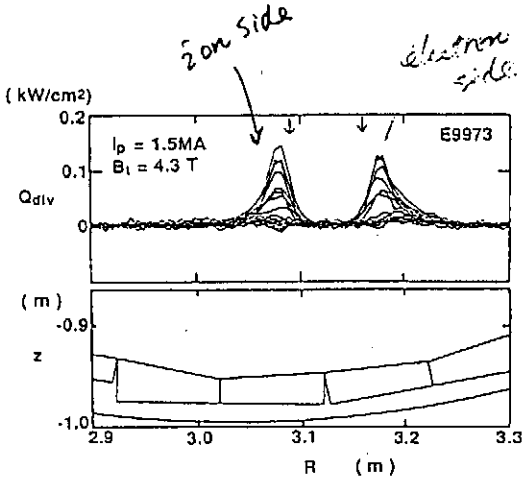

Power Loss of the LHCD Plasma

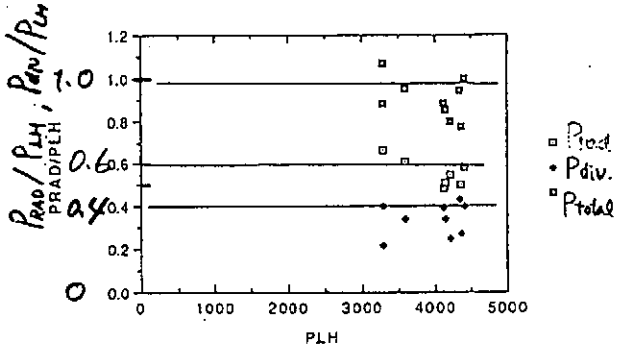

$P_{abs} \sim P_{rad} + P_{div.}$

Power Loss Balance of LHCD Plasma similar to that of NBI

FWHM of LHCD Plasma is similar to that of NBI Plasma

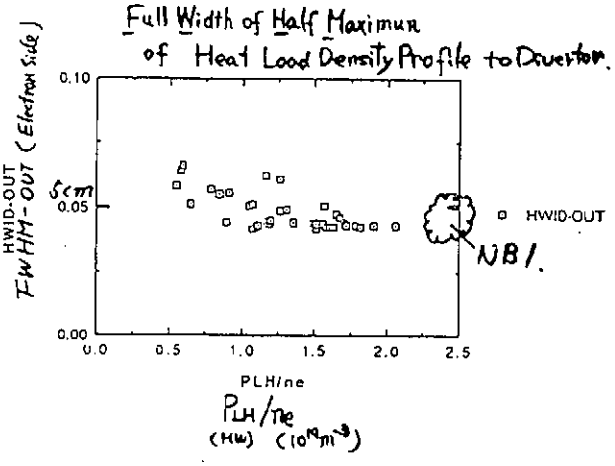

$FWHM^{LHCD} \sim FWHM^{NBI}$

Low $\bar{n}_e$ case ($\leq 1\times10^{19}$ m^{-3})

Heat Load to electron side of divertor much larger than ion side.

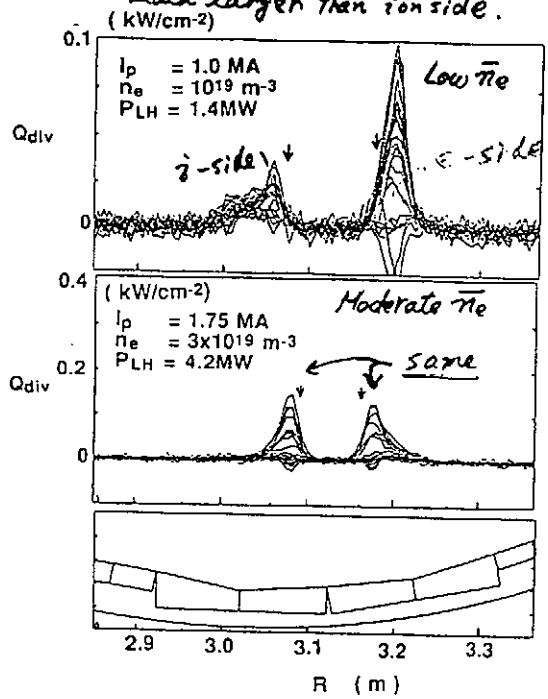

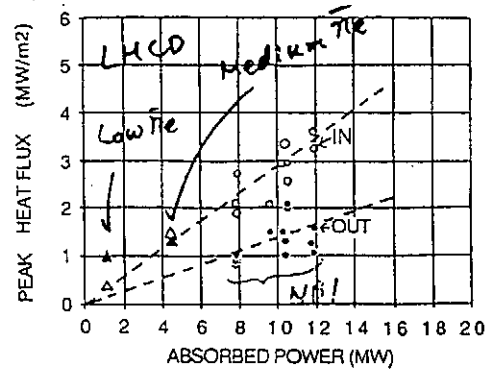

Recent Observation in JT-60U

Direct Loss of Fast Electrons

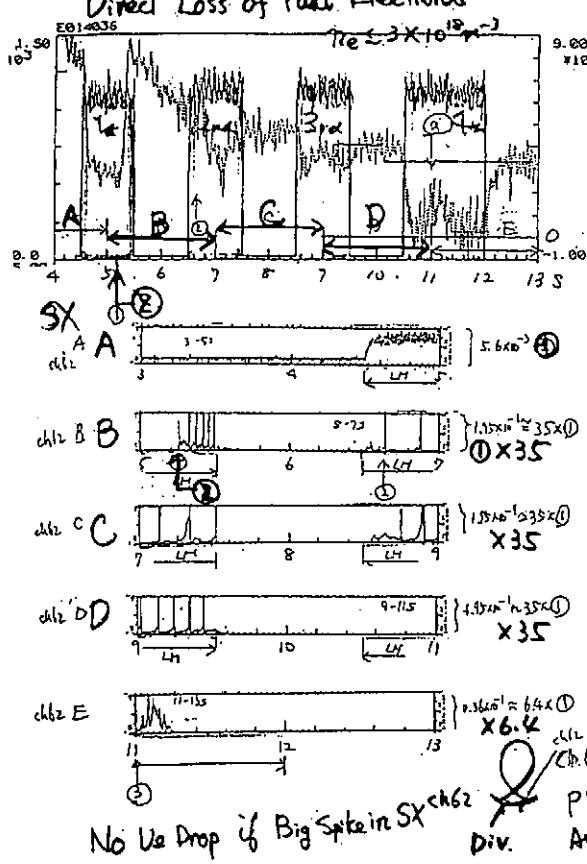

Example of Hot Spot.

due to Disalignment of First Wall.

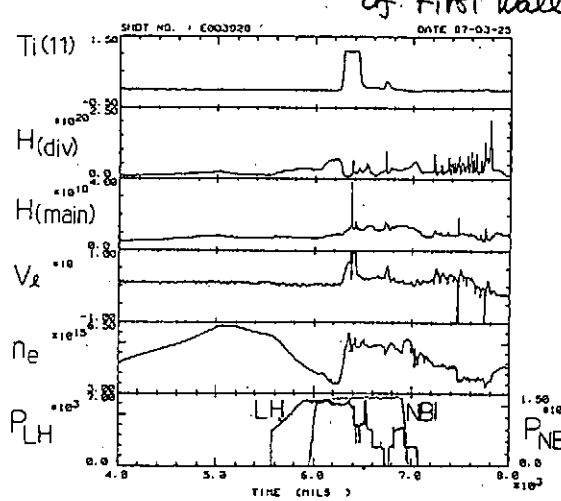

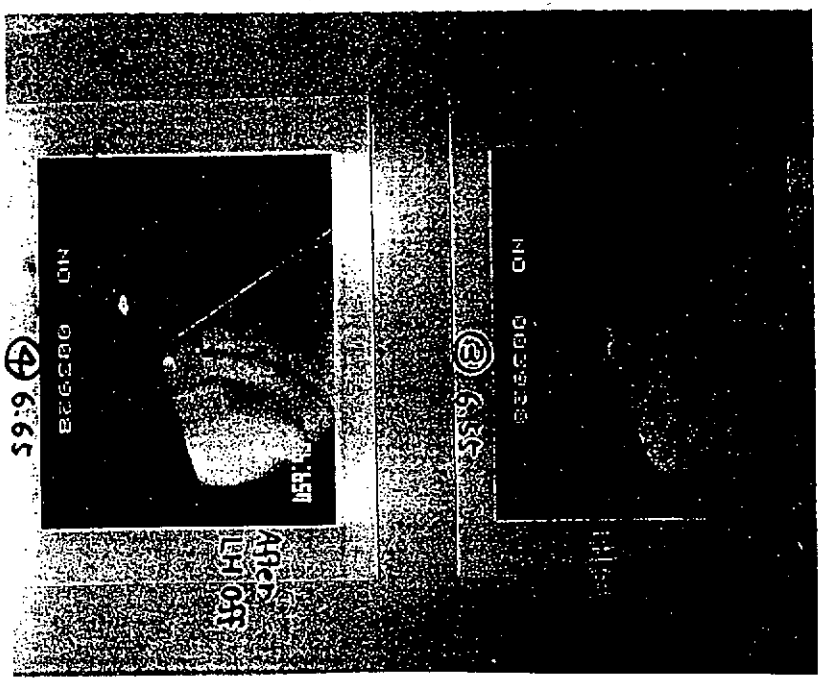

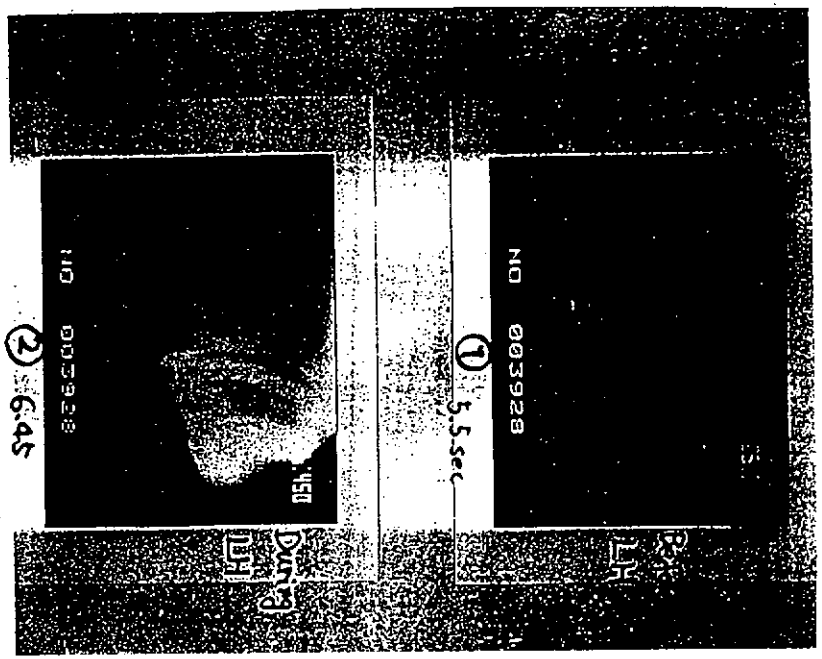

Hot Spot
due to Disalignment
of the First Wall

JT-60 T.C Wall
1987

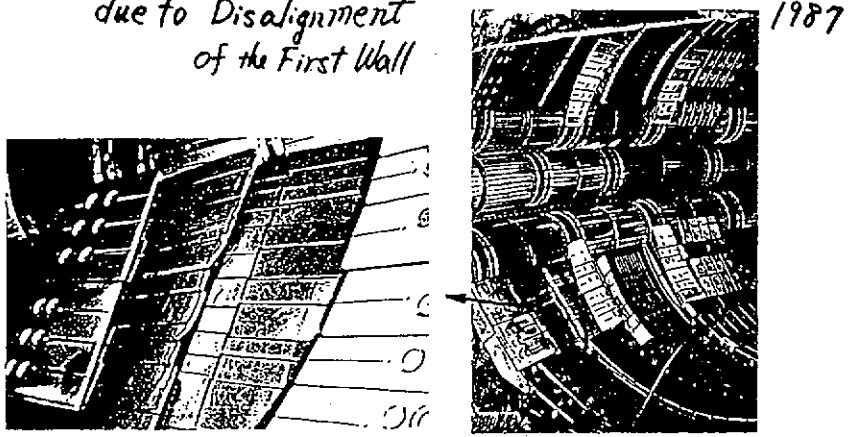

Bellows Cover Liner

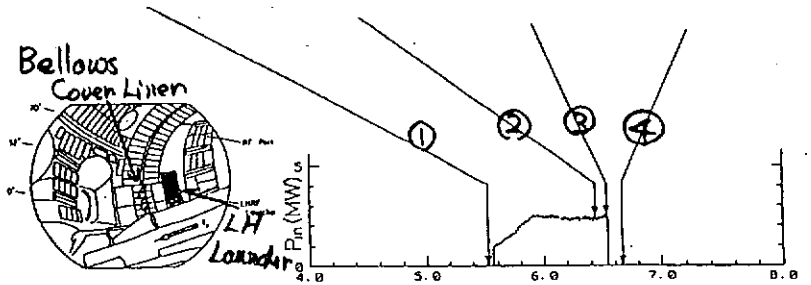

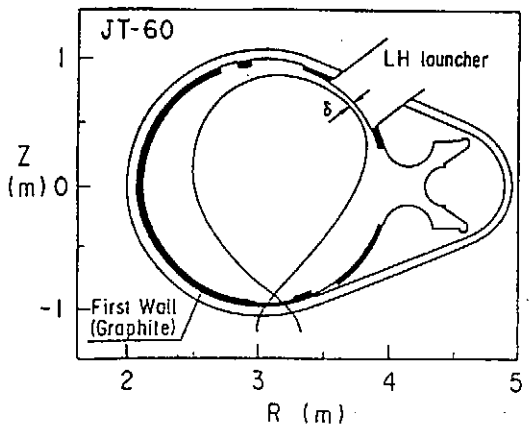

Heat Load to Launcher Head

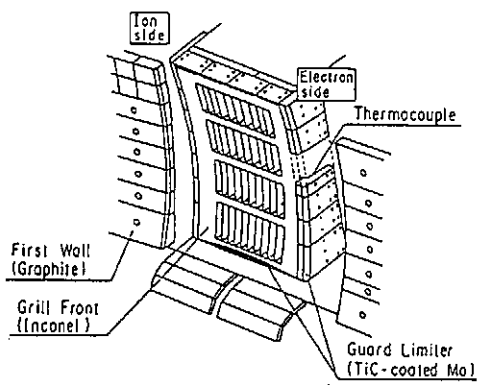

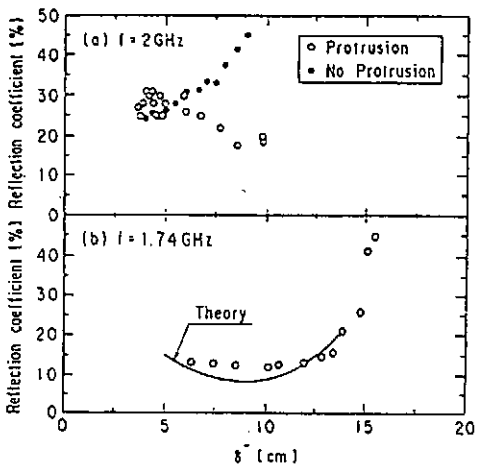

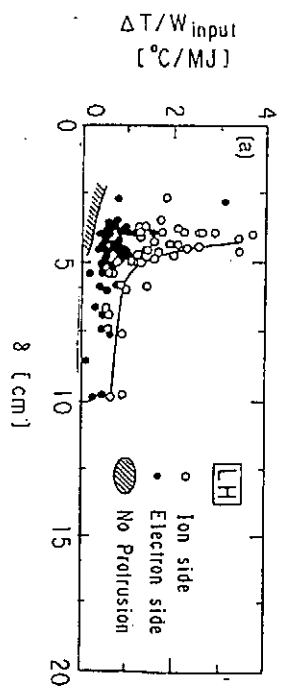

Summary 1

LHCD Program in JT-60U

-Plan-

1. 2-3 MW in 1991~92 / ~ 10 MW from 1993
2. High Performance LHCD
   $\eta_{CD} \sim 0.5 \times 10^{20} m^{-2} A/W$, CDP ~ $5 \times 10^{20} m^{-2} MA$
3. To confirm the feasibility of Reactor Application
4. LHCD Physics
   Propagation/Absorption, Profile, MHD

-Initial Results-

1. ~ 2 MA Current Drive at $n_e = 3 \times 10^{18} m^{-3}$
2. $\eta_{CD}^{exp} \propto \eta_{CD}^{th}$
3. Identification of the LHW Dispersion Relation
4. Sawtooth Suppression / j(r) Control / HX Profile / Plasma Rotation

Summary 2

Power Balance and Limitation of the LHCD Application

-Divertor Heat Load-

1. Power Balance of the LHCD Plasma is similar to that of NBI/OH Plasma (P_{RAD}, P_{DIV}, P_{ABS})
2. No Notable Difference of the Divertor Heat Load Profile $FWHM^{LHCD} \sim FWHM^{NBI}$ if $n_e > 1 \times 10^{19} m^{-3}$
3. Hot Spot occurs in cases of Disalignment of the First Wall, Error Field, especially in Limiter and/or very Low Density.
4. Direct Loss of the fast Electrons was observed in quite Low Density Plasma.

No Inherent Bad Effect due to the Presence of the Fast Electrons in Divertor Discharge with Medium or High Density.

-Heat Load to the Launcher Head-

1. Heat Load is negligible in Case of No Protrusion but Poor Coupling at $\Delta \sim 10$ cm.
2. $\Delta > 5$ cm / 2 GHz is required in Case of Protrusion but Good Coupling even at $\Delta \sim 10$ cm.
3. Need some Optimization and Further Study.

SOL/Divertor Plasma Performance during Auxiliary Heating/Current Drive in JT-60U

Michiya Shimada, Kiyoshi Itami, Nobuyuki Asakura,
Nobuyuki Hosogane, Shunji Tsuji, Katsuhiro Shimizu,
Hirotaka Kubo, Tatsuo Sugie,
Hiroo Nakamura and JT-60 team

Japan Atomic Energy Research Institute
Naka-machi, Naka-gun, Ibaraki-ken, Japan 311-01

Key questions
*SOL/Divertor Plasma Transport
*Impurity Generation/Shielding/Transport in SOL/Divertor

Contents
*Wall Conditioning(He GDC)
*Divertor Plasma Characteristics
*Particle/Power Balance (Heat Load of Div. Plate)
*Carbon Impurity Generation Mechanism
*Transport Analysis of Divertor Plasma

After GDC, Z_{eff} decreased by 1 to 2.

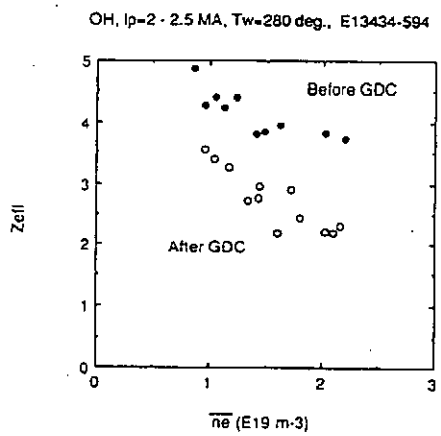

He Glow Discharge Cleaning (GDC)
Pressure ~ 0.1 Pa
Discharge Voltage ~ 400 - 500 V
Discharge Current ~ 0.8 - 1.5 A

1 hour	before First Discharge
1 hour	during Lunch Time
1 hour	during Supper Time

After GDC, n_O/n_e decreased by a factor of two to 1 %.

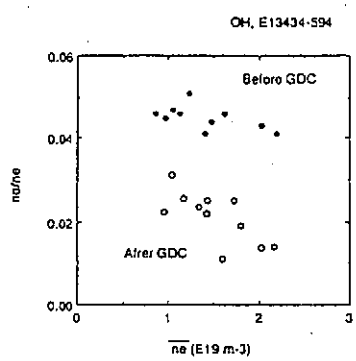

No change of n_C/n_e with GDC.

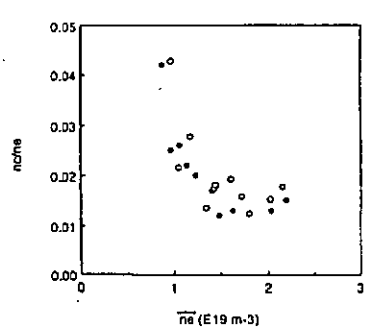

Impurity concentration was reduced in discharges with Tw = 150 °C

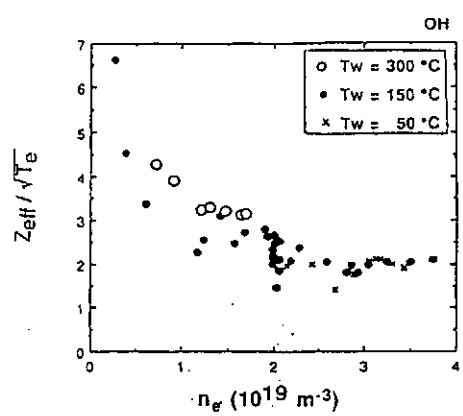

$Z_{eff}/\sqrt{T_e}$ in discharges with different temperatures of the vacuum vessel

Z_{eff} ~ 3 - 3.6 in high power NB heated discharges

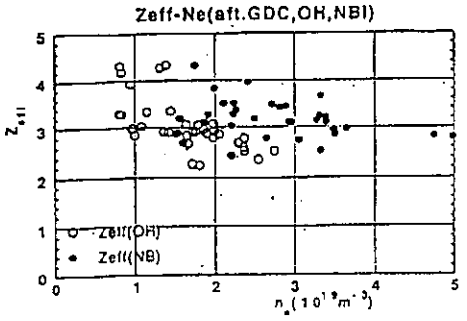

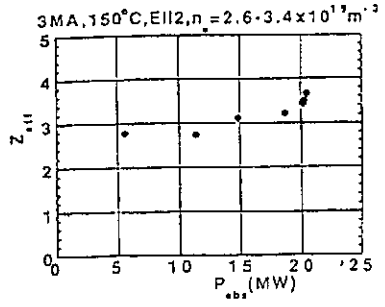

JT-60 shutdown Oct '89

Upgrade in

Volume	~50 → ~100 m^3	
I_p	3.2 →	6 MA (5MA achieved)
gas	H_2/He →	D_2
P_{NB}	26 →	40 MW (22MW achieved)

Experiments started in Apr. '91

Recent Achievements

- $I_p \leq 5$ MA
- $P_{NB} \leq 22$ MW
- $W \leq 5.1$ MJ
- neutron ~ 1.3×10^{16}/s ($Q_{DT} \sim 0.2$)
- $T_{io} \sim 20$ keV
- H-mode
- $\frac{\Delta \tau_E}{\tau_E} \lesssim 40\%$ ($\dot{W} \sim 0$), 70% ($\dot{W} \neq 0$)

SOL/Divertor Studies

Problem

ITER Steady State Scenario
→ Carbon Runaway

- Lack of Database on
  SOL/Divertor with High Power H-mode

heat flux $\Phi = \frac{P_{out}}{2\pi N R \delta_{SOL}}$ (N: #of nulls)

Equivalent $P_{out}^{JT\text{-}60U} \sim P_{out}^{ITER} \cdot \frac{N^{JT\text{-}60U}}{N^{ITER}} \cdot \frac{R^{JT\text{-}60U}}{R^{ITER}}$

$\sim 200\text{MW} \cdot \frac{1}{2} \cdot \frac{3}{6} \sim 50\text{MW}$ (40MW in '92)

- Lack of Impurity Physics in
  Generation
  Shielding
  Transport (//, ⊥)

Langmuir Probe Array on JT-60U Divertor Plates

15 channels
material: graphite, JET design
6mm(dia), 5mm SR, Protrusion: 1mm
Single probe mode
Sweeping frequency: 10 Hz
Sweeping voltage: -200 to 60 Volts

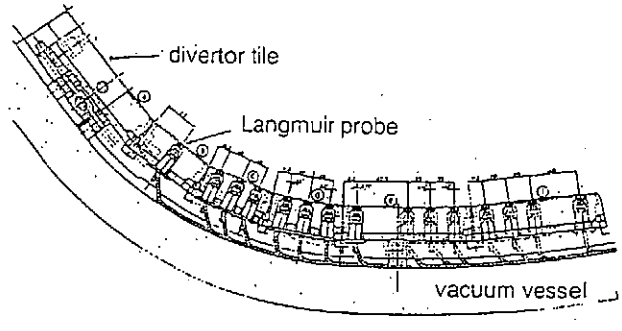

T_e and n_e Profiles on Divertor Plates (OH)

The effective area of the probe:

$$A = A_{para} \times \cos\theta + A_{perp} \times \sin\theta$$

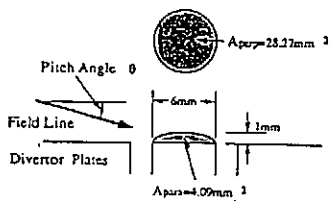

T_e on *electron side* of the divertor (outer side when the direction of the ion grad-B drift is toward the divertor) is higher than that on *ion side*.

An increase of the main plasma density from 0.6×10^{19} m^{-3} to 2.8×10^{19} m^{-3} results in reduction of the peak T_e from 80 eV to ~10eV and increase of n_e from $0.2 \times 10^{19} m^{-3}$ to $2.8 \times 10^{19} m^{-3}$.

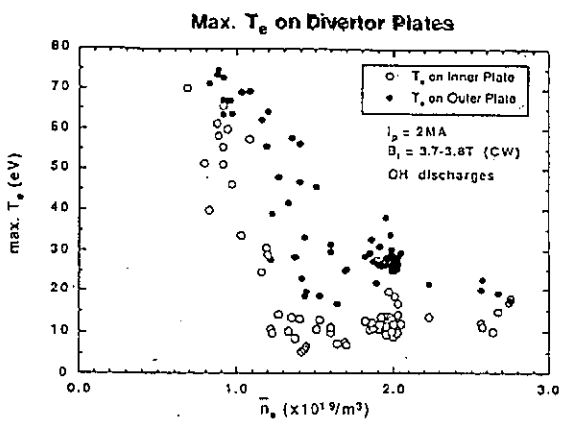

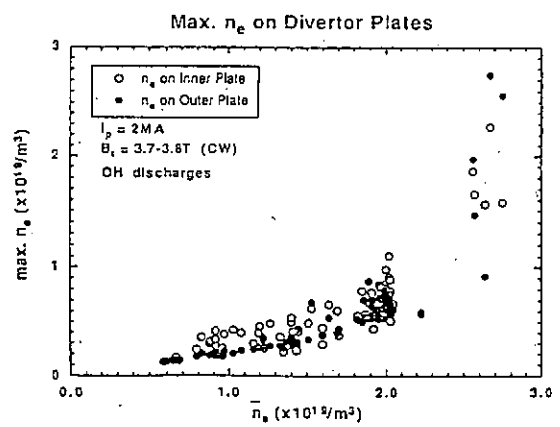

As the main plasma density increases, asymmetry in electron temperature between the inner divertor and the outer divertor increases.

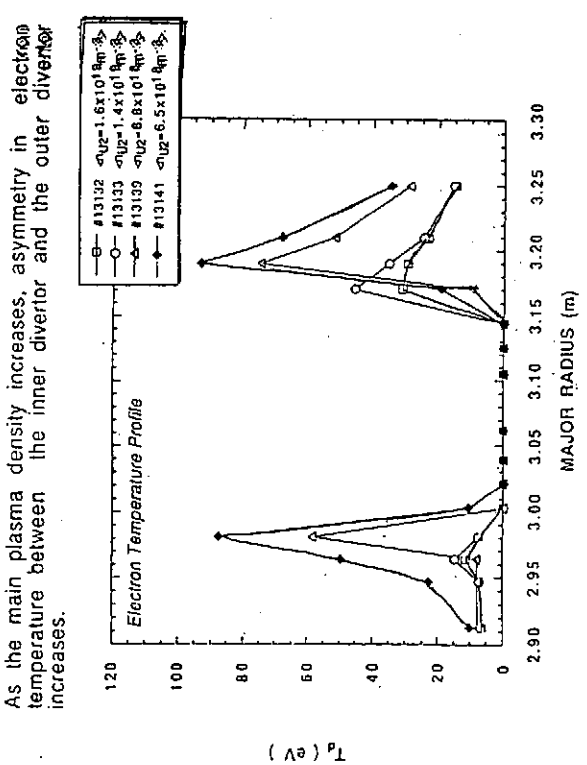

Asymmetry of the electron density is not large enough to salisfy the electron pressure balance.

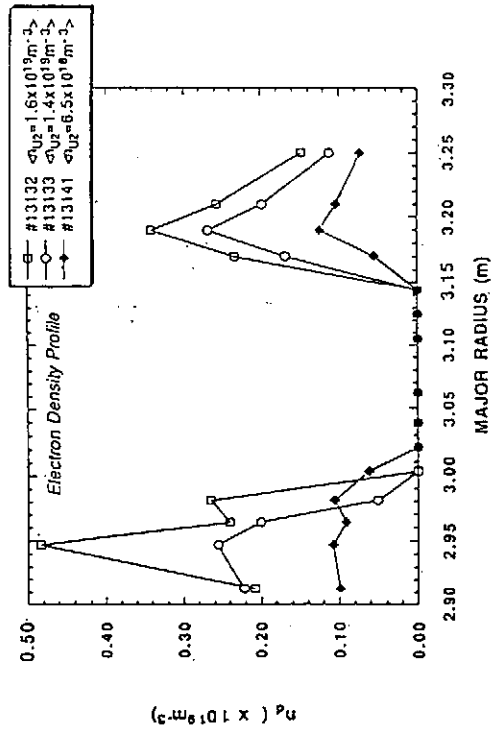

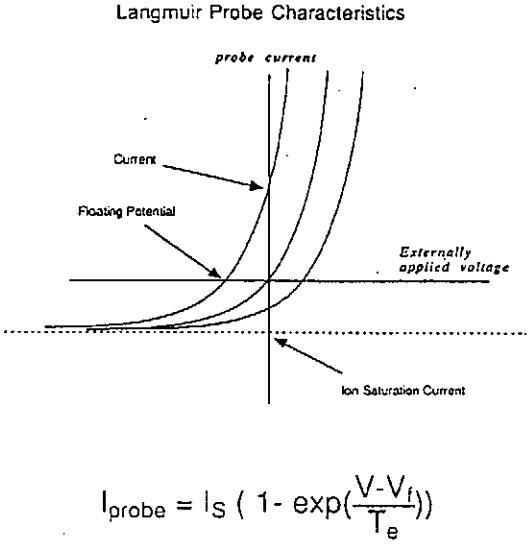

$$I_{probe} = I_S \left(1 - \exp\left(\frac{V-V_f}{T_e}\right)\right)$$

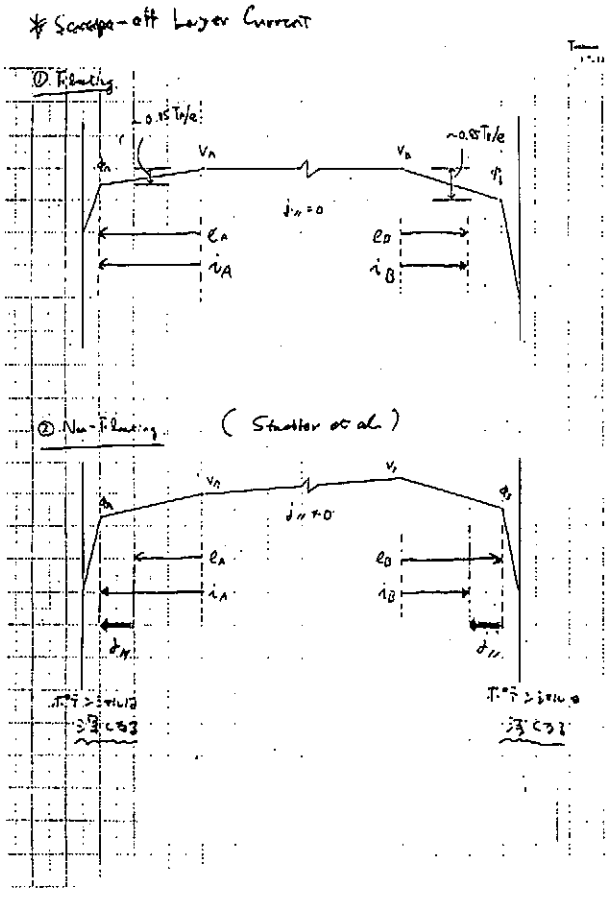

Current onto the divertor is described by scrape-off layer current in the higher density plasma.

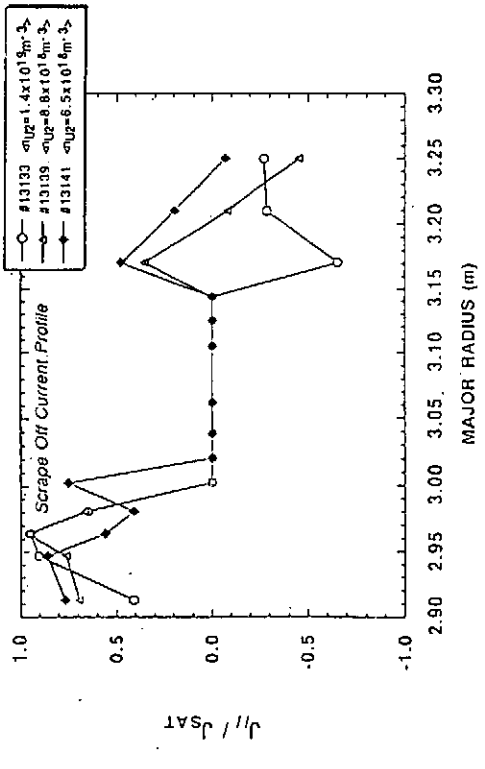

When the direction of toroidal field is reversed, the direction of divertor current as well as the electron temperature profile is reversed.

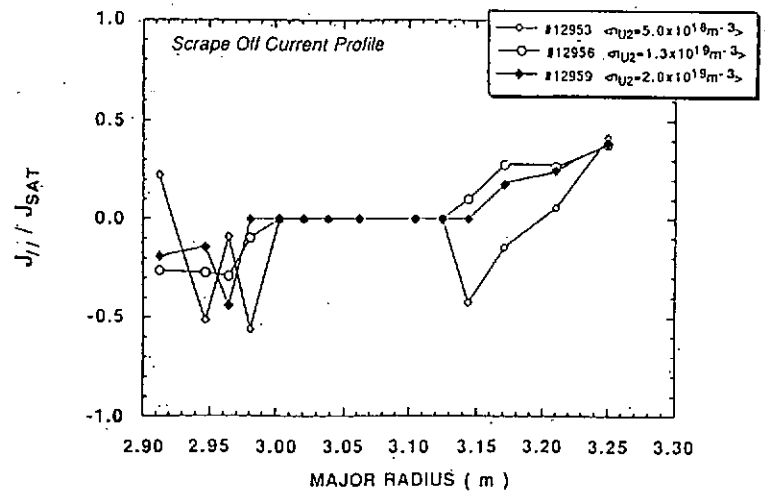

Scrape-off current is explained by a simple transport model within a factor of 2.

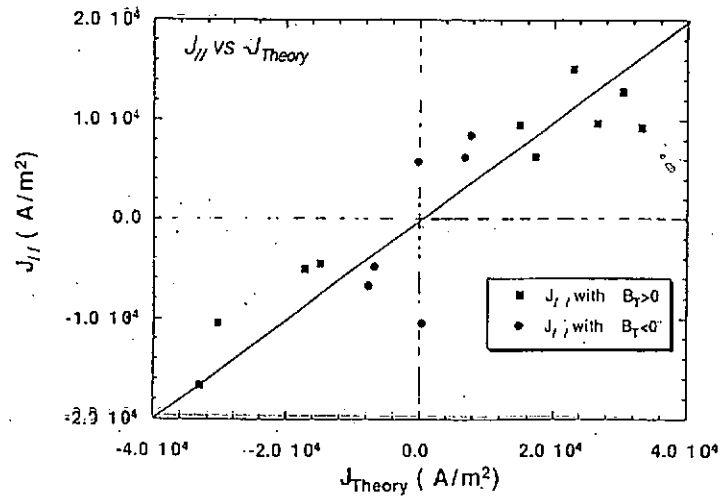

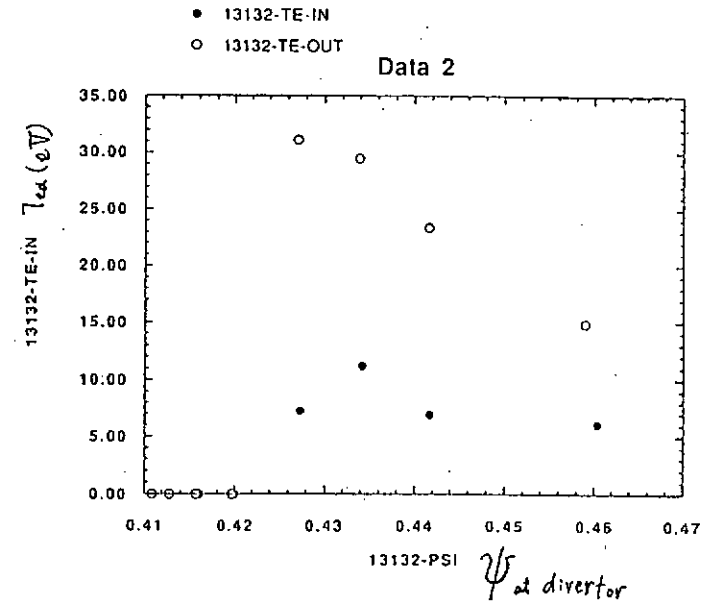

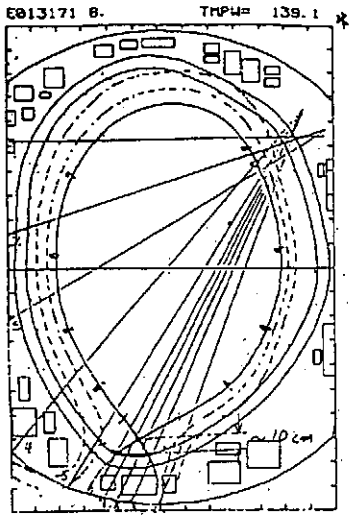

Viewing chord of Hα detector array

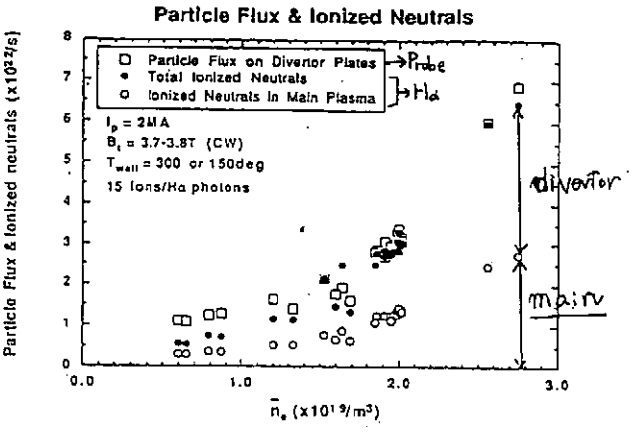

Total ionized particle flux measured by Hα detector array agrees with particle flux at the divertor measured by Langmuir probes.

$$S_I\ (\text{個/s}) = \sum_{i=1}^{40} \phi_i \cdot \varepsilon(n_e) \cdot 2\pi R \cdot \Delta\ell_i$$

ϕ_i : Hα intensity (photons/s·m²)

$\varepsilon(n_e)$: number of ionization/photon emission
= 15 /photon (at $n_e \sim 10^{19}/m^3$)
(Ref. JAERI-M 87-028)

$$\Gamma_\perp = \int S_{ion}\, dV$$

Langmuir Probe ⋮ Hα ⋮

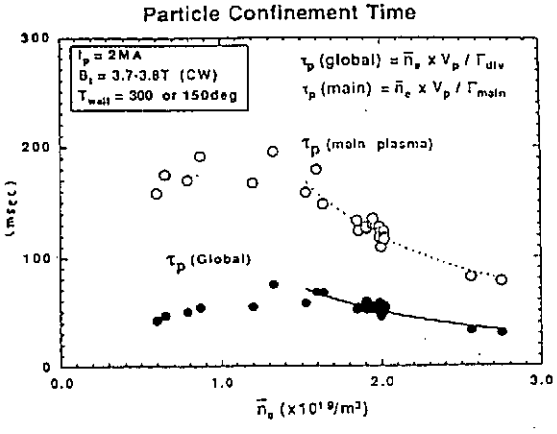

The global particle confinement time τ_p^{global} (= $n_e \times V_p / \Gamma_{div}$) has been calculated by paerticle flux.

In the density regime of $n_e > 1.3 \times 10^{19} m^{-3}$, τ_p^{global} decreases from 200ms to 80 ms, proportional to n_e^{-1}

In high density regime, the flux amplification factor, defined by

$$M = 1 + \frac{\Gamma_{ion}}{\Gamma_0} = \frac{\Gamma_{ion}+\Gamma_0}{\Gamma_0} \approx \frac{\Gamma_{div}}{\Gamma_{main}} = \frac{\tau_{main}}{\tau_{global}},$$

ranges from 2.5 to 3.0.

Preliminary

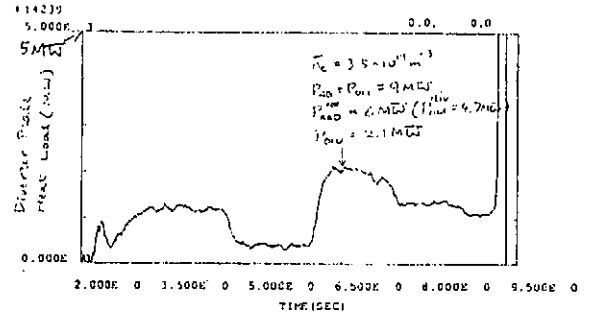

Preliminary

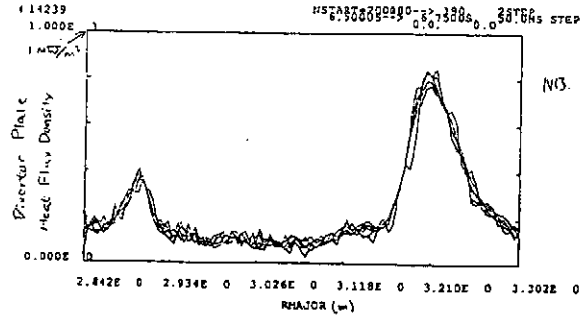

Preliminary

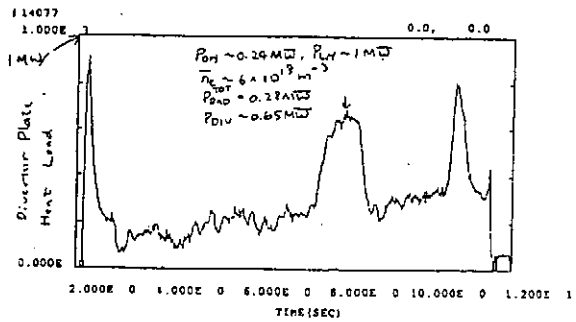

Preliminary

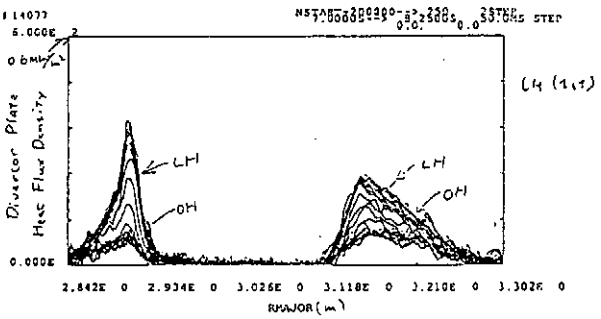

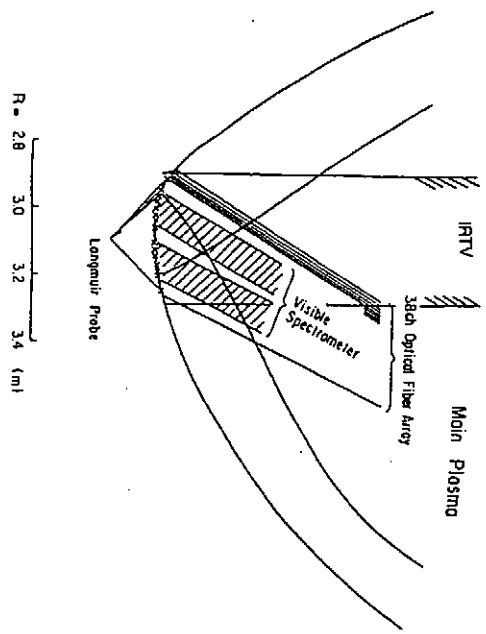

Investigation of carbon production process

Observation

Spectrometer
- C II 3s ^{2}S - 3p ^{2}D → Γ_C (observation)
- Dα
- O II 3s ^{2}P - 3p ^{2}P

Langmuir Probe
- T_e^{Div}
- n_e^{Div}

(IRTV)
- T_w

Sputtering Yield
- O (Chemical)
- C (Self-sputtering)
- D (Physical)
- (Chemical)

→ Γ_C (calculation)

Carbon production is explained by sputtering with oxygen, deuterium, and carbon (self-sputtering)

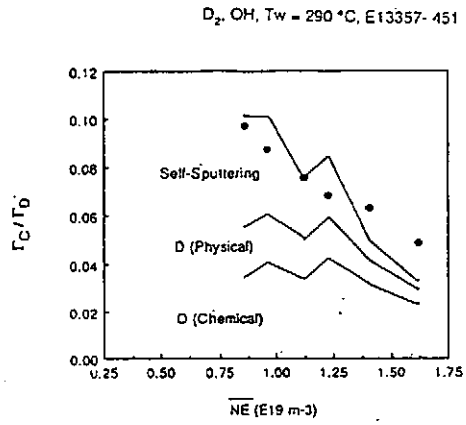

Good Agreement between Calculation and Observation for Carbon Production

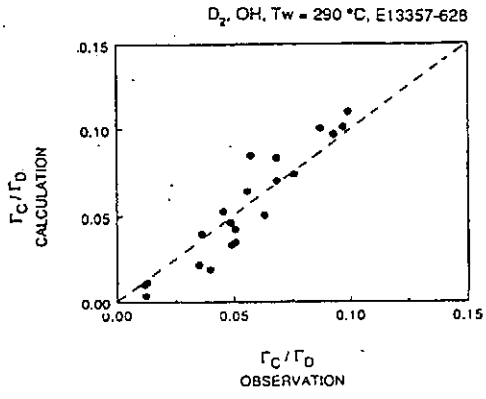

* Divertor Simulation
Simple Divertor Model

Fluid equations

- Ti = Te
- the cross field transport effect is negligible
- the electron heat conduction is the dominant loss in the energy transport

$$\nabla_{//}(nV_{//}) = S_n$$
$$\nabla_{//}(nm_iV_{//}^2) + \nabla_{//}(2nT) = S_P$$
$$\nabla_{//}q_{//} = \nabla_{//}(-\kappa_{//}\nabla_{//}T) = S_E$$
$$\kappa_{//}\ [W(eV)^{-1}m^{-1}] = \kappa_0 T^{5/2}\ ,\quad \kappa_0 = 3.07\times10^4 / \ln\Lambda$$

Boundary conditions at the divertor plate

$$(n_d, T_d)\ ,\ q_{//}(\xi_d) = \gamma n_d T_d V_{//d}\ ,\ V_{//d} = \sqrt{2T_d/m_i}$$

source terms

$S_n = n_e n_0 \langle\sigma V\rangle_I$

$S_P = 0$

$S_E = -E_{ion} S_n$

$$\int -S_E\, dV \doteq 0.2\, Q_{th}$$

The outside divertor plasma together with the scrape off layer is modeled and is divided into the 8 flux tubes.

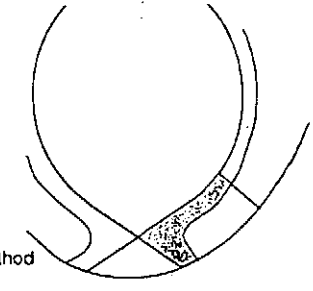

neutral transport model

- 2D MONTE-CARLO
- MHD-equilibrium
- wall reflection model
- path length estimator method

Neutral Transport Model

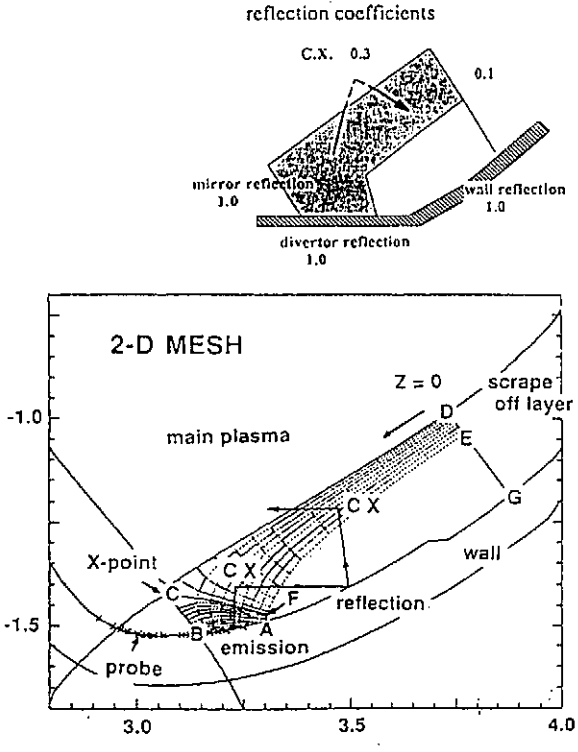

Comparison of H_α intensity with exp. data

Shot : E12953

(I_p = 2 MA, B_T = 3.5 T, $\bar{n}_e = 0.8\times10^{19}$ m^{-3})

$n_{ed} = 0.1\times10^{19}$ m^{-3}, T_{ed} = 84 eV

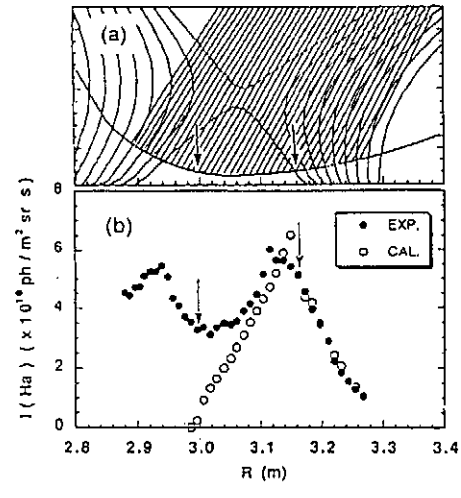

Fig. 8 (a) H_α monitor viewing the divertor plate consists of 38 channels.
(b) Calculated profile of H_α radiation intensity for the low temperature case. The measurement data is also displayed by the closed symbols.

Estimation of cross field heat diffusivity

$\chi_\perp$ can be evaluated from $T^{up}(x)$, $q_{//}^{up}(x)$ at the upstream of the divertor plasma.

Total heat flux $$Q_\perp(0)=\int q_{//}^{up}(x)\,dA_{//}$$

heat flux from the flux tube-1 to the tube-2

$$Q_\perp(1)=Q_\perp(0)-q_{//}(1)A_{//}(1)$$

heat diffusivity

$$\chi_\perp(1)=\frac{Q_\perp(1)}{S\cdot n\cdot(T(1)-T(2))/\Delta X}$$

$\chi_\perp = 3\sim 3.5\ m^2/s$

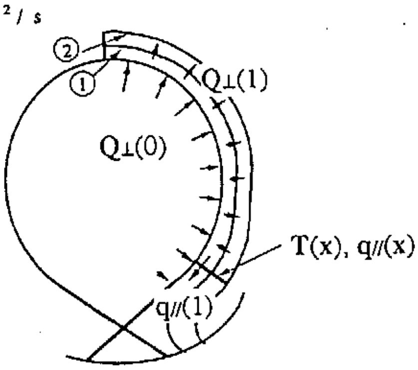

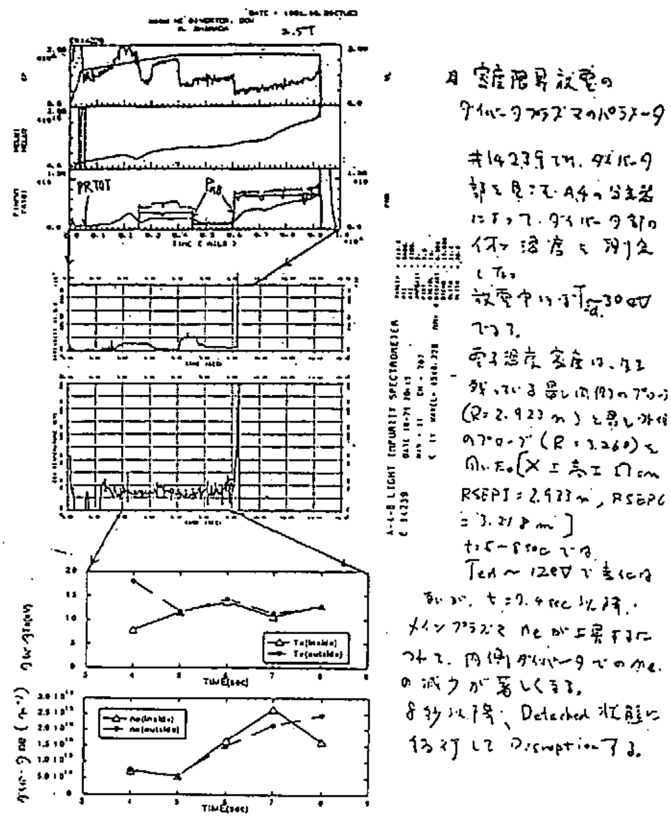

SUMMARY

Te and ne Profiles on Divertor Plates
As the electron density of the main plasma increases, asymmetries in electron temperature and heat flux become large. These asymmetries in temperature, density and current profiles are reversed when the toroidal field is reversed.

Scrape-off Layer Current
The parallel current along the magnetic field in the scrape-off layer, of which density is up to $2\times10^4 A/m^2$, is measured. the experimental results is explained by a simple transport model within a factor of two.

Particle Recycling
Global particle recycling measured by Hα detectors agrees with the particle flux at the divertor.

Divertor Simulation
Simple divertor code is being developed to model divertor plasma. This code successfully reproduce the particle recycling around the divertor in OH plasmas.

Summary

By He glow discharge cleaning and lowering the temperature of the vacuum vessel, impurity concentration was reduced.

Carbon production was explained by sputtering with oxygen (chemical sputtering), deuterium (physical sputtering), and carbon (self-sputtering). The chemical sputtering with deuterium is not important.

Nov. 20. 1991
NIFS Japan

Simulation Study of SOL Plasma Transport and the Scaling Laws.

presented at US-Japan workshop on
"RF heating and current drive in confinements systems tokamaks"

by SANAE-I. ITOH

In colaboration with
Dr. N. UEDA & Dr. K. ITOH

Acknowledgements:
Drs. A. Fukuyama, M. Sugihara, T. Takizuka
JFT-2M gr.

Achievement and Targets

Long (Steady) Power Handling

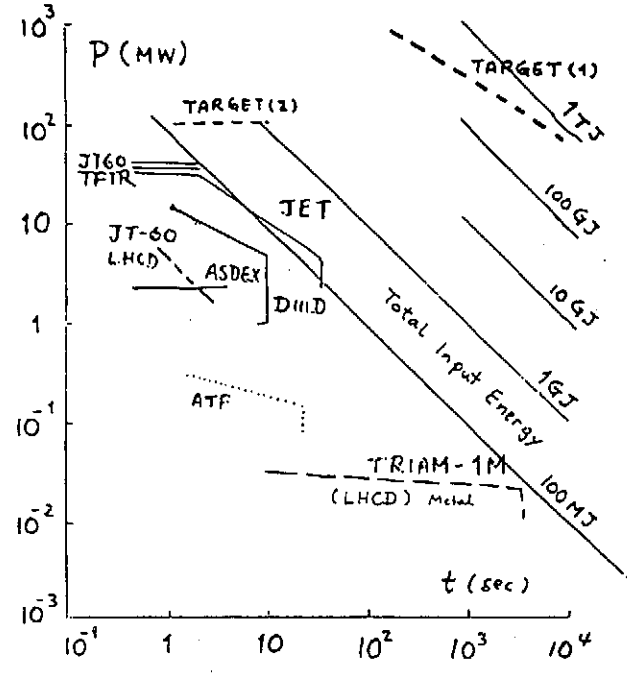

Outline

- Numerical analysis on SOL plasma and divertor plasma in tokamak
  by 2D transport (time-dependent) code
  Unified Edge-Divertor Analysis code
  (UEDA code)
  - Model, Basic eq.
  - Application to JFT-2M
  - Scaling Laws of $n_{b.d.}$; $T_{b.d}$ on Γ, Q.
- Divertor condition (Dense-Cold) is discussed using an empirical τ_p scaling (on JT60/60U)
- Discussion and Perspective for Future

Model

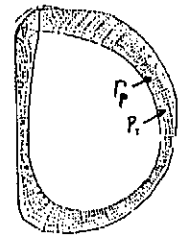

- Axisymmetric Divertor Configuration
- Given sources from core plasma
  (Γ_p, P_T)
- Plasma
  - Multiple fluid model (i, e, α···)
  - Transport coefficient

$$\vec{q} = -K_\perp \nabla_\perp T - K_\parallel \nabla_\parallel T + K_\wedge \hat{b} \times \nabla T$$

Anomalous Classical

$$K_\perp = 2n D_B$$
$$D_\perp = \tfrac{1}{2} D_B$$

- Boundary condition on divertor

$$V_\parallel = C_s$$
$$K_\parallel \nabla_\parallel T_e = C_e n T V_\parallel \quad : C_e = 1.8$$
$$\nabla_\theta T_i = 0$$

- Neutral Particles
  Monte Carlo code
  (DEGAS)

・time dependent

Fluid Equations ・PIC

$$\frac{\partial n_i}{\partial t} + \nabla\cdot(n_i\vec{v}) = S, \quad \cdots \text{連続の式 } (n_e\cdot n_i)$$

$$\rho_i\left(\frac{\partial}{\partial t} + \vec{v}\cdot\nabla\right)v_{//} = -\frac{B\theta}{Bh_z}\frac{\partial p}{\partial z} - Sv_{//}, \quad // \text{ 運動方程式}$$

$$v_\psi = -\frac{1}{h_\psi}\frac{D}{n_i}\frac{\partial n_i}{\partial\psi} \quad \perp \text{ Diffusion}$$

$$\rho_e\left(\frac{\partial}{\partial t} + \vec{v}\cdot\nabla\right)\left(\frac{3kT_e}{2m_e} + \frac{1}{2}\vec{v}\cdot\vec{v}\right) = -\nabla\cdot(p_e\vec{v}) + \vec{v}\cdot\nabla p_e - \nabla\cdot\vec{q}^e - E^eS - Q_{ei} - \vec{\gamma}_{rad},$$

エネルギー輸送 電子

$$\rho_i\left(\frac{\partial}{\partial t} + \vec{v}\cdot\nabla\right)\left(\frac{3kT_i}{2m_i} + \frac{1}{2}\vec{v}\cdot\vec{v}\right) = -\nabla\cdot(p_i\vec{v}) - \vec{v}\cdot\nabla p_e - \nabla\cdot\vec{q}^i - E^iS + Q_{ei} - Q_{cx},$$

エネルギー輸送 ion

$$\vec{q}^i = -\kappa^i_{//}\nabla_{//}T_i - \kappa^i_\psi\nabla_\psi T_i + \frac{5}{2}\cdot\frac{n_iT_i}{|\Omega_i|m_i}(\vec{b}\times\nabla T_i),$$

$$\vec{q}^e = -\kappa^e_{//}\nabla_{//}T_e - \kappa^e_\psi\nabla_\psi T_e - \frac{5}{2}\frac{n_eT_e}{\Omega_e m_e}(\vec{b}\times\nabla T_e).$$

} heat fluxes

S : volume source (ion) (n_e)

Qei : energy exchange e − i

Qcx : charge exchange loss (n_o)

Qrad : radiation loss (Impurity ...)

Degas

// モデル (Assumption) //

・$D_\perp$ ($\frac{1}{2}D_B$), $\chi_\perp$ ($2D_B$ $\chi = 2nD_B$)

・$\chi_{//}$ classical

・e − i charge neutrality.

..... Thermo electric field など .....

// 境界条件 //

プラズマ境界 ・Γ_T, Q_T, given

.... nTV/τ_E, nV/τ_p assumed.

シースパラメータ プレート

$v_o = \sqrt{(T_e+T_i)/\rho_s}$ Bohm sheath criterion

$\nabla T_{e//} = -(_e n_e v_{//} T_e/\kappa^e_{//}$

2次電子放出なし

$\nabla T_{i\theta} = 0$

Wall 壁 $\partial T/\partial\psi = \partial P/\partial\psi = 0$.

Scaling Study JFT-2M (B = 1.4T)

ccw

Fig. 2

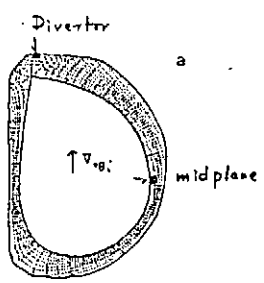

Simulation range

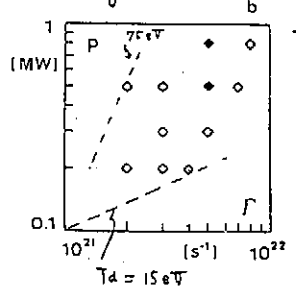

Td(Peak)

$\simeq 30\,P/\Gamma$(eV)

Td = 15eV

JFT-2M : Case Dense but not cold

$P_T = 0.8$ MW, $\Gamma_p \simeq 5\times10^{21}/s$ ($\bar{n}_e = 3\times10^{19}/m^3$, $\tau_p = 25$ms)

Fig. 3

b

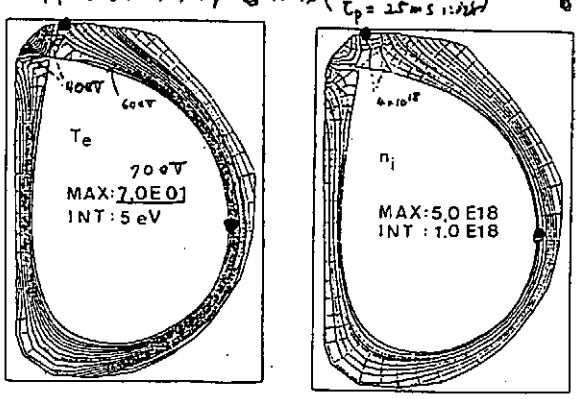

c

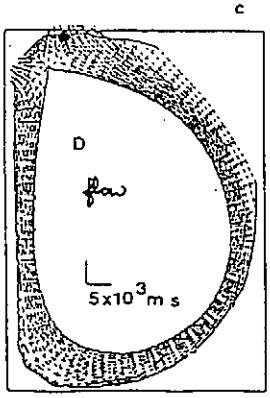

d

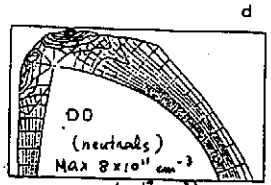

e

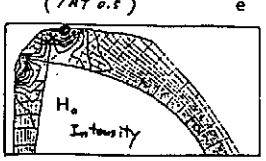

Example: JFT-2M $P_T = 0.5$MW, $\Gamma_p = 5\times10^{21}$/s ($n_e = 5\times10^{}$, $\tau_p =$)

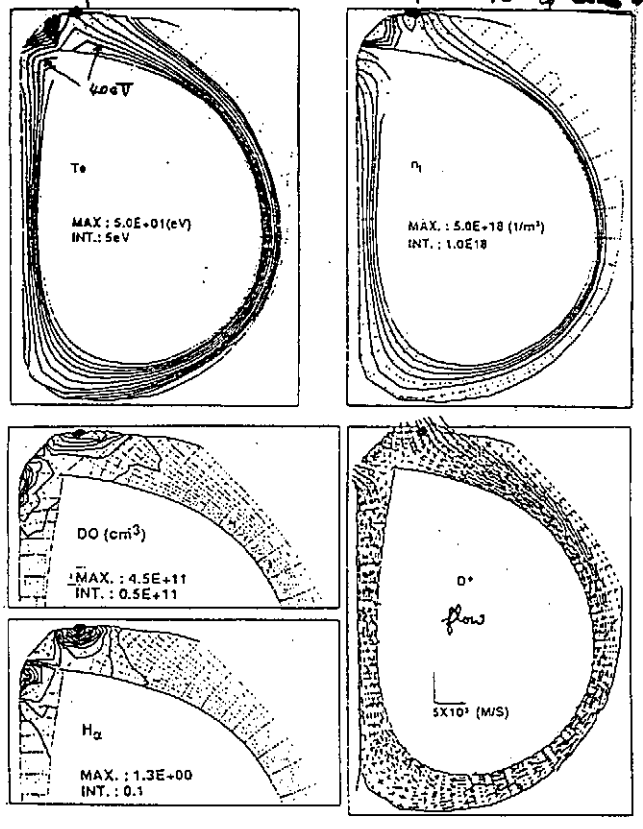

Fig. 2

midplane

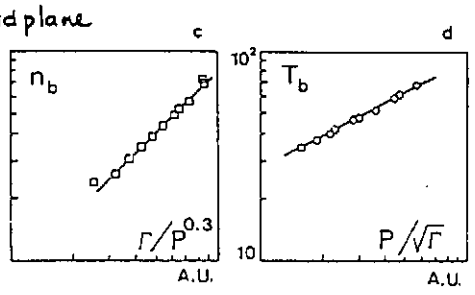

diverter

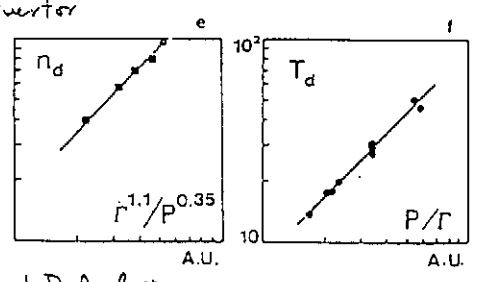

c.f. 1-D Analysis

Heat and Density channel widths

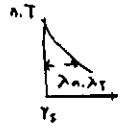

midplane

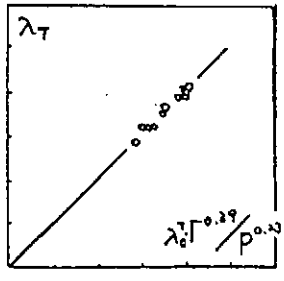

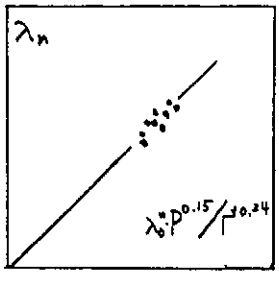

Scaling Laws:

Boundary.

$n_b \propto \Gamma_{out}^{1} P_{out}^{-0.3}$ $\quad T_{b.e} \propto \Gamma_{out}^{-0.45} P_{out}^{0.5}$

$\lambda_n = d\,\Gamma_{out}^{-0.44} P_{out}^{0.15}$ $\quad \lambda_T \propto d\,\Gamma_{out}^{0.4} P_{out}^{-0.13}$

Diverter

$n_d \propto \Gamma_{out}^{1.1} P_{out}^{-0.35}$ $\quad T_{d.e} \propto \Gamma_{out}^{-1} P_{out}^{1}$

$n_d \propto (n_b)^{1.1}$ ……(may be $\propto \bar{n}$)

where

$d = 1.8$ cm (JFT-2M for $\Gamma_{out} = 10^{21}$/s, $P_{out} = 100$kW)

$T_{d.e}$ (peak)

$= 30\, P_{out}(\text{MW})/\Gamma_{out}(10^{22}/\text{s})$

Cold Divertor Condition

$$T_d = \frac{P_{out} - P_{rad}}{\gamma G \Gamma_{out}}$$

γ : transmission coeff.

$G \simeq \frac{1}{1-g}$: multiplication factor

$1-g$: impinging neutrals

$$\left(\Gamma_{out} = \frac{n \nabla_p}{\tau_p} \right)$$

$$T_d = \frac{P_{out}\, \tau_p}{\gamma G\, n \nabla_p}$$

$$\tau_p = 0.05\, P^{-0.5} n_e^{-1} I_p^{(0)} B^{\delta} a$$

[JT-60 τ_p scaling — Tsuji et al. ; This conf. — Shimada et al.]

$$T_d = \frac{2.5\sqrt{P}}{n^2 kaR} \left(\frac{B}{B_{0.5}}\right)^{\delta} \quad (\delta > 0) \quad < 10\,eV \ (:\text{goal})$$

$$\bar{n} > n_c \left[P_{out} \right]$$

$I_p \left(\tau_p \to h_p \tau_p \right) \Rightarrow n_c \to \sqrt{h_p}\, n_c$

(h_p : enhancement factor of τ_p)

Divertor Heat Load

$$\lambda_p \propto \frac{\Gamma_{out}^{0.4}}{P_{out}^{0.33}}$$: temperature fall-off length (characteristic heat channel width)

$$\Gamma_{out} = \frac{n \nabla_p}{\tau_p}$$

$$\tau_p \propto P^{-0.5} \bar{n}^{-1}$$

$$\lambda_p \propto \left(\frac{n \nabla_p}{P_{out}^{-0.5} \bar{n}^{-1}} \right)^{0.4} P_{out}^{-0.33}$$

$$\simeq n^{0.8} \nabla_p^{0.4}$$

Heat Load $\propto P_{out(tot)} / \lambda_n$

$$\propto P \cdot n^{-0.8}$$

Divertor Temperature

$$\int_0^{\tau} \text{heat load}\, dt$$: Bloom.

REACTOR-grade Plasma case study

〈 H-mode-like 〉

FER [a=1.2 b=2.15 / R=4.6 B=4.6 / I_p = 5.9 MA]

P = 60 MW

$\Gamma = 1.2 \times 10^{23}$/s, Γ_α / Γ_i : 6%

IAEA Nice 1989

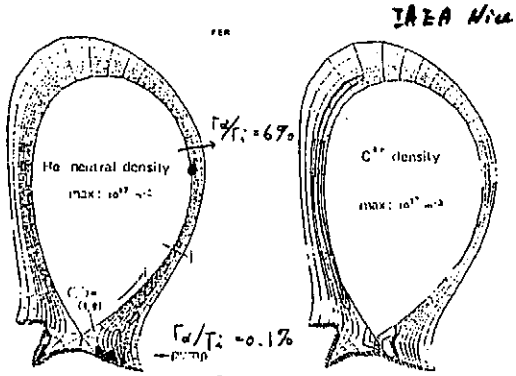

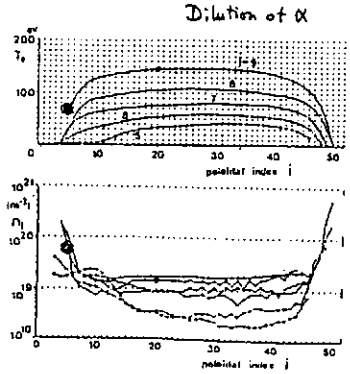

$\tau_E = 2.7\, \tau_{L(H)}$

$\tau_p \simeq 20\, \tau_{pL}$ (JT-60)

Constraints for Core-Plasma Performance

— ダイバータプラズマへの影響を中心に —

S.-I. Itoh, et al., Fusion Tech. 16 ('89) 346.

(1) β-value limit

$$\beta < \beta_c(\%) = g \frac{I_p}{aB_t}, \quad g = 2.7$$

(2) q-value limit

$$q_{95X} \geq 3$$

(3) Density limit

$$\bar{n}_e < \bar{n}_c = 0.4 \frac{I_p}{a^2} (0.1P)^{\alpha}, \quad \alpha = 0.25$$

(4) Current-drive efficiency

$$I_p < \frac{CT}{nR} P_{in}, \quad C = 0.026$$

(5) Cold divertor plasma

$$T_{div} < 10eV, \quad T_{div}(eV) = \frac{2.5\sqrt{P}}{n^2 aR}$$

(6) Ash exhaust (preliminary)

$$\frac{n_\alpha V}{\tau_p} > 10^{24} s_0$$

(9) Neutron wall loading

$$P_N < 1 \sim 1.5\ MW/m^2$$

Scaling laws used for extrapolation

(7) Energy confinement scalings (3 kinds) τ_E

Power law 1 (PK-law) 87-88

$$\tau_E^P = 0.103\, H^{0.5}\, R^{1.39}\, I_p^{0.81}\, \bar{n}^{0.41}\, B^{0.15}\, a^{0.58}\, R^{0.03}\, P^{-0.5}$$

Power law 2 (K-G law) 84-5

$$\tau_E^{KG} = 0.045\, H^{0.5}\, R^{1.39}\, I_p^{1.15}\, \bar{n}^{0.26}\, B^{0.08}\, a^{0.43}\, R^{0.03}\, P^{-0.5}$$

Offset-linear law (OT law) 88

$$\tau_E^O = C_1 H^{0.5} R a^2 + C_0 (H/2)^{0.5} I_p^{1.5} a^{0.5} R^{1.5} P^{-1}$$

$C_1 = 0.085, \quad C_0 = 0.038.$

(8) Particle confinement scaling τ_p

Extended JT-60 scaling

$$\tau_p = 0.03\, \bar{n}^{-1} (a/4.5)^{\delta}\, a\, P^{-0.5}, \quad \delta \approx 1.5$$

Offset-linear law

Steady-state operation regime 20MA

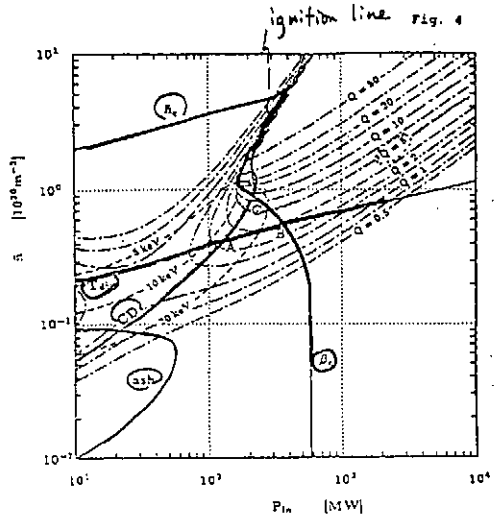

CD(Yn) is a next, good confinement needed.

Fig.4
Steady-state operation regime for standard parameters, I_p = 20 MA, and offset-linear (OT) law. Equi-Q lines are drawn as Q = 0.5, 0.7, 1, 1.5, 2, 3, 5, 7, 10, 15, 20, 30, ∞. At the point A, P_{ain} = 130 MW and Q = 2.3. Q_{max} = 8.5 is realized with P_{in} = 215 MW at the point C.

(ref. BS) 11.5

Operation Regime (ref. 13) predicted by Power law

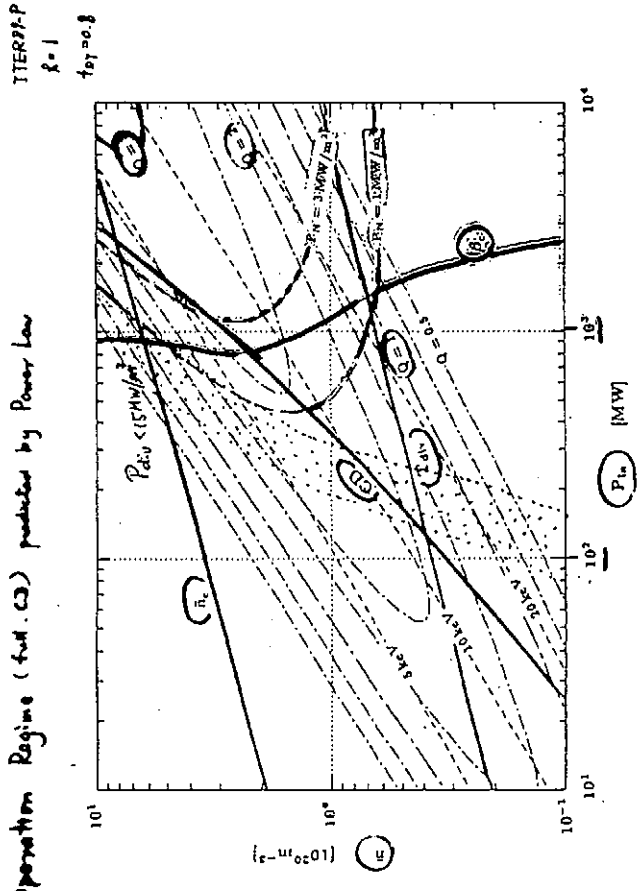

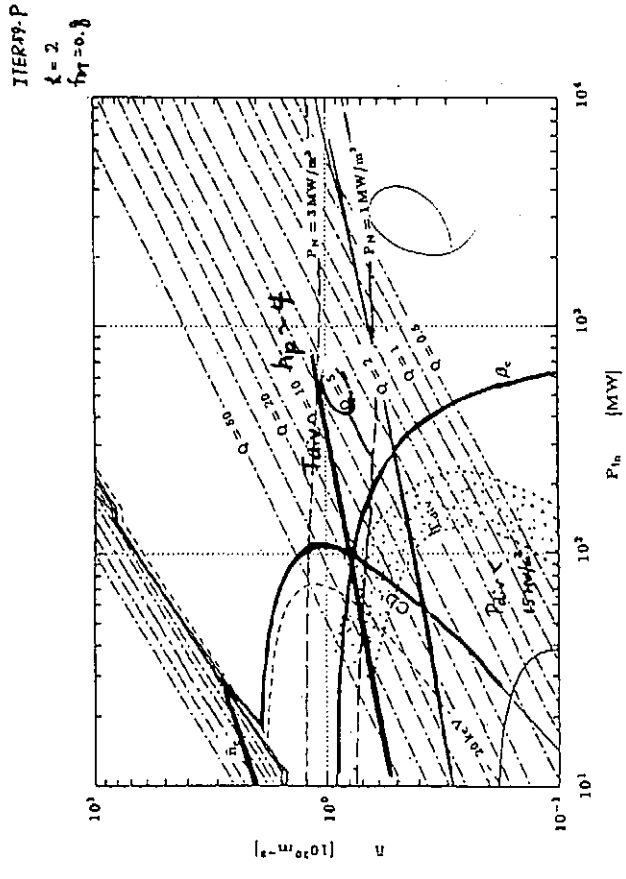

ANOMALOUS TRANSPORTS CORRELATED WITH THE HELICITY TRANSPORT

Z. Yoshida
University of Tokyo

in collaboration with
A. Hasegawa
Osaka University
and
H.R. Strauss, E. Hameiri
Courant Institute of Mathematical Sciences

- Helicity Transport = Transport of $j_{//,0}$
- Helicity Flux through a Magnetic Surface
  → correlated phenomena (anomalous transports)
- Spontaneous Fluctuations Resulting a Helicity Flux
  → electron heat flux, particle flux, resistance anomaly

HELICITY BALANCE EQUATION

$$\frac{d}{dt}\int_\Omega A\cdot B\,dv$$

$$= -\int_{\partial\Omega} n\{(-\partial_t A)\times A + 2B\varphi\}ds - 2\int_\Omega E\cdot B\,dv$$

F_h : helicity flux $\quad \sim \eta j\cdot B$ + (wave-particle interactions) ⇓ dissipation of $j_{//,0}$

Ω : arbitrary volume in plasma

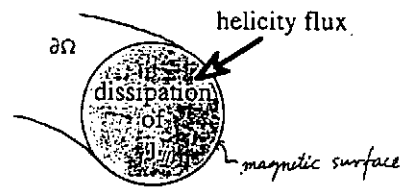

HEAT AND PARTICLE TRANSPORTS CORRELATED WITH HELICITY TRANSPORT

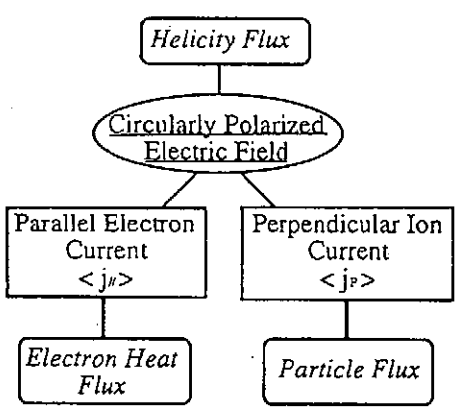

SLAB PLASMA MODEL

geometry

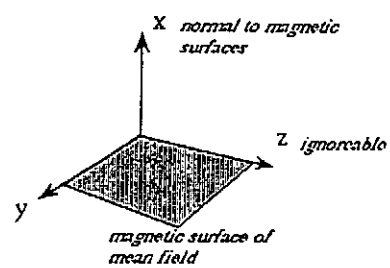

perturbations

$A_1 = \nabla u \times \nabla z + \psi\nabla z \quad B_1 = \nabla\psi \times \nabla z - (\Delta u)\nabla z$

Coulomb gauge, $\varphi = 0$ at $x = 0$.

assumption

- k is almost parallel to the magnetic surface (local modes).

HELICITY FLUX, PARALLEL CURRENT AND POLARIZATION CURRENT

helicity flux

$$\langle F_h \rangle_x \equiv \langle -(\partial A_1)\times A_1 \cdot \nabla x \rangle = \langle \psi(\partial_x u) - (\partial_x \psi)(\partial_z u) \rangle = \frac{i\omega}{4} A_\perp \times A_\perp^* \cdot \nabla x + \text{c.c.}$$

nonlinear parallel current

$$\langle j_{//} \rangle_x \equiv \langle (j \cdot b) b \cdot \nabla x \rangle$$

$$= \frac{(b_0 \cdot \nabla y)}{\mu_0 B_0} \langle (\partial_z \Delta u)(\partial_y \psi) \rangle - \frac{(j_0 \cdot \nabla z)}{B_0^2} \langle (\Delta u)(\partial_y \psi) \rangle$$

$$= \frac{1}{\mu_0 B_0} \langle (\partial_z \Delta u)(ik_{//}\psi) \rangle - \frac{j_{//0}}{B_0^2} \langle (\Delta u)(ik_\perp \psi) \rangle$$

nonlinear polarization current

$$\langle j_P \rangle_x = \frac{\rho_m}{B_0^2} \langle (v_1 \cdot \nabla) E_1 \rangle \cdot \nabla x$$

$$= -\frac{\rho_m (b_0 \cdot \nabla y)}{B_0^2} \langle (\partial_{t,x,y} u)(\partial_t \psi) + (\partial_x^2 \varphi_1)(\partial_t \psi) \rangle$$

HEAT AND PARTICLE FLUXES CORRELATED WITH HELICITY FLUX

(Z. Y. & A. Hasegawa, IAEA 1990, D-I-6)

- Isotropic perturbation in the perpendicular direction.
- Finite average in $k_{//}$.

0. $< j_{//} >_x$ and $< F_h >_x$ are correlated by

$$\langle j_{//} \rangle_x = \frac{-(k_{//}/\omega)k^2}{2\mu_0 B_0} \langle F_h \rangle_x$$

1. $< j_{//} >_x$ gives the frictional electron heat flux:

$$\langle q_e^s \rangle_x \equiv \langle q_e^s \cdot \nabla x \rangle = C_z T_e n_e \langle j_{//} \rangle_x / (-en_e)$$

$$= \frac{C_z T_e (k_{//}/\omega)k^2}{2\mu_0 B_0 e} \langle F_h \rangle_x .$$

where $C_z = 0.71$ if $Z=1$.

2. $< j_{//} >_x$ and $< j_P >_x$ give particle flux:

$$\langle \Gamma \rangle_x = -\langle j_{//} \rangle_x / e = \langle j_P \rangle_x / e = \frac{(k_{//}/\omega)k^2}{2\mu_0 B_0 e} \langle F_h \rangle_x .$$

Here ambipolar condition should be satisfied:

$$\partial_x^2 \varphi_1 = [1 - (v_A k/\omega)^2] \partial_{t,x,y} u .$$

SPONTANEOUS FLUCTUATIONS AND HYPER RESISTIVITY

(Z. Y. & A. Hasegawa, Phys. Fluids B, 1991)

The tearing-mode turbulence results in the hyper-resistivity, which parallels the divergence of the helicity flux caused by turbulent reconnections.

We write $E_{1//} = \eta j_{//} - D\Delta j_{//}$

$$B = \nabla\psi \times \nabla z + B_z \nabla z$$
$$v_\perp = \nabla\phi \times \nabla z + v_z \nabla z$$

Then

$$\langle F_h \rangle_x = -2B_{z0} \langle \phi_1 \cdot B_{x,1} \rangle = -2B_{z0} \langle \phi_1 \cdot \partial_y \psi_1 \rangle$$

$$= -\frac{2B_{z0}}{\mu_0 j_{//0}} \left\langle \frac{\gamma}{k_x} \psi_1^2 \right\rangle$$

$$= -B_{z0} D_0 \nabla j_{//0}$$

$$D_0 = \frac{1}{2} \sum_k \frac{\gamma_k}{(\partial_x k_{//})^2} |B_{x,k}|^2 \ln \left(\frac{x_k^2}{(x - x_k)^2 + \gamma_k^2 / (\partial_x k_{//})^2} \right) .$$

NONLINEAR PARALLEL CURRENT FOR FLUCTUATIONS WITH $k_{//} \approx 0$

When there is a gradient of $j_{//0}$, a spontaneous helicity flux results from the tearing mode turbulence, which yields correlated anomalous transports. We obtain

$$\langle j_{//} \rangle_x = \frac{(j_0 \cdot \nabla z)}{B_0^2} \langle (B_{x,1})(\partial_y \psi_1) \rangle = \frac{j_{//0}}{B_0^2} \langle \partial_x v_{z0} \rangle \langle \gamma^{-1} k_\perp^2 \psi_1^2 \rangle .$$

We can relate this flux with the helicity flux

$$\langle j_{//} \rangle_x = \frac{-x_k \partial_x v_{z0} \lambda^2}{\mu_0 B_0} \left\langle \left(\frac{k_\perp}{\gamma} \right)^2 \right\rangle \langle F_h \rangle_x .$$

The heat and particle fluxes are directed inward to the plasma (opposite to the direction of the diffusion of $j_{//0}$).

$$\langle q_e^s \rangle_x = \frac{-C_z T_e}{e} \langle j_{//} \rangle_x = \frac{C_z T_e \partial_x j_{//0}^2}{2e^2 n_{e,0}} \left\langle \gamma^{-1} \left(\frac{B_{x,1}}{B_0} \right)^2 \right\rangle .$$

$$\langle \Gamma \rangle_x = \frac{-1}{e} \langle j_{//} \rangle_x = \frac{\partial_x j_{//0}^2}{2e^2 n_{e,0}} \left\langle \gamma^{-1} \left(\frac{B_{x,1}}{B_0} \right)^2 \right\rangle .$$

The average charge neutrality condition reads

$$v_{z,1} \cdot \partial_x^2 \psi_0 + [(\delta_\lambda \lambda)^2 (v_A k_\perp / \gamma)^2 + 1] \partial_x v_{z0} \cdot \partial_x \psi_1 = 0 .$$

COMPARISON WITH THE STOCHASTIC THERMAL CONDUCTION

Let us assume that both $j_{//,0}$ and $T_{e,0}$ have a same magnitude of characteristic length δ_X of spatial distributions. Here, a finite gradient in $T_{e,0}$ is necessary to compare our result with the stochastic conduction, while the electron pressure gradient should not be large in order to avoid inconsistency with our previous assumption.

Then we obtain

$$|q^{\tilde{u}}_{e,x}| / |q^{\tilde{b}}_{e,x}| \simeq v^2_{z,0} / \left(v_{e,th}\gamma\delta_x\right) = \xi_e v_{z,0} / \left(\gamma\delta_x\right),$$

where ξ_e is the electron streaming factor which is typically of the order of 10^{-3}. In normal tokamak parameters, both $v_{e,th}$ and the Alfvén velocity v_A are of the order of 10^7 m/s. The growth rate γ of the tearing modes are normally much smaller than $1/v_A\delta_X$. When $\gamma/v_A\delta_X$ is of the order of 10^{-3}, then the present heat flux $q^{\tilde{u}}_e$ makes a significant contribution to the total electron heat transport.

SUMMARY

1. Circularly polarized component of perturbed electric field correlates the helicity flux, parallel electron current and polarization ion current.

2. The heat and particle fluxes have been estimated, which are correlated with the helicity transport. The heat and particle transports accompanied by the helicity transport are unavoidable consequences of the anomalous transport of $j_{//}$.

Consistency of Current Drive and Divertor Conditions for Steady State and Hybrid Operation in ITER

M.Sugihara, Y.Murakami, H.Kimura,
T.Nakazato, T.Tsunematsu, Y.Shimomura

JAERI

US-Japan Workshop on RF Current Drive
Nov. 18-21, 1991

Contents

Steady State Operation
- Steady State Operation Space
- Simple Model for Peak Divertor Load
- Divertor Load for Steady State Operation
- Possibility for Improvement

Hybrid Operation for Long Burning
- Hybrid Operation Space
- Improvement by Inductive Flux

Steady State Operation Space

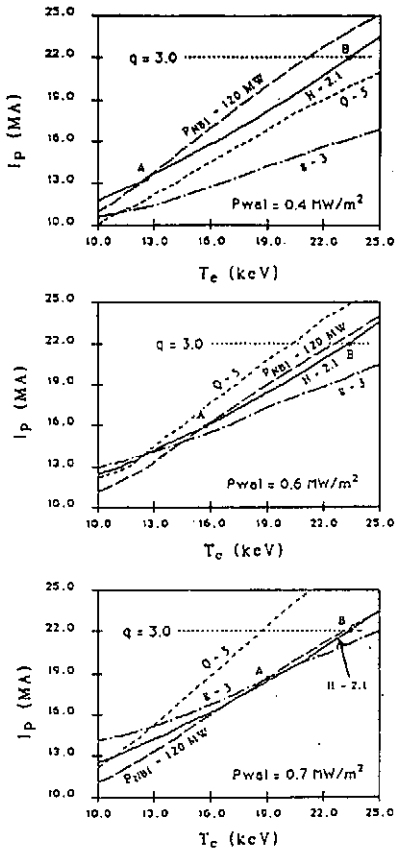

Simple Model for Peak Divertor Heat Load

Harrison-Kukushkin Model used in ITER

$$W_{div} \approx \frac{P^{14/9}}{\langle n \rangle^{7/9} \chi_\perp^{7/9}}$$

Itoh's Model

$$W_{div} \approx \frac{P^{1.0}}{\langle n \rangle^{0.4}}$$

$\chi_\perp$ = const. : HK model

$\chi_\perp$ = Bohm type : Itoh's model

Both models are normalized to 5 MW/m² in the ignition operation mode of ITER :

P = 116 MW, P_α=216 MW (P_f=1080 MW)
P_r=100 MW
$\langle n \rangle$ = 1.22×10^{20} m^{-3}

HK Model

Simple analytic heat transport along and across field line in SOL

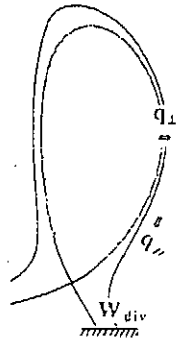

(1) $q_\perp = n_s \chi_\perp \frac{\partial T}{\partial r} \approx \frac{n_s \chi_\perp T}{\Delta}$

(2) $\nabla \cdot \vec{q} = 0 \Rightarrow \frac{q_{//}}{L} \approx \frac{q_\perp}{\Delta}$

(3) $q_{//} \approx \frac{T^{7/2}}{L}(1-\theta^{7/2})$

$$\Delta \approx \frac{(n_s \chi_\perp)^{7/9}}{q_\perp^{5/9}} \frac{L^{4/9}}{(1-\theta^{7/2})^{2/9}}$$

$$W_{div} \approx \frac{P^{14/9}}{\langle n \rangle^{7/9} \chi_\perp^{7/9}}$$

Considerations on relation between HK and Itoh's model

Starting from HK model

$$W_{div} \approx \frac{P^{14/9}}{(n)^{7/9}\chi_{\perp}^{7/9}}$$

When $\chi_{\perp}$ is Bohm type

$\chi_{\perp} \propto T/B$

Estimation of T

$\Gamma P \propto (nT)^2 \Rightarrow T \propto (\Gamma P)^{0.5}/n$
(pressure balance along field line)

P-dependence
if $\Gamma \propto P^{0.1}$ ($P^{0.5}$ when $\tau_p \propto 1/P^{0.5}$)
$W_{div} \propto P^{0.8\text{-}1.2}$ ($P^{1.0}$ when $\tau_p \propto 1/P^{0.5}$)

n-dependence
if $\Gamma \propto n$
$W_{div} \propto n^{-0.4}$

Difference of $\chi_{\perp}$ could explain two different models:

Constant $\chi_{\perp}$: HK model
Bohm type $\chi_{\perp}$: Itoh's model

JT-60 NB heating

W_{div} vs P

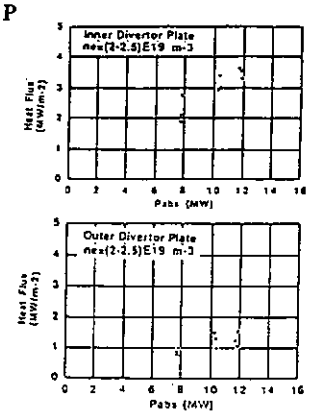

Half width vs <n>

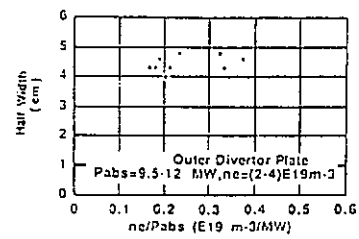

(Itami, Nakamura et al : JAERI-M90-066)

JT-60 LHCD

Half width vs <n>

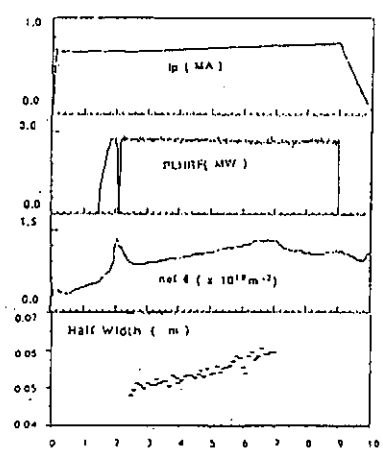

(Itami, Nishitani et al : JAERI-M90-066)

Divertor heat load at operation point A estimated by two simple models

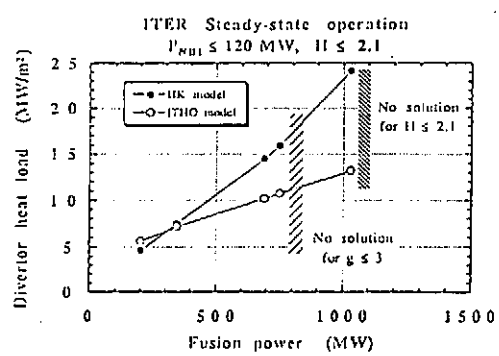

- Both models predict that steady state operation with required wall load for nuclear testing (>1 MW/m²) results in significantly higher divertor heat load than in ignition operation
- Improvement to reduce divertor heat load will be necessary to realize SS operation
- Substantial difference in predicted values by both models, so improvement on divertor model should also be very important

Possibility for reducing divertor heat load in Steady State operation

Operation: with lower temperature / higher density (A)

: with lower current drive power (B)

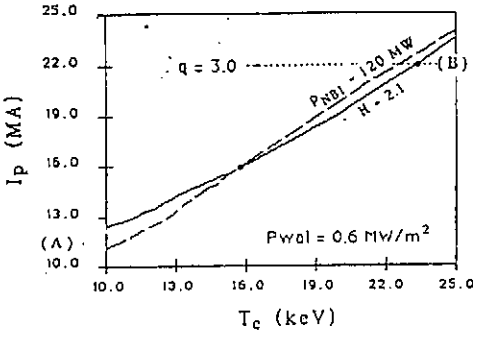

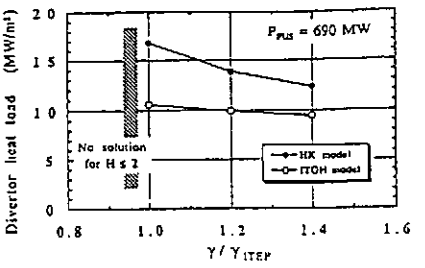

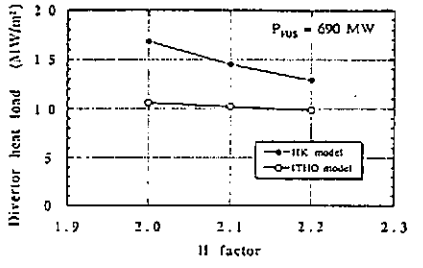

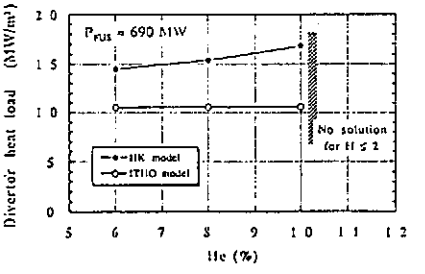

Typical examples

- Current-drive
  - Current drive efficiency
  - Bootstrap current
- Improving confinement
  - H factor
  - Helium concentration

Best operation point for divertor heat load

(A) : highest density with full CD power
(B) : smallest CD power

depends on the divertor model, and (B) is not the best one in the HK model, while (A) and (B) provides very similar divertor heat load in the Itoh's model.

Example: all improvements are included (H=2.2, $η/η_{ITER}$=1.4, He=5%)

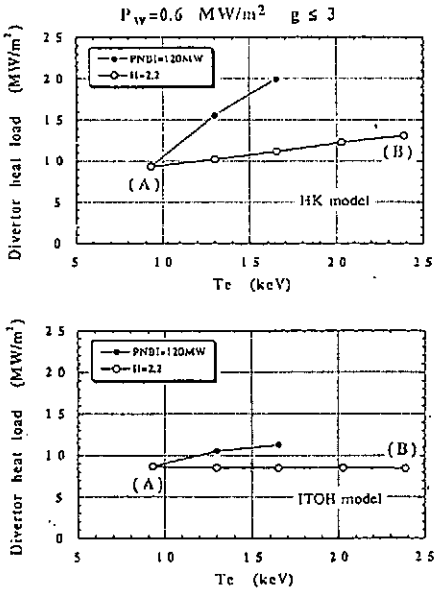

Hybrid Operation

Hybrid operation space to satisfy the engineering requirements:

Wall load > 1 MW/m²
Burn time > 1000 s

Example:
P_W =0.6 MW/m² (≈1 at test region) with 2000s burn

P_{NBI} = 80 MW

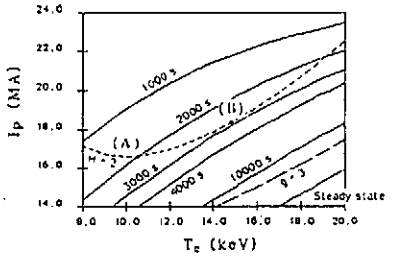

P_{NBI} = 115 MW

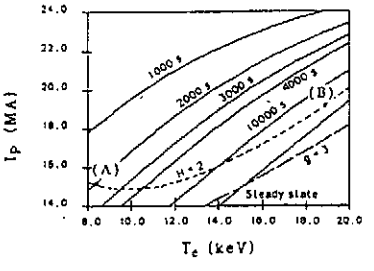

A: Operation point with lowest temperature (highest density)
B: Operation point with longest burn time

Divertor heat load is generally insensitive to the increase of CD power (in the case of HK model, it slightly decreases with CD power, which is similar to SS operation)

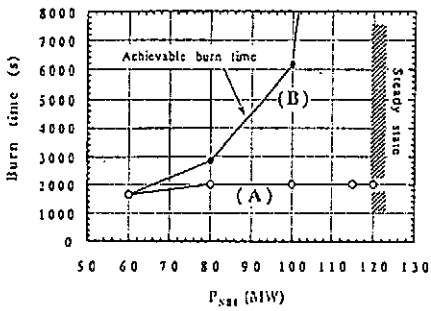

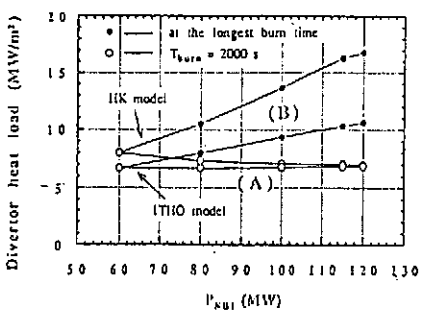

Certain degree of capability for current profile should be held in hybrid operation

(1) Maintenance of high beta

- Rather small li is needed to suppress ballooning instability near plasma center as pressure profile peaks;
  $p(\Psi) = p_0(1-\Psi)^{\alpha_p}$ (α_p is 1.5 for ITER)

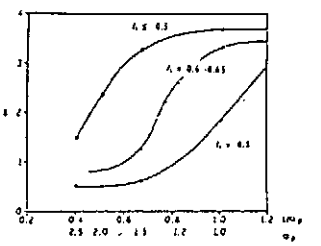

- This requirement can be relaxed as q_ψ becomes large (DIII-D)

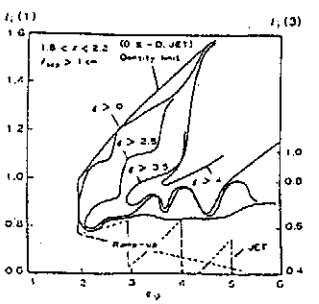

(2) Avoidance of (Monster) Sawteeth

- Steady state current profile is fairly peaked (q_0 is reduced down to 0.34) when current is driven purely inductively with neoclassical resistivity

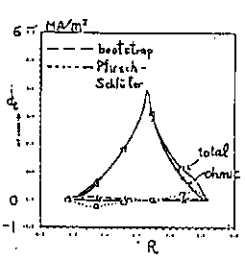

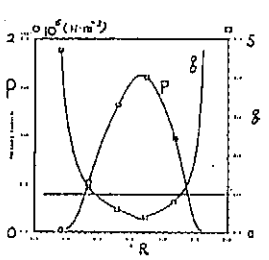

- When 1/3 of plasma current is driven non-inductively, q_0 can be maintained slightly below unity (q_0 = 0.85)

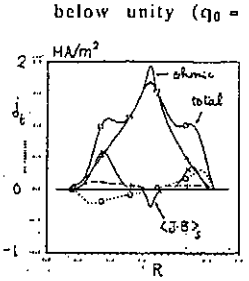

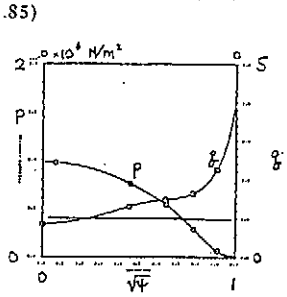

I_p = 22MA
I_e = 6MA
I_c = 38MA
I_{BS} = 2.0 MA
q_0 = 0.85
l_i = 0.90
β_J = 0.49
q = 1.88

(Tokuda, Tsunematsu)

Another issue is a probable insufficientness of current profile controllability (e.g., $I_{NBI}/I < 0.3$) for long burning.

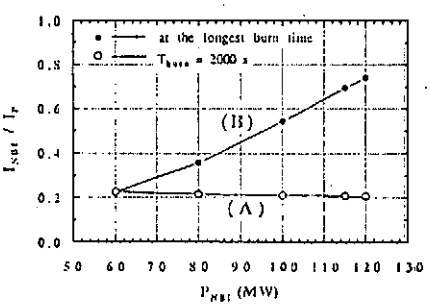

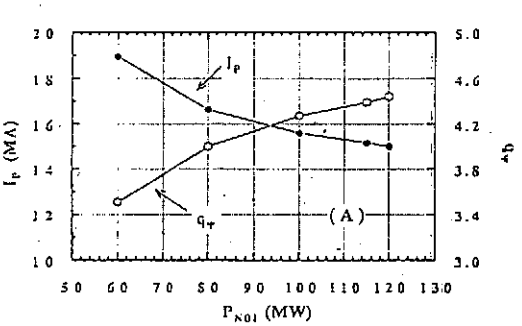

Operation point with large CD power is preferable, since requirement of profile control will probably be reduced due to increase of q_ψ.

Reduction of divertor heat load by increasing inductive flux

For fixed operation point:
Burn time is increased with same divertor load

For fixed burn time (2000s):
Divertor heat load is decreased

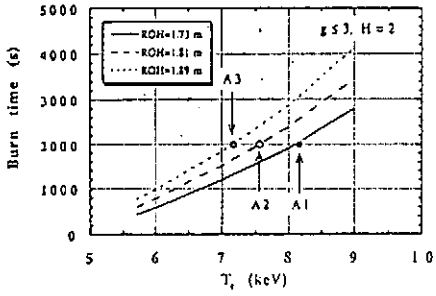

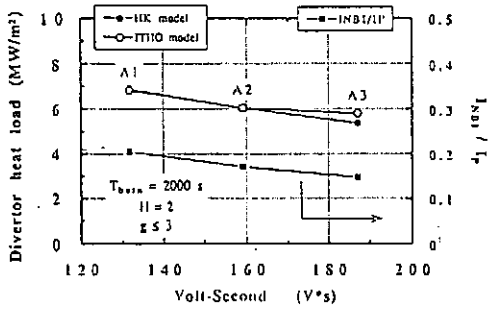

For fixed burn time operation, divertor heat load can be reduced, while the capability of profile control is decreased and the requirement of profile control will be increased (q_ψ is decreased)

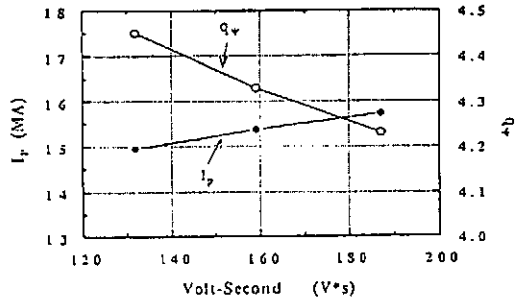

Further careful examination should be needed to identify the usefulness of increased inductive flux for inductive-dominant long burning.

Summary

1. Systems analyses on steady state and hybrid operation space in ITER are performed with respect to divertor heat load by using two typical divertor models (HK and Itoh's).

2. Both models predict substantially higher heat load, especially in steady state operation, than in ignition operation, while significant difference in the predicted values exists between two models. Improvement of the divertor models are essential to identify the feasibility of steady state operation in ITER.

3. Moderate improvement of current drive efficiency and confinement can reduce the heat load to some extent, but further substantial improvement is necessary to ensure steady state operation with reasonable heat load condition of divertor.

4. In hybrid operation, injection of full current drive power could marginally reduce the divertor heat load, and moreover, with this injection, the requirement of current profile control could be reduced.

5. Increased inductive flux can prolong burn time when non-inductive drive of about 20 % of total current is sufficient for profile control. However, the divertor heat load could not be reduced with the increased flux, since the operation point, in which the capability of profile control is reduced and the requirement will be increased, may not be realized. Further study is needed on this issue.

Group A

Status / Achievement (EC, LH, IC, Alpha ...)
Efficiency of CD of Plasma (& Profile) Control

Understanding in Progress
Current Drive
Current Profile (Direct)
Stability / Confinement (indirect)
Mistery

New Future Progress
New future Program
Possible Achievement in Control / Understanding

Group B

Motivation
Helicity
RF , DC , Transport
Synergetic Effect
Basic Understanding
Rotation Drive by non Resonant Force

Group C

View on Steady State
Heat, Particle, Current
Request from Fusion Exp. Device (ITER)
Compatibility
Heat and Current Drive
Understanding
Progress in Exp. Data
Modelling
Mistery
New Future Progress

DISCUSSION ON FAST WAVE CURRENT DRIVE
LOWER HYBRID C.D.
Group A ELECTRON CYCLOTRON C.D.

1. LIST OF DEVICES
   EXPERIMENTAL CHARACTERISTICS
   GOALS
   MAIN RESULTS
2. MAIN FEATURES OF THE INDIVIDUAL CD METHOD
   η - profile control - scaling - synergies
3. PROBLEMS – MISTERIES
4. STATUS OF THEORY – WHICH MODELLING CODES EXIST ?
5. RELEVANT TECHNOLOGICAL ISSUES
6. ITER APPLICATIONS
7. WHAT'S MISSING ? HOW CAN WE COLLABORATE ?

FAST WAVE [illegible]

1. HEATS ELECTRONS
2. UNIDIRECTIONAL EFFECTS ARE SEEN BUT CURRENT IS INDEPENDENT OF PHASE
3. FWCD THEORY HOLDS GREATEST PROMISE
   no n_e limit
   η should be like LHCD
   technology
   α particle damping seems avoidable
4. ELECTRON HEATING COMPARISON WITH THEORY IS GOOD
5. STEADY STATE CD NOT PROVEN YET

THIS IS THE METHOD WHICH IS MOSTLY FAVOURED BUT HAS LEAST EXPERIMENTAL EVIDENCE

LOWER HYBRID

1. DRIVES SS CURRENT {2 MA / 420 kA
2. EFFICIENCY NOW ~.4 (10^{20})
   APPROACHING THEORETICAL VALUE
   should achieve .5–.6
   (for ITER .35 is realistic)
3. GOOD PROSPECTS FOR I_p CONTROL
   BUT LIMITED PENETRATION
   BY T_e → HIGH EXP PRIORITY {JT60U / JET
4. DIFFUSION OF FAST ELECTRONS
   MAY OR MAYNOT BE A PROBLEM
   → MORE STUDY
5. GOOD COUPLING / COUPL. SYSTEMS
6. TEMP. BARRIER IS MAIN LIMITATION

- BETTER PHYSICS UNDERST.
- BETTER COUPLING DEVICE

ELECTRON CYCLOTRON C. D.

1. 100 kA in DIII D BUT $V_L \neq 0$
2. SAWTEETH SUPPRESSED BUT m=2 NOT STABILIZED
→ NEED MORE DATA / PHYSICAL UNDERSTANDING
3. $\eta_{ITER} = .25$ (expectation)
$\eta_0 = 0.01$ (10^{-2})
4. T-10 / DIII D SHOW PERFECT AGREEMENT WITH THEORY FOR η
5. TRAPPING EFFECT MAY ENHANCE BOOTSTRAP C.
6. BEST (THEORETICAL) LOCALIZATION → TO BE PROVEN
7. SOURCES ARE THE PROBLEM (often overstated)
8. LAUNCHER GOOD (?)

Report of Group B (Helicity & Innovation)

1) Motivation

2) Helicity

RF, DC, Transport, Rotation Drive

3) Synergies

Bootstrap, Seed Current generation, Burning Plasma

Motivation

(1) Break through is necessary
- Efficiency still low (long range)
- Applicability limited
- Not Enough Confinement
- Open up Parameter for flexibility
- Free energy of burning plasma

(2) Impact to Basic Understanding
- Transport of J, T, n, ...
- New chance for improved confinement
- Dynamic process (Sawtooth, major disruption)

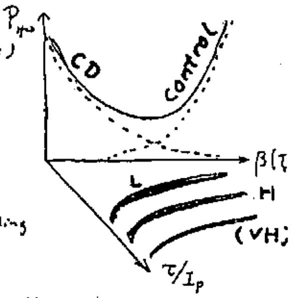

Helicity

RF: Helicity CD: Understanding of basic physics process
Local picture ⊖ wave physics
global evaluation

[rf helicity CD] ∈ [non resonant drive]

- We have now firm basis for this new Scheme (Theory)
- Experimental Evidence: Wanted

DC: Formation of Closed mag. Surface cf. SPAC

Peaked current profile (?) needs research of year or so

Generalized $(A \cdot B + \phi B) \rightarrow (\frac{c}{\omega} A + v)(\frac{c}{\omega} B + \nabla \times v)$

Test by e-beam

- Formation: Evaluate old exp.
- transport of J: J(r) problem?

Transport

$\eta J - \lambda \nabla^2 J = E$

Example of λ, $q, \Gamma = \mathcal{D} \nabla J$

Seed Current

- General Transport matrix $\begin{pmatrix} q \\ \Gamma \\ P_{\parallel e} \\ \vdots \end{pmatrix} = \begin{pmatrix} & \end{pmatrix} \begin{pmatrix} \nabla T \\ \nabla n \\ \nabla J \\ \vdots \end{pmatrix}$
heat pinch
- Sawtooth Physics / major Disruption in progress
- Fokker-Planck formalism
- non local equation $\eta J - \int \Lambda(r, r') J(r') = E$

Rotation Drive (Chan, Chiu)

Non resonant force on ions $\mathcal{F}_i^{NR} = \frac{\eta_{LH} P_{kw}}{B_T^2 N_\parallel}$ (Newton) for low frequency

Example: $n_i = 5 \times 10^{13}$, $B_T = 2T$, $N_\parallel = 10$: 0.5 N by 100 kW
NBI (80 keV, D) : ≤ 0.1 N by 100 kW

Future Progress

Synergies

Bootstrap Current

① Present exp. T-10, DIID, TFTR, JET, JT-60 Helical
90%, ~30%, ~50%, 70%, 80%

Seed current

② CDX-U exp.: Innovative $V_L = 0$, closed mag. surface
this state may be close to 100% BS state
Hope to prove may not be easy

Seed current Generation

① diffusion of J
in principle zero external supply
F.P. Eq. for ohm's Law
② Finite banana?

Burning Plasma

① BS current Carried by α-particle
10% of bulk BS current (Taguchi)
without other effects

Others

DC E-field + conventional / unconventional
Trapped particle population

In particular .....

(1) Physics of helicity CD made progress RF, DC

(2) Synergies
BS + Current Diffusion
BS + α-particle
⋮

(3) Future possible progress
$\lambda \nabla^2 J$ physics
Rotation Drive
Improved Efficiency
Free energy of burning plasma

Group C

- View on Steady State Operation
- Compatibility
- Understanding
- New Future Progress

Group C

S.-I. Itoh, M. Shimada, M. Sugihara, T. Taylor

View on Steady State Operation

- Requests from Fusion Exp. Device (ITER)
  - Plasma current ≳ 15MA — confinement, beta
  - Wall load ≳ 1MW/m² — nuclear test
  - Total power (α+CD) ≳ 250MW
  - Divertor heat load ≲ 15MW/m² — heat removal
  - Divertor temperature ≲ 30 eV — erosion
  - Low density ~ 5×10^{19} m^{-3}
  - Z_{eff} ≲ 2.2
- Requirements for divertor condition to meet these requests
  - high density / low temperature divertor

Compatibility

- Steady State Operation is difficult based on present simple model :
  - low density / high power demands
    peak heat load ≳ (2-3) times ignition operation
    peak temperature ≳ 100 eV
  - while present models need large improvement

- Possible Solutions (Breakthrough)
  - Radiative divertor : low density, compatibility with good T_e, low impurity level
  - Higher β_t operation*)
  - Edge density control
  - Biasing
  - Sweeping (magnetic, electro-static)
  - Pumped divertor
  - Ergodization

Higher β_t Operation

Good	Bad
· high bootstrap fraction	· lower confinement
· long connection length	· lower absolute beta
· radiative divertor	– Both are improved by increasing B_T :
· stability	· Synchrotron radiation?
· grassy ELM	· Technology development
	– Effort to reduce plasma current is important :
	· VH mode + 2nd stability difficult to realize simultaneously ?
	· High aspect ratio needs high performance database

Understanding : Present status is poor

- Approach of core plasma confinement is valuable

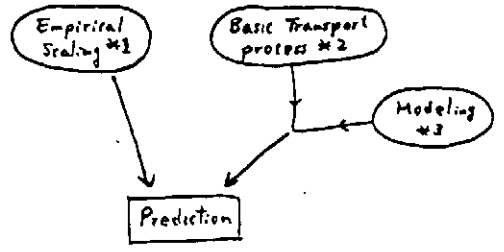

*1 Scaling of peak heat load / temperature, T_p on
(P, n, I_p, B, SN/DN --)
under ITER-relevant (ED) conditions

*2 Systematic database on
- Divertor / SOL profile data (n, T, j, P_{rad})
derivation of $\chi_\perp$, $D_\perp$
- P_{ion} / P_{elec}, fast ion trajectory
- Impurity Physics ; generation
shielding
transport
effect on τ_E / τ_p

*3 Systematic check against exp. data
Modeling of non-stationary state (ELM)
Impurity modeling

- Identification of operation regime / parameters
grassy
ELMy discharge (not possible in low β ?)
· High bootstrap with high n operation
· Effect by fast electrons ($2 \times 10^{19}\,m^{-3}$)
· How plasma can maintain Maxwellian

- Mysteries
· High energy ion on SOL
· $\nabla \cdot j \neq 0$?
· $\Gamma_{tot} / \Gamma(H) \sim 2$?
· Isotope effect
· Material effect (confinement, ---)

New Future Progress

DIII-D
Database being developed (Systematic)
Biasing effects
Pumping effects
BSCD (2nd stable core?)

JT-60U
Database (OH) on n, T, j
τ_p, τ_E heat data of high P (~40MW)
Impurity data
Generation
Shielding
Transport ($\parallel$, $\perp$)
Boronization ? → VH ?!
BSCD

GENERAL SUMMARY OF THIS US-JAPAN WORKSHOP ON RF HEATING AND CURRENT DRIVE

Participation: 8 US Scientists
30 Japanese scientists

General Categorization of Papers:

RF physics, technology & application	10
New Concepts: helicity injection; transport	6
Heating/CD and SOL/Divertor conditions	6

Detailed Categorization:

FW H/CD	5
ICRF/IBW	3
ECCD/ECH	2
LHCD	4
Helicity Injection	5
Profile control/sawtooth stabilization	4
ITER/reactor requirements	2
Bootstrap Current	2
Divertor/SOL Models	4

Show growth of workshop both in depth and breadth

RF Physics, Technology & Applications

(A) FW CD

- Electron heating established. Multiple pass absorption in evidence ± ~~agreement~~ consistent w/ theory. Extensive
- Launching of FW w/ phased spectrum demonstrate Efficient Coupling w/ loop antenna demonstrate Is loop antenna competitive w/ ITER and reactors?
- CD observed but current is dependent of phasing. Steady-state CD not demonstrated.
- FWCD holds largest promise in theory
  - α particle damping available
  - no n_e limit for penetration
  - η comparable to LHCD
  - technology available.

(B) LHCD

- Demonstrated S.S.C.D. (most data) 2MA, 4210 sec
- Efficiency ~.4 ($10^{20} m^{-2}$ A/W) for ITER .35 is realistic
- Profile control demonstrated but penetration may be limited by high T_e
- Diffusion of fast electron still a question.

(C) ECCD

- CD demonstrated, agreement w/ FP theory
- ECCD + bootstrap shown on T-10
- launcher efficient
- Sawtooth suppression proven but $n=2$ stabilization and disruption control not yet shown. Reliable theoretical model does not exist
- Theory predicts $\eta = .25$ for ITER. Recovering trapped particle reduction of η_{CD} through bootstrap enhancement may improve efficiency. Need theory and experiment
- Sources are <u>the</u> problem. RF generator not yet available

New Concepts

Motivation:

- I_{rf}
- need better η_{CD} at high density
- compatibility w/ stability
- β_p
- Profile control dir. to improve T_e
- T_e/T_p

- Fundamental physics understanding

Helicity CD:

① rf — theoretical understanding much improved over last 2 years
Experimental observation still lacking
Efficiency still low so far

② dc — formation of closed flux surface established
Current diffusion & transport still not well understood.

-5-

③ Transport — Theretical models of diffusion proposed

Experimental verification not available

If validated, full bootstrap current tokamak may be feasible

Bootstrap :-

- Significant fraction of bootstrap current has been observed in many machines
- CDX-U close to 100% internally generated current
- Is externally supplied seed current needed? Unknown both theoretically & experimentally.

Synergetic Effects :- Some preliminary observation. Not yet ~~Not yet observed~~ or convincingly demonstrated.

Plasma Rotation :- non-resonant rf force can drive plasma rotation comparable to NBI e.g. for T_E improvement Need experimental verification

-7-

③ Theory & Modeling

- 1-D model assumptions may not be realistic although some interesting predictions have come forth
- 2-D model difficult to develop
- Need some intermediate approach combining measured boundary conditions with 1-D model

Divertor/SOL Issues

① Compatibility of S.S. CD with divertor and wall loading e.g. for ITER

- Simple model ⇒ S.S. difficult to achieve. [Favors high β, high n_e (low T_e) operation]
- Constraints may be relaxed by improved T_E or innovative divertor concepts
  c.g. radiative divertor, sweeping X-point
  Significant trade-offs are still required.
- Reliability of divertor model needs to be improved. Lack experimental verification of model.

② Runaway electrons / impurity generation

- Experiments observed runaway electrons at low n_e ⇒ hot spots & impurity generation
- May be due to error fields. What is the constraint on field errors?
- ICRH also generate energetic ions, which also result in impurity generation.
- High β_T CD operation may not be compatible w/ [illegible] control. Need new ideas.

Ed. S.-I. Itoh, T. Seki

Recent Issues of NIFS Series

NIFS-PROC-1 *U.S.-Japan Workshop on Comparison of Theoretical and Experimental Transport in Toroidal Systems Oct. 23-27, 1989* ; Mar. 1990

NIFS-PROC-2 *Structures in Confined Plasmas –Proceedings of Workshop of US-Japan Joint Institute for Fusion Theory Program–* ; Mar. 1990

NIFS-PROC-3 *Proceedings of the First International Toki Conference on Plasma Physics and Controlled Nuclear Fusion –Next Generation Experiments in Helical Systems– Dec. 4-7, 1989* ; Mar. 1990

NIFS-PROC-4 *Plasma Spectroscopy and Atomic Processes –Proceedings of the Workshop at Data & Planning Center in NIFS–*; Sep. 1990

NIFS-PROC-5 *Symposium on Development of Intensed Pulsed Particle Beams and Its Applications*; Oct. 1990

NIFS-PROC-6 *Proceedings of the Second International TOKI Conference on Plasma Physics and Controlled Nuclear Fusion , Nonlinear Phenomena in Fusion Plasmas -Theory and Computer Simulation-*; Apr. 1991

NIFS-PROC-7 *Proceedings of Workshop on Emissions from Heavy Current Carrying High Density Plasma and Diagnostics;* May 1991

NIFS-PROC-8 *Symposium on Development and Applications of Intense Pulsed Particle Beams, December 6 - 7, 1990*; Jun. 1991

NIFS-PROC-9 *X-ray Radiation from Hot Dense Plasmas and Atomic Processes*; Oct. 1991